# INTRA-ARTICULAR DRUG DELIVERY SYSTEMS FOR THE TREATMENT OF OSTEOARTHRITIS

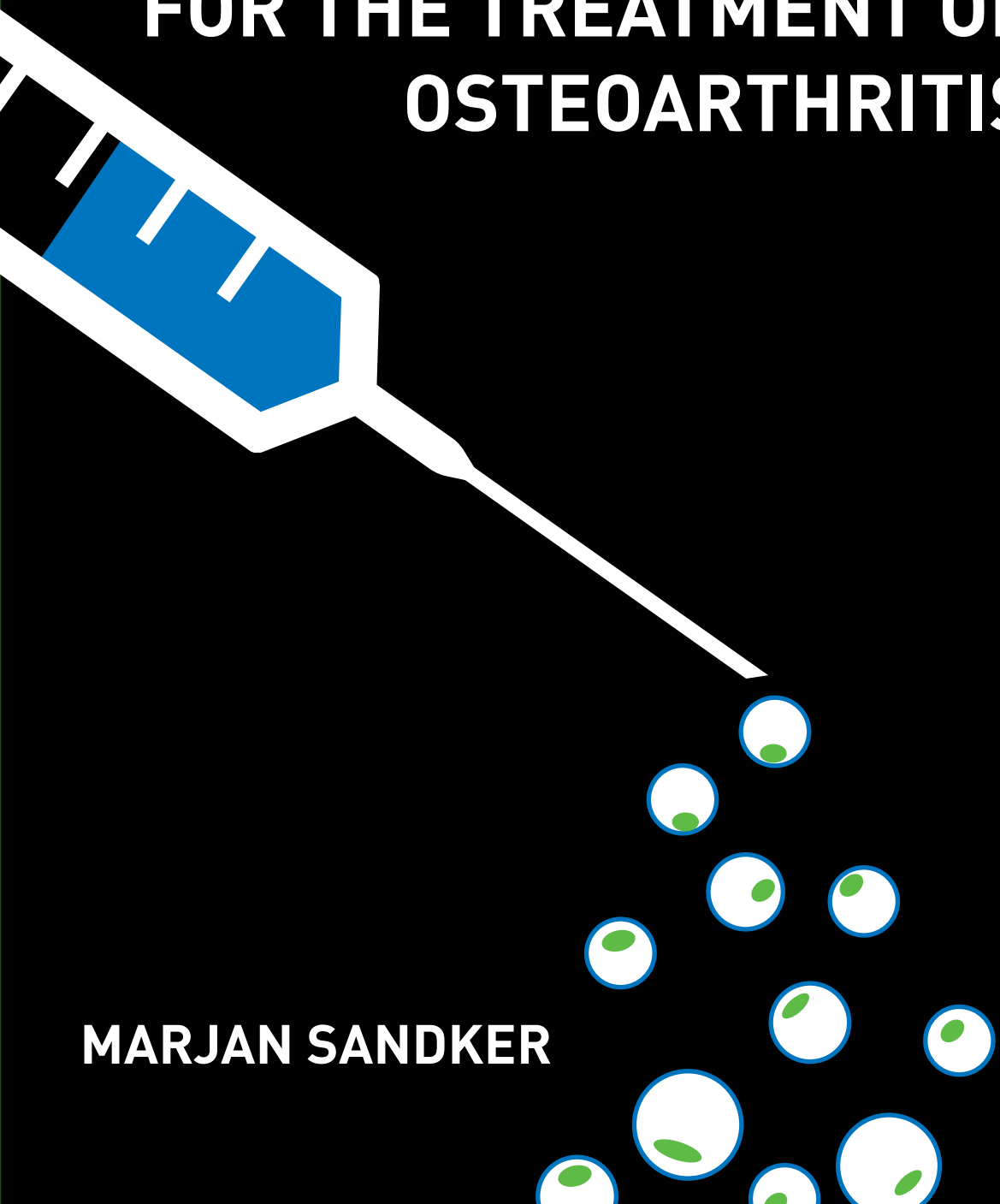

MARJAN SANDKER

# Intra-articular Drug Delivery Systems for the Treatment of Osteoarthritis

**Intra-articular Drug Delivery Systems for the Treatment of Osteoarthritis**

Maria Jannie Sandker, 2019

PhD thesis, Utrecht University, University Medical Center Utrecht, the Netherlands

ISBN 978-94-6380-215-4

The research described in this thesis was part of OAcontrol of the research program of the BioMedical Materials institute, co-funded by the Dutch Ministry of Economic Affairs, Agriculture and Innovation. This work was supported by the Dutch Arthritis Foundation

Cover by: Cover and illustrations Chapter 1 by: Bregje Jaspers, Studio 0404, Nijmegen

Layout by: Ben Graphics, Tilburg

Printed by: ProefschriftMaken, Eindhoven

# Intra-articular Drug Delivery Systems for the Treatment of Osteoarthritis

Intra-articulaire Geneesmiddelafgiftesystemen voor de behandeling van Artrose
(met een samenvatting in het Nederlands)

**Proefschrift**

ter verkrijging van de graad van doctor aan de Universiteit Utrecht
op gezag van de rector magnificus, prof.dr. H.R.B.M. Kummeling,
ingevolge het besluit van het college voor promoties in het openbaar
te verdedigen op 13 februari 2019 des ochtends te 10.30 uur

door

Maria Jannie Sandker

geboren op 12 november 1985 te Odoorn

Promotoren: Prof. dr. ir. H. Weinans
Prof. dr. ir. W. E. Hennink

Dit proefschrift werd (mede) mogelijk gemaakt met financiële steun van Nederlandse Orthopaedische Vereniging, Eslin Orthopedie, Centrum Orthopedie Rotterdam, Buchrnhornen, La-Mer Orthopedie, Anna Fonds te Leiden en Chipsoft.

# Content

# Chapter I

## General introduction

## Osteoarthritis

Osteoarthritis is the most common type of arthritis, affecting approximately 1.2 million people in The Netherlands alone [1] and this number is expected to grow in the nearby future, partly due to the increasingly ageing population. Recent numbers show that in people older than 60 years of age, 10% of men and 13% of women are affected by osteoarthritis worldwide [2]. Patients suffering from osteoarthritis may experience joint pain and loss of function, leading to disability and a reduced quality of life [3]. The pathogenesis of osteoarthritis is not fully understood yet, but it is likely a combination of different factors, amongst which obesity, age, trauma, joint malalignment and genetics play an important role [2]. Although it is thought that there are potentially critical biological differences between the age-related, post-traumatic and metabolic phenotypes of osteoarthritic, eventually all these factors lead to a disequilibrium between anabolic and catabolic activities in the joint, which in turn lead to upregulation of proinflammatory cytokines (such as Il-1B, TNF-a) and related catabolic enzymes such as matrix metalloproteinases (MMPs) and aggrecanases [4, 5]. These factors will eventually result in cartilage breakdown. The products of cartilage degradation by itself such as collagen and proteoglycan fragments can also be catabolic, hence a vicious circle of cartilage degradation is initiated. Due to the very limited healing capacity of cartilage, this will eventually lead to osteoarthritis.

## Cartilage

Synovial joints are covered with hyaline cartilage. The cells within the cartilage are named chondrocytes which produce the extra-cellular matrix (ECM), with the most important factors being collagen type 2 (COL2) and glycosaminoglycans (GAGs) [6]. GAGs are negatively charged polysaccharides; the main GAGs in cartilage are chrondoitin sulfate and hyaluronic acid [7]. GAGs are mostly linked to a core protein of aggrecan, forming proteoglycans which are highly negatively charged molecules, leading to an inflow of positive charged molecules such as sodium, potassium or calcium. The subsequent high tonicity creates water influx and causes swelling of the tissue that expands the collagen fibers and creates an internal cartilage pressure. This mechanism makes cartilage resilient to the high compressive forces of load-bearing of the joints, and thereby absorbing the forces for the articulating bones making motion painless and fluidic. In the case of osteoarthritis, there is a mismatch within the joint between catabolic and anabolic factors, leading to cartilage damage. Because of the low proliferation rate of chondrocytes and the avascular nature of cartilage, its healing capacity is limited. Once the initial damage has occurred, the proteoglycans will leak from the cartilage and with that, it will lose its water content and thereby the ability to withstand compressive forces. As a result, the chondrocytes are no longer able to maintain cartilage integrity, and the weakening of the matrix makes the damaged cartilage more susceptible for further degradation. As a

negative side effect, the presence of cartilage degradation products such as collagen and proteoglycan fragments within the synovial fluid can lead to inflammatory responses and production of catabolic cytokines, in their turn leading to further cartilage degradation and the vicious circle of degeneration known as osteoarthritis has begun.

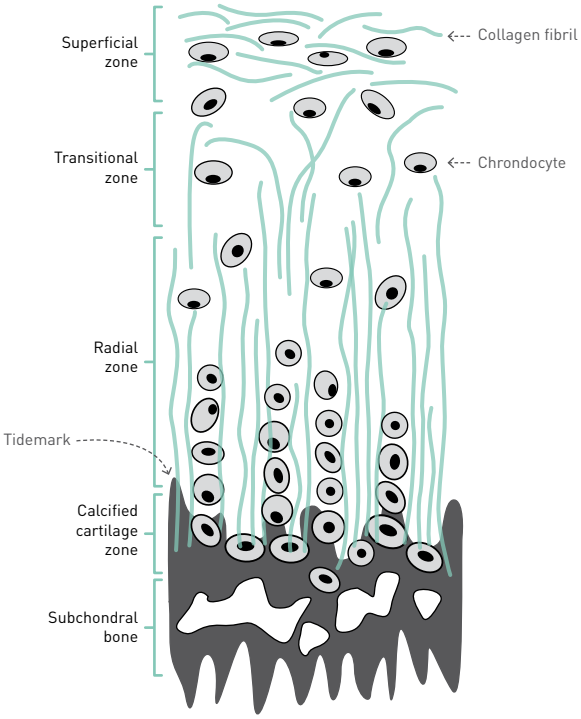


***Figure 1.*** *Cartilage.*

## Other changes in the osteoarthritic joint

Apart from the degeneration of cartilage, other structures in the osteoarthritic joint show pathological changes as well. Alterations in subchondral bone, the layer situated directly under the articular cartilage, have been identified in osteoarthritis. Bone changes mainly involve osteophyte formation and subchondral bone sclerosis. The physiological role of subchondral bone in healthy and diseased cartilage is to a large extent unknown. However, it likely plays a role in the homogenous load distribution throughout the joint as well as supplying the cartilage its nutrients and is therefore important in maintaining the homeostasis of the joint [8].

Subchondral bone is known to be dynamic and is able to adapt to changes in mechanical loading. Within the arthritic joint, weakening and loss of the cartilage will lead to an increased loading of the underlying subchondral bone, resulting in stiffening and

sclerosis. In its turn, the sclerotic subchondral bone leads to higher (peak) loading of the overlying cartilage thereby contributing to local overloading and cartilage degeneration [9]. Another radiological hallmark of OA is the formation of osteophytes which are fibrocartilage-capped bony spurs at the borders of the joint lines. The pathophysiology of osteophyte formation is not fully understood, but it is partly thought to be formed by the joint in order to expand the surface area of the joint, in an attempt to withstand the increased mechanical loading of the joint as a result of cartilage damage and degeneration. Also, local osteophyte formation is seen after ACL (anterior cruciate ligament) ruptures, limiting the translocation of the femur in correlation to the tibia and thereby facilitating stability [10]. The formation is however not solitarily linked to mechanical stress, as osteophytes are also present in osteoarthritis of the hand, joints that are usually non-weight bearing. Chronic inflammation, as seen in osteoarthritis, leads to activated macrophages which are known to produce TGF-ß [11, 12]. This cytokine in turn induces BMP production, which is known to trigger osteophyte formation [11]. Changes in bone were historically thought to be secondary to the cartilaginous changes within the joint. However, in animal models it has been shown that in early stages of osteoarthritis, bone changes are already present and that changes in subchondral bone in their turn indeed lead to cartilage degeneration, indicating that bony changes are not purely secondary to cartilage breakdown [13, 14]. This again shows that osteoarthritis is a "whole joint disease" and that its pathogenesis is very complex and pathways are intertwining.

Another structure within the joint, called the synovium, plays an important role in the osteoarthritic joint. The synovium is the lining of the joint, consisting of specialized connective tissue capable of producing lubricin and hyaluronic acid and thereby maintaining the synovial fluid volume and composition. Synovial fluid is not only a lubricant of the articulating joint, but is also very important for the nutrition of chondrocytes. Furthermore, in the synovium macrophages are present, which are cells involved in immune reactions. Historically, osteoarthritis was considered to be a non-inflammatory disease. However, in the early 1980s, it was shown through histopathology that in the majority of patients suffering from OA, the synovium shows an abundant inflammation [15] and inflammation has since been indicated to play a strong role in the pathogenesis of osteoarthritis [16]. Products of cartilage degradation, such as fibronectine fragments, are released within the synovial fluid, and initiate an inflammatory response which in turn leads to the release of multiple catabolic factors, amongst which interleukin-1-beta and tumor necrosis factor-alpha are the most important. These factors are known for their negative effects on the ECM via MMPs resulting in chondrolysis with as a resultant, a release of cartilage degradation products in the synovial fluid [17, 18]. The result is a vicious circle of inflammation and cartilage breakdown with severe osteoarthritis as an end stage. As stated before, the consensus of synovial changes in the OA joint being solely secondary to cartilage degeneration has

been abandoned. For instance, it has been shown that obesity and acute trauma can trigger an increase of local inflammatory mediators and cytokines, leading to synovitis and subsequently cartilage degeneration [19] as well as osteophytes. This indeed suggests a more prominent role of the synovium within the development of osteoarthritis than merely secondary involvement.

## Clinical presentation of osteoarthritis

Patients suffering from osteoarthritis usually present themselves with chronic joint pain, loss of function and range of motion, joint effusions, crepitus during motion and radiographic joint space narrowing. Although risk factors for the development of osteoarthritis have been identified (age, obesity, trauma, genetics), we cannot predict in an early state which patient will develop symptomatic and progressive osteoarthritis and who will not. Furthermore, symptomatic and radiographic osteoarthritis unfortunately do not always overlap. About 25% of the population aged 50 years and over shows radiographic signs of knee osteoarthritis. However, only 50% of these individuals indeed has clinical symptoms of osteoarthritis [20]. This indicates that is it very important to always use a combination of radiological and clinical signs and symptoms in diagnosing osteoarthritis. The same applies for initiating any form of therapeutic treatment, be it conservative of operative, this should never be done solely on radiographic or clinical features, but always a combination of both.

## Treatment of osteoarthritis

To date, cartilage regeneration is not yet possible, making the treatment of patients suffering from osteoarthritis purely symptomatic. The golden standard of treatment is joint replacement, but this is only considered once conservative treatment has failed. Also, joint replacement is not a very suitable option for younger patients with osteoarthritis, due to their active lifestyles and the limited lifespan of a prosthesis. In patients with malalignment of the knee joint and osteoarthritis in one knee compartment (varus or valgus osteoarthritis), one may consider an osteotomy with realignment of the joint in order to decrease the loading of the affected cartilage in one compartment of the knee, thereby decreasing pain and delaying the moment of joint replacement in these younger patients. Conservative treatment mainly consists of weight loss and physical therapy in combination with oral pain management. The drug of choice, alongside acetaminophen, is usually an NSAIDs (non-steroidal anti-inflammatory drug), amongst which the most well-known are celecoxib and ibuprofen [21]. These drugs are potent painkillers, but also act in an anti-inflammatory fashion making them an interesting platform in the treatment of osteoarthritis, since as mentioned before, chronic inflammation plays an important role in osteoarthritis. The downside of these drugs is however their possible

systemic side-effects (renal, cardiac, gastro-intestinal [21, 22], limiting their long-term use. Furthermore, only a small fraction of a systemically administered drug will eventually end up in the affected joint. To overcome these problems, intra-articular injections with drugs, such as NSAIDS, have been investigated extensively. It is also aimed that in order to reduce the number of injections for the patients, innovative formulations have to be developed which release the loaded drug in a sustained manner for prolonged periods of time, as pointed out in more detail on the next pages.

## Intra-articular injections

Osteoarthritis usually affects only one or a few joints, making direct intra-articular injections a feasible treatment option for only the affected joint and thereby circumventing the risk of systemic side-effects. Indeed, intra-articular (i.a.) injections are being widely used in the clinics, with the drug of choice usually being hyaluronic acid and/or a corticosteroid (usually triamcinolone). Recent OARSI (Osteoarthritis Research Society International) guidelines for the conservative treatment of knee osteoarthritis indeed suggest that i.a. corticosteroid injections should be considered in some patient groups (with- and without comorbidities, knee-only and multi-joint OA) when biomechanical interventions fail to relieve the pain [21]. The main problem with intra-articular injections in a joint is the rapid efflux of the injected drug from the joint, leading to a limited duration of effect. Indeed, it was shown through a meta-analysis that i.a. corticosteroid injections led to better pain reduction compared to a placebo at 1-2 weeks post-injection, however at 4-24 weeks post-injection there was very little evidence of an effect [23]. This problem of short i.a. residence time could be solved with repeating the injections multiple times, but repeated injections are uncomfortable and moreover, these can be associated with an increased risk of infections and is therefore not suitable for common practice since the risks outweigh the benefits. The use of i.a. corticosteroid injections is therefore usually limited to a maximum of 3-4 per year [24].

### Drug delivery systems

To tackle the problem of rapid efflux, drug delivery systems (DDSs) have been developed in order to extend the intra-articular drug retention times with the aim of making treatment via one single or repeated intra-articular injection with long intervals possible. In 1987, Ratcliffe *et al.* were the first to report delayed clearance of a drug from the joint by using microspheres based on crosslinked albumin as a drug delivery system [25]. Since then, a great number of different carriers for local drug delivery within the joint have been manufactured and tested. The majority of these carriers are based on liposomes, nano- and microparticles based on synthetic or natural polymers

and polymeric hydrogels [26]. Liposomes are spherical particles based on natural lipids which are formed spontaneously in water. Liposomes show good biocompatibility and are versatile delivery systems since both hydrophobic drugs (solubilized in the lipid bilayer) and hydrophilic drugs (soluble in the aqueous compartment) can be easily loaded [27]. The main drawback of liposomes is the short drug release period [28], but also the fact that release is hardly adjustable. The circulation kinetics of liposomes has been extended by PEG-ylation [29], liposomes have been embedded in HA gel to retain them at the site of injection [30] and collagen-liposome conjugates have been prepared, with the purpose of making the DDS site-adherent to cells, thereby increasing their retention time after injection [31]. A number of liposomal formulations have entered the market and are clinically used, for instance Doxil®[27, 32], a chemotherapeutic drug (doxorubicin) encapsulated in liposomes. It should be mentioned that most of the clinically used liposomal formulations are administered by intravenous injection. Formulations that are locally administered are lacking so far.
Nano- and microparticles, polymer-based (mainly PLGA = *poly (lactic-co-glycolic acid*) or natural-based (for instance alginate beads) within the nanometer and micrometer range, are investigated as sustained release formulations of drugs. Especially the polymer-based particles show a more sustained release compared to liposomes, and their lack of immunogenicity, the tunability of the drug release and reproducibility in pharmaceutical preparation make them very interesting [33]. The most commonly used polymer is PLGA (poly (lactic-co-glycolic acid), which is often used in FDA-approved formulations. For example, Lupron is a commercially available PLGA-based microsphere based drug delivery system for sustained release of testosterone after intramuscular administration in patients with advanced prostate cancer [34].

For this thesis, we developed two release platforms which are both expected to show sustained intra-articular release of drugs suitable for osteoarthritis therapy in an adjustable and predictable manner, namely thermoreversible hydrogels and polymeric monospheres.

## Thermoreversible hydrogels

Hydrogels are three-dimensional structures of cross-linked hydrophilic polymer chains [35] Up to now, the use of polymeric hydrogels has been very limited, but it was shown that hydrogels are able to minimize the burst release seen with other drug delivery systems [26]. Thermoreversible hydrogels are based on among others block copolymers of aliphatic polyesters and PEG and are soluble or form a solution at room temperature, but form a gel at body temperature (37°). This leads to ease of injectability. Moreover,

thermoreversible hydrogels showcase high encapsulation efficiency and low burst release [36-38].

## Monospheres

Monospheres are micro- or nanospheres with a narrow size distribution. Up to now, no literature is available about the use of monospheres for intra-articular drug delivery. The use of monospheres holds some potential advantages compared to polydisperse microspheres. First of all, due to the absence of coarse particles, smaller injection needles can be used, which is less traumatic for the patient. Also, monospheres lack the presence of a fraction of very small microspheres which can induce particle-induced immunoactivation [39]. Furthermore, size uniformity leads to a more precise amount of drug per microsphere, in its turn potentially leading to more reproducible between batches and predictable *in vivo* release kinetics [39].

## Celecoxib

For this thesis, the two abovementioned drug delivery systems (hydrogels and monospheres) were investigated on different levels, such as their drug release kinetics and efficacy in the treatment of osteoarthritis. In order to do so, we selected 2 different drugs for the loading of these drug delivery systems. The first one we choose was celecoxib (structure shown in figure 3), because the use of this drug for treatment of osteoarthritis has been investigated extensively. Celecoxib, a commonly used NSAID is not only a well-known painkiller, but also is anti-inflammatory by inhibiting $PGE_2$ release and thereby reducing the production of inflammatory cytokines such as IL-1 and TNF-alpha [40]. These cytokines stimulate the release of collagenase and other MMPs, which are involved in the degradation of collagen [41]. Therefore, celecoxib could potentially act as a disease modifying drug by putting a halt to the vicious circle of chronic inflammation and cartilage degradation, as well as by directly reducing the potential negative effect of $PGE_2$ on cartilage, whereas $PGE_2$ also inhibits the formation of proteoglycans [41]. Celecoxib has been loaded in different drug delivery systems for intra-articular application in different animal models, and some studies have shown promising effects on pain reduction [42] and even positive effects on cartilage, although it must be stated here that Dong *et al.* only found significant differences, when comparing to a saline control group, with their formulation combining celecoxib with Hyonate (hyaluronic acid) and not for celecoxib only [30].

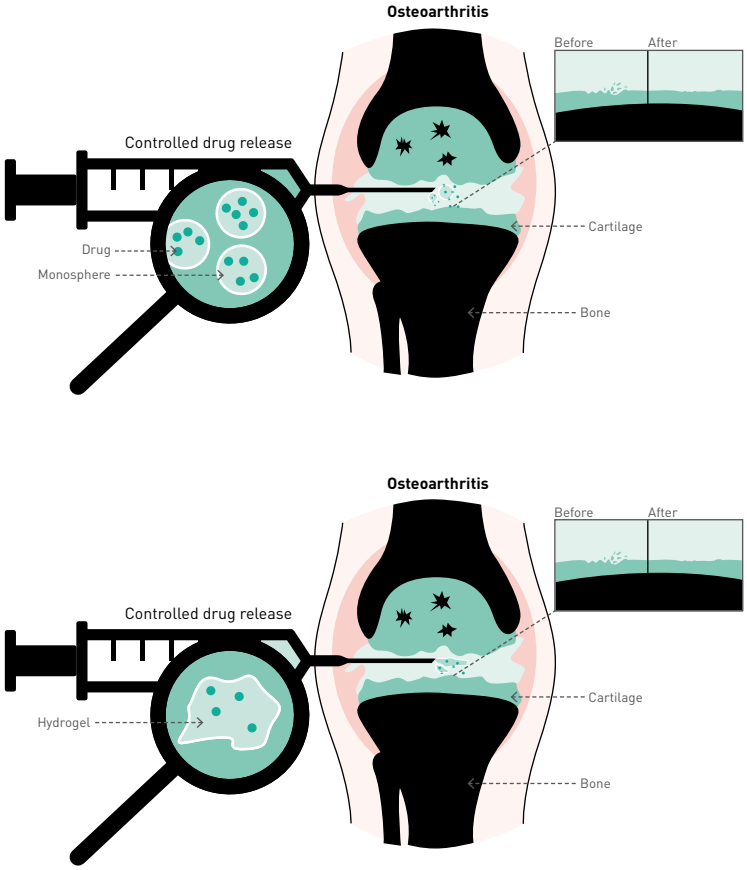


***Figure 2.*** *Illustration of the two drug delivery systems developed for this thesis (monospheres and hydrogels) and their aimed action within the osteoarthritic joint.*

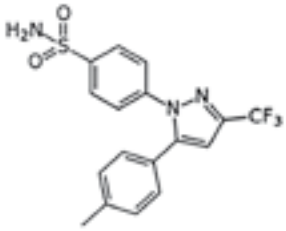


***Figure 3.*** *Chemical structure of celecoxib, an NSAID cox-2 inhibitor, thereby inhibiting* $PGE_2$.

## FK506

As a second compound, we opted a drug that to our knowledge, has not been tested for intra-articular use yet. FK506, also known as tacrolimus (structure shown in figure 4), is an immunosuppressive drug that was discovered in the 1980s by Kino *et al.*[43] and is mainly used in transplantation surgery to prevent graft rejection [44, 45]. Its mechanism of immunosupression is through calcineurin inhibition, which causes T-cell suppresion with very little effect on bone marrow cell differentiation and proliferation [46]. More recently, FK506 has also been proven to be an effective treatment option in DMARD (Disease Modifying Anti- Rheumatic Drug) -resistant or -intolerant patients with active rheumatoid arthritis [47]. Rheumatoid arthritis is a chronic inflammatory joint disease, ultimately leading to joint destruction. In patients with RA, synovial fluid concentrations of catabolic cytokines such as TNF (tumor necrosis factor), IL-1b (interleukin 1) and IL-6 (interleukin 6) have been shown to be elevated [48]. These catabolic cytokines induce their own production as well as the production of MMP's (matrix metalloproteinases) and NO, which are involved in cartilage degeneration [49]. The cartilage degradation products in turn induce the production of catabolic cytokines, and a vicious circle is developed. Although the pathogenesis of osteoarthritis has not been fully unraveled and the stimuli leading to the initial onset may be different, the process of cartilage degeneration involves the same loop of cytokines and MMPs and synovial inflammation is a commonly seen phenomenon [50, 51]. The suppressive effect of FK506, and another but less potent calcineurin inhibitor cyclosporin-A (CsA), on catabolic cytokines has been proven both *in vitro* [46, 52] and *in vivo* [53]. It has also been shown *in vivo* that calcineurin inhibition (by either FK-506 or CsA) leads to less cartilage destruction in mouse models of rheumatoid arthritis [52, 54]. It is therefore likely that this effect is (partially) achieved through the suppression of the catabolic cytokines, and that the same positive effect might be accomplished in osteoarthritis. Furthermore, calcineurin inhibition has been shown to be involved inducing chondrogenic differentiation of clonal mouse embryonic carcinoma cells [55] and improving regeneration of cartilage defects [52]. The underlying mechanism is by increasing the expression of chondrogenic markers through endogenous TGFb1 (transforming growth factor beta) production by chondrocytes [56]. TGFb1 is an anabolic cytokine, that increases proteoglycan synthesis in cartilage, and can be used as a redifferentiation factor for culture-expanded chondrocytes [57]. FK506 may exert a protective or even regenerative effect on cartilage in the development of OA by engaging in these two mechanisms hence slowing the catabolic and boosting the anabolic pathway. There are no data yet on the use and therapeutic effects of intra-articular FK506, let alone slow-released FK506.

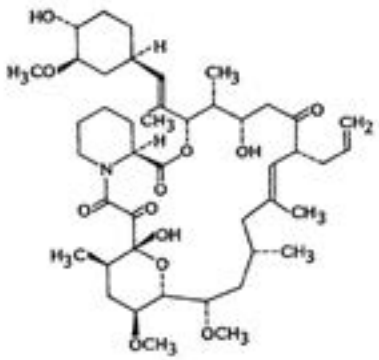

***Figure 4.*** *Chemical structure of FK506 (tacrolimus).*

## Aim and outline of this thesis

The research presented in this thesis was part of the BioMedical Materials project OAcontrol (co-funded by the Dutch Ministry of Economic Affairs, Agriculture and Innovation). The aim of this project was to develop new drug delivery systems for intra-articular use, specifically aiming at the treatment of osteoarthritis. We focused on two different drug delivery systems, celecoxib loaded thermoreversible hydrogels based on acetyl-capped poly(ε-caprolactone-co-lactide)-b-poly(ethylene glycol)-b-poly(ε-caprolactone-co-lactide)(PCLA-PEG-PCLA) triblock copolymers [58], and FK506 loaded monospheres based on poly(DL-lactide)-PEG-poly(DL-lactide)-b-poly(L-lactide) multiblock copolymers.

In **Chapter 2** we studied the *in vitro* and *in vivo* properties and performance of a new acyl-capped PCLA-PEG-PCLA based hydrogel. The intra-articular biocompatibility of this gel was tested in rats. In order to test intra-articular degradation, a blend of polymers either capped with acetyl, or with 2-(2',3',5',-triiodobenzoyl, TIB) moieties was injected in the joints. TIB can be visualize using μCT, enabling longitudinal quantification of the degradation of the gel.

In **Chapter 3,** we investigated the *in vitro* and *in vivo* properties and performance of the acetyl-capped hydrogel, described in Chapter 2, which we loaded with the drug celecoxib. *In vitr*o and *in vivo* drug release kinetics were studied. Also, intra-articular biocompatibility of this celecoxib-loaded gel was studied through both μCT-scanning and histology of injected rat knees.

In **Chapter 4** we aimed to obtain more insight into the pharmacokinetics and the duration of celecoxib release after subcutaneous administration of celecoxib-loaded

PCLA-PEG-PCLA based hydrogels with compositions differing in endcapping, injected volume, drug loading and polymer concentration (5 formulations in total). For a period of 8 weeks blood samples were taken to measure drug concentrations. From these results, we could also obtain insight into the *in vitro-in vivo* correlation in order to create a gel for which we could predict *in vivo* pharmacokinetics and release duration based on the *in vitro* release kinetics.

**Chapter 5** describes the efficacy of the celecoxib-loaded gel that was tested in Chapter 3 when injected in rat knees in which osteoarthritis was induced. Outcome measurements were not only structural (μCT-scanning and histology), but we also looked at pain management in rats by measuring hind limb weight distribution over the course of the whole experiment.

In **Chapter 6**, we developed and investigated monospheres, prepared by a micro-sieve membrane emulsification process, composed of biodegradable poly(DL-lactide)-PEG-poly(DL-lactide)-b-poly(L-lactide) multiblock copolymers, which would potentially be suitable for local sustained drug release in articular joints. Monospheres with different sizes (5, 15 and 30 μm) were tested both *in vitro* and *in vivo*. *In vivo* imaging of the monospheres after loading with a fluorescent dye was performed in order to measure their retention within the injected joints. Biocompatibility was tested in a small (rats) and a large animal model (horses), where we looked at both structural changes in terms of cartilage quality and quantity as well as inflammatory responses within the synovial cavity.

In **Chapter 7** we describe the mechanical properties of our multiblock copolymer monospheres. This is important because the release profile of the monospheres may be influenced by the applied mechanical forces. Furthermore, the mechanical properties are important for the injected joint because the monospheres could potentially harm the cartilage surface when these particles monospheres are too stiff, leading to cartilage indentations and subsequent damage. Three different sizes of monodisperse microspheres (5, 15, and 30μm) were tested in both dry and hydrated states and the Young's moduli were measured.

**Chapter 8** focusses on tacrolimus loaded monodisperse biodegradable monospheres (30 μm) based on poly(DL-lactide-PEG)-*b*-poly(L-lactide). Intra-articular biocompatibility was again tested in rats using μCT-scanning and histology after injection of different doses of tacrolimus (10 weight%) loaded monospheres (2.5, 5.0 and 10 mg) in the knee joint. Drug release kinetics were examined after intra-articular injection in horse joints. Both synovial fluid and blood samples were taken, to get insight into duration of the local release of the monospheres, but also to investigate whether the systemic

concentrations remain below levels where adverse effects can be expected. Furthermore, inflammatory markers were measured within the synovial fluid of horses injected with unloaded as well as monospheres loaded with FK506 in order to test the local anti-inflammatory actions of these loaded monospheres.

In **Chapter 9** and **10**, we discuss and summarize the findings of this thesis and provide future perspectives.


2

# Chapter 2

## In situ forming acyl-capped PCLA-PEG-PCLA triblock copolymer based hydrogels

Sandker MJ, Petit A, Redout EM, Siebelt M, Müller B, Bruin P, Meyboom R, Vermonden T, Hennink WE, Weinans H.

*Biomaterials. 2013 Oct;34(32):8002-11*

## Abstract

Sustained intra-articular drug delivery opens up new opportunities for targeted treatment of osteoarthritis. In this study, we investigated the *in vitro* and *in vivo* properties and performance of a newly developed hydrogel based on acyl-capped PCLA-PEG-PCLA specifically designed for intra-articular use. The hydrogel formulation consisted of a blend of polymers either capped with acetyl, or with 2-(2',3',5',-triiodobenzoyl, TIB) moieties. TIB was added to visualize the gel using μCT, enabling longitudinal quantification of its degradation. Blends containing TIB-capped polymer degraded in vitro (37 °C; pH 7.4 buffer) through dissolution over a period of ~20 weeks, and degraded slightly faster (~12 weeks) after subcutaneous injection in rats. This *in vivo* acceleration was likely due to active (enzymatic) degradation, shown by changes in polymer composition and molecular weight as well as the presence of macrophages. After intra-articular administration in rats, the visualized gel gradually lost signal intensity over the course of 4 weeks. Good cytocompatibility of acetyl-capped polymer based hydrogel was proven in vitro on erythrocytes and chondrocytes. Moreover, intra-articular biocompatibility was demonstrated using μCT-imaging and histology, since both techniques showed no changes in cartilage quality and/or quantity.

## 1. Introduction

Osteoarthritis (OA) is a common joint disease that affects approximately 30% of the elderly population [59]. Current treatment is mainly based on pain prevention through orally administered drugs, as often non-steroidal anti-inflammatory drugs [60], since disease modifying drugs (DMOADs) are not (yet) available. The development and application of DMOADs are hindered by the fact that it is difficult to obtain sufficient intra-articular (i.a.) concentrations, while high systemic exposure of some putative drugs leads to unwanted side-effects [60, 61]. The best local therapies for OA so far are i.a. injections (of hyaluronan or corticoid steroids), thereby circumventing the problem of sub-therapeutic local drug concentrations. However, i.a. injections also provide limited effects, due to the rapid i.a. drug turnover leading to a fast decline of the local drug concentrations to therapeutically inactive levels. For example, i.a. administration of Kenalog® (triamcinolone acetonide suspension) allows for local delivery [62], but only for a limited period of ~1 week [62-64]. Therefore, often multiple i.a. injections are given [65], leading to the risk of cartilage and joint damage and/or infections [60, 63, 65, 66]. Ideally, a single i.a. injection of a local drug delivery system (DDS) for OA would provide sustained drug concentrations in a joint in a controlled way for at least one month. Suitable drug delivery systems are easy to inject, show high encapsulation efficiency with low burst release, tunable release kinetics, and full recovery of the loaded drug. Ideal systems release a drug of interest for weeks while maintaining a therapeutically effective concentration at the target site. DDSs developed for i.a. use have, up to now, been mainly based on liposomes or polymeric nano/microparticles [67, 68]. Liposomes for local intra-articular treatment (and other non-vascular routes) usually show a short drug release duration which is hardly adjustable [28], although biological stability of liposomes can be improved by surface PEGylation [69, 70]. On the other hand, microparticle-based systems show a more controllable and sustained release [28, 71]. The main drawback of both liposome- and microparticle-based systems is their costly and non-straightforward manufacturing mainly because up scaling is challenging [28, 72, 73]. Alternatively, an *in situ* forming depot containing highly concentrated solutions (400 mg/ml) of the hydrophobic drug celecoxib in poly(ethylene glycol) 400 ($PEG_{400}$) has recently been developed [74]. Upon i.a. injection $PEG_{400}$ is diluted and celecoxib precipitates/crystallizes, allowing a sustained release by slow dissolution (~10 days). This shows the potential i.a. use of *in situ* forming depots, but modulating release rates and durations using this system are not possible [75]. Temperature-responsive gelling systems (composed of ABA triblock copolymers with a PEG middle block flanked by polyester blocks of divers compositions, dispersed in aqueous medium) do meet desirable DDS properties including high encapsulation efficiency, low burst and good drug recovery. They can be injected as a solution and transform into a gel after injection [36-38, 76, 77]. Moreover, terminal hydroxyl-end group modification of the

polyester–PEG–polyester triblock copolymers enables further modulation of rheological and degradation/dissolution properties of aqueous and temperature-responsive gelling systems [78, 79]. Indeed, we previously showed that the rheological properties of aqueous systems containing acyl-capped poly(ε-caprolactone-*co*-lactide)-*b*-poly(ethylene glycol)-*b*-poly(ε-caprolactone-*co*-lactide) (PCLA–PEG–PCLA) are easy to modulate [80].
Getting more insight into the *in vivo* behavior of DDSs is a crucial step towards clinical applications for treatment in a joint. In that respect, it is pivotal to determine whether a DDS forms a depot that is retained at the injection site and to investigate its degradation kinetics. Fluorescent particles [81, 82] and dye-loaded microparticles [81] are examples of visible DDSs used previously. For both systems, the initial distribution of the particles after administration can be visualized, however due to diffusion and release of the dyes from the DDSs, biodegradation kinetics cannot be investigated. To circumvent this problem, dyes have been covalently bound to polymeric particles [83]. This method facilitates visualization, but only through *ex vivo* sectioning, hence lacking longitudinal follow-up possibilities of particle quantification and spatiotemporal distribution. Non-invasive *in vivo* imaging of DDSs can be achieved by, for instance, computed tomography (CT) using iodine containing moieties that confer a degree of X-ray opacity [84, 85]. Indeed, others have shown that different systems, for instance polymethacrylate-based microparticles [86, 87] and hydrogels, containing covalently bound 2-(2′,3′,5′,-triiodobenzoyl) moieties (TIB) are suitable for *in vivo* visualization.
In the current study, we investigated the potential of biodegradable, temperature-responsive gelling systems made of an aqueous acyl-capped PCLA–PEG–PCLA triblock copolymer dispersion for *in vivo* use, and in particular i.a. application. Primarily, we assessed the real-time degradation kinetics of the gel both *in vitro* and *in vivo* (subcutaneous and i.a.) in a non-invasive manner. For this, we modified the hydroxyl end groups of PCLA–PEG–PCLA with 2-(2′,3′,5′,-triiodobenzoyl) moieties (TIB) to obtain radiopaque gels suitable for long-term *in vivo* visualization using μCT. Secondly, the cytocompatibility and i.a. biocompatibility of the gels were tested.

## 2. Methods and materials

### 2.1. Materials

L-Lactide was obtained from Purac Biochem BV, The Netherlands. Hexabrix 320®, a clinical iodine-based contrast agent, was obtained from Guerget, The Netherlands. All other chemicals were obtained from Aldrich and used as received.

### 2.2. Synthesis of TIB chloride

2-(2′,3′,5′,-Triiodobenzoyl) (TIB) chloride was synthesized as described previously [88]. Briefly, 2,3,5-triiodobenzoic acid (10.5 g; 21 mmol) was dissolved in dichloromethane (100 ml), followed by the addition of a catalytic amount of dimethylformamide (10 mg, 0.14 mmol). An excess of oxalyl chloride (10 ml; 79 mmol, –COCl/COOH = ~8 mol/mol) was added drop wise and the mixture was stirred for two days at room temperature. Volatiles were evaporated under reduced pressure and the remainder was stripped with toluene three times to yield 9.3 g (85%) of TIB chloride. Characterization of TIB chloride dissolved in $CDCl_3$ was done with $^1H$ NMR using a Varian Oxford, operating at 300 MHz. $^1H$ NMR spectra were referenced to the signal of chloroform at 7.26 ppm.

### 2.3. Synthesis of acetyl-capped ($PCLA_{2\times1700}CL_{2.5}$Acet) and TIB-capped PCLA–PEG–PCLA ($PCLA_{2\times1700}CL_{2.5}$TIB and $PCLA_{2\times750}CL_{5.7}$TIB) polymers

The acetyl-capped and TIB-capped PCLA–PEG–PCLA triblock copolymers ($PCLA_{2\times1700}CL_{2.5}$Acet and $PCLA_{2\times1700}CL_{2.5}$TIB, respectively) used in this study were essentially synthesized and characterized as described previously [80]. In short, l-lactide and ε-caprolactone dissolved in toluene were polymerized with $PEG_{1500}$-diol as a macroinitiator in the presence of tin(II) 2-ethylhexanoate as a catalyst. The exact amounts used in the synthesis are summarized in Table 1. For $PCLA_{2\times1700}CL_{2.5}$ and $PCLA_{2\times750}CL_{5.7,}$a caproyl/lactoyl (CL/LA) molar ratio of 2.5/1 and 5.7/1 mol/mol, respectively were used. Subsequently, acylation of the hydroxyl end-groups using an excess of acetyl chloride or TIB chloride (ratio chloride/OH groups = 4 mol/mol) resulted in the formation of acetyl-capped and TIB-capped PCLA–PEG–PCLA respectively, with a yield of ~85%.TIB-end group: 8.40–7.60 ppm ($I_{8.0}$, m, 2H, Ar H) [89-91]. Acetyl-end group: 2.14–2.12 ppm ($I_{2.13}$, $CH_3$–CO–O–$CH(CH_3)$–); 2.03–2.05 ppm ($I_{2.04}$, $CH_3$–CO–O–$(CH_2)_5$–)[79, 92-95] and 2.10–2.08 ppm ($I_{2.09}$, $CH_3$–CO–O–$C(H_2)_2$–O–) as shown in figure. S1.

The composition of acyl-capped PCLA–PEG–PCLA was established from integral of signals belonging to methine protons of LA subdivided in four quadruplets ($I_{5.1}$), methylene protons of PEG ($I_{3.6}$ at 3.72–3.55 ppm), methylene protons of CL subdivided in two triplets ($I_{2.4}$ + $I_{2.3}$). The degree of modification was calculated from the ratio between protons of the end groups and methylene protons of PEG ($I_{3.6}$ at

3.72–3.55 ppm). TIB-end group ($I_{8.0}$) at 8.40–7.60 ppm ($I_{8.0}$, m, 2H, Ar H) [78, 89-91] as previously described [78].

***Table 1**. Characteristics of acetyl-capped and TIB-capped PCLA-PEG-PCLA triblock copolymers.*

| **Polymer** | **Acetyl-capped $PCLA_{1700}$-$PEG_{1500}$- $PCLA_{1700}$** | **TIB-capped $PCLA_{1700}$-$PEG_{1500}$- $PCLA_{1700}$** | **TIB-capped $PCLA_{750}$-$PEG_{1500}$- $PCLA_{750}$** |
|---|---|---|---|
| Abbreviation | $PCLA_{2x1700}Cl_{2.5}$Acet | $PCLA_{2x1700}Cl_{2.5}$TIB | $PCLA_{2x750}Cl_{5.7}$Acet |
| PEG feed [g] | 50 | 50 | 50 |
| ε-Caprolactone feed [g] | 88 | 88 | 45 |
| Lactide feed [g] | 10 | 10 | 5 |
| Acetyl chloride feed [g] | 10 | 0 | 0 |
| TIB chloride feed [g] | 0 | 9.3 | 9.3 |
| Aimed $M_{n,PCLA}$ [g $mol^1$] | 4900 | 4900 | 3200 |
| PCLA/PEG[a] | 2.1/1 | 2.1/1 | 1.1/1 |
| CL/LA [mol/mol][b] | 4.9/1 | 5.7/1 | 4.4/1 |
| DM [%][c] | 93 | 90 | 90 |
| Mn[d] [g $mol^1$] | 4700 | 3100 | 3400 |
| PDI[e] | 1.4 | 1.2 | 1.3 |

*a Weight ratio of PCLA to PEG determined by $^1$H NMR.*
*b Weight ratio of ε-caprolactone to L-lactide determined by $^1$H NMR.*
*c Degree of modification represents the number of end groups per triblock copolymer determined by $^1$H NMR.*
*d Mn determined by GPC.*
*e Polydispersity index determined by GPC.*

## 2.4. Characterization of $PCLA_{2\times1700}CL_{2.5}$Acet, $PCLA_{2\times1700}CL_{2.5}$TIB and $PCLA_{2\times750}CL_{5.7}$TIB

Molecular weights ($M_n$ and $M_w$) of the synthesized polymers were determined by GPC as described previously [78]. The characteristics of $PCLA_{2\times1700}CL_{2.5}$Acet, $PCLA_{2\times1700}CL_{2.5}$TIB and $PCLA_{2\times750}CL_{5.7}$TIB are given in Table 1.

## 2.5. Preparation of $PCLA_{2\times1700}$CL2.5Acet/$PCLA_{2\times750}CL_{5.7}$TIB and $PCLA_{2\times1700}$CL2.5Acet/$PCLA_{2\times1700}CL_{2.5}$TIB blends

$PCLA_{2\times1700}CL_{2.5}$Acet and $PCLA_{2\times1700}CL_{2.5}$TIB or $PCLA_{2\times750}CL_{5.7}$TIB were separately dissolved in 15 ml ethyl acetate at a concentration of 500 mg/ml. The solutions were mixed to achieve specific ratios and the obtained mixtures were transferred to 11 cm

petri dishes. The solvent was removed under nitrogen flow for 48 h (gas chromatography analysis indicated a residual ethyl acetate content < 0.5%).

## 2.6. Preparation of the aqueous dispersions

21 ml PBS buffer (44 mm $Na_2HPO_4$; 9 mm $NaH_2PO_4$; 72 mm NaCl; pH 7.4) was added to 7 g $PCLA_{2\times1700}CL_{2.5}$Acet, $PCLA_{2\times1700}CL_{2.5}$Acet/$PCLA_{2\times1700}CL_{2.5}$TIB or $PCLA_{2\times1700}CL_{2.5}$Acet/$PCLA_{2\times750}CL_{5.7}$TIB blend in 50 ml centrifuge tubes to yield systems with 25 wt% solid content. Samples were heated for 15 min at 50 °C and vortexed thoroughly. Next, the samples were stored at 4 °C for 48 h to allow formation of homogeneous systems.

## 2.7. Rheological characterization

Oscillatory stress was applied to the $PCLA_{2\times1700}CL_{2.5}$Acet/$PCLA_{2\times750}CL_{5.7}$TIB system (25 wt% in buffer) from 10 to 400 Pa with 10 points per decade using a TA AR-G2 rheometer equipped with a Peltier plate (1° steel cone, 20 mm diameter with solvent trap). The run duration was 2 min and the time between runs was <30 s. Rheological analysis of 70 µl samples of $PCLA_{2\times1700}CL_{2.5}$Acet/$PCLA_{2\times750}CL_{5.7}$TIB systems (25 wt% in a 280 mOsm/L buffer) was done by dynamic mechanical analyzer (DMA, TA Instruments). A static force sweep of 5 N/min, starting at 0.1 N, was applied on a sample-loaded syringe (2 ml).

## 2.8. *In vitro* degradation behavior

$PCLA_{2\times1700}CL_{2.5}$Acet/$PCLA_{2\times750}CL_{5.7}$TIB (25/75 *w*/*w*) systems of 25 wt% solid content were used to study degradation properties of gels under physiological conditions (37 °C, pH 7.4). Samples (300 µl) cooled to 4 °C were transferred via a syringe into glass vials (8.2 × 40 mm). The closed vials were placed at 37 °C to induce a sol-to-gel transition. After 30 min, 700 µl phosphate buffer was added. At different time points, the buffer was removed, the weight of residual gels was measured, and fresh buffer was added. In addition, samples were freeze-dried for further analysis (dry weight and analysis by GPC and $^1$H NMR).

## 2.9. *In vitro* cytocompatibility of $PCLA_{2\times1700}CL_{2.5}$Acet

Cytocompatibility tests of the $PCLA_{2\times1700}CL_{2.5}$Acet gel (25% in PBS) were performed on primary equine chondrocytes. Full thickness cartilage was harvested from metacarpophalangeal joints from four horses and digested in 0.15% collagenase type II in DMEM (10% FBS, 100 U/ml penicillin, 100 U/ml streptomycin,

25 mm Hepes) overnight. Then, the digest was filtered through a 100 µm cell strainer, and centrifuged (10 min; 1500 rpm; 4 °C). The supernatant was aspirated and the pellet resuspended in PBS and centrifuged (10 min; 1500 rpm; 4 °C); this step was repeated twice. Subsequently, PBS was aspirated and cells were resuspended in DMEM/F12 supplemented with 5% FBS, 100 U/ml penicillin, 100 U/ml streptomycin, 0.5% Fungizone, 0.085 mm vitamine C, 1% glutamax and cultured (37 °C; 5% $CO_2$). Cytocompatibility of the gel was assessed by AlamarBlue (Invitrogen) assay. Cells were seeded in 96-well plates at $10^4$ cells per well in 100 µl DMEM/F12 containing aforementioned supplements and incubated (37 °C; 5% $CO_2$) for 24 h. Then 100 µl of $PCLA_{2\times1700}CL_{2.5}$Acet, Pluronic® F-127 (a non-ionic copolymer frequently used for cell culture; positive control) or SDS (sodium dodecyl sulfate; negative control) were dissolved in DMEM/F12 (1% ITS, 100 U/ml penicillin, 100 U/ml streptomycin, 0.5% Fungizone, 0.085 mm vitamine C, 1% glutamax and 5 mg/ml BSA) at concentrations ranging from 0.001 to 2.0 mg/ml. After 24 h incubation, DMEM/F12 was replaced by 100 µl fresh medium containing AlamarBlue (1:10) followed by 24 h incubation at 37 °C and the absorbance was measured at 570 nm. Cytocompatibility is expressed as relative viability; cells cultured in blank DMEM/F12 medium served as a control which was set at 100%.

Hemolytic activity of $PCLA_{2\times1700}CL_{2.5}$Acet and its dissolving buffer (44 mm $Na_2HPO_4$; 9 mm$NaH_2PO_4$; 72 mm NaCl) was measured. PBS solution containing 1% Triton X-100 was used as a positive, and PBS as a negative control. Equine erythrocytes were isolated from fresh citrate treated blood, washed with PBS by four centrifugation cycles (10 min; 1000 rpm; 4 °C). The erythrocyte pellet was diluted 10-fold in 150 mm NaCl. Next, 50 µl of 25 wt% polymer or buffer were added to a 450 µl erythrocyte suspension, and incubated at 4 or 37 °C for 1 h under constant shaking. Eppendorfs were centrifuged (5 min; 2000 rpm) and 60 µl supernatant was transferred into a flat bottom 96-well plate. Hemoglobin content was obtained by measuring absorbance at 540 nm.

## 2.10. *In vivo* experiments

Sixteen 16-week-old (400–450 g) male Wistar rats (Charles River Nederlands BV, Maastricht, the Netherlands) were housed in the animal facility of the Erasmus Medical Center, with a 12-h light–dark regimen, at 21 °C. Animals were fed with standard food pellets and water *ad libitum*. The Animal Ethic committee of the Erasmus Medical Center, Rotterdam, the Netherlands, approved all conducted procedures.

*In vivo* retention and degradation of $PCLA_{2\times1700}CL_{2.5}$Acet/$PCLA_{2\times750}CL_{5.7}$TIB (25/75) blends (25 wt%, in buffer) was assessed in a first group of six rats. Four rats received a subcutaneous injection of 100 µl $PCLA_{2\times1700}CL_{2.5}$Acet/$PCLA_{2\times750}CL_{5.7}$TIB (25 wt% solid content) each; the other two rats received an injection of 50 µl in the knee joint. The gels were scanned regularly to visualize degradation longitudinally. All rats received

two additional s.c. injections of 100 µl $PCLA_{2\times1700}CL_{2.5}$Acet/$PCLA_{2\times750}CL_{5.7}$TIB which were excised at predetermined time points, dried and analyzed by GPC and $^1$H NMR. In a second group of rats ($n$ = 10), *in vivo* biocompatibility was assessed. Each rat received an injection at $t$ = 0 of 50 µl aqueous dispersion of $PCLA_{2\times1700}CL_{2.5}$Acet (25 wt% solid content) in the left knee and 50 µl of saline in the right knee (control). Of both knees µCT scans were acquired before gel injection and at 6 and 12 weeks, to visualize potential cartilage degeneration (using a contrast agent). Simultaneously, each rat received a 500 µl 25% $PCLA_{2\times1700}CL_{2.5}$Acet subcutaneous injection (tibia region) in order to follow *in vivo* gelling properties and degradation kinetics. The total s.c. gel volume was measured at set time points using a skin fold meter.

## 2.11. µCT-imaging

*In vitro*: Vials containing $PCLA_{2\times1700}CL_{2.5}$Acet/$PCLA_{2\times750}CL_{5.7}$TIB or $PCLA_{2\times1700}CL_{2.5}$Acet/$PCLA_{2\times1700}CL_{2.5}$TIB were scanned at different time points during *in vitro* degradation. Scans were performed using the following scanner settings: isotropic voxelsize of 35 µm; 55 kV; 170 mA; 35 mm field of view; 0.5 mm Al filter; 0.8 rotation step over 198°; frame averaging of 3.

Group 1: Scans were performed $t$ = 0, 1 day, 4 days, 1 week and thereafter on a weekly base until the $PCLA_{2\times1700}CL_{2.5}$Acet/$PCLA_{2\times750}CL_{5.7}$TIB blend was no longer visible. The following scan settings were used; isotropic voxelsize of 35 µm; 55 kV; 170 mA; field of view 35 mm; a 0.5 mm Al filter; 0.8 rotation step over 198° with a frame averaging of 3.

Group 2: cartilage quality (sulfated glycosaminoglycan (sGAG) content) and quantity (thickness) was measured with *in vivo* µCT arthrography. Therefore, knees were injected with a radiographic contrast (Hexabrix mixed with 10 µg/ml Epinephrine) as described previously [96, 97]. Influx of Hexabrix into the cartilage correlates inversely with sGAG content [98, 99] to detect early changes in cartilage quality using *in vivo* µCT arthrography [96, 97]. After injecting Hexabrix, rats were placed in a custom made scanner bed fixing the hind limb in extended position. Scans were performed using the following scanner settings: isotropic voxelsize of 35 µm; 55 kV; 170 mA; 35 mm field of view; 0.5 mm Al filter; 0.8 rotation step over 198°; frame averaging of 2.

## 2.12. µCT data analysis

Raw µCT images were converted into 3D reconstructions using the reconstruction software nRecon version 1.5 (SkyScan). With 3D Calc software segmentation into binary images [100] took place creating a mask overlaying bone and Hexabrix in the original gray value images of the first group (ImageJ; NIH, http://imagej.nih.gov.eur.idm.oclc.org/ij/index.html) [96]. Subsequently, regions of interest (ROI's) were drawn around the patellar cartilage (40 slices) for which attenuation and thickness were calculated.

In the datasets of the second group (gel degradation) as well as the *in vitro* degradation images, ROI›s were drawn directly around the visible gels in the reconstructed images. Subsequently, segmentation took place between gel and surrounding tissue and attenuation and volume of the gels were calculated.

## 2.13. Histology

Following the last scan, the rats of the first group ($n$ = 10) were killed and the knee joints were fixed with formalin, decalcified and embedded in paraffin. Next, 6 µm sections were prepared sagitally at 300 µm intervals and stained with Safranin-O. Patellar, tibial (lateral/medial) and trochlear cartilage were scored using a modified Mankin scoring system (0, normal cartilage; 1, slight reduction; 2, moderate reduction; 3, severe reduction; 4, no dye noted) [101] for GAG-staining and a modified Pritzker score for structure composition (0, surface intact; 1, surface discontinuity; 2, vertical fissures; 3, erosion; 4, denudation; 5, deformation) [102]. Both scores were multiplied by number representing the affected area (1 < 10%; 2 = 10–25%; 3 = 25–40%; 4 > 40%). Final score is expressed as a percentage of the maximal score (GAG-depletion: 16; structural score: 20). Then the average of all regions per knee was calculated, resulting in total knee joint scores ranging from 0% (not affected) to 100% (severe OA in >40% of the joint). At the same time, also the site of the $PCLA_{2\times1700}CL_{2.5}$Acet depot including the surrounding tissue was resected *en-bloc*, fixed in 4% paraformaldehyde (48 h at 4 °C), embedded in paraffin and sectioned at 6 µm. These sections were dewaxed and pre-treated with heat mediated antigen retrieval (Dako S1699, Glostrup, Denmark) at 90 °C for 20 min. Subsequently, sections were incubated with CD68 (1:100, Acris, Herford, Germany) for 60 min and visualized with PO link and label kit (Biogenex, Fremont, CA, USA), followed by a DAB (3,3′-diaminobenzidine) substrate. Sections were dried overnight and mounted with Vectamount (Vector laboratories, Burlingame, CA, USA).

## 2.14. Statistical analysis

Differences in µCT-data and histological scoring between the gel-injected and saline-injected knees were analyzed using type-1, two-tailed, paired *T*-tests. *In vitro* biocompatibility data were analyzed using one-way ANOVA with Bonferroni correction for multiple testing. All data are presented as mean ± SD, $p$-values <0.05 were considered significant.

## 3. Results and discussion

### 3.1. Synthesis and characterization of $PCLA_{2\times1700}CL2.5Acet$/ $PCLA_{2\times1700}CL_{2.5}TIB$

($PCLA_{2\times1700}CL_{2.5}TIB$) and TIB–$PCLA_{750}$–$PEG_{1500}$–$PCLA_{750}$–TIB ($PCLA_{2\times750}CL_{5.7}TIB$)$^1$H NMR analysis showed the presence of characteristic peaks of $PCLA_{2\times750}CL_{5.7}TIB$ for methine protons of LA, methylene protons of PEG and methylene protons of CL at 5.25–4.95, 3.65–3.55 and 2.50–2.10 respectively (Supplementary data: figure S1) [78-80]. A CL content of 87 wt% CL (CL/LA = 2.1 mol/mol) was found by $^1$H NMR which is slightly lower than the feed (90 wt%), a finding in accordance with previous data. The extent of acylation (calculated by comparison of the integral of the aromatic peaks of TIB groups to the methylene peak of PEG) was 1.8, indicating ~90% TIB capping. The $M_n$ of $PCLA_{2\times750}CL_{5.7}TIB$ and $PCLA_{2\times1700}CL_{2.5}TIB$ (determined by $^1$H NMR) was respectively 3400 g/mol and 3100 g/mol the $M_n$ determined by GPC relative to PEG standards showed equal values (Table 1).

### 3.2. Selecting a blend suitable for longitudinal in vivo gel visualization

$PCLA_{2\times1700}CL_{2.5}TIB$ was synthesized, but appeared to be too hydrophobic and consequently did not form a homogeneous suspension in buffer. In order to obtain homogeneity, it was mixed with $PCLA_{2\times1700}CL_{2.5}Acet$ at different $PCLA_{2\times1700}CL_{2.5}Acet$/ $PCLA_{2\times1700}CL_{2.5}TIB$ ratios (25/75 *w*/*w*, 50/50 *w*/*w* and 75/25 *w*/*w*; all 25 wt% solid content). μCT scanning (Table 2) revealed that of these three different blends, only the 75/25 $PCLA_{2\times1700}CL_{2.5}Acet$/$PCLA_{2\times1700}CL_{2.5}TIB$ blend formed a homogeneous suspension. The acetyl-/TIB-capped polymer ratio slightly influenced attenuation (higher TIB-ratios equaled a higher attenuation). Based on the minor differences in attenuation combined with the formation of a heterogeneous blend, the 25/75 $PCLA_{2\times1700}CL_{2.5}Acet$/ $PCLA_{2\times1700}CL_{2.5}TIB$ blend was injected i.a. However, the μCT scan revealed that radiopacity of this blend was too low for longitudinal *in vivo* visualization. In order to be able to inject a homogeneous blend and follow this over time, a blend with a higher wt% of TIB was used which was obtained by TIB capping of a triblock copolymer with the same PEG molecular weight but with a shorter PCLA chains ($PCLA_{2\times750}CL_{5.7}TIB$). This polymer was blended with $PCLA_{2\times1700}CL_{2.5}Acet$ and all $PCLA_{2\times1700}CL_{2.5}Acet$/ $PCLA_{2\times750}CL_{5.7}TIB$ blends (25/75, 50/50, 75/25) were homogenous. Importantly, the attenuation greatly increased as compared to the blends containing $PCLA_{2\times1700}CL_{2.5}TIB$. Based on the good attenuation and heterogeneity, the blend containing the highest TIB content (75%) was injected intra-articular and was indeed well visible. This blend is therefore suitable for longitudinal μCT visualization and all following experiments were consequently performed using this blend.

***Table 2.*** *μCT analysis of in vitro scanned blends with different polymer compositions ($PCLA_{2\times1700}CL_{2.5}TIB$ vs $PCLA_{2\times750}CL_{5.7}TIB$) and acetyl-/TIB-capped ratios.*

| Polymer blend (Acetyl-/TIB-capped ratio) | $PCLA_{2\times1700}CL_{2.5}Acet/PCLA_{2\times1700}CL_{2.5}TIB$ (75/25) | $PCLA_{2\times1700}CL_{2.5}Acet/PCLA_{2\times1700}CL_{2.5}TIB$ (50/50) | $PCLA_{2\times1700}CL_{2.5}Acet/PCLA_{2\times1700}CL_{2.5}TIB$ (25/75) | $PCLA_{2\times1700}CL_{2.5}Acet/PCLA_{2\times750}CL_{5.7}TIB$ (75/25) | $PCLA_{2\times1700}CL_{2.5}Acet/PCLA_{2\times750}CL_{5.7}TIB$ (50/50) | $PCLA_{2\times1700}CL_{2.5}Acet/PCLA_{2\times750}CL_{5.7}TIB$ (25/75) |
|---|---|---|---|---|---|---|
| Attenuation (a.u.) | 25.0 | 30.4 | 35.8 | 39.3 | 58.3 | 60.5 |
| homogeneity[a] | + | +/- | - | + | + | + |
| Intra-articular visibility[b] | n.t. | n.t. | too low | n.t. | n.t. | good |

*a.u.: arbitrary unit.*
[a] *- : Heterogeneous; +/-: slight heterogeneous areas; +: homogenous.*
[b] *n.t.: not tested.*

## 3.3. Rheological properties of $PCLA_{2\times1700}CL_{2.5}Acet/PCLA_{2\times750}CL_{5.7}TIB$ (25/75) blend

The $PCLA_{2\times1700}CL_{2.5}Acet/PCLA_{2\times750}CL_{5.7}TIB$ (25/75) blend at 25 wt% in buffer was a gel at temperatures below 10–15 °C and rapidly phase-separated at higher temperatures (as seen on the μCT images). This behavior is different from the behavior of only $PCLA_{2\times1700}CL_{2.5}Acet$ at 25 wt% in buffer and is likely due to the hydrophobicity of the TIB moieties as also observed for hexanoyl-capped PCLA–PEG–PCLA [80]. However, the cold $PCLA_{2\times1700}CL_{2.5}Acet/PCLA_{2\times750}CL_{5.7}TIB$ gel could be manually injected through a 27 G needle (normally used for i.a. injection into a rat knee) and DMA analysis confirmed that a force of 5.8 N was required to expel the gel from the syringe, which is slightly higher than the force required to expel air or $PCLA_{2\times1700}CL_{2.5}Acet$ dispersion (~4 °C) from the syringe (1.5 and 1.8 N, respectively).

To get more insight into the rheological properties of $PCLA_{2\times1700}CL_{2.5}Acet/PCLA_{2\times750}CL_{5.7}TIB$ (25 wt% in buffer), oscillatory stress experiments were performed (figure 1). At ~4 °C, the gel had a storage modulus ($G'$) of 350 Pa and a tan $\delta$($G''/G'$) of 0.6 at an oscillatory stress below 200 Pa. However, at an oscillatory stress of around 250 Pa the gel started to loosen and its $G'$ decreased to <30 Pa with an increase in tan $\delta$ to 5. After releasing and subsequently applying the same oscillatory stress, the exact same $G'$ and tan $\delta$ patterns were found during subsequent stress applications. These findings indicate thixotropic behavior of the gel and explain its injectability through a thin 27 G needle. Thixotropic behavior of aqueous PEG/polyester temperature-responsive systems has not been reported yet, but is very similar to what was reported for thixotropic systems based on charged hydrogel microspheres [103]. In the sol state,

the polyester–PEG copolymer forms micelles with a hydrophobic polyester core and a hydrated PEG shell [38, 79, 92]. The flow in thixotropic systems is likely due to weakening/loosing interactions that exist between the particles.

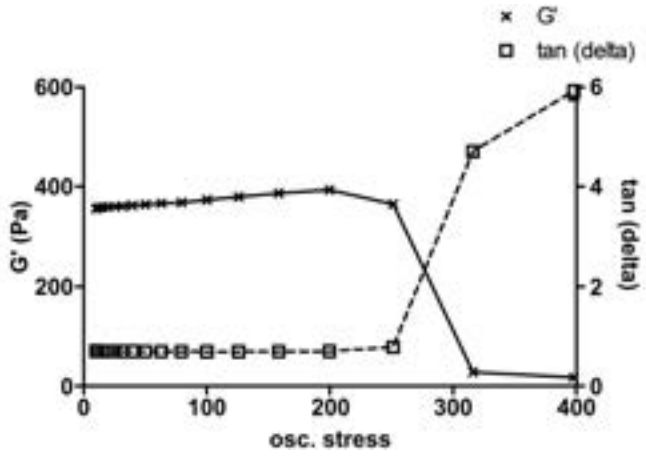


***Figure 1.*** *Stress sweeps of 25 wt% sample containing* $PCLA_{2\times1700}CL_{2.2}Acet/PCLA_{2\times750}CL_{5.7}TIB$ *(25/75) at 4 °C. Three consecutive measurements (<30 s between measurements) were performed at 1 Hz.*

## 3.4. *In vitro* degradation behavior of 25 wt% $PCLA_{2\times1700}CL_{2.5}Acet/PCLA_{2\times750}CL_{5.7}TIB$ (25/75) blend

Upon incubation of $PCLA_{2\times1700}CL_{2.5}Acet/PCLA_{2\times750}CL_{5.7}TIB$ blend of 25 wt% in PBS buffer (pH 7.4; 37 °C), a ~20 wt% decrease in wet weight was observed during the first 2 h which was not accompanied by loss in dry weight. Most likely, phase-separation of the gel into a polymer-rich and polymer poor phase occurred without degradation and/or dissolution of the triblock copolymers. During the next ~30–40 days of incubation, a linear decrease in wet weight from 80 to 50 wt% was observed, accompanied by a ~10% decrease in dry weight. Thereafter, wet and dry weight stabilized at ~50% and ~90%, respectively, until day 80. Then, both wet and dry weight dropped substantially at a constant rate until complete degradation at ~130–140 days (figure 2). These findings are very similar to the *in vitro* degradation previously reported for acyl-capped PCLA–PEG–PCLA blends [80].

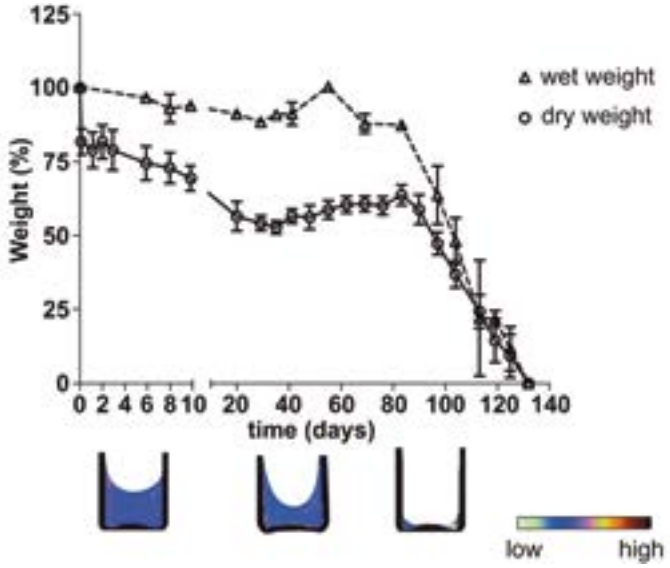


***Figure 2.*** *In vitro degradation of gels composed of* $PCLA_{2\times1700}CL_{2.2}Acet/PCLA_{2\times750}CL_{5.7}TIB$ *blends (25 wt% in buffer) presented as loss (%) of wet (n = 6) and dry weight (n = 2) over time. Experiments were performed in PBS at 37 °C. Under the graph, representative μCT images are depicted for the corresponding time points on the x-axis, showing a decline in volume and attenuation (see color scheme) during degradation. (For interpretation of the references to color in this figure legend, the reader is referred to the web version of this article.)*

The drop in volume could be depicted accurately using μCT. Also, the changes in dry weight correlated well with the attenuation values acquired using μCT; samples containing 90–100% of the initial dry weight showed an attenuation of 60.7 ± 3.5 whereas for samples containing <50% of the initial dry weight, this value dropped to 36.6 ± 2.2. These findings prove that μCT is indeed a useful surrogate for longitudinal follow-up of gel degradation kinetics.

The $M_n$ of the residual polymer mixture of $PCLA_{2\times1700}CL_{2.5}Acet/PCLA_{2\times750}CL_{5.7}TIB$ gels (GPC analysis) as well as the copolymer composition ($^1H$ NMR analysis) remained constant during the entire duration of *in vitro* degradation (data not shown). This demonstrates that degradation of the gel took place through polymer dissolution and not by chemical polymer degradation, which is in line with our previous data on other acyl-capped PCLA–PEG–PCLA systems [80].

### 3.5. Subcutaneous degradation of 25 wt% $PCLA_{2\times1700}CL_{2.5}$Acet and 25 wt% $PCLA_{2\times1700}CL_{2.5}$Acet/$PCLA_{2\times750}CL_{5.7}$TIB blend (25/75)

Upon s.c. injection of 25% $PCLA_{2\times1700}CL_{2.5}$Acet, a depot was formed immediately that could be palpated easily. Total gel volume remained stable for 2 weeks after which the volume started to decrease and complete degradation was observed in a range of 4–12 weeks. Although these data give a good indication of *in vivo* gelation and degradation kinetics, this method lacks accuracy on quantification and no distinction could be made between gel volume and possible fibrous tissue present at the injection site. Also, no longitudinal details about the type of degradation (e.g. surface or bulk erosion, loss in wet or dry weight) could be obtained using this method. In order to facilitate reliable and accurate longitudinal *in vivo* degradation data, the $PCLA_{2\times1700}CL_{2.5}$Acet/$PCLA_{2\times750}CL_{5.7}$TIB blend was used for the rest of the degradation experiments. $PCLA_{2\times1700}CL_{2.5}$Acet/$PCLA_{2\times750}CL_{5.7}$TIB showed a 25% drop in volume within the first day after s.c. injection, while attenuation (proportional to the total amount of TIB–polymer present in the gel) remained stable during this phase (figure 3). This is in line with our *in vitro* observations of early phase separation in a polymer rich and a polymer poor phase (figure 2). Subsequently, a decline in attenuation was observed between day 1 and day 21, while the volume of the gel hardly changed during this period (which is quite similar to the findings on s.c. degradation of $PCLA_{2\times1700}CL_{2.5}$Acet were no volume changes were found during the first 2 weeks). This indicates that the polymers dissolved while wet volume was maintained. Subsequently, attenuation stabilized at a value of ~20 while the gel volume decreased slowly, indicating a gradual gel degradation with equal degradation rates for wet and dry weight. The s.c. gel degradation followed a pattern with regions of high attenuation in the center surrounded by lower attenuation in the peripheral regions. This indicates that degradation occurs mainly at the surface while the polymer within the center of the depot remained unchanged, a phenomenon that has been shown before for other biomaterials implanted in animals [104-106].

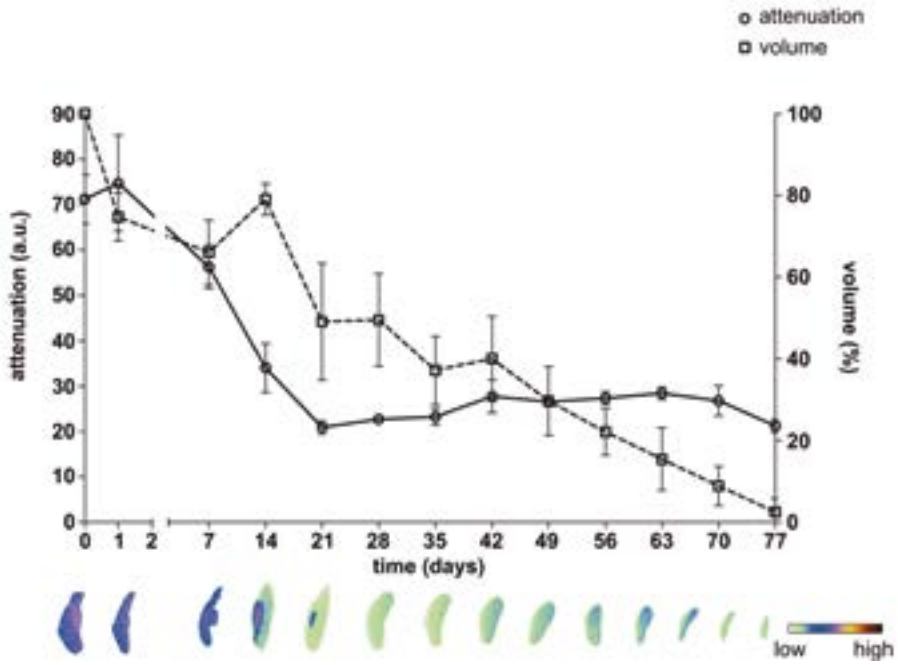


***Figure 3.*** *Volume (%) and attenuation (arbitrary unit) changes over time following s.c. injection of 25% $PCLA_{2\times1700}CL_{2.5}Acet/PCLA_{2\times750}CL_{5.7}TIB$ blend (n = 4). For each time point, representative CT-images of the s.c. depots are depicted under the graph, with the color representing the attenuation of the gel.*

GPC analysis showed that during *in vivo* gel degradation the peak of the polymer broadened towards longer retention time, hence shorter $M_n$, accompanied with an increase in PDI (figure 4). This indicates the formation of polymer entities with shorter chain lengths, which is not in line with the findings for *in vitro* degradation. In addition, the composition of residual polymer determined by $^1$H NMR significantly changed in time (figure 5). The CL content increased from 37 wt% at day 0 to 56 wt% at day 75, and the LA weight fraction increased during the same time frame from 7 to 16 wt%. On the other hand, the PEG weight fraction decreased from 37 wt% (day 0) to 12 wt% (day 75). These changes in composition are likely due to chain scission at the PEG–PCLA bonds and dissolution of the PEG rich chains [107], as also observed previously for structurally related gels [80]. This indicates that, opposed to *in vitro*, the *in vivo* degradation did not only take place by dissolution, but also by another (active) degradation mechanism [107, 108]. Others have previously shown that macrophages secrete enzymes including lipase, known for catalyzing PCL and PLLA degradation [104, 105]. Immunohistochemistry on the excised subcutaneous $PCLA_{2\times1700}CL_{2.5}Acet$ depots indeed showed positive CD68 staining, indicating macrophage infiltration (figure 6). It is therefore very likely that enzyme-catalyzed degradation also played a significant role in the *in vivo* (active) degradation of our PCLA–PEG based gels. TIB-

content remained more or less stable over the course of degradation, proving that the attenuation changes observed by μCT were in fact due to gel degradation and not chain cleavage of the TIB-capped polymer.



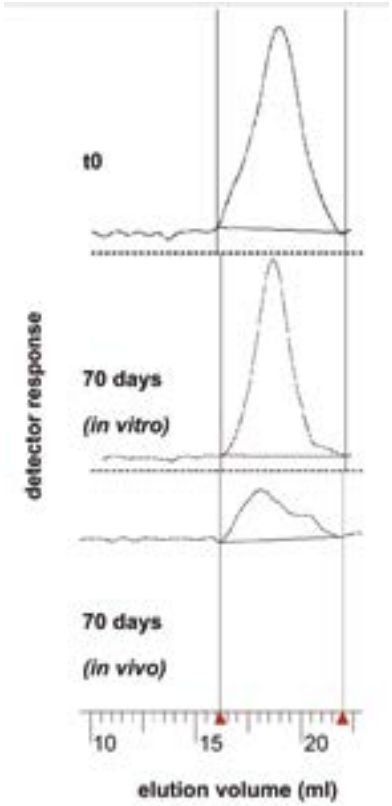


***Figure 4.*** *GPC chromatograms of the $PCLA_{2\times1700}CL_{2.5}Acet/PCLA_{2\times750}CL_{5.7}TIB$ depots in time in vitro and in vivo. No changes were observed during the in vitro degradation, while in vivo a broadening of the polymer peak occurred which indicates shorter chain lengths thus (active) polymer degradation.*

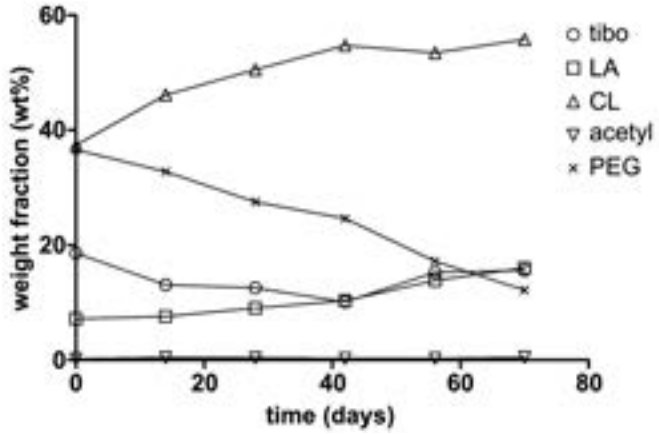


***Figure 5.*** *In vivo degradation of 25 wt% $PCLA_{2\times1700}CL_{2.5}Acet/PCLA_{2\times750}CL_{5.7}TIB$ gels after s.c. injection in time. The graph shows the weight fraction of CL, LA, TIB and acetyl, PEG, determined by $^1H$ NMR.*

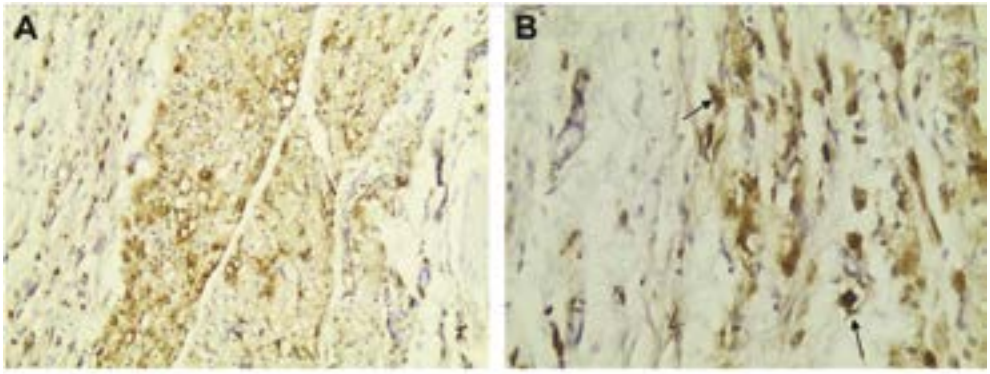


***Figure 6.*** *Representative images of immunohistochemistry CD68 staining of the excised subcutaneous depot at t = 12 weeks. A) Macrophage infiltration (deep brown staining), surrounded by fibrous tissue at the site of the depot, indicating active degradation of the gel in vivo (magnification 10×). B) The same image in a higher magnification (20×); the dark arrows indicate macrophages.*

### 3.6. Intra-articular injection of $PCLA_{2\times1700}CL_{2.5}Acet/PCLA_{2\times750}CL_{5.7}TIB$ blend (25/75)

Directly after i.a. injection of $PCLA_{2\times1700}CL_{2.5}Acet/PCLA_{2\times750}CL_{5.7}TIB$, the gel volume distributed to the supra-patellar pouch (figure 7). After 8 days, ~50% of the initial injected volume was still present within this pouch and ~25% remained at day 14. At 3 weeks, traces of the depot were still visible but the signal was too weak for proper quantification and 4 weeks post-injection no gel could be detected. It is very important for a DDS that is specifically designed for i.a. application to stay within the injected joint for a period of time long enough to release the incorporated drug in a timescale where it can be effective for joint repair and/or pain relief. Although the $CL_{2.2}Acet/CL_{5.7}TIB$ blend could indeed be traced for a period of 3 weeks within the knee joint, complete degradation was much faster compared to s.c. application (12 weeks). Multiple factors might contribute to this large difference. Most importantly, the geometry and size of the gel in the i.a. situation are quite different from the s.c. situation (confined environment). The injected i.a. volume is smaller and also, due to dispersion and mechanical loading in the joint the geometry is quite different with higher surface/volume ratio compared to s.c. application, leading to faster degradation. In addition, the mechanical stress in the weight bearing joint may even create smaller sequestered gel particles that subsequently become phagocytosed by macrophages. In case these particles become smaller than 5 μm and stay detached from the larger gel-depot-mass, they could leave the joint with the normal physiological (daily) efflux of synovial fluid directly through gaps within the fenestrated synovial tissue [28, 109]. While the results that were found for the i.a. injected $PCLA_{2\times1700}CL_{2.5}Acet/PCLA_{2\times750}CL_{5.7}TIB$ blend are very promising and rendered good longitudinal visualization, quantification was more difficult. Firstly, i.a. dispersion of the gel makes volume and attenuation values less reliable compared to the s.c. depot. Secondly, differentiation between the $PCLA_{2\times1700}CL_{2.5}Acet/PCLA_{2\times750}CL_{5.7}TIB$ blend and structures within of the joint is hindered due to similar attenuations most likely leading to an underestimation of the amount of gel at later time points. Despite this, the i.a. degradation data clearly show that our gel has the capacity to sustain within the joint for a period of time that, to our knowledge, has not been shown before for any other gelling systems [28].

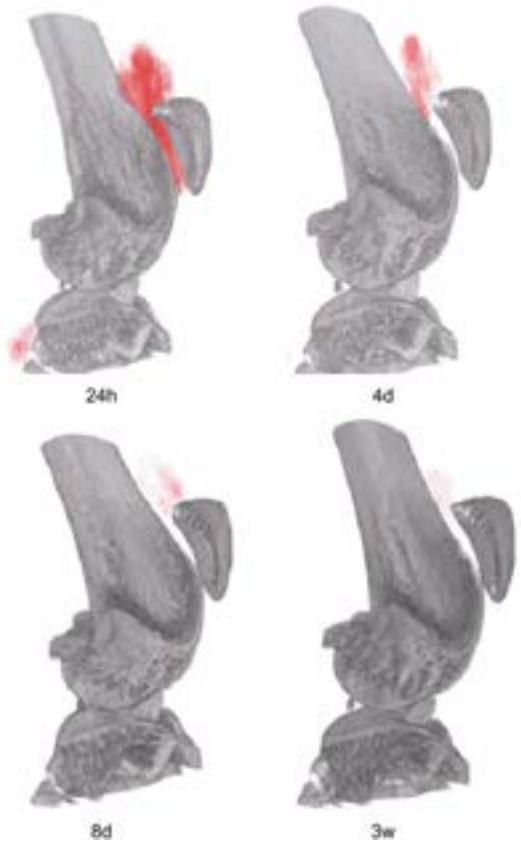


***Figure 7.*** *Reconstructed 3D μCT images of i.a. injected* $PCLA_{2\times1700}CL_{2.5}Acet/PCLA_{2\times750}CL_{5.7}TIB$. *The gel (red) was contained i.a. while slowly degrading over time. At the 4-week scan, the gel was no longer visible.*

## 3.7. In vitro cytocompatibility of $PCLA_{2\times1700}CL_{2.5}Acet$

In terms of cytocompatibility and *in vivo* biocompatibility, we are interested in the purest form of the gel ($PCLA_{2\times1700}CL_{2.5}Acet$) since this is the formulation that would eventually be used for i.a. treatment and is representative for the acyl-capped PCLA–PEG–PCLA family. Also, the TIB-group might have a (negative) effect on cytocompatibility and/or i.a. biocompatibility. Therefore, primary equine chondrocytes were incubated with $PCLA_{2\times1700}CL_{2.5}Acet$ (up to 2 mg/ml). The viability of the cells was not affected when compared to medium only or F-127 (negative control). Also, no differences in hemolytic activity were observed for erythrocytes incubated with $PCLA_{2\times1700}CL_{2.5}Acet$ (in buffer) or its buffer alone at body temperature (37 °C). The results on viability and hemolytic activity prove good cytocompatibility of the gel (figure 8). Previously, similar results were found for uncapped polymers [110] and our findings demonstrate that cytocompatibility of the polymers was not jeopardized by capping acetyl groups.

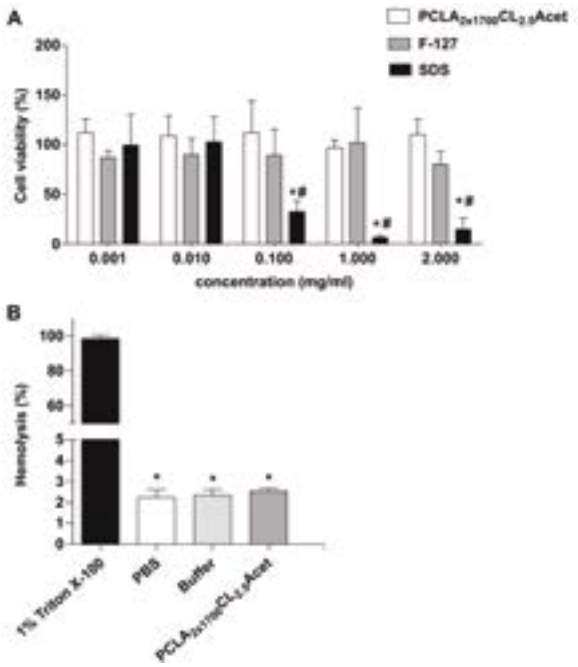


***Figure 8.*** *In vitro $PCLA_{2\times1700}CL_{2.5}$Acet biocompatibility. A) Viability of primary equine chondrocytes after addition of $PCLA_{2\times1700}CL_{2.5}$Acet compared to positive control (F-127) and negative control (SDS) detected by AlamarBlue assay. Primary equine chondrocytes cultured with culture medium only served as a control and were set as 100% viability (n = 4). Values are depicted as Mean ± SD, *p < 0.05 vs $PCLA_{2\times1700}CL_{2.5}$Acet, #p < 0.05 vs F-127. B) Hemolytic activity of $PCLA_{2\times1700}CL_{2.5}$Acet (gel) and its buffer. PBS was set as a negative control while 1% Triton X-100 was set as a positive control (n = 3). *p < 0.05 vs 1% Triton X-100.*

## 3.8. Intra-articular biocompatibility of $PCLA_{2\times1700}CL_{2.5}$Acet

Left knees were injected with 25 wt% $PCLA_{2\times1700}CL_{2.5}$Acet; right knees received a saline injection and served as a control ($n$ = 10, minus $n$ = 1 due to incomplete Hexabrix influx). No toxic responses such as joint redness/swelling or changed locomotion occurred during the entire 12-weeks follow-up period in neither gel injected nor control knees. At 0, 6 and 12 weeks post-injection the patellar cartilage did not show any significant thickness nor attenuation differences with the contralateral control side (figure 9a). Histology of the joint samples after 12 weeks ($n$ = 10) confirmed these findings (figure 9b); GAG-depletion score for the gel injected knees was 13 ± 7% vs 10 ± 3% for the control knees and no structural changes were seen (0%). These findings show that the $PCLA_{2\times1700}CL_{2.5}$Acet gel is safe for i.a. use.

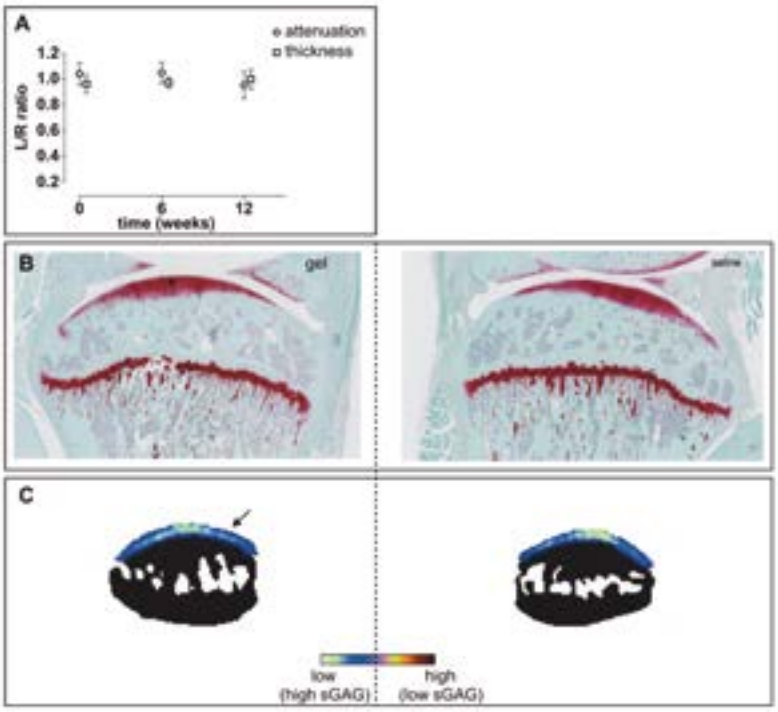


***Figure 9.*** *A) Graph representing left (gel)-to-right (saline) ratio of patellar cartilage attenuation and thickness at 3 time points (n = 10).* ***B)*** *Representative histological images of the tibia plateau (* indicating the cartilage) and* ***C)*** *μCT images (patella) of 25 wt% $PCLA_{2\times1700}CL_{2.5}$Acet-injected (left images) and saline-injected (right images) knees 12 weeks after injection (arrow indicating the cartilage); no changes in cartilage thickness and attenuation occurred (see color scheme; a low attenuation represents high sGAGs thus good cartilage quality).*

## 4. Conclusion

Acyl-capped PCLA–PEG–PCLA polymers form a hydrogel depot that degrades gradually both s.c. and i.a. *In vivo* degradation of the gel depot differed from *in vitro* degradation and was driven both by dissociation and active degradation by macrophages. The desirable degradation kinetics combined with the excellent intra-articular biocompatibility makes these gels suitable for intra-articular drug delivery.

## Acknowledgments

Mike de Leeuw, Dr. Theo Flipsen and Dr. Leo G.J. de Leede from InGell Labs BV are gratefully acknowledged for their support and valuable discussion. This research was partly supported by a grant of the Ministry of Economic Affairs, The Netherlands (BMM/TerM P2.02).

## Supplementary data

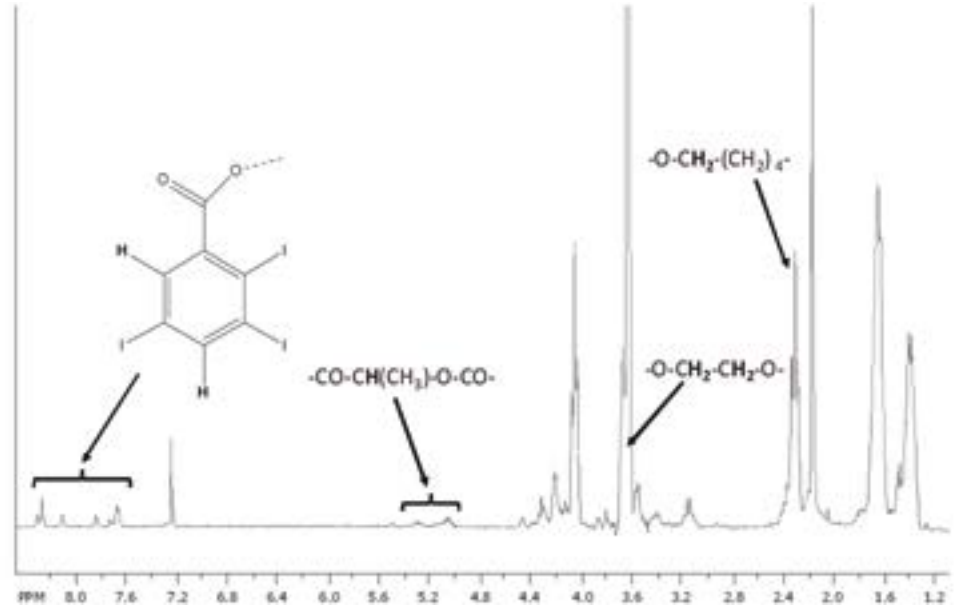


***Figure S1.*** *$^1$H NMR spectra of TIB-capped PCLA–PEG–PCLA in $CDCl_3$. The characteristic peaks at 5.25–4.95, 3.65–3.55, 2.50–2.10 and 8.40–7.60 ppm correspond to methine protons of LA, methylene protons of PEG, methylene protons of CL , and aromatic protons of TIB-end groups respectively.*


3

# Chapter 3

## Release behavior and intra-articular biocompatibility of celecoxib-loaded acetyl-capped PCLA-PEG-PCLA thermogels

Sandker M, Petit A, Müller B, Meyboom R, van Midwoud P, Bruin P, Redout EM, Versluijs-Helder M, van der Lest CH, Buwalda SJ, de Leede LG, Vermonden T, Kok RJ, Weinans H, Hennink WE.

*Biomaterials. 2014 Sep;35(27):7919-28.*

## Abstract

In this study, we investigated the *in vitro* and *in vivo* properties and performance of a celecoxib-loaded hydrogel based on a fully acetyl-capped PCLA-PEG-PCLA triblock copolymer. Blends of different compositions of celecoxib, a drug used for pain management in osteoarthritis, and the acetyl-capped PCLA-PEG-PCLA triblock copolymer were mixed with buffer to yield temperature-responsive gelling systems. These systems containing up to 50 mg celecoxib/g gel, were sols at room temperature and converted into immobile gels at 37 °C. *In vitro*, release of celecoxib started after a ~10-day lag phase followed by a sustained release of ~90 days. The release was proven to be mediated by polymer dissolution from the gels. *In vivo* (subcutaneous injection in rats) experiments showed an initial celecoxib release of ~30% during the first 3 days followed by a sustained release of celecoxib for 4–8 weeks. The absence of a lag phase and the faster release seen *in vivo* were likely due to the enhanced celecoxib solubility in biological fluids and active degradation of the gel by macrophages. Finally, intra-articular biocompatibility of the 50 mg/g celecoxib-loaded gel was demonstrated using μCT-scanning and histology, where no cartilage or bone changes were observed following injection into the knee joints of healthy rats. In conclusion, this study shows that celecoxib-loaded acetyl-capped PCLA-PEG-PCLA hydrogels form a safe drug delivery platform for sustained intra-articular release.

## I. Introduction

Celecoxib (Figure 1) is a non-steroidal anti-inflammatory drug (NSAID) and a selective inhibitor of cyclo-oxygenase-2 (COX-2), approved as Celebrex® for the pain management of, amongst others, rheumatic diseases and osteoarthritis [111]. Some authors even consider celecoxib to have anti-catabolic and/or even anabolic potential on cartilage, however, there is quite some conflicting data and further research is needed regarding this topic [41, 112, 113]. Celecoxib has a very low aqueous solubility (<1 μg/ml) with a large apparent volume of distribution (>1 l/kg) due to its high plasma protein binding (~97%) [114]. Concerns have risen about the systemic toxicity of celecoxib, mainly on myocardial muscles [115], and consequently there is a need for formulations reducing its toxicity. One way to reach this goal is to develop formulations, which are able to locally release drugs for a prolonged period. These drug delivery systems (DDSs) ideally lead to therapeutically effective local concentrations while plasma concentrations remain below toxic level. Moreover, not only the exposure is targeted and localized, but also patient compliance is greatly improved compared to daily oral administration.

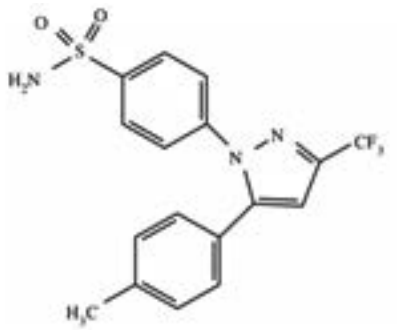


***Figure 1.*** *Chemical structure of celecoxib, a NSAID cox-2 inhibitor.*

Other desired DDS properties are ease of injection, high encapsulation efficiency (preferably 100%), and a low burst release to prevent high drug concentrations (and consequently possible toxic side effects) shortly after administration. In addition, the ideal DDS should have tunable release kinetics and show full recovery of the loaded drug. Injectable DDSs developed for the controlled release of celecoxib have been based up to now mainly on micro/nano-particles composed of poly(lactide-*co*-glycolide) (PLGA)[116-121]. These systems show some limitations in encapsulation efficiency (as low as 50%), burst release (as high as 60%), and recovery rates (as low as 25%) which all together hinder their clinical applicability [116-121]. Recently, highly concentrated solutions of celecoxib in PEG400 (400 mg/ml) were used as *in situ* forming depots

after injection in equine joint cavities [74]. Upon injection, PEG400 is diluted in the synovial fluid of the joints and celecoxib subsequently precipitates/crystallizes. Its release is achieved by slow dissolution of the celecoxib precipitates/crystals, which is however difficult to predict and control and the crystals may harm the cartilage.

Temperature-responsive aqueous formulations of 'ABA' triblock copolymers composed of PEG as middle block flanked by polyester blocks of diverse compositions, are systems that fulfill the aforementioned desired DDS properties [36, 37, 58, 77, 78, 80, 122-126].

Importantly, these gels offer the possibility of complete encapsulation of hydrophobic drugs with release kinetics that can be modulated [123, 127, 128]. Systems based on PLGA-PEG-PLGA loaded with paclitaxel were clinically evaluated up to Phase IIa in oncology for targeted delivery to the tumor *via* intralesional injection or placement into the tumor cavity [129]. The drug release from these systems is mediated by a combination of diffusion and chemical polymer degradation, which takes around six weeks (both *in vitro* and *in vivo*) [123, 127, 128]. For some applications, however, longer release times are required. To slow down hydrolysis and thereby increase the degradation time, PLGA blocks have been replaced by poly (ε-caprolactone-*co*-lactide) (PCLA) blocks. Indeed, gels based on PCLA-PEG-PCLA (depending on the ratio of caproyl units (CL) to lactoyl units (LA)) are more stable compared to PLGA-based gels. For instance, systems with PCLA blocks containing 70% mol CL showed a complete degradation time of approximately six months [110, 130]. Moreover, modification of the terminal hydroxyl groups of these triblock copolymers allowed modulation of mechanical properties and provided extended degradation time of temperature-responsive gelling systems made of these copolymers [58, 78, 80, 92].

In this study, we investigated the feasibility of acetyl-capped PCLA-PEG-PCLA triblock copolymer based temperature-responsive gelling systems as an intra-articular drug delivery system for celecoxib. We characterized the systems (the *in vitro* release and gel degradation), examined the *in vivo* release kinetics of a subcutaneous injected formulation and the biocompatibility of the same formulation after intra-articular injection.

## 2. Materials and Methods

### 2.1. Materials

Celecoxib was obtained from LC Laboratories, USA. Hexabrix 320®, a clinical iodine-based contrast agent, was obtained from Guerget, The Netherlands. All other chemicals were obtained from Aldrich and used as received.

### 2.2 Synthesis of acetyl-capped PCLA-PEG-PCLA

The acetyl-capped PCLA-PEG-PCLA triblock copolymer used in this study was synthesized and characterized as described previously[80]. In short, in a three-neck round-bottom flask equipped with a Dean Stark trap and a condenser, PEG1500 (50 g), l-lactide (22 g), ε-caprolactone (88 g) and toluene (150 ml) were introduced and, while stirring, heated to reflux (~140 °C; i.e. the boiling point of toluene is 111 °C but that of the mixture is ~140 °C) under a nitrogen atmosphere. The solution was azeotropically dried by distilling off toluene/water (ca. 50% vol of the initial volume). Next, the solution was cooled to ~90 °C and tin(II) 2-ethylhexanoate (5 mmol per mol PEG1500) was added. Ring-opening polymerization was carried out at 110–120 °C overnight under a nitrogen atmosphere. The solution was cooled to room temperature and dichloromethane (100 ml) and triethylamine (6 mol per mol PEG1500) were added. Then, the solution was cooled to 0 °C in an ice bath, and while stirring, an excess of acetyl chloride (10 g, ratio acetyl chloride/PEG = 4 mol/mol) was added drop wise and acylation was allowed to proceed for 3 h. Next, dichloromethane was removed under vacuum at 60–65 °C, ethyl acetate (100 ml) was subsequently added and triethylamine hydrochloride salts were removed by filtration. The polymer was precipitated by adding a 1:1 mixture of hexane and diethyl ether (290 ml). Upon storage at –20 °C, the polymer separated as a waxy solid from which non-solvents containing unreacted monomers and the excess of acyl chloride could be decanted easily. The precipitated polymer was dried in vacuo and obtained in yield of 85%. The polymer was characterized by 1H NMR and GPC as previously described [58].

### 2.3. Miscibility of celecoxib in $PEG_{1500}$ and in PCLA-PEG-PCLA

Celecoxib, $PEG_{1500}$ and PCLA-PEG-PCLA were separately dissolved in ethyl acetate (300, 150 and 300 mg/ml, respectively). The solutions were mixed to prepare celecoxib/PEG1500 mixtures with weight ratios between 10/90 and 80/20 (w/w) as well as celecoxib/PCLA-PEG-PCLA mixtures with weight ratios between 5/95 and 70/30 (w/w). The solutions (1–10 ml) were transferred into 6-cm Petri dishes. Next, the solvent was removed under nitrogen flow for 48 h.

## 2.4. Solubility of celecoxib in $PEG_{1500}$/buffer and in PCLA–PEG–PCLA/buffer systems

100 mg of celecoxib/PEG1500 (10/90 w/w) mixture was added to 750 μl PBS buffer pH 7.4 (44 mm Na2HPO4, 9 mm NaH2PO4, 72 mm NaCl, 0.02% wt NaN3). Similarly, 260–830 mg of celecoxib/PCLA-PEG-PCLA mixtures 10/90 to 80/20 were added to 750 μl PBS to yield celecoxib-loaded aqueous PCLA-PEG-PCLA of 25% wt gel formulations. Samples were vortexed for 1 min and then incubated at 4 °C for 48 h. To check for possible presence of celecoxib crystals, the samples were investigated under a microscope (Nikon Eclipse TE2000U) and analyzed by X-ray diffractometry as described previously [80].

Celecoxib/PEG1500/buffer mixtures were further filtered with standard GPC/HPLC syringe filters (0.45 μm), and the amount of celecoxib in the transparent filtrates was measured by UPLC (see paragraph 2.8).

## 2.5. Differential Scanning Calorimetry (DSC) analysis

The thermal properties of celecoxib and the polymers ($PEG_{1500}$ and PCLA-PEG-PCLA) as well as those of the celecoxib/polymer mixtures were determined by DSC (TA Instruments DSC Q2000 apparatus). Samples of ~10 mg in closed aluminum pans were heated under a nitrogen flow at a rate of 50 ml/min from room temperature to 170 °C and kept at this temperature for 5 min. Next, the samples were cooled to −80 °C with a rate of 10 °C/min, followed by a second heating cycle at the same rate to 170 °C. Using the second heat run, the glass transition temperature ($Tg$) was set as the midpoint of heat capacity change and the melting enthalpy ($\Delta H$) as the integration of the endothermic area.

## 2.6. Gelling properties of celecoxib–loaded PCLA–PEG–PCLA systems

Vial tilting to visually characterize sol and gel state of celecoxib-loaded PCLA-PEG-PCLA 25% wt systems was performed at 4 °C, room temperature and at 37 °C after 30 min of incubation. Immobility of the systems for 10 min with the vial upside down was used to discriminate between mobile sols and immobile gels [80, 124].

Rheological characteristics of the systems were monitored by oscillatory temperature sweep experiments using a TA AR-G2 rheometer equipped with a Peltier plate (1° steel cone, 20 mm diameter with solvent trap) at 1% strain and a frequency of 1 Hz. The solvent trap of the Peltier plate was filled with water to prevent dehydration of the samples during measurement. A 70 μl sample (cooled to 4 °C) was introduced between the rheometer plates (pre-cooled to 4 °C), and subsequently heated from 4 to 50 °C under oscillatory force with a heating rate of 1 °C/min.

## 2.7. Degradation and release behavior of celecoxib-loaded PCLA-PEG-PCLA gels

The *in vitro* degradation and release behavior of unloaded and loaded (0.125, 1.25 and 50 mg celecoxib per g gel) PCLA-PEG-PCLA 25% wt gel was investigated in PBS buffer pH 7.4 (same composition as described in section 2.4) with or without 0.2% wt Tween® 80. Tween® 80 (sorbitan oleate ester, $M$ = 1310 g/mol) is a surfactant with a critical micelle concentration (CMC) of 0.02 mm, i.e. 0.0026% wt [131], which increases the solubility of celecoxib [121, 132]. Celecoxib solubility in PBS buffer pH 7.4 with Tween® 80 was investigated. Therefore, an excess of celecoxib (~10 mg) was added to 1 ml of PBS with 0.1–2.0% wt Tween® 80 (i.e. above its CMC), which was incubated for 24 h at room temperature and after centrifugation for 5 min at 3500 rpm the celecoxib concentrations in the supernatant were determined by UPLC (see paragraph 2.8).
For the *in vitro* degradation and release, 6 g of dry celecoxib/PCLA-PEG-PCLA mixture was added to 21 ml PBS buffer pH 7.4. Samples were heated for 15 min at ~50 °C (i.e. above the melting temperature of the polymer in dry state), subsequently vortexed (1 min) and then incubated at 4 °C for 48 h to allow formation of homogeneous dispersions. Subsequently, 300 µl sample cooled to 4 °C was transferred into glass vials (8.2 × 40 mm) using a syringe. The vials were incubated at 37 °C to allow gel formation, 30 min later 700 µl PBS buffer pH 7.4, with or without 0.2% wt Tween® 80 was added. At predetermined time points, the buffer was removed, the weight of the remaining gels was measured and fresh buffer was added. In addition, gel samples were freeze-dried and analyzed for their dry weight and for the average number molecular weight (Mn) of the polymer by GPC as described previously [80]. The buffer samples that were taken during the release experiments were observed under a microscope (Nikon Eclipse TE2000U) and celecoxib concentrations were determined by UPLC (see paragraph 2.8).

## 2.8. Determination of celecoxib concentration in in vitro release samples

The celecoxib concentration in the different release samples was determined by UPLC using a Waters UPLC system equipped with a Waters column (BEH C18 1.7 µm, size: 2.1 × 100 nm). Celecoxib was dissolved in DMSO at 5 mg/ml. This celecoxib solution was diluted 10 times with DMSO and subsequently with buffer containing Tween® 80 to prepare celecoxib standards used for calibration (final celecoxib concentration ranged from 0.5 to 100 µg/ml). Two eluents containing 0.1% vol trifluoroacetic acid (TFA) were used: 95/5 v/v acetonitrile/water (Eluent A) and 45/45/10 v/v/v methanol/acetonitrile/water (Eluent B), the elution rate was 0.08 ml/min, and the column temperature was 50 °C. A gradient was run from 100% Eluent A to 100% Eluent B in 2 min and kept at 100% B for 10 min before returning to 100% Eluent A. Detection was performed with a UV detector at 254 nm and the injection volume was 10 µl. The retention time of celecoxib was 10.5 min with a total run time of 16 min. The autosampler temperature

was 20 °C. The release samples were analyzed undiluted and after a 4× dilution with acetonitrile (ACN) to dissolve gel particles, if present.

## 2.9. In vivo celecoxib release study

The Animal Ethic committee of the Erasmus Medical Center, Rotterdam, The Netherlands, approved all conducted procedures (agreement number EMC2255(116-11-02)). Six 14-week-old (400-450 g) male Wistar rats (Charles River Nederland BV, Maastricht, the Netherlands) were housed in the animal facility of the Erasmus Medical Center, with a 12-h light-dark regimen, at 21°C. Animals were fed standard food pellets and water *ad libitum*. Experiments started after an acclimatization period of 2 weeks. To investigate the *in vivo* celecoxib release kinetics from the gel, six rats were injected subcutaneously in the neck region with 500 µl aseptically prepared PCLA-PEG-PCLA 20 % wt gel loaded with 50 mg/g celecoxib. Experiments (see Figure S.1 in the supplementary file) showed that there is no difference in *in vitro* release kinetics between the 20 and 25 % wt. The 20 % wt formulation had the right viscosity for injection (the viscosity of the 25% formulation was too high) and was therefore selected for investigation of the *in vivo* performance. At predetermined time points between 0 and 100 days, blood samples (500 µl) were taken from the lateral tail vein using Vacutainer SST™ II Advance (BD Plymouth) tubes that contain Silica (clot activator). After spinning down the cells (3500 rpm, 10 minutes), 100 µl of serum was taken and extracted with ethyl acetate [133]. Briefly, 100 µl serum was mixed with 100 µl internal standard (200 ng paracoxib in 5% BSA). Then, 200 µl 0.1 M Na acetate buffer (pH 5.0) was added, followed by ethyl acetate (1 ml) and the samples were vortexed for 10 min. Then, samples were centrifuged at 11,000 rpm for 10 minutes and stored at -80 °C for at least 30 minutes. The upper ethyl acetate phases were transferred into HPLC glass vials and evaporated under nitrogen atmosphere. After evaporation, the samples were dissolved in 100 µl of methanol:acetate buffer (3:1 vol:vol) of which 5 µl was injected onto a Kinetex® $C_{18}$ (30 × 3.0 mm, particle size of 2.6 µm) analytical column (Phenomenex, Utrecht, NL). Separation was performed at a flow rate of 500 µl/min, with a total runtime of 3 minutes. The mobile phases consisted of acetonitrile:water (1:1 vol:vol) (A), and acetonitrile:methanol (1:1 vol:vol) (B). Samples were separated using the following gradient A/B vol/vol: 0-0.6 minutes, ; 0.6-0.7 minutes, 100/0 to 30/70; 0.7-1.6 minutes, 30/70 to 0/100; 1.6-2.4 minutes, 0/100; 2.4-2.7 minutes, 0/100 to 100/0; 2.7-3.0 minutes, 100/0 at a column temperature of 40 °C. The column effluent was introduced by an atmospheric pressure chemical ionization (APCI) interface (Sciex, Toronto, ON) into a API3000 mass spectrometer. For maximal sensitivity and for linearity of the response, the mass spectrometer was operated in multiple-reaction monitoring (MRM) mode at unit mass resolution. Peaks were identified by comparison of retention time and mass spectra of standards. For each component two ion transitions

were monitored, celecoxib: 380.3→316.3 and 380.3→276.3 (collision energy: -50 V, both), and paracoxib: 369.3→250.2 and 369.3→234.2 (collision energy: -30 V, both). The following MS parameters were used: nebulizer gas: 10 psi; curtain gas: 10 psi; ion current: -2 μA; source temperature: 500 °C; gas flow 1: 30 psi; gas flow 2: 20 psi: decluster potential: -70 V and entrance potential: -10 V. Data were analysed with Analyst software version 1.4.2 (Applied Biosystems, Nieuwerkerk a/d IJssel, The Netherlands). Celecoxib peak areas were corrected for the paracoxib recovery, and concentrations were calculated using a celecoxib reference line ranging from 0.5 ng to 1000 ng/ml. The reference line was linear in this range (r = 0.9997). Further calculations on the pharmacokinetics were done using the freeware PK solver [134].



## 2.10. Intra-articular biocompatibility of celecoxib loaded PCLA-PEG-PCLA 25 wt% gels

Five 14-week-old (400–450 g) male Wistar rats (Charles River Nederland BV, Maastricht, the Netherlands) were housed in the animal facility of the Erasmus Medical Center, with a 12-h light–dark regimen, at 21 °C. The animals (kept under the same conditions as described in 2.9) were used to investigate intra-articular biocompatibility of celecoxib-loaded temperature-responsive gels composed of PCLA-PEG-PCLA of 25% wt polymer in PBS buffer with pH 7.4 (without NaN3) loaded with 50 mg celecoxib/g gel. Gels were prepared aseptically and 50 μl (cooled to 4 °C) was injected directly into the joint cavity through the patellar tendon using Luer-lock® syringes mounted with 27G needles. After injection, the knee was flexed and extended several times to distribute the gel throughout the whole knee joint. Contralateral knees were injected with saline to serve as a negative control.

12 weeks post injection, the animals were euthanized and both knee joints were harvested for equilibrium partitioning of a contrast agent using μCT (EPIC-μCT) analysis, a method that has a strong correlation with cartilage sulfated-glycosaminoglycan (sGAG) content, which is a direct measurement for cartilage quality [135, 136]. All samples were incubated in a 40% Hexabrix solution (diluted with PBS) for 24 h at room temperature [99]. EPIC-μCT was performed on a Skyscan 1076 *in vivo* μCT scanner (Skyscan, Kontich, Belgium), using previously described scan settings [36]. In all EPIC-μCT datasets, X-ray attenuation (arbitrary gray values inversely related to sGAG content) and thickness (μm) were calculated for cartilage of the medial and lateral tibial plateau [99]. Using Skyscan analysis software, all datasets were segmented using a fixed attenuation threshold between air (30) and subchondral bone (120). In all segmented μCT datasets, regions of interest (150 slices) were drawn around the cartilage of the medial and lateral plateau of the tibia separately and for these regions, cartilage attenuation and thickness (μm) were calculated, osteoarthritic knee joints from a previous article in rats of the same age, sex and species as the animals as in our current study were used [136]. In short,

a strenuous running protocol was combined with 3 unilateral i.a. papain injections, leading to cartilage damage. The above-mentioned protocols for EPIC-μCT scanning as well as data analysis were used.
Directly following the EPIC scan, knee joints were fixed with buffered formaldehyde, decalcified and embedded in paraffin for histological analysis. 6-μm sections were prepared sagitally at 300-μm intervals and stained with Safranin-O with a fast green counterstain to image the distribution of the GAGs. All staining was performed at once in order to minimize artefacts between samples.

### 2.12. Statistical analysis

All data was normally distributed (Shapiro–Wilk >0.05) and Levene's tests ($p > 0.05$) verified the equality of variances in the tested samples (homogeneity of variance) for all tested parameters. Differences in μCT-data between the gel-injected and saline-injected knees within the same animal were analyzed using type-1, two-tailed, paired *T*-tests for all outcome parameters (SPSS Inc., Chicago, USA). When comparing differences between means of the knees injected with celecoxib-loaded gel or saline to the OA induced knees (PRO), type-1, two-tailed, unpaired *T*-tests were performed for all outcome parameters. All data are presented as mean ± SD, *P*-values <0.05 were considered significant.

## 3. Results and discussion

### 3.1 $^1$H NMR and GPC analysis of the acetyl-capped PCLA-PEG$_{1500}$-PCLA

The acetyl-capped PCLA-PEG$_{1500}$-PCLA copolymer used in this study was synthesized by ring opening solution polymerization of a mixture of l-lactide and ε-caprolactone using PEG$_{1500}$ as initiator and tin(II) 2-ethylhexanoate as catalyst, followed by capping of the terminal hydroxyl with acetyl groups by reaction with an excess of acetyl chloride as previously described [58]. It was aimed to synthesize a fully actelyated polymer with two PCLA blocks of 1700 g/mol and with a CL/LA molar ratio of 2.5. 1H NMR analysis and GPC analysis showed that the polymer had two PCLA blocks of 1600 g/mol with a molar CL/LA ratio of 2.2, hence slightly below the feed value as previously reported [58]. The degree of acylation was almost quantitative. The characteristics of the synthesized triblock copolymer are summarized in Table 1.

***Table 1.*** *Characteristics of the acetyl-capped PCLA-PEG-PCLA triblock copolymer used in this study.*

| **Polymer** | **Acetyl-capped PCLA-PEG$_{1500}$-PCLA** |
|---|---|
| Mn,PCLA [g/mol][a] | 1600 |
| CL/LA ratio [mol/mol][b] | 2.2/1 |
| Average CL-sequence length | 4.9 |
| Degree of acylation [%][c] | 93 |
| Mn,NMR [g/mol][d] | 4800 |
| Mn,GPC [g/mol][e] | 5100 |
| PDI[f] | 1.38 |

[a] *Molecular weight of each PCLA block determined by $^1$H NMR.*
[b] *Molar ratio of CL to LA in PCLA determined by $^1$H NMR.*
[c] *Determined by $^1$H NMR.*
[d] *Number average molecular weight determined by $^1$H NMR.*
[e] *Number average molecular weight determined by GPC, relative to PEG standards.*
[f] *Polydispersity determined by GPC.*



## 3.2. Miscibility of celecoxib with PEG and acetyl-capped PCLA-PEG-PCLA triblock copolymer

The thermogram of PEG$_{1500}$ showed no *T*g and a melting endotherm at ~50 °C ($\Delta H$ = 156 J/g), which is in accordance with literature [137]. The thermogram of celecoxib showed no *T*g and a melting endotherm at 165 °C ($\Delta H$ = 102 J/g), also in accordance with literature [138, 139]. The thermogram of the celecoxib/PEG$_{1500}$ mixture (10/90 w/w) showed a melting endotherm at ~50 °C ($\Delta H$ = 138 J/g), which can be ascribed to melting of PEG. Similarly, the thermograms of celecoxib/PEG$_{1500}$ mixtures (30/70 and 40/60 w/w) showed melting enthalpies of the PEG endotherm at ~50 °C (ΔH of 77 and 2 J/g, respectively) whereas no melting endotherm of celecoxib was observed. However, the thermograms showed a *T*g at –47 and –33 °C, respectively, which likely can be ascribed to miscibility of celecoxib and PEG (Fox equation, see below). Hence celecoxib/PEG$_{1500}$ mixtures with weight ratios 10/90, 30/70 and 40/60 have an amorphous celecoxib/PEG$_{1500}$ phase and crystalline PEG$_{1500}$ domains. Upon further increase in celecoxib weight ratio, the thermograms of the celecoxib/PEG$_{1500}$ mixtures (50/50 and 80/20 w/w) showed a further increase of the *T*g (–23 and 25 °C, respectively) and no melting endotherm of PEG and celecoxib. Hence, these mixtures were composed of an amorphous celecoxib/PEG$_{1500}$ phase only. Table 2 summarizes the thermal properties of celecoxib/PEG$_{1500}$ mixtures.

***Table 2.*** *Thermal properties of celecoxib/$PEG_{1500}$ mixtures as determined by DSC.*

| Celecoxib [% wt] | $PEG_{1500}$ [% wt] | $T_g$ [°C] | $T_m$ [°C] | ΔH [J/g] |
|---|---|---|---|---|
| 0 | 100 | Not detectable | ~50[a] | 156 |
| 10 | 90 | Not detectable | ~50[a] | 138 |
| 30 | 70 | –47 | ~50[a] | 77 |
| 40 | 60 | –33 | ~50[a] | 2 |
| 50 | 50 | –23 | Not detectable | Not detectable |
| 80 | 20 | 25 | Not detectable | Not detectable |
| 100 | 0 | Not detectable | 165[b] | 102[b] |

[a] *Melting due to PEG.*
[b] *Melting due to celecoxib.*

Figure 2 shows that the reciprocal $T_g$ of celecoxib/$PEG_{1500}$ mixtures linearly decreases with increasing celecoxib weight fraction ($F_{Celecoxib}$), which indicates that the $T_g$ of these mixtures follows the Fox Equation (equation 1) in which $F_{Celecoxib}$ and $F_{Polymer}$ are the weight fraction of celecoxib and $PEG_{1500}$, respectively.

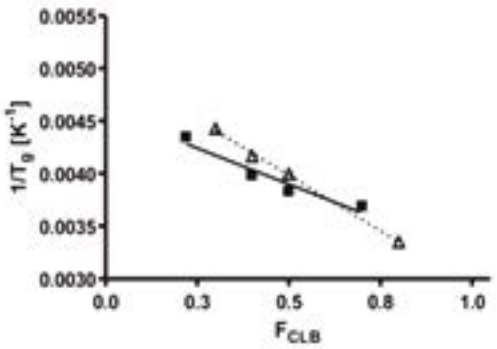


***Figure 2.*** *Reciprocal Tg of celecoxib/PCLA-PEG-PCLA (squares) and celecoxib/PEG1500 (triangles) mixtures as a function of celecoxib weight fraction ($F_{celecoxib}$).*

Extrapolation of the weight fraction of celecoxib to 100% and 0 (100% $PEG_{1500}$) gives a calculated *T*g for celecoxib and $PEG_{1500}$ of 70 and –70 °C respectively, which is only slightly deviating of the reported *T*g of celecoxib and PEG (51 °C[139] and –60 °C [137], respectively). The results therefore confirm that celecoxib and $PEG_{1500}$ are miscible, which is in line with the reported miscibility of celecoxib with $PEG_{6000}$ [138] and $PEG_{400}$ [36, 140]. Evidence of the miscibility of drugs structurally related to celecoxib (i.e. drugs containing –SO2N- moieties) and PEG has been discussed elsewhere [138, 140-143]

and, FTIR analysis showed the occurrence of intermolecular interactions and hydrogen bonding but also non-polar interactions between PEG and the studied drugs.
The thermograms of PCLA-PEG-PCLA and its mixtures with celecoxib are shown in figure S3. The thermogram of PCLA-PEG-PCLA showed a *T*g at –58 °C, which can be ascribed to the *T*g of the PCLA domains [37, 78, 80, 122, 124] and a crystallization exotherm at ~–40 °C (38 J/g), as well as a melting endotherm at 10–40 °C ($\Delta H$ = 40 J/g), which can be ascribed to melting of PEG as we showed previously that this polymer does not show crystallinity of the CL-rich domains because the CL sequence length are too short, i.e. less than 5 CL units [37, 78, 80, 122, 124]. With increasing celecoxib content, the thermograms of celecoxib/PCLA-PEG-PCLA mixtures (5/95 and 17/83 w/w) showed an increasing *T*g (–55 and –47 °C, respectively), a crystallization exotherm at higher temperature and of lower enthalphy (–30 °C ($\Delta H$ = 25 J/g) and 0 °C ($\Delta H$ = 1 J/g), respectively), which is likely attributed to miscibility of celecoxib and PCLA-PEG-PCLA. In line herewith, these thermograms also showed a melting endotherm at ~10–40 °C and of decreasing melting enthalpy ($\Delta H$ = 33 and 13 J/g, respectively). Hence these systems have amorphous celecoxib/PCLA/PEG domains and PEG crystals. Upon further increase of the celecoxib weight fraction, the thermograms of celecoxib/PCLA-PEG-PCLA mixtures (22/78, 40/60, 50/50 and 70/30) showed a further increase in *T*g (–43 to –2 °C, respectively), and no crystallization/melting endotherm. This shows that these systems consist of one amorphous celecoxib/PCLA/PEG phase. Table 3 summarizes the thermal properties of celecoxib/PCLA-PEG-PCLA mixtures.

***Table 3.*** *Thermal properties of celecoxib/PCLA-PEG-PCLA mixtures as determined by DSC.*

| **Celecoxib [% wt]** | **PCLA-PEG-PCLA [% wt]** | **Tg [°C]** | **Tm [°C]** | **ΔH [J/g]** |
|---|---|---|---|---|
| – | 100 | –58 | 0–25[a] | 38 |
| 5 | 95 | –55 | –10–20[a] | 33 |
| 17 | 83 | –47 | 10–20[a] | 13 |
| 22 | 78 | –43 | Not detectable | – |
| 40 | 60 | –22 | Not detectable | – |
| 50 | 50 | –12 | Not detectable | – |
| 70 | 30 | –2 | Not detectable | – |
| 100 | 0 | – | 165[b] | 102 |

[a] *Melting due to PCLA-PEG-PCLA.*
[b] *Melting due to celecoxib.*

As can been seen in figure 2, the reciprocal *T*g of celecoxib/PCLA-PEG-PCLA mixtures linearly decreases with increasing celecoxib weight fraction (Fox Equation [144], see Equation (1)) confirming that celecoxib and PCLA-PEG-PCLA are miscible. Extrapolation of the weight fraction of celecoxib to 100% and 0 (100% PCLA2x1700CL2.5Acet) gives a calculated *T*g for celecoxib and PCLA-PEG-PCLA of 49 and –56 °C respectively, which is in good agreement with the reported *T*g of celecoxib (51 °C [139] and of PCLA-PEG-PCLA (–58 °C, Table 3). The presence of favorable interactions between celecoxib and PCLA-PEG-PCLA is in line with the miscibility of celecoxib with PLGA[116-119] and might be ascribed to hydrogen bonding between the N–H groups of celecoxib and the carbonyl CO groups of polymers as described for celecoxib/PLGA and celecoxib/polyvinylpyrrolidone systems [145]. Because of favorable interactions of celecoxib with both PEG and PCLA, celecoxib is soluble to more than 70% wt in the acetyl-capped PCLA-PEG-PCLA.

## 3.3. Phase behavior of aqueous celecoxib-loaded PCLA-PEG-PCLA systems

Visualization by light microscopy and X-ray diffraction analysis were performed on aqueous systems (25% wt PCLA-PEG-PCLA in buffer) with celecoxib/PCLA-PEG-PCLA ratios between 0/100 to 50/50 w/w. In systems of celecoxib/PCLA-PEG-PCLA ratios from 0/100 to 17/83, no crystals were detected, but above a concentration of 70 mg/g celecoxib, needle-shaped crystals (~500 × 1 μm) were observed and identified as celecoxib crystals by X-ray analysis (see figure S4 in the supplementary file). Although celecoxib is molecularly dispersed in celecoxib/PCLA-PEG-PCLA mixtures (with celecoxib loading from 22% to 70% wt, Table 3 and figure S2), it (partly) crystallizes upon addition of buffer. The solubility of celecoxib in PEG1500/buffer mixtures (10/90 w/w, corresponding to the same PEG content as in PCLA-PEG-PCLA 25 wt% systems) was only ~35 μg/g, meaning that, because celecoxib is highly soluble in PCLA-PEG-PCLA 25% wt systems (~50 mg/g), celecoxib is solubilized in the hydrophobic PCLA domains of the system. The high solubility of celecoxib in aqueous PCLA-PEG-PCLA 25% wt systems (~50 mg/g) is in line with the reported good solubility (~5–15 mg/g) of other hydrophobic drugs such as paclitaxel [123], cyclosporine A [123], docetaxel [128] and indomethacin [127] in other structurally-related temperature-responsive gelling systems based on PLGA-PEG-PLGA.

## 3.4. Gelling properties of celecoxib-loaded PCLA-PEG-PCLA 25 % wt systems

Photographs of aqueous PCLA-PEG-PCLA 25% wt systems with a celecoxib load of 1.25 mg per g formulation are shown in figure 3A. At 4 °C and room temperature,

the samples were sols, whereas they formed immobile opaque gels at 37 °C, similar to samples without celecoxib. This sol-to-gel conversion between 21 and 37 °C occurred in all tested celecoxib-loaded PCLA-PEG-PCLA 25 wt% systems containing up to 50 mg/g celecoxib.

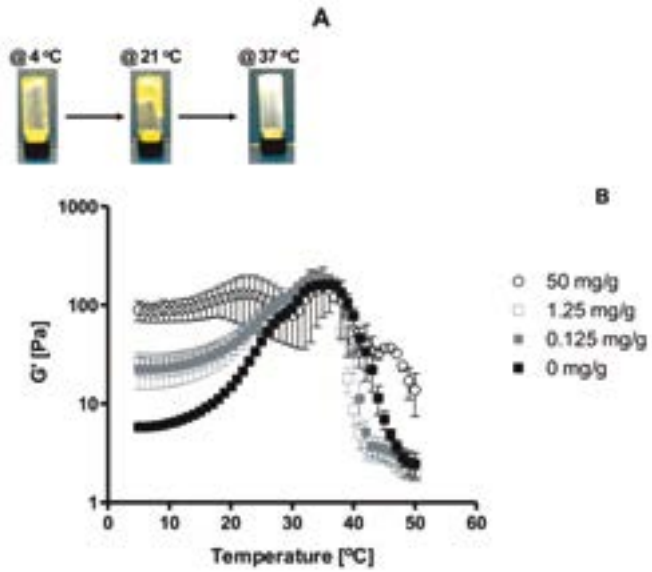


***Figure 3.*** *Phase behavior and rheological properties of celecoxib-loaded PCLA-PEG-PCLA systems of 25% wt in PBS buffer pH 7.4. 3A shows photographs of systems containing 1.25 mg celecoxib per g PCLA-PEG-PCLA formulation at 4, 21 and 37 °C. 3B shows the temperature-dependent storage modulus G' of systems containing different celecoxib loadings (*n = *3). Error bars represent the standard deviation.*

Figure 3 shows the temperature-dependent storage modulus (G′) of PCLA-PEG-PCLA 25 wt% systems with different celecoxib loadings (up to 50 mg/g containing fully dissolved celecoxib, see paragraph 3.3). The G′ of the unloaded systems was below 10 Pa at 4 °C, and increased to 100 Pa at 40 °C. Above 40 °C, a drop in G′ was observed which is likely caused by phase separation of the systems and loss of contact between the gel phase and the plate of the rheometer. The G′ of systems loaded with 1.25–50 mg/g celecoxib at 4 °C increased with increasing celecoxib loading from ~10 to 100 Pa, but these values were independent of the celecoxib loading at temperatures above 25 °C. Despite the observed increase an increase of G′ with increasing celecoxib loading (up to 50 mg/g), no significant effect on the sol-to-gel transition temperature of the systems was detected. The effect of drug loading on rheological properties of temperature-responsive systems has been described in literature before, but the underlying mechanism for the observed effects is not yet fully understood [128, 146, 147]. However, it was shown that a lowering of the sol-to-gel transition temperature of the systems, measured by

rheological measurements or vial tilting, was observed with increasing drug loading as reported for systems made of PLGA-PEG-PLGA loaded with docetaxel [128], PEGylated-camptothecin [146] as well as that of paclitaxel in systems composed of sulfamethazine-capped PCLA-PEG-PCLA copolymers [147].

## 3.5. In vitro release and degradation of celecoxib-loaded gels.

Degradation and release behavior of PCLA-PEG-PCLA 25% wt gels with or without celecoxib (1.25 mg/g) was investigated at 37 °C in PBS buffer (pH 7.4) in the absence and presence of Tween® 80 (to ensure sink conditions for celecoxib; solubility of celecoxib in buffer without Tween® 80 was <1 μg/ml while addition of 0.2% Tween® 80 increased it to 500 μg/ml). Degradation of gels without celecoxib and with 1.25 mg celecoxib/g loaded gels in the presence of Tween® 80 as well as that of 1.25 mg/g celecoxib-loaded gels in the absence of Tween® 80 started after a lag time of ~10 days in a sustained manner over ~100 days (figure S5A in the supportive information). Hence, no difference in gel degradation behavior in the presence and absence Tween® 80 was observed. The *M*n of the polymer of the residual gels did not change in time (figure S4B in the supportive information). This shows that the *in vitro* degradation of the gels loaded with 1.25 mg/g celecoxib was not affected by the celecoxib load and occurred *via* polymer dissolution, in line with previous data [80]. Hence, Tween® 80 is not required to solubilize celecoxib (and respect sink conditions) during the *in vitro* release experiments. Previously, we reported [58] that the gels in PBS first swelled (lag time in dissolution) to reach <20% wt polymer content and thereafter start to dissolve. However, no swelling was observed in PBS containing Tween. This makes the lag time in dissolution difficult to explain and warrants further research, but is likely linked to disentanglement of the polymer chains. The release of celecoxib started after the lag time of ~10 days (figure 4A), after which, a sustained release was maintained until day 75, where it reached a plateau at 40% of the loaded amount. The chromatograms of the samples showed an injection peak with high absorption at 254 nm, which is hypothesized as a peak corresponding to micelles/gel particles loaded with celecoxib. Full recovery of celecoxib was achieved only after dilution of the release samples with ACN, which likely led to the disassembly of the celecoxib-loaded micelles present in the samples. This might be linked to the fact that gels made of triblock copolymers release (flower-like) micelles loaded with drug as reported previously [148].

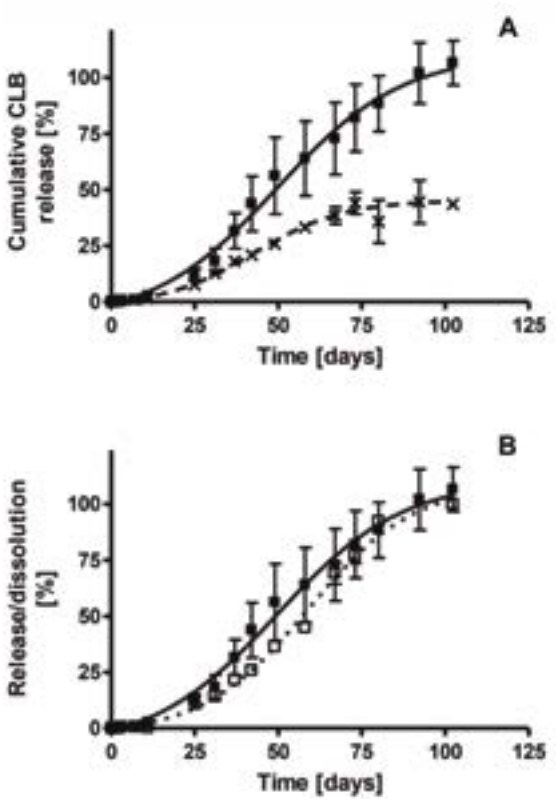


***Figure 4.*** *Release and degradation behavior (*n = *6) of PCLA-PEG-PCLA 25% wt gels loaded with 1.25 mg celecoxib/g gel at 37 °C in the presence of Tween® 80 (0.2% wt). 4A shows celecoxib release before (crosses) and after (closed squares) dilution of the release samples with acetonitrile. 4B shows celecoxib release (closed symbols) and polymer dissolution (open symbols).*

In line with the release of celecoxib-loaded micelles, the release of celecoxib followed the polymer dissolution (figure 4B), demonstrating that celecoxib release was mediated by polymer dissolution as earlier reported for other temperature-responsive gelling systems based on amphiphilic copolymers, loaded with hydrophobic drugs like paclitaxel [123, 148, 149] and indomethacin [150]. The observed release lag phase might be due to the high solubility of celecoxib in the gels (50 mg/g) compared to its solubility in Tween® (~50 μg/ml).

## 3.6. Effect of the celecoxib loading on its release from PCLA-PEG-PCLA 25 wt% gels

The release of celecoxib from PCLA-PEG-PCLA 25% wt gels with different celecoxib loadings in the presence of Tween® 80 is shown in figure 5A. Independent of the drug

loading, the release started after a lag phase of ~10 days, after which the drug was released in a sustained manner to reach 100% release at day 75–100, depending on the drug loading. Dissolution time of the gels increased from 75 days for gels loaded with 0.125 mg/g to 100 days for gels loaded with 1.25 mg/g and 50 mg/g (figure 5B). This observation suggests that celecoxib affects gel stability, which can be ascribed to the hydrophobicity of the celecoxib and its interactions with PCLA-PEG-PCLA, thereby influencing the mechanical integrity of the gel (figure 3). The effect of loading on the release of drugs from temperature-responsive systems has been reported in other studies and is controversial [123, 147, 150, 151]. No effect of drug loading on the release of paclitaxel from PLGA-PEG-PLGA systems (loading up to 20 mg/g) was reported [123] as well as from sulfamethazine-capped PCLA-PEG-PCLA hydrogels (loading up to 10 mg/g)[147]. However, PLGA-PEG-PLGA systems showed longer release periods with increasing drug loading of docetaxel [128] and bee venom peptide (up to 8 mg/g) [150]. Finally, faster release of salmon calcitonin was observed from PEG-PLGA-PEG gels with increasing loading (loading up to 5 mg/g) [151].

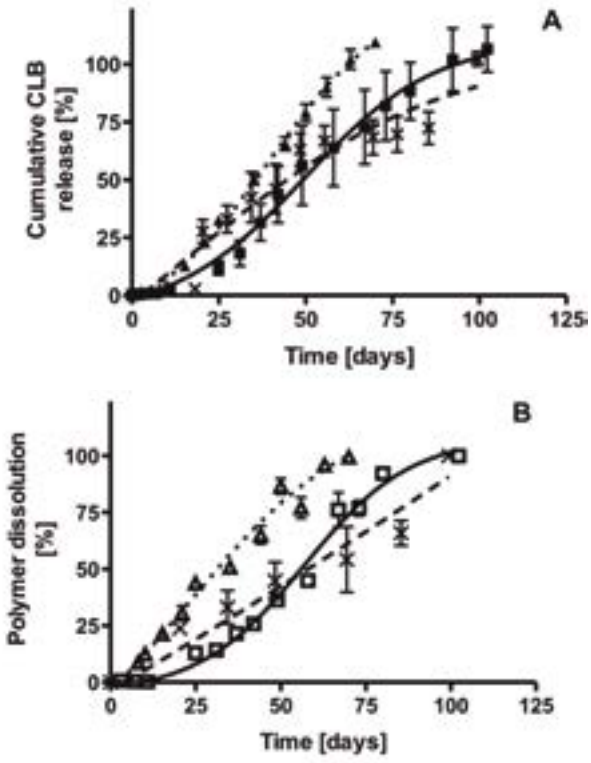


***Figure 5.*** *Release and degradation behavior (*n = *6) of PCLA-PEG-PCLA 25% wt gels loaded with 0.125 (triangles), 1.25 mg/g (squares) and 50 mg/g (crosses) at 37 °C. 5A shows celecoxib release after dilution of the release samples with acetonitrile. 5B shows polymer dissolution in the presence of Tween® 80 (0.2% wt).*

## 3.7 *In vivo* pharmacokinetics of 20 % wt gels containing 50 mg/g celecoxib

The designed gel is aimed for local release of celecoxib in the knee while minimizing the systemic exposure. However, the small total volume of synovial fluid in rat knees (<50 µl) does not allowed for synovial fluid sampling after intra-articular administration in order to monitor local pharmacokinetics. Therefore, the serum levels acquired from rats with subcutaneous administration of the gel with the highest celecoxib loading (50 mg/g) were utilized to gather insight in the *in vivo* duration and kinetics of celecoxib release from the gel. Figure 6 shows the serum concentration of celecoxib in time after subcutaneous injection of 500 µl 20% PCLA-PEG-PCLA containing 50 mg/g celecoxib, with a *C*max of 705 ± 322 ng/ml after 8 h. After 24 h, celecoxib concentrations dropped to 278 ± 103 ng/ml and from day 3, a continuous and sustained drug release was observed with average serum concentrations between 5 and 80 ng/ml for a period of 4–8 weeks after injection. 4 out of the 6 animals still showed measurable celecoxib serum concentrations at the end of the experiment (8 weeks). Total area under the curve (AUC) was 2565 ± 396 (ng × d/ml) with the initial peak in the first day accounting for 17% and the peak of the first 3 days for 30% of the total release, meaning that around 70–80% of the dose was released in a sustained mode over 4–8 weeks.

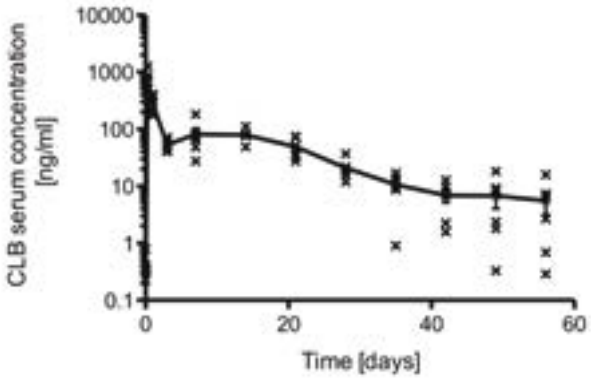


***Figure 6.*** *In vivo release of celecoxib from 20% wt gels with 50 mg celecoxib per g gel. The serum concentrations of celecoxib after injection of 500 µl subcutaneously in rats are shown. Each dot represents the individual measurements; error bars represents standard error of the mean (*n = *6).*

*In vivo*, no lag time of celecoxib release from the gel was observed, in contrast to what was observed *in vitro*, where the lag time was linked to a gel dissolution lag time (see figure 4). In our previously conducted experiment using unloaded gel (500 µl) of similar composition, the same difference was observed with the absence of an *in vivo* lag time, while *in vitro* this was present [122]. Another observation is the significantly faster release *in vivo* compared to *in vitro* for both the previously conducted experiments [122]

and the celecoxib-loaded gels of the current study. Non-linearity of level A *in vitro*/*in vivo* correlations (IVIVCs) was addressed by Dunne and coworkers [152] and is likely explained by the complex phenomena that govern release and absorption *in vivo* compared to *in vitro* models. The absence of an *in vivo* lag phase might be due to the enhanced celecoxib solubility in biological fluids likely caused by the relatively high protein binding of celecoxib [111, 153, 154]. Differences in gel degradation kinetics were shown to be influenced by the *in vivo* presence of macrophages as well as differences in gel depot geometry with a larger surface area and therefore multi-directional diffusion of the gels *in vi*vo [122, 155, 156]

## 3.9. Intra-articular biocompatibility of 25 % wt gels containing 50 mg/g celecoxib

In a previous study, we have shown good intra-articular biocompatibility of unloaded PCLA-PEG-PCLA 25% wt gels [122]. Now, we want to show that loading these gels with the highest amount of celecoxib does not jeopardize this biocompatibility. This formulation is representative for the lower celecoxib/PCLA-PEG-PCLA ratios as well, and by showing the combination of highest amount of polymer (25% wt) with the highest celecoxib loading (50 mg/g) does not harm the injected joint, we can conclude that the other formulations would also be safe. Healthy knees ($n$ = 5) of 16-wk old Wistar rats were injected with 50 µl gel of high polymer content (25% wt) containing 50 mg/g celecoxib, while the contralateral knees of these rats served as a control (50 µl saline injection). During the entire follow-up period, no clinical signs of a toxic response, such as joint redness/swelling or changed locomotion occurred. The EPIC-µCT (figure A&B) of these 5 rats showed significantly ($p$ = 0.025) thicker cartilage in the lateral compartment of celecoxib-loaded gel injected knees compared to saline (230 ± 13 vs. 205 ± 12 µm), with no difference in attenuation (70.7 ± 1.5 vs. 71.2 ± 1.1). Medially, the celecoxib-loaded gel injected knees showed significantly ($p$ = 0.033) higher attenuation values, indicating a lower amount of sGAGs, compared to saline injected knees (69.3 ± 1.3 vs. 65.6 ± 2.5) while no significant difference in thickness was present (276 ± 17 vs. 301 ± 17 µm).

All values of healthy knees injected with either saline or celecoxib-loaded gel remained within the range of what is normally seen in healthy cartilage [136]. It should be noticed that due to the high sensitivity of EPIC-µCT very subtle differences in cartilage quality and quantity that would have remained unnoticed when using less quantitative techniques like histology, are picked up. To better understand the clinical relevance of our values, we compared them to what was found earlier for knees in which osteoarthritis was induced [136]. These osteoarthritic knees indeed showed significantly ($p$ < 0.01) worse attenuation and cartilage thickness values for both compartments, with

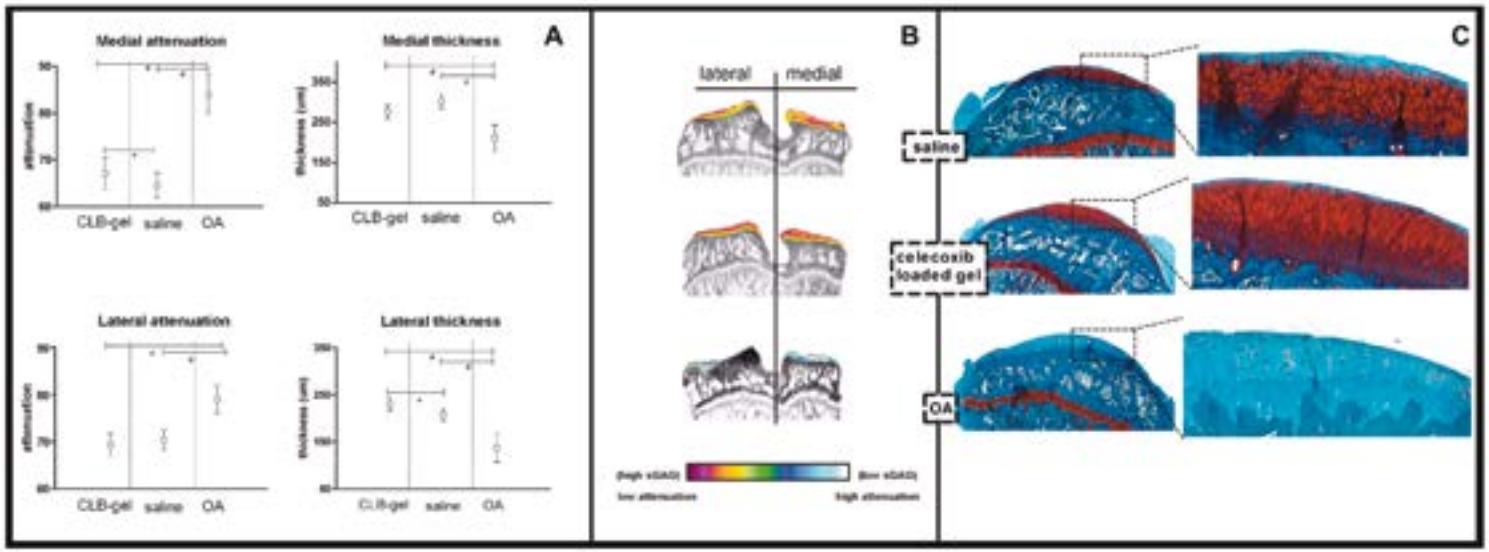


***Figure 7.*** *Intra-articular biocompatibility of celecoxib-loaded gel (50 mg/g; 50 µl).* ***A*** *shows the thickness and attenuation of both the medial and lateral tibial plateau of the different groups (celecoxib-gel* (n = 5)*, saline injected* (n = 5)*, OA* (n = 9)*) measured by EPIC-µCT 12 weeks after intra-articular injection of either celecoxib-loaded gel, saline of papain (OA). *significant difference* ($p < 0.05$) *between celecoxib-loaded gel and saline injection (paired t-test); #significant difference* ($p < 0.05$) *between saline or celecoxib loaded gel injection and OA model (unpaired t-test).* ***B*** *shows representative EPIC-µCT images of the three different groups.* ***C*** *shows representative sagital histological images of the knees of the three different groups stained with Saf-O directly following the EPIC-µCT. The findings of EPIC-µCT are supported by the histology, since for both saline and gel-injected knees the cartilage stains red, indicating healthy GAG-rich cartilage whereas the osteoarthritic knee shows almost fully GAG-depleted cartilage.*

(respectively medial and lateral) attenuation values of 84.1 ± 4.1 and 79.0 ± 3.0 and cartilage thickness of 211 ± 33 and 137 ± 29 μm.
Our findings of *in vivo* and EPIC scanning were supported by histology (representative images are shown in figure 7C). No differences in safranin O staining (the presence of sGAGs in the cartilage is indicated by the red color (in web version)) were seen between knees injected with celecoxib-loaded gel and the saline control. Also, both saline and celecoxib-loaded gel injected knees did not show structural changes (e.g., clefts or fissures) of the cartilage. Figure 7C also shows an osteoarthritic (OA) knee and in agreement with the results on *in vivo* μCT and EPIC scanning, the cartilage is almost fully depleted of sGAGs.

Since bone changes are also a feature of osteoarthritis [10], scans were inspected for bone changes in terms of osteophyte formation. Neither in the saline injected knees, nor the knees injected with celecoxib-loaded gel these changes occurred. Histologically, also no bone changes were seen.
The findings on both cartilage and bone show that celecoxib-loaded PCLA-PEG-PCLA 25% wt gel is safe for intra-articular use. A next step will be to apply these celecoxib-loaded gels in an osteoarthritis model in order to achieve positive treatment effects in these joints.

## 4. Conclusions

Acetyl-capped PCLA-PEG-PCLA based gels show good potential as a drug delivery system for the sustained and local release of celecoxib with desirable release kinetics (*in vitro* as well as *in vivo*) and intra-articular biocompatibility. Therefore, this drug delivery system has great potential in the field of orthopedics, especially for the local treatment of osteoarthritis.

## Acknowlegdment

Mike de Leeuw and Dr. Theo Flipsen are gratefully acknowledged for their support and valuable discussions. Jan Wever (Polyvation BV) is thanked for carrying out the GPC measurements. This work is part of the BMM/Term program (Project P2.02) and the Dutch Ministry of Economic Affairs is thanked for the financial support.

## Supplementary data

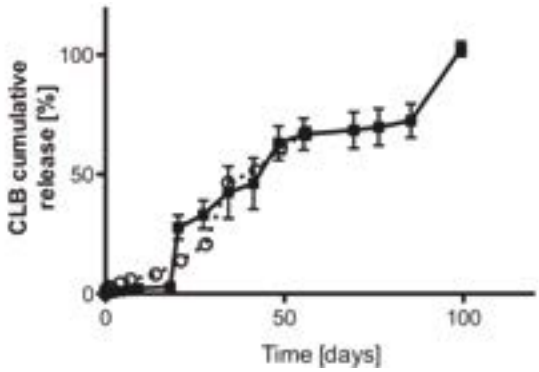


***Figure S1.*** *Release (*n *= 3) of PCLA-PEG-PCLA 25 wt% gels (closed squares) and 20 wt% gels (open circles) loaded with 50 mg celecoxib/g gel at 37 °C in the presence of Tween® 80 (0.2 wt%).*

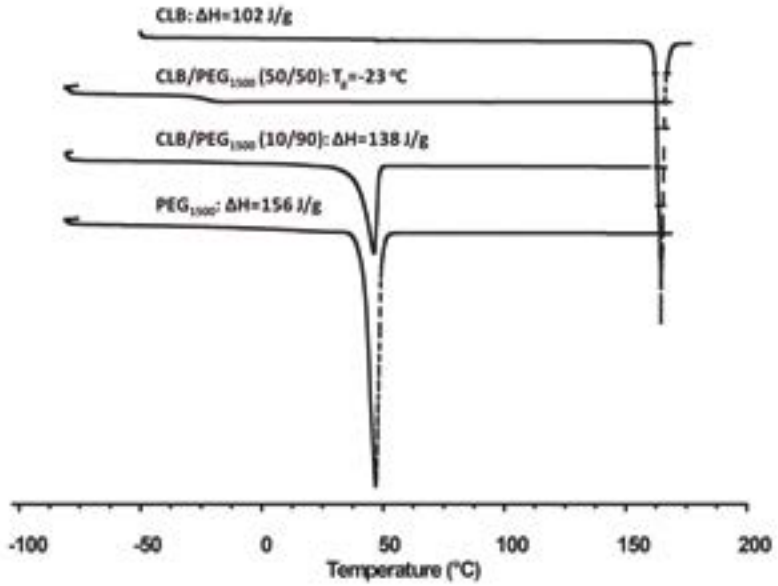


***Figure S2.*** *DSC thermograms of $PEG_{1500}$, celecoxib and their mixtures (second heating).*

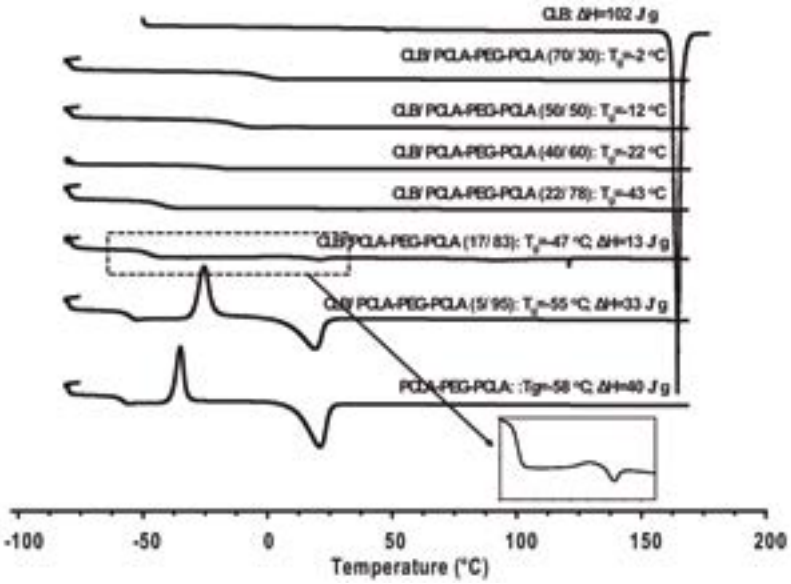


***Figure S3.*** *DSC thermograms of acetyl-capped PCLA-PEG-PCLA, celecoxib and their mixtures (second heating). The insert shows the thermograms of celecoxib/PCLA-PEG-PCLA mixture (17/83 w/w) between −60 and +50 °C.*

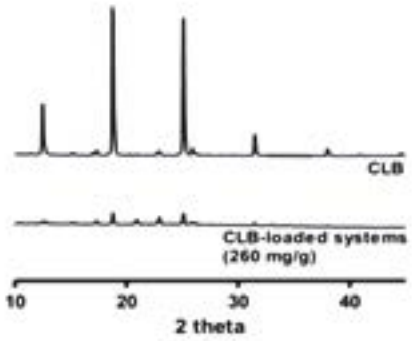


***Figure S4.*** *X-ray diffraction pattern of celecoxib and a representative sample at 260 mg/g celecoxib containing celecoxib crystals.*

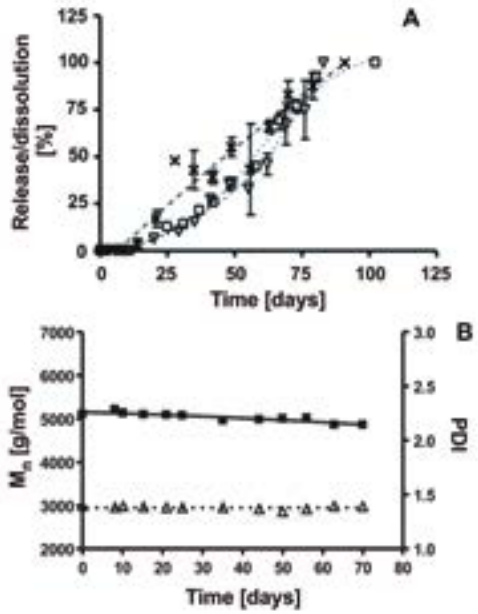


***Figure S5.*** *Effect of Tween® 80 and celecoxib on the degradation of PCLA-PEG-PCLA gels.* ***A*** *shows dissolution rate of the polymers from the gels without celecoxib (crosses) in the presence of Tween® 80 as well as that of gels with 1.25 mg/g celecoxib in the presence of Tween® 80 (squares) and in the absence of Tween® 80 (triangles).* ***B*** *shows the* $M_n$ *(squares) and PDI (triangles) of the polymers in the residual acetylated PCLA-PEG-PCLA gels loaded with 1.25 mg/g celecoxib in the presence of Tween® 80 as determined by GPC.*


4

# Chapter 4

## *In Vivo* Pharmacokinetics of Celecoxib Loaded Endcapped PCLA-PEG-PCLA Thermogels in Rats after Subcutaneous Administration.

Maria J Sandker, Paul M. van Midwoud, Wim E. Hennink, Leo G.J. de Leede, Alan Chan, Harrie Weinans.

*Eur J Pharm Biopharm. 2018 Jul 31; pii: S0939-6411(18)30655-6*

## Abstract

Injectable thermogels based on poly(ε-caprolactone-co-lactide)-b-poly(ethylene glycol)-b-poly(ε-caprolactone-co-lactide) (PCLA-PEG-PCLA) containing an acetyl- or propyl endcap and loaded with celecoxib were developed for local drug release. The aim of this study was to determine the effects of the composition of the celecoxib/PCLA-PEG-PCLA formulation on their *in vivo* drug release characteristics. Furthermore, we want to obtain insight into the *in vitro-in vivo* correlation. Different formulations were injected subcutaneously in rats and blood samples were taken for a period of 8 weeks. Celecoxib half-life in blood increased from 5 h for the bolus injection of celecoxib to more than 10 days for the slowest releasing gel formulation. Sustained release of celecoxib was obtained for at least 8 weeks after subcutaneous administration. The release period was prolonged from 3-6 weeks to 8 weeks by increasing the injected volume from 100 to 500 μL, which also led to higher serum concentrations in time. Propyl endcapping of the polymer also led to a prolonged release compared to the acetyl endcapped polymer (49 versus 21 days) and at equal injected dose of the drug in lower serum concentrations. Increasing the celecoxib loading from 10 mg/mL to 50 mg/mL surprisingly led to prolonged release (28 versus 56 days) as well as higher serum concentrations per time point, even when corrected for the higher dose applied. The *in vivo* release was about twice as fast compared to the *in vitro* release for all formulations. Imaging of organs of mice, harvested 15 weeks after subcutaneous injection with polymer solution loaded with infrared-780 labelled dye showed no accumulation in any of these harvested organs except for traces in the kidneys, indicating renal clearance. Due to its simplicity and versatility, this drug delivery system has great potential for designing an injectable to locally treat osteoarthritis, and to enable tuning the gel to meet patient-specific needs.

# I. Introduction

Celecoxib is a non-steroidal anti-inflammatory drug (NSAID) and a selective inhibitor of cyclo-oxygenase-2 (COX-2) [157]. Celecoxib is taken orally once or twice a day in pain management, for instance, by patients with osteoarthritis [111]. To reach local therapeutic concentrations, high daily dosing is necessary due to the low oral availability and the fact that only a small portion of the administered dose reaches the inflamed joints. Celecoxib is 97% protein bound, with a large apparent volume of distribution (> 1 L/kg), suggesting extensive distribution into tissues [111, 139]. High systemic concentrations are unwanted since concerns have risen about the toxicity of celecoxib, for instance in myocardial function [115]. The best option to decrease the risk of systemic side-effects is through local administration of the drug in the target tissue. Direct intra-articular injection of a drug in patients with osteoarthritis is not desirable due to rapid intra-articular drug wash-out combined with the fact that repeated intra-articular injections are not patient friendly and pose a potential risk of infection [158]. Therefore, research has been focused on the development of injectable drug delivery systems based on hydrogels with a well-controlled and sustained release [36, 92, 159-164]. We have previously shown in a relevant animal model that acetyl endcapped poly(ε-caprolactone-co-lactide)-poly(ethylene glycol)-poly (ε-caprolactone-co-lactide) (PCLA-PEG-PCLA) based thermoreversible hydrogels have excellent potential for the local release of celecoxib with sustained *in vivo* release kinetics of 4–8 weeks. In addition, good biocompatibility after both subcutaneous and intra-articular administration was observed [165, 166]. Recently, intradiscal injections of PCLA- PEG-PCLA hydrogels loaded with celecoxib were performed in ten client-owned dogs with chronic low back pain, of which 9 out of 10 dogs showed clinical improvement [167].

These PCLA-PEG-PCLA hydrogels are very interesting for different applications, since release kinetics of these polymer systems are likely tunable by changing multiple factors. Firstly, the volume of injected gel and thus the therapeutic dose can be altered. Secondly, the polymer concentration in the formulation can be changed, which leads to variation in network density of the gel, thereby influencing the release kinetics. Thirdly, the capping group of hydroxyl ends of the tri-block copolymer can be altered, resulting in different release characteristics. As a last factor, the amount of the drug in the formulation can be changed. Indeed, in a previous study we demonstrated that increasing the celecoxib concentration resulted in longer *in vitro* releases [165]. The chosen animal model was the rat model, due to the extensive information available of oral administration of celecoxib in rats, and to be able to compare the obtained results with other studies [153, 168].

The primary aim of this study was to determine the effects of the injection volume of the formulation, polymer concentration and capping group of celecoxib/PCLA-PEG-PCLA formulations on the *in vivo* drug release. The second aim of the present study was

to get insight into the relation between the *in vitro* and *in vivo* release characteristics of the formulations.

## 2. Materials and methods

### 2.1. Materials

Celecoxib was obtained from LC Laboratories, USA. All other chemicals were obtained from Sigma Aldrich.

### 2.2. Synthesis of acetyl- and propyl endcapped PCLA-PEG-PCLA

The acetyl- and propyl endcapped PCLA-PEG-PCLA triblock copolymers used in this study were synthesized and characterized as described previously [58]. In short, a three-neck round-bottom flask equipped with a Dean Stark trap and a condenser was used. PEG1500, L- lactide, ε-caprolactone and toluene were introduced and, while stirring, heated to reflux (~140 °C) under a nitrogen atmosphere. The Dean stark apparatus was used in azeotropic drying by distillation of toluene/ water (ca. 50% volume of the initial volume). Next, the solution was cooled down to < 80 °C and tin(II) 2-ethylhexanoate was added. Ring- opening polymerization was carried out at 110–120 °C overnight under a nitrogen atmosphere. The solution was cooled down to room temperature and dichloromethane and triethylamine were added. Subsequently, the solution was cooled to 0 °C in an ice bath, and while stirring, an excess of acetyl chloride or propyl chloride (depending on the required endcap) was added dropwise and acylation/propylation was allowed to proceed for three hours. Next, dichloromethane was removed under vacuum at 60–65 °C, ethyl acetate was subsequently added and triethylamine hydrochloride salts were removed by filtration. The polymer was precipitated by adding a 1:1 mixture of pentane and diethyl ether. Upon storage at –20 °C, the polymer separated as a waxy solid from which non-solvents containing unreacted monomers and the excess of acyl chloride could be decanted easily. The precipitated polymer was dried under vacuum and obtained in yield of 85%. The polymer was characterized by $^{1}$H NMR and GPC, as described previously [80].

### 2.3. Preparation of PCLA-PEG-PCLA celecoxib formulations

The formulations were prepared by mixing 5 g of PCLA-PEG-PCLA with 20 mL PBS buffer (43 mM Na2HPO4, 9 mM NaH2PO4, 75 mM NaCl; pH 7.4, 280 mOsm/kg) (20% formulation) or 5 g of PCLA-PEG-PCLA with 15 mL PBS buffer (25%). Celecoxib was added to these formulations at a final concentration of 10 or 50 mg/mL. Since autoclaving has no negative effect on the formulations, all formulations were

autoclaved for 15 min at 121 °C [166]. After cooling down to approximately 40 °C, the mixtures were vortexed for 2 min and subsequently incubated at 4 °C for 48 h to allow formation of homogeneous polymer solutions. Rheological analysis of 300 µL of the polymer solutions was determined as described previously [165]. An overview of the formulations prepared for this study is given in Table 1.

***Table 1.*** *Description of the different formulations used for in vivo studies.*

| Formulation | Endcapping | Injected volume (µL) | Celecoxib concentration (mg/mL) | Celecoxib dose (mg) | Polymer concentration in PBS (% w/w) |
|---|---|---|---|---|---|
| A | Acetyl | 500 | 10 | 5 | 25 |
| B | Acetyl | 100 | 50 | 5 | 20 |
| C | Acetyl | 500 | 50 | 25 | 20 |
| D | Acetyl | 500 | 10 | 5 | 20 |
| E | Propyl | 500 | 10 | 5 | 20 |



## 2.4. *In vivo* celecoxib release

The Animal Ethics Committee of the Erasmus Medical Center, Rotterdam, The Netherlands, approved all conducted procedures (agreement number EMC2255(116-11-02)). It was previously shown that there is a gender difference in the pharmacokinetics of celecoxib in rats, with celecoxib being eliminated from the plasma 4-times faster in males compared to females [168]. Only male rats were used in our study. Fourteen-week-old (400–450g) male Wistar rats (Charles River Nederland BV, Maastricht, The Netherlands) were housed in the animal facility of the Erasmus Medical Center, with a 12-h light-dark regime, at 21 °C. Animals were fed standard food pellets and water ad libitum. Experiments started after an acclimatization period of 2 weeks. To investigate the pharmacokinetics of the different PCLA-PEG-PCLA/celecoxib formulations, rats (6 animals per group (5 groups in total)) were injected subcutaneously in the neck region with aseptically prepared and autoclaved PCLA-PEG-PCLA formulations as described in Table 1.

As a control for absolute bioavailability and determination of the elimination half-life of celecoxib, nine rats received an intravenous bolus injection of 200µL celecoxib. Since the aqueous solubility of celecoxib is limited, it was dissolved in polyethylene glycol (PEG) 400:water in a 2:1 ratio (w/v) in a concentration of 10 mg/mL as described before by Paulson *et al.*[168]. At predetermined time points between 0 and 56 days, blood samples (500µL) were taken from the lateral tail vein and collected in Vacutainer SSTTM II Advance (BD Plymouth) tubes that contained silica (clot activator). After spinning down the cells (3500 rpm, 10 min), celecoxib was extracted from the serum

using ethyl acetate [166]. In total, 100 µL serum was mixed with 100 µL internal standard (200 ng/ mL parecoxib in 5% BSA). Then, 200 µL 0.1 M sodium acetate buffer (pH 5.0) was added, followed by ethyl acetate (1 mL) and the samples were vortexed for 10 min. Subsequently, samples were centrifuged at 11,000 rpm for 10 min and stored at –80 °C for 30 min. The upper ethyl acetate phase was transferred into HPLC glass vials and evaporated under nitrogen atmosphere. Next, the residues were dissolved in 100 µL of methanol and celecoxib concentration in the samples was analyzed by LC-MS. Per sample, 5µL was injected onto a Kinetex® C18 (30 * 3.0 mm, particle size of 2.6 µm) analytical column (Phenomenex, Utrecht, NL). Separation was performed at a flow rate of 500 µL/min, with a total run time of 3 min. The mobile phases consisted of acetonitrile/ water (1/1 v/v) (A), and acetonitrile/methanol (1/1 v/v) (B). Samples were separated using the following gradient A/Bv/v: 0–0.6 min, 100/0; 0.6–0.7 min, 100/0–30/70; 0.7–1.6 min, 30/70–0/ 100; 1.6–2.4 min, 0/100; 2.4–2.7 min, 0/100–100/0; 2.7–3.0 min, 100/ 0. Column temperature was set at 40 °C. The column effluent was introduced by an atmospheric pressure chemical ionization (APCI) interface (Sciex, Toronto, ON) into an API3000 mass spectrometer. For maximal sensitivity, the mass spectrometer was operated in negative ion multiple-reaction monitoring (MRM) mode. Peaks were identified by comparison of retention time and mass spectra of standards. For each component two ion transitions were monitored, celecoxib: 380.3 → 316.3 and 380.3 → 276.3 (collision energy: –50 V), and parecoxib: 369.3→250.2 and 369.3→234.2 (collision energy: –30V). The following MS parameters were used: nebulizer gas: 10 psi; curtain gas: 10 psi; ion current: –2 µA; source temperature: 500 °C; gas flow 1: 30 psi; gas flow 2: 20 psi: decluster potential: –70 V and entrance potential: –10 V.

## 2.5. Data analysis

LC-MS data were analyzed with Analyst software version 1.4.2 (Applied Biosystems, Nieuwerkerk a/d IJssel, The Netherlands). Celecoxib peak areas were corrected for the parecoxib recovery, and concentrations were calculated using celecoxib standards prepared in rat serum ranging from 0.5 to 1000 ng/mL. The calibration curve was linear in this range (r = 0.9997). Single blood sample data were used to construct the plasma level curves.

The pharmacokinetic characterization of celecoxib was analyzed using PK Solver, Version 2.0, an add-in program for pharmacokinetic and pharmacodynamic data analysis in Microsoft Excel [134]. Non-compartmental modeling was carried out according to conventional pharmacokinetic principles. The fraction released *in vivo* was determined by dividing the total area under the curve (AUC) at different time points by the AUC0-∞.

### 2.6. *In vitro* celecoxib release

Formulations that were subcutaneously injected in rats were also studied for their in vitro release characteristics. In total, 100 or 500 μL formulations were transferred into cell culture tubes (16*100mm) using a syringe. The tubes were incubated for 15 min at 37 °C to allow gel formation. Next, 5 mL PBS buffer (43 mM Na2HPO4, 9 mM NaH2PO4, 75 mM NaCl; pH 7.4, 280 mOsm/kg) with 0.2% w/w Tween® 80 for the lower dose and 1% w/w Tween® 80 for the higher dose was added, and formulations were shaken at 300 RPM. Tween® 80 was added to solubilize the released celecoxib and to maintain sink conditions. At predetermined time points, samples of 2.5 mL were withdrawn and 2.5 mL fresh PBS was added. The celecoxib concentration in the different release samples was determined by LC-UV as described in the Supporting Information. Supplementary data associated with this article can be found, in the online version, at https://doi.org/10.1016/j.ejpb.2018.07.026.



### 2.7. *In vivo* imaging in mice

All experimental procedures for in vivo imaging were approved by the Subcommittee on Research Animal Care at Leiden University Medical Center. Male FVB mice (4–8weeks of age, from the LUMC breeding facility) were used for the experiment. Two mice were injected subcutaneously with 10 μL of a solution containing 20% acetyl end- capped polymer solution loaded with a near-infrared dye (IR-780 iodide). IR-780 iodide was chosen due to its poor aqueous solubility, like celecoxib. The total dose of near-infrared dye was 0.05μg. Fifteen weeks after subcutaneous injection, the mice were sacrificed, dissected, and *ex vivo* scans of the site of injection and all major organs were made to check the redistribution of the dye to the rest of the body.

Fluorescence imaging was performed with an IVIS spectrum animal imaging system (Perkin Elmer/Caliper LifeSciences, Hopkinton, MA). For spectral unmixing, an image cube was collected on the IVIS Spectrum with 18 narrow band emission filters (20 nm bandwidth) that assist in significantly reducing autofluorescence by the spectral scanning of filters and the use of spectral unmixing algorithms. Fluorescence regions were identified and spectrally unmixed using Living Image 4.3.1 software.

## 3. Results and discussion

### 3.1. *In vivo* pharmacokinetics of a single IV bolus injection (4 mg/kg celecoxib)

Intravenous (IV) administration of a single dose of 4mg/kg celecoxib was performed as described previously by Paulson *et al.* [168]. A 200 μL solution of polyethylene glycol 400/saline (2:1, v/v) containing 10 mg/mL CLB was injected to obtain reference serum

samples with different celecoxib concentrations over time and to enable calculation of the relative bioavailability for the SC administered gel formulations. The serum concentration after IV administration is shown in figure 1.

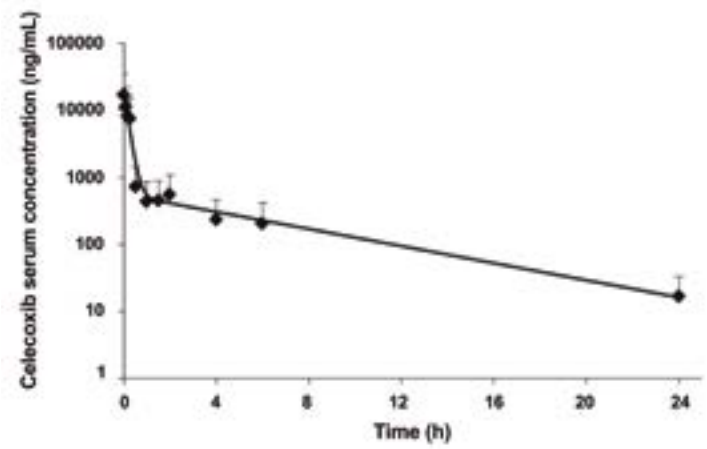


***Figure 1.*** *Celecoxib serum concentrations measured after intravenous injection of 200 µL of 10 mg/mL celecoxib in PEG400/water solution (n=3 per time point, mean ± SEM).*

By definition, the first sampling point after IV administration is the Cmax (10 min after administration), followed by a rapid decline of the serum drug concentration. Twenty-four hours post-injection, the drug concentration was only 0.1% of the Cmax. figure 1 shows that the celecoxib serum concentration versus time plot can be divided in a distribution phase (first two hours) followed by an elimination phase (2–24 h). The $t_{1/2}$-values of the distribution phase (α) and the elimination phase (β) were 0.1 and 4.7 h respectively, which is in line with the results of Paulsen *et al.* (t1/2 = 3.7 h) [168]. The calculated pharmacokinetic values are given in Table 2. The clearance of the drug was 8.6 mL/min/kg (dose/AUC0–∞; 2,000,000 ng/7753 ng/mL * h = 258 mL/hr [=8.6 mL/min/kg]). This value is very close to what was found earlier for clearance of celecoxib in male rats (7.8mL/min/kg [168]). Furthermore, the AUC0-∞ of our reference group (7.8 µg/mL * h) is the same as that found by Paulson *et al.*, 8.6 µg/mL * h (2.15 µg/ml * h for a total dose of 1 mg/kg, while our dose was 4 mg/kg; 4 * 2.15 = 8.6 µg/mL * h). Since our results are very similar to previous pharmacokinetic values obtained in a different study [168], we consider these results consistent and therefore they were used to evaluate the *in vivo* kinetics of the different slow release formulations of Table 1.

***Table 2**. Pharmacokinetic parameters of celecoxib after a single IV administration (2.0 mg dose, 4 mg/kg) in rats.*

| Parameter | Unit | Values |
|---|---|---|
| Dose | mg | 2.0 |
| $t_{1/2}$ Alpha | h | 0.1 |
| $t_{1/2}$ Beta | h | 4.7 |
| $AUC_{0-\infty}$ | ng/mL*h | 7753 |

## 3.2. Effect of polymer concentration of the hydrogel formulation on celecoxib release



Figure 2 shows the serum concentrations of celecoxib after injection of formulation A and D (Table 1). The difference between the two formulations is the polymer concentration (25% versus 20%, respectively). Cmax (150–190 ng/mL) was reached after 1 day, followed by a gradual drop of celecoxib concentration during the next 28 days (from 190 to 0.06 ng/mL). These results show that the injected formulations released the loaded celecoxib during at least 28 days. The results of figures 1 and 2 were used to calculate the bioavailability of celecoxib after SC administration [169]:

Bioavailability = (AUCsc ∗Doseiv)/(AUCiv ∗Dosesc)

It appears that the bioavailability for formulation A and D was 96% and 99% respectively, which demonstrated that the full dose of formulated celecoxib was released and reached the bloodstream during the 4-week period. Half-life ($t_{1/2}$) for both formulation A and D was calculated using PK Solver according to conventional pharmacokinetic principles [134]. Since the rate of decline of the celecoxib serum concentration is not due to elimination alone, but also due to other factors, such as absorption rate and/or distribution rate, the observed half-life is called apparent half-life. An apparent half-life of 4 days (Table 3) was obtained and a sustained release of 28 days was reached for both formulations. No significant differences were observed between the two formulations.
Rheological analysis showed that the storage modulus of the 25% thermogel (220 Pa at 40 °C) was higher than that of the 20% thermogel (166 Pa at 40°C). Therefore, it was anticipated that longer release would be obtained for the 25% polymer formulation compared to the 20% one. However, no differences in the *in vivo* pharmacokinetics were observed. The release of drugs from gels is dependent on the diffusion of the drug through the gel and erosion of the gel. Obviously, the differences in erosion and diffusion between the 20 and 25% gels are not that large.

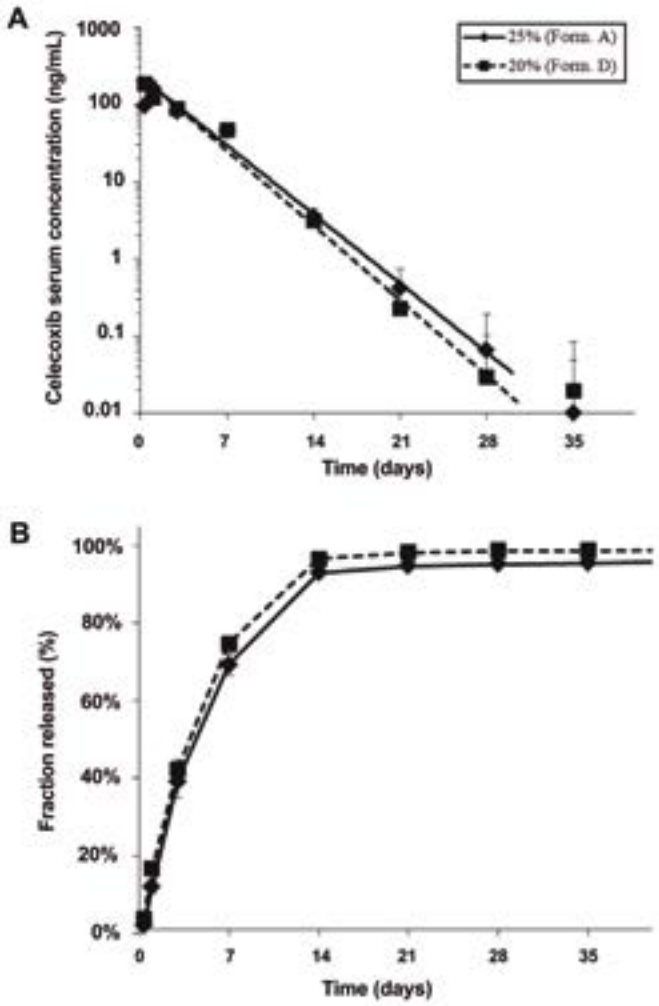


***Figure 2.*** *Effect of polymer concentration of the formulation on in vivo celecoxib release; (**A**) the celecoxib serum concentrations after subcutaneous injection of Formulation A and D (mean ± SEM, n=6) and (**B**) cumulative fraction absorbed/released from Formulation A and D.*

## 3.3. Effect of celecoxib loading of the hydrogel formulation on celecoxib release

The effect of celecoxib loading on the release was determined by comparing a 20% gel containing 10 mg/mL celecoxib (formulation D) with the same gel containing a five-time higher loading (50 mg/mL, formulation C). The injection volume was the same for both formulations. Celecoxib serum concentration after injection of the gel with 10 mg/mL celecoxib led to a Cmax of 186 ± 64 ng/mL 8 h post-injection, while the observed Cmax after administration of the gel with 50 mg/mL celecoxib was 695 ± 322

ng/mL. This means that the Cmax indeed scales, within the experimental error, with the administered dose (Table 3). In case of the 50 mg/mL loading, celecoxib concentrations dropped to 278 ± 103 ng/mL after 24 h and from day 3, a continuous and sustained drug release was observed with average serum concentrations between 80 and 5 ng/mL 4–8 weeks after injection. At week 7 as well as at week 8, 3 out of the 6 animals still showed measurable celecoxib serum concentrations, respectively between 9 and 18 and 6–16 ng/mL. The fact that there is still a fair amount of celecoxib measurable in the serum at the end-point (8 weeks) indicates that a full drug release from the gel was not achieved at this point in time yet.

For formulation C, an initial peak in the 24 h accounted for 17% and the first 3 days for 30% of the total release, after that the dose was released in a sustained mode over the course of 4–8 weeks (figure 3). For formulation D, the initial release after 24 h was 17% and the release in the first 3 days accounted for 43% of the total release, the remaining 60% was released in a sustained mode over 1–4 weeks.

The bioavailability was 99% for formulation D while this was only 64% for formulation C. This means that for formulation C, there is 36% celecoxib "missing". There is no reason to believe that other kinetic properties play a role or that the rest of the celecoxib was excreted in a different way (lymphatic system) without being measured in the bloodstream [74, 170]. Therefore, it is highly likely that this amount is still present subcutaneously and will be released after the 8-week period.

The sustained release period was greatly prolonged by increasing the celecoxib loading in the formulation. The formulation containing 10 mg/mL celecoxib showed a 3 week (21 days) release profile, whereas the formulation containing 50mg/mL celecoxib showed more than 8weeks (56 days) release. Due to the higher dose (50mg/mL and 10 mg/mL represent a total dose of 25 mg versus 5 mg respectively), the serum concentrations were higher, but after 2 weeks the difference in serum concentration was more than 5-times higher, which cannot be explained solely by the higher drug loading. This phenomenon might be explained by celecoxib-polymer interactions.

We have shown previously that with increasing celecoxib loading of the gels, the dissolution time of the gels increased and thus concluded that the celecoxib loading has an effect on the stability of the gel through the hydrophobicity of the celecoxib and its interaction with PCLA-PEG-PCLA [165]. Furthermore, the high amount of encapsulated celecoxib led to the presence of celecoxib in a partly crystallized state within formulation C (50mg/mL), which was not the case for formulation D (10 mg/mL). At a concentration of 10 mg/mL the celecoxib is fully dissolved, and at a celecoxib concentration of 50 mg/mL needle shaped crystals were observed (see figure 4) [166]. It takes time before the crystals dissolve, and therefore the formulation with the fully dissolved drug will release its content faster than the formulation with celecoxib in a partly crystallized state [74].

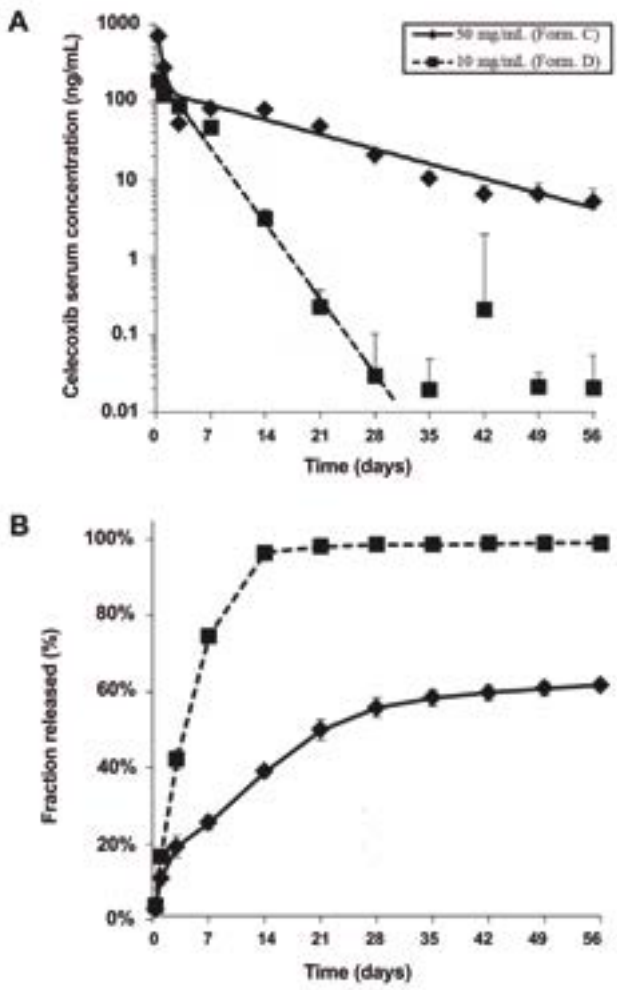


***Figure 3.*** *Effect of celecoxib loading of the formulation (50 mg/mL versus 10 mg/mL) on celecoxib release; (**A**) the celecoxib serum concentrations after subcutaneous injection of Formulation C and D (mean ± SEM, n=6) and (**B**) cumulative fraction absorbed/released from Formulation C and D.*

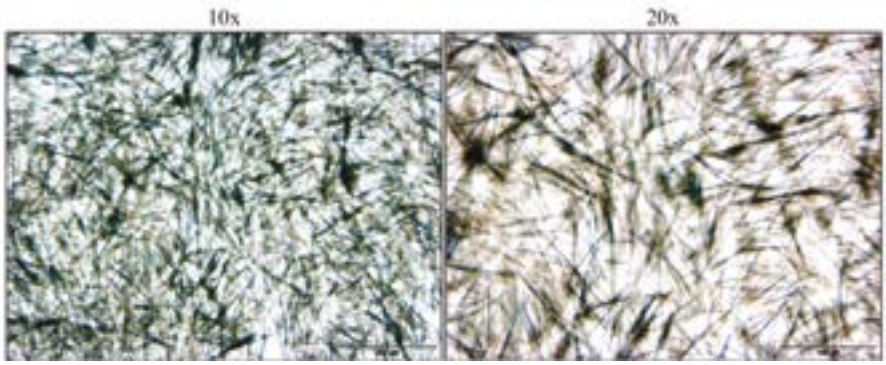


***Figure 4.*** *Microscopic evaluation of formulation C, 20% acetyl endcapped polymer in PBS containing 50 mg/mL celecoxib (magnification 10x and 20x).*



## 3.4. Effect of injected volume

Formulation B and C, which are identical (same polymer, same polymer concentration, and celecoxib concentration) except for the injected volume (100 µL versus 500 µL), were compared for their *in vivo* release characteristics (see figure 5). The injected dose of celecoxib was therefore 5-times higher for formulation C than for formulation B. Due to this dose difference, the Cmax was much higher for formulation C than for B (695 and 206 ng/mL, respectively). The initial release of celecoxib is coming from the outer surface of the depot. As seen by us and by others, hydrogels form a spherical shape when injected subcutaneously [122, 171]. A spherical 500 µL depot has an outer surface of approximately 300 $mm^2$ (radius is ~5 mm) compared to 100 $mm^2$ for a 100 µL depot (radius is ~3 mm). This means that the absolute amount of celecoxib at the outer surface of a 500 µL depot is approximately 3-times higher as compared to a 100µL depot. This 3-fold difference is also observed in the Cmax, of formulation C compared to formulation B (see Table 3).

The apparent serum half-life was prolonged from 7 to 11 days when injecting a 500 µL depot instead of 100 µL. In case of formulation B, the celecoxib concentrations dropped from 205ng/mL to an average of 27 ± 20 ng/mL after 3 days, followed by a continuous and sustained release with average serum concentrations between 4 and 25 ng/mL for 2–6 weeks. For Formulation B, a relative bioavailability of 100% was calculated showing that this composition led to a complete release of the encapsulated celecoxib.

Changing the injected volume did not only have an effect on the serum concentrations per time-point as described above, but also had a direct effect on the release period from the depot; the 500µL formulation C led to a release period of 8 weeks, while injection of 100 µL formulation B led to a sustained release of 3–6 weeks. This difference can also be explained by the larger volume of the depot, since it takes longer for the larger depot

to fully degrade. Consequently, the celecoxib release from the larger depot is prolonged compared to the smaller depot.
As stated before (Section 3.3), the bioavailability of formulation C is only 64% and it is highly likely that the remaining 36% was still present subcutaneously at the 8-week time-point at which the *in vivo* experiments ended. This indicates that the actual release period from formulation C is probably longer than 8 weeks.

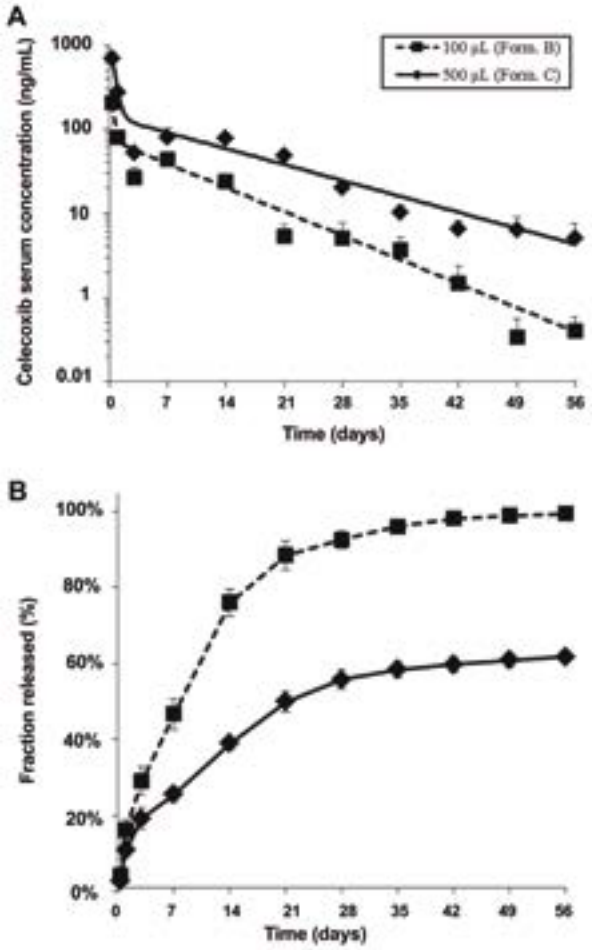


***Figure 5.*** *Effect of injection volume on celecoxib release; (**A**) the celecoxib serum concentrations after subcutaneous injection of Formulation B and C (mean ± SEM, n=6) and (**B**) cumulative fraction absorbed/released from Formulation B and C.*

### 3.5. Effect of polymer type

To determine the effect of a different endcap on the in vivo release kinetics of celecoxib, a formulation was tested where the acetyl-endcap of the PCLA-PEG-PCLA triblock copolymer (Formulation D) was replaced by a propyl group (Formulation E). This propyl group theoretically results in stronger hydrophobic interactions and thereby forming a stronger gel when the temperature is above the gelling temperature (> 28 °C). Both formulations (D and E) showed a ~100% relative bioavailability, whereas the Cmax after administration of formulation E was significantly lower compared to formulation D (94 versus 186 ng/mL (Student's t-test, $p = 0.01$)). In addition to a lower initial release for formulation E, also a more sustained release after 3 days was obtained compared to formulation D (figure 6). After 4 weeks, the serum concentration for formulation E was 5 ± 2 ng/mL while this was almost zero (0.1 ± 0.1 ng/ml) for formulation D. Finally, the propyl encapped polymer showed a sustained release up to 49 days, whereas the acetyl endcapped polymer had a release of only 21 days. This data all points to a stronger gel for formulation E than for D, which can likely be ascribed to the more hydrophobic propyl capping groups which in turn slows down the release of the loaded celecoxib.

Interestingly, at day 21, a celecoxib concentration of 1.2 ng/mL was determined for formulation E in all six rats, whereas this concentration increased to 5.2 ng/mL at day 28. Since the lower concentration at day 21 was determined in all six rats it is unlikely due to an analytical artifact. A plausible explanation of this phenomenon is that there is a biphasic drug release. Up to 21 days, the celecoxib release is diffusion driven, but after these 3 weeks polymer degradation starts to occur, leading to the second phase of celecoxib release [172].

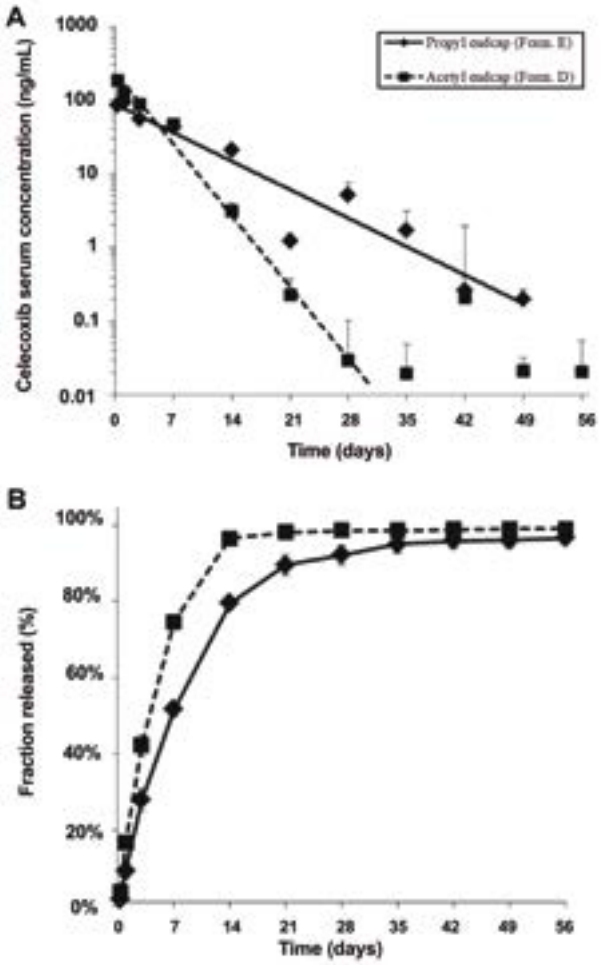


***Figure 6.*** *Effect of polymer type on celecoxib release; (**A**) the celecoxib serum concentrations after subcutaneous injection of Formulation D and E (mean ± SEM, n=6), and (**B**) cumulative fraction absorbed/released from Formulation D and E.*

***Table 3.*** *Pharmacokinetic parameters of celecoxib after subcutaneous administration of different polymer formulations containing celecoxib in rats.*

| | | Formulation | | | | |
|---|---|---|---|---|---|---|
| **Parameter** | | **A** | **B** | **C** | **D** | **E** |
| Dose | mg | 5 | 5 | 25 | 5 | 5 |
| $AUC_{0-\infty}$ | ng/mL*d | 778 | 811 | 2508 | 800 | 792 |
| $t_{1/2}$ | days | 4.1 | 7.3 | 10.6 | 4.0 | 6.9 |
| Cmax | ng/mL | 159 | 205 | 695 | 186 | 94 |
| F | % | 96% | 100% | 64% | 99% | 98% |

*AUC= Area under the curve; $t_{1/2}$= apparent half-life; Cmax= maximum serum concentration; F= biological availability*



## 3.6. *In vitro-in vivo* correlation (IVIVC)

The *in vitro* release characteristics of the formulations of Table 1 are shown in the Supporting Information. The drug release *in vitro* followed the same trends as observed *in vivo*. No differences in release were observed between the formulation with 20% w/w polymer (A) versus 25% w/w polymer (B), while increasing injection volume (100µL versus 500µL; formulation B versus C) led to a prolonged release period. When changing the endcapping from acetyl to propyl, we observed a prolonged release *in vitro* as well as *in vivo*. The same is observed when changing the celecoxib loading from 10 mg/mL (D) to 50 mg/mL (C); the *in vivo* trend of prolonged release was also seen *in vitro*.
For all tested formulations, the *in vivo* release was 2 times faster compared to the *in vitro* situation. As reported previously, this might be due to the presence of enzymes or macrophages at the site of injection resulting in a faster release *in vivo* compared to *in vitro* [74, 173-175]. Although we observed similar trends *in vitro* as *in vivo* with changing the different properties of the gels, no level A correlation was obtained (a point-to-point relationship between in vitro dissolution and the *in vivo* input rate, which is usually linear [176]). In a previous study, we found that *in vitro*, erosion of the gel (acetyl-endcapped) led to the release of celecoxib and the *in vivo* release was faster due to both the gel depot geometry (larger surface area) as well as the *in vivo* presence of macrophages, leading to a faster degradation of the gel and therefore a faster release of the encapsulated celecoxib [122, 165].

## 3.7. *In vivo* imaging of tissue distribution of the subcutaneous injected gel

The distribution of the gel after subcutaneous injection was visualized by injecting a near-infrared dye (IR-780 iodide) loaded formulation (20% acetyl endcapped polymer). The physical properties of IR-780 iodide are different compared to celecoxib, but it is a

lipophilic compound like celecoxib to mimic the encapsulation of lipophilic compounds in the hydrogel. Fifteen weeks after injection, the animal was sacrificed and the organs were harvested and scanned using fluorescence imaging (figure 7).
The scan of the injected subcutaneous area showed that there was still some formulation present 15 weeks post-injection. No accumulation of the formulation was observed in the harvested organs. The only detected signal was coming from the kidneys, which indicates that renal clearance of the formulation as expected is the primary route of excretion as opposed to biliary excretion [168].

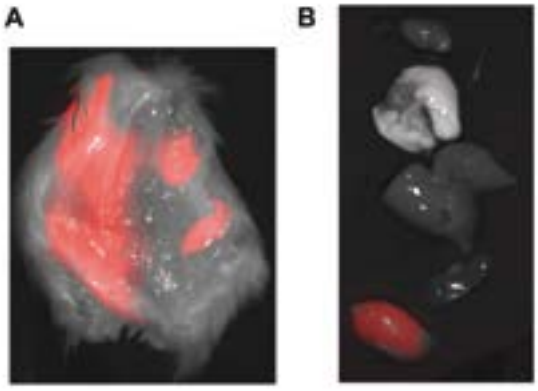


***Figure 7.*** *(**A**) IVIS images of the site of injection and (**B**) the harvested organs 15 weeks after subcutaneous injection.*

## 4. Conclusion

PCLA-PEG-PCLA thermogels loaded with celecoxib show sustained *in vivo* release up to 8 weeks and are therefore an excellent candidate for sustained local drug delivery. The properties of this thermogel-celecoxib formulation can be altered, leading to tunable release profiles. The apparent *in vivo* half-life of celecoxib was extended from 5 h (bolus injection) to more than 10 days. It was shown that the drug release *in vivo* was about two times faster than *in vitro*, which might be due to faster *in vivo* gel degradation due to the presence of enzymes and or macrophages. Tweaking the gel design (endcapping of the polymer, celecoxib loading or injected volume) leads to different release patterns, with even up to over 8 weeks release period. Therefore, it is possible to steer and even personalize the release based on disease- or patient-specific needs.

## Acknowlegdments

This work is part of the BMM/Term program (Project P2.02) and the Dutch Ministry of Economic Affairs is thanked for the financial support. This study was co-sponsored by the Dutch Arthritis Society, ReumaNederland (LLP-12).

## Supporting information

### *In vitro* celecoxib release

Formulations that were subcutaneously injected in rats were also tested on their in vitro release characteristics. In total, 100 or 500 µL samples were transferred into cell culture tubes (16 * 100 mm) using a syringe. The tubes were incubated at 37°C to allow gel formation, 15 minutes later 5 mL PBS buffer, pH 7.4, with 0.2% wt Tween® 80 for the lower dose and 1% wt Tween® 80 for the higher dose was added and formulations were shaken at 300 RPM. Tween® 80 was added to determine sink conditions. At predetermined time points, buffer was refreshed by taken 2.5 mL buffer from the tube and add 2.5 mL fresh PBS. The celecoxib concentration in the different release samples was determined by UHPLC using an Agilent 1290 UHPLC system equipped with a Waters column (BEH C18 1.7 µm, 2.1 * 100 mm). Celecoxib was dissolved in acetonitrile at 1 mg/mL. This celecoxib solution was diluted with 75% acetonitrile and 25% buffer solution containing Tween® 80 to prepare celecoxib standards used for calibration (final celecoxib concentration ranged from 0.05 to 10 µg/mL). Two mobile phases containing 0.1% vol. trifluoroacetic acid (TFA) were used: 95/5/0.1 v/v/v acetonitrile/water/TFA (mobile phase A) and 99.9/0.1 v/v acetonitrile/TFA (mobile phase B), the elution rate was 0.3 mL/min, and the column temperature was 40°C. A gradient was run from 65% mobile phase B to 100% mobile phase B in 3 min and kept at 100% mobile phase B for 1 min before returning to 65% mobile phase B. Detection was performed with an UV detector at 254 nm and the injection volume was 5 µL. The retention time of celecoxib was 1.5 min with a total run time of 8 min (including column equilibration). The autosampler temperature was 8°C. The release samples were diluted 1:3 with 100% acetonitrile (final concentration of 75% acetonitrile) and the gels were 10-times diluted with 75% acetonitrile / 25% water to dissolve the gel.

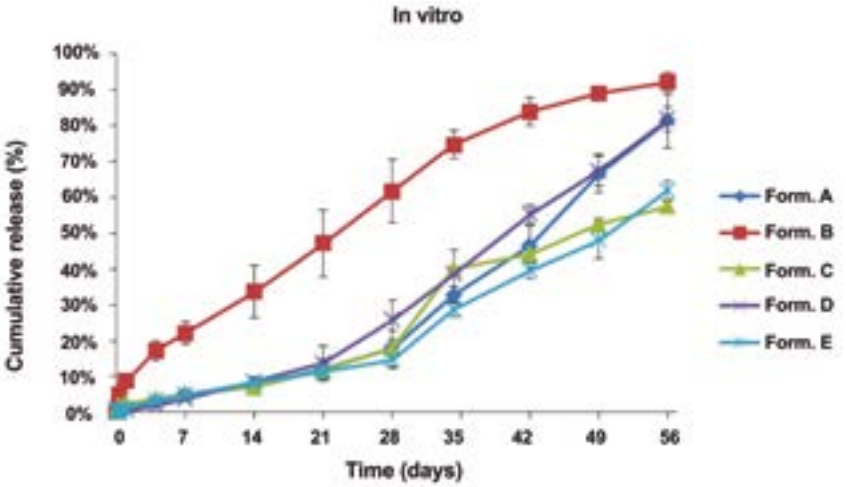


***Figure S1.*** *Cumulative in vitro release of 6 different formulations containing celecoxib (mean ± SD, n=3).*

For formulation A, C, D and E no significant differences were observed for the first three weeks, afterwards different release patters were observed. *In vitro* the release is only from one side (the top) where *in vivo* the release is three dimensional. It is anticipated that the celecoxib release for the first 3 weeks is only due to diffusion and afterwards by degradation/erosion of the gel. No level A correlation was obtained, but the trend seen *in vitro* is similar to *in vivo*. No significant difference between formulation A and D, and for both formulations 80% release after 56 days. Formulation E (with propyl endcap) has a slower *in vitro* release as formulation D (acetyl endcap), only 60% release after 56 days for formulation E and 80% for formulation D. The slowest release was observed for formulation C, only 55% celecoxib release after 56 days. However, when lowering the gel volume from 500 µL to 100 µL (comparing formulation C with B), a much faster *in vitro* release was observed. This was also to be expected since the *in vitro* release is only from the top and by lowering the volume, the thickness of the depot is decreased and for this reason a much faster release was obtained.


5

# Chapter 5

## *In-vivo* efficacy of intra-articular injection of celecoxib-loaded thermoreversible hydrogels in a Rat Model of Osteoarthritis

Maria J Sandker, Paul van Midwoud, Stuart Koelewijn, Erik de Blois, Marion de Jong, Christina Muller, Nicoline M. Korthagen, Michiel Beekhuizen, Laura Creemers, Wim E. Hennink, Harrie Weinans

*Submitted*

## Abstract

We investigated the efficacy of an intra-articular (i.a.) controlled release formulation of celecoxib based on a thermoreversible hydrogel composed of acetyl-capped PCLA-PEG-PCLA triblock copolymer for the treatment of osteoarthritis in a rat model. The target of celecoxib is $PGE_2$, which is directly linked to inflammation and pain in osteoarthritis. First, we proved in an *in vitro* environment, that the celecoxib released from the gel retained its pharmacological activity by suppressing $PGE_2$ release from osteoarthritic chondrocytes during the three-week study duration. Osteoarthritis was induced in the left knee of rats by intra-articular low dose papain injections in combination with a moderate exercise protocol. Two days after induction, the osteoarthritis induced knees were treated with either a single intra-articular injection of celecoxib loaded hydrogel, or an injection of a celecoxib suspension, while the total dose of celecoxib was equal. A third (control) group received one saline injection. All groups experienced pain after induction of osteoarthritis, which was quantified by measuring lower hind limb load distribution at several time-points during the study. However, 5 days after treatment, no signs of pain were detectable in any of the groups, including control animals. The μCT scanning showed that the celecoxib suspension led to more cartilage loss of the lateral compartment (compared to saline control), while this negative effect of celecoxib was abolished by releasing it in a sustained manner from the hydrogel. The hydrogel formulation group also showed significantly more macrophage activity in the affected knee as compared to both the celecoxib suspension group and the control animals (saline), determined by folate SPECT scans. The latter likely indicates the presence of more anti-inflammatory (M2) macrophages in the joints induced by the slow release celecoxib formulation. Although no chondropositive effects of the celecoxib-loaded hydrogel has been shown in this animal model, injection of the formulation proved to be active and superior to injection of the celecoxib suspension. This study demonstrates the potential of this thermoreversible hydrogel drug delivery system for intra-articular use within the context of osteoarthritis.

## 1. Introduction

Osteoarthritis (OA) is a common joint disease and the most prevalent musculoskeletal disorder [59]. The pathogenesis of OA is mainly unknown, but it is likely a combination of different genetic, biochemical and biomechanical factors all leading to a failure of the chondrocytes to maintain cartilage integrity [177]. This failure is initiated by disequilibrium between anabolic and catabolic activities, leading to upregulation of catabolic enzymes (such as matrix metalloproteinases (MMPs) and aggrecanases) and proinflammatory cytokines and mediators such as e.g. IL-1B, TNF-a and $PGE_2$. These factors will eventually give rise to cartilage breakdown, leading to joint degeneration and full progression of OA [4, 5]. Although there are no disease modifying drugs available for OA at present, there are some drugs of interest. One of these drugs is celecoxib, a selective COX-2 inhibitor, a known analgesic which also exhibits anti-inflammatory activities via selective COX-2 inhibition, leading to a decrease of its principal enzymatic product $PGE_2$ [178]. By targeting the inflammation and its catabolic effects, one could possibly slow down the destructive pathway seen in osteoarthritis. However, although promising chondroprotective properties of celecoxib were shown in an *in vitro* environment, *in vivo* results have been less encouraging. Mastbergen *et al.* [113] were able to show promising chondroprotective properties of celecoxib in an *in vitro* environment, *in vivo* these positive results could not be replicated. Dogs with induced OA showed no differences between treatment with oral celecoxib and a placebo [179]. The authors suggest that the beneficial effect of the drug might have been counteracted by an increase in weight-bearing of the diseased joint in the celecoxib group due to the analgesic effects, leading to a progression of the OA. Recently, Fukai *et al.* were not able to show a chondroprotective effect of celecoxib in mice with surgically induced OA. In all these studies, the drug was administered via the oral route. Oral administration of drugs is also the basis of symptomatic treatment of OA in humans [21], but systemic exposure may lead to side-effects and the drug concentration reaching the joint is minimal and therefore potential chondroprotectivity may not be fully displayed. In patients were oral drug administration is not leading to the desired pain relief, intra-articular injections solely targeting the affected joint are usually the next step. These intra-articular injections are widely used in the clinics (corticosteroids, hyaluronic acid), but while multiple injections are often required, they only provide limited effects [23]. This failure is mainly due to rapid efflux of the injected drugs from the joint, providing only short-term pain relief. Jiang *et al.* [180] showed a positive effect of celecoxib injections directly into the joint, but they had to inject on a weekly basis, making the translation to a clinical situation not feasible. To tackle the problem of rapid efflux, different drug delivery systems (DDSs) ensuring sustained IA drug concentrations have been developed [28, 67, 68] and extended IA drug retention times have been demonstrated [25, 181]. Dong *et al.* [30] showed no chondropositive effect of liposomal celecoxib, although there was a slight effect on pain

reduction, lasting for only 24 hours. This very limited effect was likely due to the rapid release of the drug from the liposomes. When combining the celecoxib-liposomes with hyaluronate, the drug release and consequently also pain relief could be extended to 48 hours and also some minor chondropositive effects were found on histology with this combined therapy [30]. A major disadvantage of liposomal formulations is that it is difficult to control the release kinetics of entrapped drugs [182].

Using a DDS with tailored and sustained drug release would, based on these results, very likely lead to more distinct effects in the treatment of OA, both on pain reduction and on ameliorating cartilage destruction. Besides liposomes, another major group of intra-articularly applied DDSs are nano/microspheres-based [68, 183, 184]. Recently, highly concentrated solutions of celecoxib in PEG400 (400 mg/ml) were used as *in situ* forming depots after injection in equine joint cavities [74]. The release from this DDS is governed by crystal dissolution making the release difficult to predict and the presence of crystals could potentially harm the cartilage. Moreover, they did not test this suspension in an OA model to look at therapeutic ability or pain reduction. More recently, a study was presented in which celecoxib loaded PEA (polyester amide) microspheres were injected intra-articularly in rats with surgically induced OA [42, 185]. However, no beneficial (or therapeutic) effects of these microspheres on cartilage were found. Release of the drug *in vivo* was tested indirectly by measuring prostaglandin $E_2$ ($PGE_2$) release, a cytokine that is inhibited by celecoxib [186]. $PGE_2$ release per mg knee homogenate was lower for the group that received celecoxib loaded microspheres compared to unloaded microspheres or saline. However, no control group with freely injected celecoxib (so without the use of a DDS) was included, so whether there is an additional effect of the use of PEA microspheres for intra-articular release of celecoxib compared to just injecting celecoxib directly in the OA joint remains unclear from these results.

In a previous article [122] we demonstrated the biocompatibility and intra-articular degradation kinetics of a PCLA-PEG-PCLA based hydrogel; a novel DDS with favorable properties such as ease of injectability, biocompatibility, and drug release that can be tailored for both duration and concentration. Following these encouraging results, we loaded this gel with celecoxib and showed sustained *in vivo* release of 4~8 weeks (after subcutaneous injection) while showcasing excellent intra-articular biocompatibility [165]. The next step in our research is therefore to evaluate this celecoxib loaded gel in an OA disease model in order to investigate the potential of this DDS for the treatment of OA, not only focusing on structural recovery of cartilage and bone, but also clinical symptoms like pain and inflammation, which is one of the most important aspects of human OA. In this study, we aimed to evaluate the disease modifying effects of celecoxib loaded hydrogels on cartilage and joint macrophage activation, as well as the effects on pain, measured by weight bearing of the affected joint, and mechanical loading.

## 2. Methods and materials

### 2.1. Materials

Celecoxib was obtained from LC Laboratories, USA; TNFα was obtained from Ebioscience. Hexabrix 320®, a clinical iodine-based contrast agent, was obtained from Guerget, The Netherlands. All other chemicals were obtained from Sigma-Aldrich (Saint Louis, USA) and used as received.

### 2.2 Synthesis of acetyl-capped PCLA-PEG-PCLA and celecoxib loaded acetyl-capped PCLA-PEG-PCLA hydrogels

The acetyl- capped PCLA-PEG-PCLA triblock copolymers used in this study was synthesized and characterized as described previously [122]. In short, in a three-neck round-bottom flask equipped with a Dean Stark trap and a condenser, $PEG_{1500}$ (50 g), L-lactide (22 g), ε-caprolactone (88 g) and toluene (150 ml) were introduced and, while stirring, heated to reflux (~140 °C; i.e. the boiling point of the mixture) under a nitrogen atmosphere. The solution was azeotropically dried by distilling off toluene/water (ca. 50 % vol of the initial volume). Next, the solution was cooled down to <80 °C and the catalyst tin(II) 2-ethylhexanoate (5 mmol per mol $PEG_{1500}$) was added. Ring-opening polymerization was carried out at 110-120 °C overnight under a nitrogen atmosphere. The solution was cooled down to room temperature and dichloromethane (100 ml) and triethylamine (6 mol per mol $PEG_{1500}$) were added. Then, the solution was cooled to 0 °C in an ice bath, and while stirring, an excess of acetyl chloride (10 g, ratio acetyl chloride/PEG = 4 mol/mol) was added drop wise and acylation was allowed to proceed for three hours. Next, dichloromethane was removed under vacuum at 60-65 °C, ethyl acetate (100 ml) was subsequently added and triethylamine hydrochloride salts were removed by filtration. The polymer was precipitated by adding a 1:1 mixture of pentane and diethyl ether (290 ml). Upon storage at -20 °C, the polymer separated as a waxy solid from which non-solvents containing unreacted monomers and the excess of acyl chloride could be decanted easily. The precipitated polymer was dried in vacuo and obtained in yield of 85 %. The polymer was characterized by $^1$H NMR and GPC as previously described.

The celecoxib loaded formulations were prepared by mixing 5 g of PCLA-PEG-PCLA polymer with 15 mL PBS buffer (43 mM $Na_2HPO_4$, 9 mM $NaH_2PO_4$, 75 mM NaCl; pH 7.4, 280 mOsm/kg), so the final polymer concentration was 25% w/w Two formulations were prepared by adding celecoxib to the 25% polymer solution. A formulation containing 50 mg/g celecoxib was prepared for the animal study and a formulation containing 1.25 mg/g celecoxib for the cell studies. The formulations were autoclaved for 15 minutes at 121°C, and after cooling down to approximately 40°C the

mixtures were vortexed (2 min) and then incubated at 4°C for 48 h to allow formation of a homogeneous polymer solution.

## 2.3 Cell culture in presence of celecoxib-loaded PCLA-PEG-PCLA hydrogel: cytocompatibility and bioactivity

Anonymous use of redundant tissue for research purposes is part of the standard treatment agreement with patients in the University Medical Center Utrecht [187]. The cell culture experiments were performed as follows; 1 vial of $1x10^6$ Passage 2 chondrocytes from OA patients was defrosted and diluted in 25 ml expansion medium (DMEM 31965 + 10%FCS + pen/strep). Then, 1 ml of cell suspension was added to each bottom compartment of a transwell plate (24 wells) and incubated at 37°C (5% $CO_2$) for 21 days. Chondrocytes, similarly to many other cell types, respond to TNF-α stimulation (a well-known inflammatory stimulus) by producing $PGE_2$ via COX-2. This mechanism can be blocked by specific COX-inhibitors, amongst which celecoxib, leading to reduction of the inflammatory reaction. Four different conditions were tested to evaluate bioactivity (e.g. reduction of $PGE_2$ production) of celecoxib released from PCLA-PEG-PCLA 25 wt% gels: 1) cells + TNFα; 2) cells + TNFα + unloaded gel *(negative control)*; 3) cells + TNFα with a bolus of celecoxib (1.0 μM) *(positive control)*; 4) cells + TNFα with celecoxib loaded PCLA-PEG-PCLA 25% (1.25 mg/g). For the experiments in presence of the gel, 200 μl PCLA-PEG-PCLA in sol state without or with celecoxib (1.25 mg/g, total dose 250 μg) were placed in the transwell inserts (1-μm membrane). The gels were allowed to form for 30 min at 37 °C and washed with 1 ml DMEM in order to remove any leachables. After that, the medium of the cells was refreshed to remove dead cells, and the transwells containing the gel were transferred to the 24 wells plate with the cells. A celecoxib solution, with a final concentration in culture medium of 1.0 μM, was added to the positive control wells during every medium renewal. One hour after addition of the celecoxib solution or the celecoxib-loaded gels, TNFα was added to a final medium concentration of 10 ng/ml and subsequently the plates were placed back in the incubator. Samples were taken every 3 days for a total period of 21 days from each well and stored at -80°C until analysis. To determine released $PGE_2$ by the cells into the medium a prostaglandin E assay was performed (R&D; catalog number KGE004B) according to the protocol. To correct the $PGE_2$ values for total amount of cells per sample the pico-green DNA assay was performed according to the manufacturer's protocol (Quant-iT™ PicoGreen ® dsDNA). After each harvesting time point, the transwells with the gels were transferred into a fresh plate with cells. For the last time points at day 21, 50 μl medium was harvested to perform a lactate dehydrogenase (LDH)-test to check viability of the cells that were incubated with the celecoxib-loaded gel in accordance with the manufacturer's protocol (Roche). The medium sample was mixed with dye solution (1:1) and incubated at room

temperature. After 15 min of incubation, a stop solution was added, and absorbance was read at 490 nm, with a reference filter at 655 nm. Results are presented in arbitrary units (AU).

## 2.4 Animal model

The Animal Ethic committee of the Erasmus Medical Center, Rotterdam, the Netherlands, approved all conducted procedures. Twenty-four 16-week-old (400-450g) male Wistar rats (Charles River Nederlands BV, Maastricht, the Netherlands) were housed in the animal facility of the Erasmus Medical Center, with a 12-h light-dark regimen, at 21°C. Animals were fed standard food pellets and water *ad libitum*. Experiments started after an acclimatization period of 2 weeks. Rats were weighed at the start of the experiment and at the endpoint after 3 weeks.



## 2.5 Induction of osteoarthritis

OA was induced unilaterally in the animals using intra-articular papain injections in the left knee joints (70 µl) in combination with a moderate exercise protocol as described previously. Left knee joints were injected once with a 70 µl solution consisting of 3 units of papain (type IV, double crystallized, 15 units/mg, Sigma-Aldrich, St. Louis, MO, USA) with 5 µL 0.03M L-cystein (Sigma-Aldrich). Contralateral right knees were used as healthy internal controls. The rats ran on a motorized rodent treadmill (LE-8700; Panlab Harvard Apparatus, Barcelona, Spain) during the entire experimental period (3 weeks) for a period of 30 minutes daily at a speed of 0.3 m/s. This protocol is an adjusted version of the one described by Siebelt *et al.* [136] where 3 consecutive injections with 9 papain units were used. We choose to use a less severe protocol, where osteoarthritic changes in cartilage thickness and quality can be found, however bony changes in terms of subchondral plate thickness changes, osteophyte formation and pore formation were not observed. Therefore, in the current study, we focused on the effects on cartilage and not bone. The rationale behind this, is that we did not test a prophylactic drug, but instead we started treatment after OA induction, which is closer to the actual clinical use of a potential treatment for OA, since patients present themselves when they already have symptoms rather than being treated prophylactic. Also, we wanted to be certain that there were no interfering effects between the injected drug and following papain injections within the same joint.

## 2.6 Treatment groups

The 24 rats were randomly divided in 3 groups of 8. They received their treatment 2 days after the start of OA induction via the intra-articular papain injection as described above.
group 1: intra-articular injection of 50 µl of 25wt% gel containing 50 mg/ml celecoxib
group 2: intra-articular injection of 50 µl suspension in saline, containing 50 mg/ml celecoxib
group 3: intra-articular injection of 50 µl saline (untreated)

## 2.7 The effect of celecoxib on hind limb weight distribution (pain assessment)

As a quantitative measurement of pain, hind limb weight distribution was measured using an incapacitance tester (Linton Instrumentation, Norfolk, UK) as described previously [188]. Therefore, all rats of the 3 treatment groups were placed on the incapacitance tester in a position with both hind limbs on two separate force plates. The force on each plate (in grams) was measured over a period of 3 seconds in which the rat did not move. Measurements were conducted five times subsequently during measurement days and these 5 measurements were used to calculate the weight on the affected limb as a percentage of total weight distributed by both hind limbs. The first measurement took place to check baseline values (-2 days), directly after these measurements the left knees were injected with papain to start the OA induction. After two days, the second measurements took place to verify the effect of OA induction before starting the different treatments. Directly following this second measurement, the rats were treated according to the different treatment groups presented in paragraph 2.6. After starting the treatment, measurements were done at 2, 5, 12, 16 and 19 days after the first treatment. Hence, day 0 is considered the first treatment day.

## 2.10 Measurements of therapeutic effect of celecoxib on tissue level

*EPIC imaging:* At end point, the rats were killed and the knee joints were dissected into femur, tibia and patella with removal of the surrounding soft tissue. These samples were incubated for 24 hr in 40% Hexabrix solution (Hexabrix 320, Mallinckrodt, Hazelwood, MO, USA) at room temperature in order to achieve equilibrium between the contrast agent and the sGAG content of the cartilage. The influx of Hexabrix into cartilage correlates well with the inverse of sGAG content; therefore, cartilage quality and degeneration are measurable using µCT (expressed as attenuation). Samples were scanned using the following settings: isotropic voxelsize of 18 µm, 60 kV, 170 mA, 885 ms exposure time, 35 mm field of view, 0.5 mm Al filter, 0.8 rotation step over 198°, frame averaging of 3.

μCT data analysis: Obtained images were converted into 3D reconstructions using nRecon software, version 1.5 (Skyscan). In all EPIC-μCT datasets, X-ray attenuation (arbitrary gray values inversely related to sGAG content) and thickness (μm) were calculated for cartilage of the medial and lateral tibial plateau. Using Skyscan analysis software, the datasets were segmented using a fixed attenuation grey value threshold between air (grey value 30) and subchondral bone plate (grey value 120). In all segmented μCT datasets, regions of interest (150 slices) were drawn around the cartilage of the medial and lateral plateau of the tibia separately and for these regions, cartilage attenuation and cartilage thickness (μm) were calculated.

*SPECT macrophage imaging:* Folate SPECT imaging was performed to image macrophage activity according the protocol described earlier [189, 190]. In short, DOTA-Bz-folate (EC0800, kindly provided by Endocyte Inc., West Lafayette, USA) was radiolabelled with $^{111}InCl_3$ (Covedien, Petten, The Netherlands) resulting in a specific activity of 50 MBq/nmol 111In-DOTA-folate. At the end of the experiment (after 3 weeks), each rat was injected with 60 MBq of 111In-DOTA-folate into the tail vein, 24 hours before scanning. Animal placing was similar to that described in the μCT section. Scans were performed on the NanoSPECT/CT (Bioscan Inc., Washington DC, USA), with the following settings; 1.5-mm diameter pinhole tungsten-based collimators, 350 mm x 28 mm field of view. For anatomical reference, a fast (200 μm) helical micro-CT was performed. Energy peaks were set at 170 keV and 240 keV. Scans were performed midfemur to midtibia resulting in an acquisition time of 40 minutes.

*SPECT/CT analysis*: SPECT data were reconstructed using HiSPECT software (Scivis) at an isotropic voxel size of 600 μm, where CT data were automatically co-registered. The Region of Interest (ROI) in which photon emission was determined consisted of a cylindrical shape around the knee from the distal part of the patella to the proximal part of the tibial plateau. Of these ROI's, radioactivity was measured using InVivoScope software (Bioscan) and expressed as kBq/mm$^3$ to yield macrophage activity per volume. For all rats, the absolute difference in measured radioactivity (kBq/mm$^3$) of the OA knee joint compared to the healthy internal control joint was calculated, and means of the groups were compared to check for differences in macrophage activation between the treatment groups.

## 2.11 Statistical analysis

Differences in between treated OA knees and healthy control knees within the same animal were analyzed using type-1, two-tailed, paired T-tests for all outcome parameters (SPSS Inc., Chicago, USA). When comparing differences between means of the knees of the three different treatment groups, type-1, two-tailed, unpaired T-tests were performed

for all outcome parameters. All data are presented as mean ± SD, *P*-values <0.05 were considered significant. For the cell experiments, statistical analysis was performed using SPSS 20 software (SPSS Inc., Chicago, IL, USA). Results are presented as mean ± standard deviation. Statistical significance was considered when p values were less than 0.05. Differences in $PGE_2$ production between the different conditions were determined by univariate analysis of variance. A post-hoc test with Bonferroni correction was applied when 5 conditions were compared to each other.

## 3. Results

### 3.1 In vitro release of celecoxib from the gel in the presence of cells and bioactivity of the released celecoxib

Celecoxib is a very stable drug, which is only metabolized by the liver (predominantly by cytochrome P450 2C9 coenzyme) into inactive metabolites lacking COX-2 inhibition capacity [191, 192]. This is confirmed by the fact that only the celecoxib peak (and no metabolites/degradation products) was observed in the chromatograms of the release samples. However, to confirm that celecoxib after release retained its full pharmacological activity, its efficacy to inhibit COX-2 and the production of $PGE_2$ human chondrocytes was assessed. Briefly, primary human chondrocytes were incubated with celecoxib-loaded PCLA-PEG-PCLA (1.25 mg/g) gels. Cell viability at day 21 was 99.2 ± 1.9% and 98.6 ± 1.6% for respectively the control and the cells cultured with celecoxib-loaded gel, showing good cytocompatibility of the gels. Over the 21-day period of the experiment with refreshment of the cell medium every 3 days, the ability of celecoxib released from the gel to actively inhibit COX-2 and subsequently block the release of $PGE_2$ was investigated by activating an inflammatory ($PGE_2$) activity in the cells by adding TNFα to the medium (figure 1). Compared to the control, the addition of the unloaded (blanc) PCLA-PEG-PCLA gel did not result in either an increase nor decrease of $PGE_2$ release. As expected, cells exposed to TNFα showed a significant ($p<0.05$) increase in $PGE_2$ release (figure 1). The added bolus of celecoxib as well as the celecoxib released from the loaded PCLA-PEG-PCLA25 wt% gel (1.25 mg/g) were able to almost fully block the $PGE_2$ release by the activated chondrocytes. After a burst release within the first week, up to 15 μg/ml in 3 days; a steady state of 4 μg celecoxib/3 days was released in 1 mL medium, determined by UPLC as described previously [165].

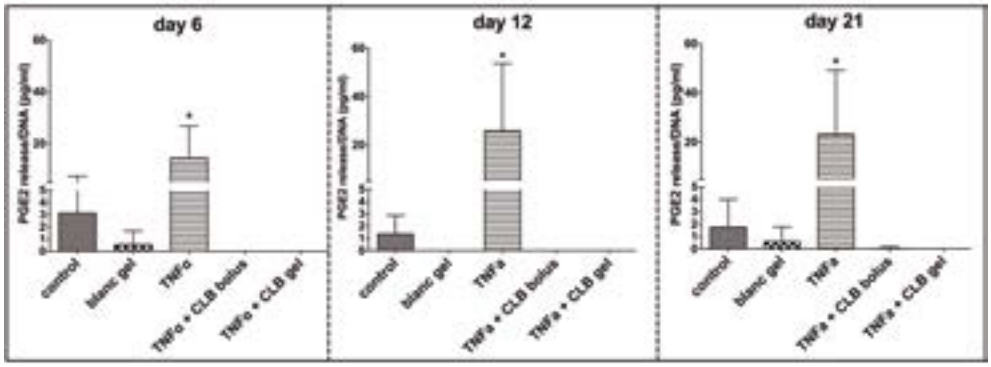


***Figure 1:*** *$PGE_2$ release, normalized for total DNA content, of chondrocytes cultured in medium only (control), medium with PCLA-PEG-PCLA 25 wt% gel (blanc gel), medium with TNFα (TNFα) to induce $PGE_2$ release in addition of a bolus celecoxib (TNFα+CLB bolus), celecoxib-loaded PCLA-PEG-PCLA 25 wt% gel (1.25 mg/g) (TNFα+CLB gel). Data are presented as mean ± SD (n=2 donors/4 measurements per donor). * = $p < 0.05$*



## 3.2 Weight gain of the rats

Average bodyweights of the rats at baseline were respectively 366.5 g (345-382 g), 389.3 (375-406 g) and 372.5 g (354-390 g) for the groups treated with celecoxib-loaded gel, with the celecoxib suspension and with saline. During the full study period of 3 weeks, in which all rats received a papain injection combined with daily treadmill running and an intra-articular treatment of either celecoxib-loaded gel, celecoxib suspension or saline control, average bodyweights increased slightly to respectively 374 g (355 – 386 g), 402.5 (380-424 g) and 380 g (365-400 g), which was only statistically significant for the saline group. In a previously conducted study by our group, we also observed that increase in bodyweight was either non-significant or very low due to the running protocol combined with the papain injection [136]. We can conclude that no systemic side-effects of both intra-articular treatment with celecoxib (via the gel or suspension) occurred in terms of weight loss (>10% of the total body weight is considered a sign of distress).

## 3.3 Hind Limb Weight Distribution

At baseline (two days before treatment, *t = -2 days*), all groups had equal weight distribution over both hind legs (shown as % of bodyweight distributed over the left hind limb: celecoxib-loaded gel 48±5%); celecoxib suspension group 47±3%; saline group 49±4% (figure 2). Two days after the start of OA induction through papain injection (left knee) combined with the running protocol *(t = 0)*, all groups clearly showed the effect of this induction in terms of weight bearing of the affected limb (celecoxib-loaded gel 33±7%; celecoxib suspension group 33±8%; saline group 33±8%), indicating the

occurrence of pain of the inflicted joint. Directly after these measurements, treatment was provided in all groups. Two days later (*t = 2 days*) the weight distribution was monitored again, showing a weight distribution over the affected limb that increased compared to the previous time point to ~45 for all groups (celecoxib-loaded gel 45±5%; celecoxib suspension group 47±6%; saline group 42±9%). Five days after the start of the treatment, weight distribution over the affected limb was significantly more than what was seen at baseline in all groups (celecoxib-loaded gel 58±8%; celecoxib suspension group 60±9%; saline group 58±12%). At the next time point (*t = 12 days*), for all groups the equilibrium between left and right returned to 50% and stayed the same throughout the experiment (*19 days*) with no differences between groups.

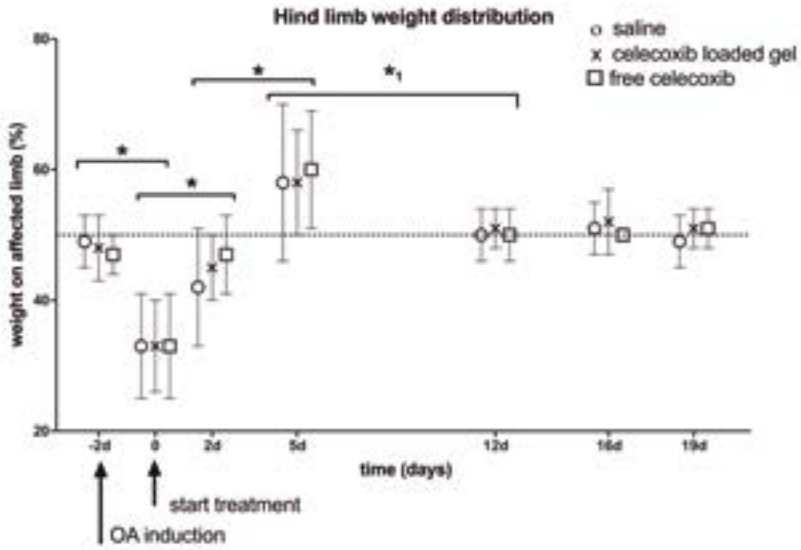


***Figure 2.*** *Hind limb weight distribution of rats before and after induction of OA, treated with celecoxib loaded hydrogel (○) or celecoxib suspension (X) or saline (□) as a negative control (Y-axis shows the percentage of total weight put on the affected limb. The dotted line marks the point of 50% weight distribution, where both OA and healthy knees are loaded equally. *: p<0.05, difference between time points for all individual groups and the groups combined, *1: P<0.05 between time points for combined groups and all individual group, except for the celecoxib suspension group.*

## 3.4 Osteoarthritic changes of articular cartilage

In a previous study, it was shown that multiple intra-articular papain injections combined with moderate exercise for 6 weeks induced severe sGAG depletion from both medial and lateral cartilage compartments of the tibia plateau [136]. As explained in the introduction, we adjusted this protocol to achieve a milder OA type. At the end

of the experiment (after 3 weeks of running), cartilage of both the medial and the lateral compartment was affected by OA compared to the contralateral healthy control joint (right knees). For the different groups, the attenuation in μCT grey values during the EPIC imaging of both lateral and medial tibial plateau was much higher in the affected joint compared to the internal healthy control, indicating loss of sGAGs, which is an early sign of OA (figure 3a). Both quality (attenuation) and quantity (thickness) of the cartilage were significantly affected by the OA induction, showing reduced cartilage thickness and higher attenuation (indicating less sGAG content of the cartilage) for all three groups ($p<0.001$), independent of the treatment. The model adaptation indeed led to a less severe OA model, with less loss of cartilage thickness compared to the previous study [193]. Medially, none of the groups showed a significant loss of cartilage thickness when compared to their contralateral healthy control joint. For the lateral compartment, all groups showed some loss of cartilage thickness when compared to their internal control; this difference was significant for the group treated with celecoxib-loaded gel ($p=0.03$) and the celecoxib suspension group ($p=0.01$), but not for the saline group ($p=0.08$).



When comparing the affected OA knees treated with celecoxib suspension or celecoxib-loaded gel to the untreated OA knees (saline), no significant differences were found for attenuation. For cartilage thickness, a significant difference was found in the medial compartment between the group treated with the celecoxib-loaded gel versus the group treated with the celecoxib suspension, where the joints injected with the gel showed thicker cartilage compared to the group treated with the suspension (218 ± 30 μm versus 176 ± 29 μm; $p=0.02$, figure 3a). Cartilage thickness of the saline treated group was in between these two values; 206 ± 29 μm, with no significant difference compared to both treatment groups (Figure 3a). The differences between these groups however, seem to represent differences between the animals and not so much an effect of the treatment itself since for this measurement, no significant differences were found between the affected and the healthy control knees in all groups. For cartilage thickness of the lateral compartment, significant differences were only found between saline treated knees and celecoxib suspension treated knees, with more severe thinning of the cartilage found in the knees treated with the celecoxib suspension (192 ± 31 μm versus 148 ± 39 μm; $p=0.02$). The group treated with the celecoxib-loaded gel showed an average of 169 ± 35 μm for this measurement, which is not significantly different from both other groups.

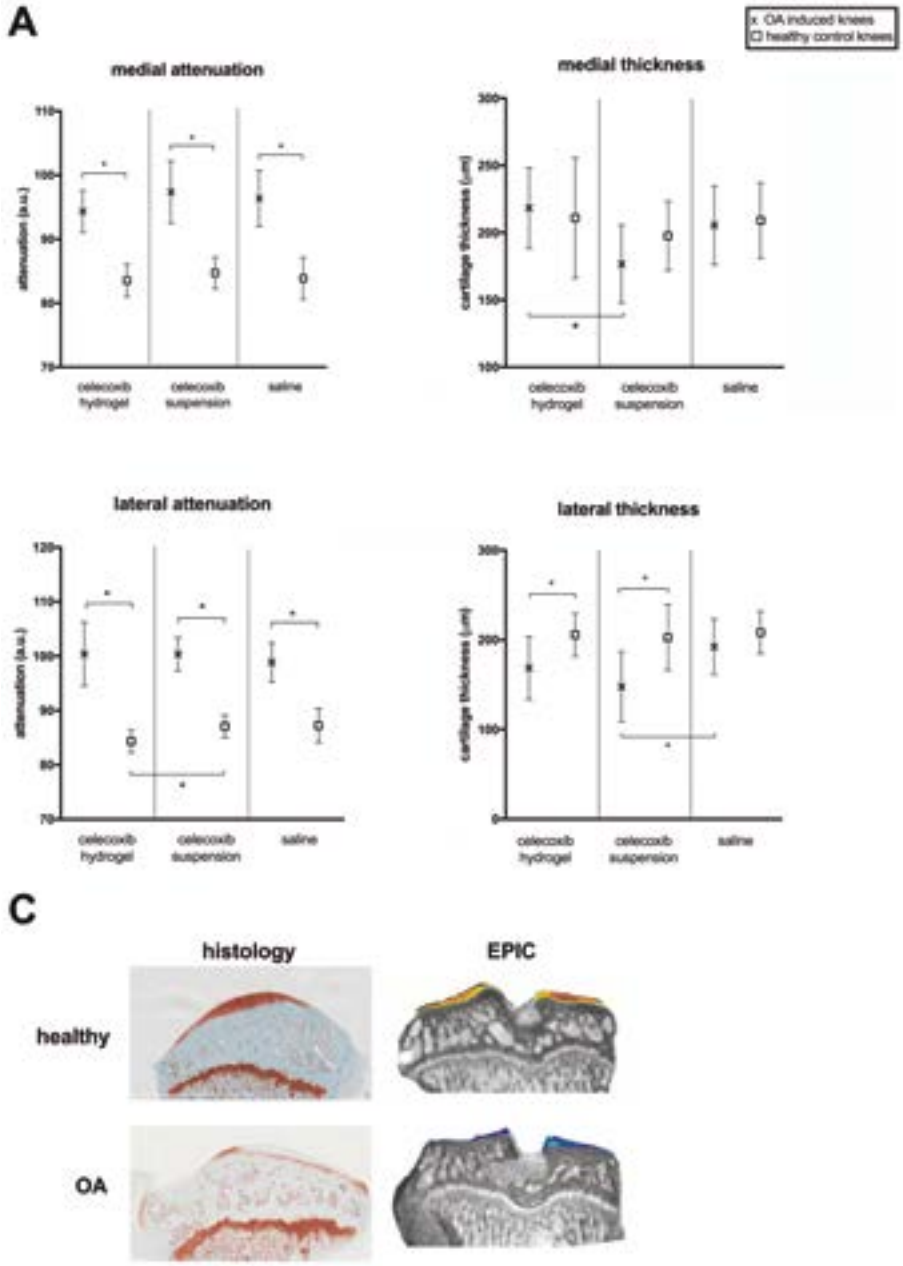


***Figure 3-a*** *EPIC-µCT scanning at t=3 weeks, to determine cartilage thickness (µm) and attenuation (arbitrary units) of knee joints in which OA (**x**) was induced and after 2 days treatment was started with saline (negative control), celecoxib suspension or celecoxib loaded hydrogel. The contralateral knees are healthy controls (‡). Data are shown as mean ± SD, p<0.05 is considered significant. *: significant differences were found for both lateral and medial attenuation for all groups, with higher attenuation (lower cartilage quality) for the OA knees compared to their healthy counterparts. Lateral thickness was affected in the OA knees for all groups, except for the saline group (control) where this difference was*

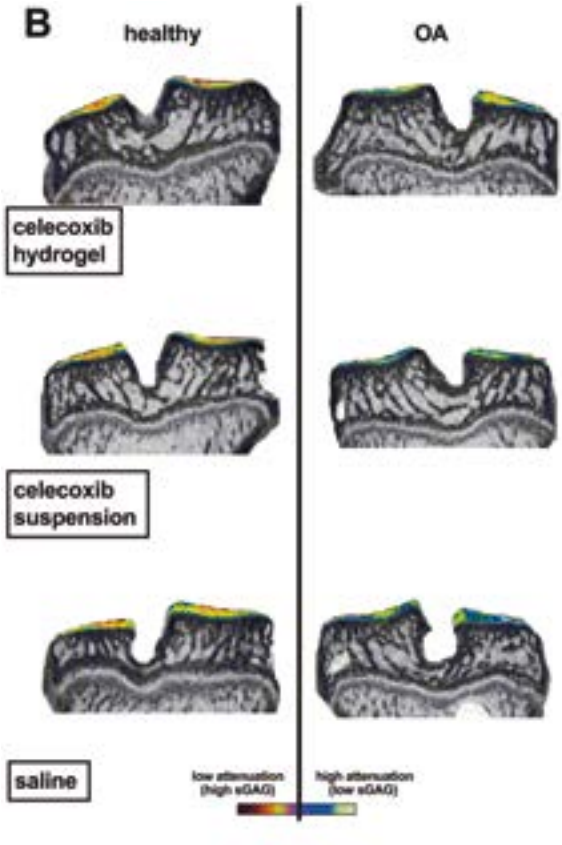




*not significant. Significant differences between treatment groups: the celecoxib hydrogel group showed thicker medial cartilage compared to the celecoxib suspension group. The celecoxib suspension group showed thinner lateral cartilage compared to the saline treated group (negative control).**b** representative EPIC-µCT images of the data presented in figure 3-a. Both the OA induced knees and the contralateral healthy knees of representative rats of all three groups are depicted (Celecoxib hydrogel treated, celecoxib suspension treated and saline treated). The color of the cartilage represents the attenuation, a quantitative measurement of the sGAG content and therefore the quality of the cartilage. The color bar at the bottom of the figure depicts the correlation between the different colors and the attenuation. **c** Histological and EPIC-µCT images of the same osteoarthritic and healthy knee, showing excellent representation of the cartilage quality and quantity by EPIC, when compared to histology. EPIC scanning is superior to histology, since it is a quantitative measurement, whereas histological scoring is semi-quantitative.*

## 3.5 Macrophage activation

Macrophage activation can be visualized and quantitatively measured in animals via SPECT-imaging after intra-venous administration of $^{111}$In-EC0800. Each animal received 60 MBq of $^{111}$In-EC0800 under isoflurane anesthesia at the end of the experimental protocol (*t = 3 weeks*), and both activity and absolute differences in activity between the OA induced knee and contralateral healthy knee are shown for all treatment groups (figure 4). All groups showed an increased radioactive uptake in their OA-induced knee joints compared to their internal healthy control joints (figure 4a). This is in accordance with previous results, where it was shown that synovial macrophages are activated and measurable with the use of SPECT, even though the OA model used in our current study is much milder [136]. When comparing the absolute differences between healthy and affected joints between groups, the joints injected with celecoxib loaded gel showed a significant higher radioactive uptake, indicating more pronounced macrophage activation when compared to joints treated with either saline or celecoxib suspension (figure 4b). We found no significant difference when comparing the saline treated group to the celecoxib suspension treated group.

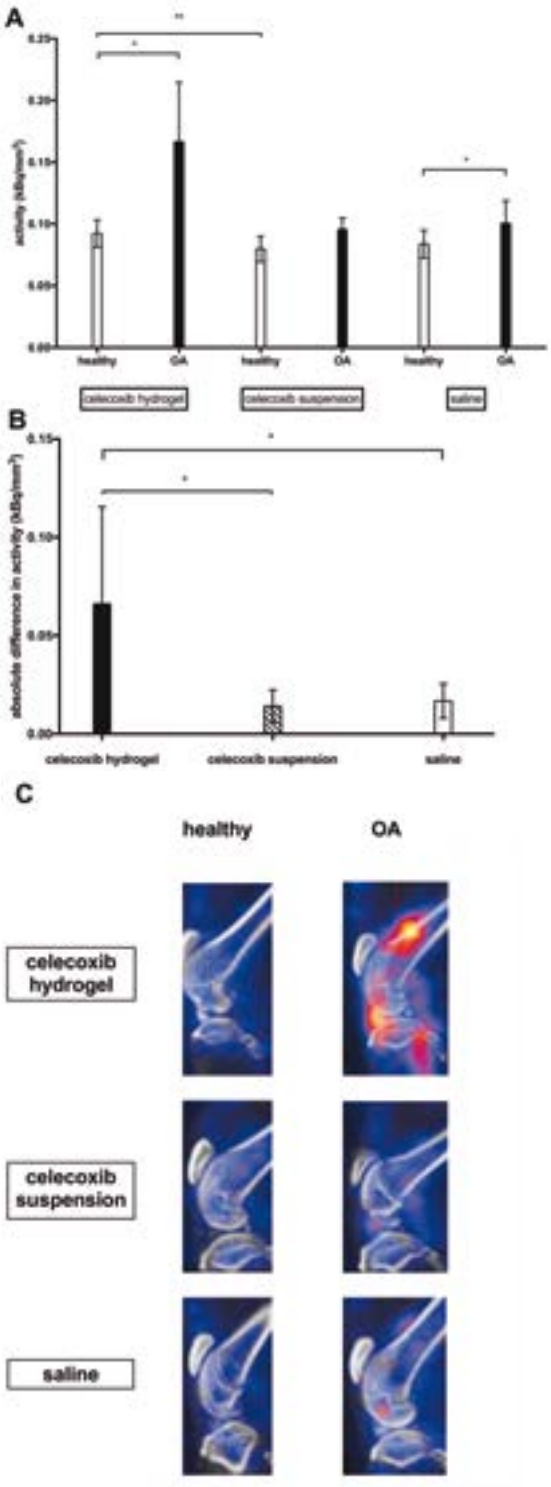


***Figure 4.*** *Macrophage activation determined in healthy versus OA induced knees, treated with saline, celecoxib suspension or celecoxib loaded hydrogels, after injection of $^{111}$In-EC0800 using single-photon emission computed tomography/computed tomography (SPECT/CT). Scans were performed at t=3 weeks. *= P<0.01, **= P<0.05.* ***a.*** *Quantitative outcome of measured radioactivity in healthy versus OA joints, normalized to the size of the analyzed cylindrical region of interest for groups treated with intra-articular celecoxib loaded hydrogel, celecoxib suspension or saline (negative control)* ***b.*** *Absolute differences per animal were calculated to correct for differences in biodistribution of $^{111}$In-EC0800 between the different groups (celecoxib loaded hydrogel, celecoxib suspension, saline)* ***c.*** *Representative SPECT/CT images showing the macrophage activity of healthy knees, versus OA knees, after treatment with celecoxib loaded hydrogel, celecoxib suspension and saline (negative control) at t=3 weeks.*

## 4. Discussion

In the current study, we evaluated the effects of sustained intra-articular celecoxib release from PCLA-PEG-PCLA hydrogels, compared to intra-articular treatment with celecoxib suspension and saline (negative control) in an OA model in rats.

*In vitro*, the celecoxib released from the loaded PCLA-PEG-PCLA hydrogel was, similar to a celecoxib bolus, able to almost fully block $PGE_2$ release by activated chondrocytes. This demonstrates that celecoxib released from the gel was indeed bioactive. Since $PGE_2$ has been proven to contribute to hyperalgesia and the erosion of cartilage and juxta-articular bone [194], sustained release of bioactive celecoxib from the hydrogel could be an efficient intra-articular (anti-inflammatory) treatment option for OA.

As expected, OA induction inflicted pain in all the animals, measured by a decrease of weight bearing over the affected joint. Five days after the start of intra-articular treatment, we observed something unexpected in all groups; weight bearing over the affected limb of ~60%. Recovery from the initial pain of OA induction would in theory lead to a return to baseline, with a 50% weight distribution over the treated affected limb. Since the saline group showed increased weight bearing over the affected limb after 5 days as well, we are not observing a treatment effect of celecoxib. It could however be a sign of overcompensation; daily running with a painful left limb due to the papain injection could cause temporary overuse of the healthy side (right), causing for instance sore muscles. At *t = 5 days*, this compensatory pain on the right side could have been measurable because the pain caused by the papain injection on the left side had subsided. While we already know from our previous studies that the celecoxib loaded gel does not cause adverse effects in the injected joints in terms of cartilage damage [165], now we have shown that the sustained intra-articular presence of celecoxib loaded hydrogels also does not cause any discomfort or pain of the injected joint. For a potential clinical translation of the celecoxib loaded hydrogel in the future, this is an important finding.

Celecoxib blocks $PGE_2$ release, and with the sustained release from the gels, a more pronounced $PGE_2$ blockage leading to less pain and inflammation compared to the celecoxib suspension, would have been expected. However, since the inflicted pain in our current model was short-term, we were unable to measure such an effect. As described in our introduction, Mastbergen *et al.* [195] and Janssen *et al.* [42] were both unable to show positive effects of celecoxib on cartilage in a surgical OA model. They both hypothesize that a chondropositive effect of celecoxib was possibly masked due to a positive effect of celecoxib on pain, leading to an increased loading of the affected joint, causing more cartilage damage in their surgically induced OA knees. However, based on our results presented here, this effect is rather unlikely, since no significant differences in hind limb weight distribution were found between the groups injected with celecoxib suspension, the celecoxib loaded hydrogel and saline control.

OA induction led to macrophage activation in all groups. When macrophages become activated, they can differentiate in different subtypes, which can crudely be divided in M1 and M2. However, this dichotome distribution of macrophages was recently recognized to be much more complex, since it is now appreciated that macrophages are present in a whole spectrum where M1 and M2 phenotypes can partially overlap [196]. On one end of the spectrum, M1, or classically activated macrophages, are activated through the cell-mediated immune response and are thought to be mainly pro-inflammatory and have an important role in the host defense against infections [197]. On the other side of the spectrum are M2, or alternatively activated macrophages, that mainly promote anti-inflammatory actions and are linked to tissue repair [198] When performing folate-SPECT scanning, folate-receptor positive macrophages, which are predominantly of the M2 type, are specifically targeted [199]. Increased macrophage activation found after inducing OA is not only M1 driven (inflammation), but M2 (repair) is also activated since the joint is trying to maintain homeostasis. This is indeed confirmed by the fact that the OA induced knees treated with saline showed higher activity on the folate-SPECT (measuring mainly M2) compared to their healthy contralateral knees.



Treatment with celecoxib loaded hydrogels led to higher macrophage activation compared to joints treated with either saline or celecoxib suspension. This result is similar to an earlier finding with intra-articular injections with triamcinolone acetonide, a corticosteroid; Siebelt *et al.* [193] found that the use of triamcinolone led to an increased macrophage activation in an OA model. It has been shown that glucocorticosteroids can trigger macrophages to differentiate in a specific M2 subtype known as regulatory macrophages, which produce IL-10 and are therefore considered to be mainly anti-inflammatory [200]. Siebelt *et al.*, indeed confirmed *(in vitro)* that triamcinolone steered the macrophages towards an M2 (anti-inflammatory) phenotype that is folate receptor positive. However, this M2 activation did not lead to any positive nor adverse effects on cartilage compared to saline treated controls. What they did observe was a very distinct reduction of osteophyte formation following intra-articular treatment with triamcinolone. Since osteophyte formation is linked to chronic inflammation [201], this is an understandable effect of M2 activation. The same effect of reduced osteophyte formation was shown for celecoxib loaded PEA (polyester amide) microspheres in a surgically induced OA model in rats [185]. In our current study, the OA model was relatively mild and no osteophytes occurred. Therefore, we were not able to show a potential beneficial effect of celecoxib loaded hydrogels on osteophyte formation.

Although Tellegen *et al.* [185] found no significant differences in M2 related folate receptor-beta expression (at the endpoint after 16 weeks), the highest dosage of celecoxib loaded microspheres led to a decrease of the M1 related iNOS (inducible nitric oxide synthases) expression of the OA induced knees. Timur *et al.* [202] recently found similar results; they showed that $PGE_2$ release by Hoffa's fat pad harvested from OA knees was mainly associated with the expression of genes correlated with M1 macrophages.

Hoffa's fat pad is an infrapatellar structure within the knee, and the last years it has been more and more recognized as an important player, next to the synovium, in the role of inflammation in the development of OA [203]. Celecoxib was able to modulate these M1 macrophages towards the more favorable M2 subtype [202]. Overall, the results within the Orthopedic research field seem to indicate that celecoxib, similar to glucocorticosteroids, steers the macrophage population towards the M2 phenotype while decreasing the M1 activity [185, 202]. A reduction of M1 activity is very important; Utomo *et al.* recently showed that M1 macrophages have a direct negative effect on OA cartilage, whereas M2 macrophages did not directly affect the cartilage, nor are able to counteract the pro-inflammatory actions [204].

Based on our results, combined with the abovementioned literature, we hypothesize that the macrophage activation following intra-articular treatment with celecoxib-loaded hydrogel was mainly of the M2 type, thus part of a repair process in the inflicted joint. This is further supported by the lack of negative effects on cartilage, which would be expected with an activation of the M1 subtype, and the absence of measurable pain at the 3-week mark. Moreover, a previously conducted study in which our celecoxib loaded hydrogel (with the same composition and the same amount of celecoxib loading) was injected in horse joints, histology of the synovial membrane of the injected joints showed no signs of inflammation at the end mark (28 days) [166].

Treatment with celecoxib suspension did not show a significant difference when compared to saline. This can be explained by the fact that we tested macrophage activity 3 weeks post-treatment, and unlike the celecoxib loaded hydrogels, the celecoxib suspension does not lead to a sustained release and was therefore not able to give a long-lasting effect.

In the field of cancer research, there are several publications where the opposite of the abovementioned effects of celecoxib on macrophages seems to be true and celecoxib modulates the macrophages towards a predominantly M1 phenotype, which is tumor suppressive [205-207]. It has been shown that macrophages can adapt to particular environments and thereby adapt their role to be organ and tissue specific [208]. Cytokine expression of macrophages differs greatly depending on their site of residence [208]. This site specificity of macrophages and consequently different cytokine expression could explain the different reactions to celecoxib between synovial macrophages and macrophages in other organs.

In our current study, quantitative and qualitative cartilage measurements performed using EPIC μCT scanning showed more severe thinning of the cartilage of the lateral compartment in the celecoxib suspension group compared to the saline treated group. These values indicate that the intra-articular celecoxib suspension had a slight negative effect on the already weakened cartilage (sGAG loss due to the OA induction) and that this phenomenon was less prominent when celecoxib was administered in the form of a gel, since no significant differences were found between the saline treated animals and

celecoxib loaded hydrogel treated animals. Negative effects of intra-articular celecoxib administration on cartilage has not been described by other research groups. Janssen *et al.* found no differences between OA knees that were treated with saline (negative control), unloaded PEA (polyesther amide) microspheres and celecoxib loaded microspheres; no chondropositive effects occurred, but also no negative effects were observed at *t = 12 weeks* post-injection [42]. A major difference between the results presented by Janssen *et al.* and our results is our use of quantitative EPIC-μCT images to very accurately determine cartilage quality and quantity where the whole cartilage was measured, while Janssen *et al.* used semi-quantitative histological scoring systems, during which only one or two sections were scored per joint. Since our method is far more sensitive, it is much more likely that small differences will be picked up, which might have been overlooked when only using histology for cartilage scoring. Jiang *et al.* presented a study in 2010, in which they showed significant chondropositive effects of weekly intra-articular injections with celecoxib suspension in a surgical OA model in rabbits, when compared to saline treatment [180]. Since weekly injections are not an option in the clinical situation, they conducted the same experiment by administrating celecoxib loaded liposomes [30]. With the celecoxib loaded liposomes, no significant differences were found between treated animals and saline treated knees on histological examination of the cartilage. Again, only histology was used and subtle differences might have been missed. Furthermore, the liposomes released showed almost 75% of the celecoxib *in vitro* within the first 24 hours upon injection [30]. Therefore, it is rather unlikely for this formulation to have an extended effect on the disease progression after only one single injection and it is possible that the fast release of celecoxib from the liposomes is the main reason this group was not able to reproduce their chondropositive effects that were observed in their prior study with multiple injections of celecoxib suspension. A major disadvantage of trying to compare results between different studies, is the fact that a lot of different animals and/or different OA models as well as different treatment protocols were used between different research groups. Therefore, the differences in results on cartilage between the different studies might very well be the result of differences in experimental set ups rather than real treatment differences. In order to gain reliable, reproducible and comparable results, it would be desirable to only have a selected number of OA animal models for all research groups to work with. The mild protective effect of the hydrogel on the chondronegative effects of celecoxib in our current rat model could be explained by various mechanisms. First of all, the use of a hydrogel leads to a sustained release of celecoxib, in contrast to the celecoxib suspension which would likely lead to a peak concentration within the first hours. This peak concentration could be toxic and potentially harm the cartilage. Secondly, as described in section 3.5, the sustained release of celecoxib from the hydrogel led to an increased macrophage activity compared to saline and celecoxib suspension treated joints. These macrophages were

most likely of M2 phenotype, reducing inflammation and leading to a decreased release of cytokines and enzymes that could potentially harm the cartilage.

## 5. Conclusions

The treatment of OA with intra-articular celecoxib suspension led to mild cartilage damage, where the release of celecoxib from a hydrogel prevented this from happening. Unfortunately, no chondroprotective effects of celecoxib were found in our current study, which could be a result of the relatively mild OA induced in this specific model or of the dose of the administered drug not reaching its therapeutic range. Since we observed no adverse effects of the celecoxib loaded hydrogel, a dose-finding study is recommended. The celecoxib loaded hydrogel led to a significant difference in macrophage activation compared to both saline and the celecoxib suspension, with a phenotype most likely of the anti-inflammatory (M2) spectrum. For the OA model used in this study, pain was only present shortly after OA induction. In the clinical situation, however, the primary complaint of patients suffering from OA is pain. Therefore, presenting a DDS that could potentially set the phenotype of the macrophages from a pro-inflammatory to an anti-inflammatory phenotype, thereby actively reducing pain, is very attractive for the treatment of OA.

## Acknowlegdment

This research was partly supported by a grant of the Ministry of Economic Affairs, The Netherlands (BMM/TerM P2.02).

# Chapter 6

## Degradation, intra-articular retention and biocompatibility of monospheres composed of [PDLLA-PEG-PDLLA]-b-PLLA multi-block copolymers

Sandker MJ, Duque LF, Redout EM, Chan A, Que I, Löwik CWGM, Klijnstra EC, Kops N, Steendam R, van Weeren R, Hennink WE, Weinans H.

*Acta Biomater. 2017 Jan 15;48:401-414*

## Abstract

In this study, we investigated the use of microspheres with a narrow particle size distribution ('monospheres') composed of biodegradable poly(DL-lactide)-PEG-poly(DL-lactide)-*b*-poly(L-lactide) multiblock copolymers that are potentially suitable for local sustained drug release in articular joints. Monospheres with sizes of 5, 15 and 30 μm and a narrow particle size distribution were prepared by a micro-sieve membrane emulsification process. During *in vitro* degradation, less crystallinity, higher swelling and accelerated mass loss during was observed with increasing the PEG content of the polymer. The monospheres were tested in both a small (mice/rat) and large animal model (horse). *In vivo* imaging after injection with fluorescent dye loaded microspheres in mouse knees showed that monospheres of all sizes retained within the joint for at least 90 days, while the same dose of free dye redistributed to the whole body within the first day after intra-articular injection. Administration of monospheres in equine carpal joints caused a mild transient inflammatory response without any clinical signs and without degradation of the cartilage, as evidenced by the absence of degradation products of sulfated glycosaminoglycans or collagen type 2 in the synovial fluid. The excellent intra-articular biocompatibility was confirmed in rat knees, where μCT-imaging and histology showed neither changes in cartilage quality nor quantity. Given the good intra-articular retention and the excellent biocompatibility, these novel poly(DL-lactide)-PEG)-poly(DL-lactide)-*b*-poly(L-lactide)-based monospheres can be considered a suitable platform for intra-articular drug delivery.

## I. Introduction

To this date, disease modifying drugs are not available for the treatment of OA (osteoarthritis), the most common joint disease [59] and the current treatment is mainly based on pain prevention/reduction with orally administered drugs, often non-steroidal anti-inflammatory drugs (NSAIDs) [209]. Due to the chronic nature of OA in combination with the short half-life and poor distribution of drugs in general, and in this case more specifically NSAIDs to the joint [210-212], oral medication has to be taken daily for a long period and in high dosages. This high systemic exposure can in its turn lead to unwanted side-effects [61, 209]. To circumvent these adverse effects, intra-articular injections (mainly hyaluronan or corticosteroids) have been used quite extensively in clinical practice, but this route of drug delivery has as a major drawback that the injected substance is rapidly released from the joint with daily synovial fluid turnover [62, 63, 65], making multiple injections necessary. Ideally, a single intra-articular injection of a local drug delivery system (DDS) for OA would provide sustained drug concentrations in the injected joint in a controlled way for a longer period of action. Drug delivery systems can significantly improve pharmacokinetics of therapeutic compounds, which is especially relevant for the treatment of chronic diseases and for compounds with a narrow therapeutic window, since systemic plasma concentrations can be reduced with concurrent reduction of undesirable side-effects [213, 214]. Moreover, the use of registered drugs and drug candidates, which generally are inactivated and eliminated from the body before even entering the joint, would benefit for therapeutic outcome when administered locally to the tissue of interest. Biodegradable DDSs are attractive for clinical applications since their degradation products are eliminated via metabolic routes and/or excreted by the kidneys, obviating the need for surgical removal. To date, several biodegradable DDSs for intraarticular delivery have been developed, including liposomes, hydrogels and polymeric nano/microparticles [28, 67, 68, 122]. Poly(DL-lactide) (PDLLA) and poly(DL-lactide-co-glycolide) (PLGA) are the most widely used biodegradable polyesters for use in sustained release microparticles. However, a limitation of PDLLA and PLGA is that acidic degradation products that are formed upon hydrolysis of the ester bonds accumulate in the polymer matrix due to which the *in situ* pH in the microparticles may drop significantly [215, 216]. The acidic micro-environment has been reported to negatively impact the stability of pH sensitive therapeutic agents such as proteins [217] and cause irregular release profiles of encapsulated actives [218] as well as dose-dumping of acidic degradation products which may evoke significant foreign body reactions [219]. Controllable and sustained drug release has been observed with microparticle-based systems prepared by different manufacturing processes [28, 71], where emulsification/solvent evaporation is the most commonly used method [220-222]. Nevertheless, the difficulty to control particle size with this technique and the broad particle size distribution of the obtained microspheres

leads to difficulties in formulation reproducibility and poor injectability [39, 223]. Microsieve membrane emulsification allows the preparation of uniformly sized particles with average size ranging from tens of nanometers to several hundreds of micrometers [224, 225]. The advantages of membrane emulsification include 1) excellent control over the particle size and narrow particle size distribution and 2) mild process conditions as no shear forces are needed to form the droplets. Due to the absence of coarse particles, which could potentially block the injection needle, monospheres can be administered less painfully compared to polydisperse microspheres since smaller injection needles can be used [39, 226]. Monospheres also lack the presence of a fraction of very small microspheres which can induce particle-induced immunoactivation [39]. Furthermore, size uniformity enables the microspheres to deliver a more precise amount of drug per microsphere, optimization of the drug release kinetics and hence more reproducible and predictable *in vivo* pharmacokinetics [227, 228]. The Shirasu Porous Glass (SPG) membranes have been widely used to prepare uniformly sized microparticles [229]. Microsieve™ emulsification is an alternative membrane emulsification technique preparation of monodisperse microspheres (monospheres™) [230]. Contrary to other membrane-based droplet and particle production methods, the droplet size (and thus the particle size) is solely determined by the membrane design and independent of other process parameters. As a consequence, scalability of the process is straightforward and can be achieved by simply increasing the number of pores of the microsieve membrane or by adding more microsieves to the process.

In the present study, we used a series of novel phase separated poly(DL-lactide)-PEG-poly(DL-lactide)-*b*-poly(L-lactide) multi-block copolymers ([PDLLA-PEG-PDLLA]-*b*-PLLA) obtained by polymer chain extension of telechelic poly(L-lactide) diol (PLLA) and poly(DL-lactide)-PEG-poly(DL-lactide) diol (PDLLA-b-PEG-b-PDLLA) with 1,4 butanediisocyanate [231]. To prepare microspheres with a narrow size distribution ('monospheres') by means of microsieve membrane emulsification. By varying the ratio of the rigid, semi-crystalline poly(L-lactide) blocks (PLLA) and the soft amorphous poly(DL-lactide)-PEG-poly(DL-lactide) blocks, the hydrophilicity and swelling degree of these multi-block copolymers can be tailored, which allows control over drug release kinetics. Drug release from [PDLLA-PEG-PDLLA]-*b*-PLLA multi-block copolymers is generally controlled by diffusion through the swollen polymer network, which is in contrast to PDLLA and PLGA polymers, where release is in general controlled by degradation of the polymer matrix [232]. Another advantage of the (PDLLA-PEG-PDLLA]-*b*-PLLA multi-block copolymers is that, due to swelling of the polymer matrix, acidic degradation products do not accumulate in the polymer matrix, but are released instead, leading to the preservation of a less acidic micro-environment as compared to PLGA or PDLLA polyesters.

Besides, due to the hydrophilic and swellable nature of the PDLLA-PEG-PDLLA]-*b*-PLLA multi-block copolymers used in the present study, it is expected that acidic

degradation products will not accumulate in the polymer matrix, which is anticipated to positively contribute to the preservation of the integrity and bioactivity of the encapsulated therapeutic agents [215, 233, 234].
In the current study, we investigated the suitability of monospheres composed of biodegradable PDLLA-PEG-PDLLA]-*b*-PLLA multi-block copolymers with different block ratios as a platform for local intra-articular drug delivery. Intra-articular retention and biocompatibility of these monospheres were assessed in rodents (mice and rats) as well as horses. Like humans, horses suffer from OA, with up to 60% of equine lameness being OA-related [235, 236]. Lameness is the leading cause of economic loss in the equine industry, making effective new therapies for equine OA very valuable. Furthermore, the horse is an accurate translational model for human OA since they both develop OA spontaneously [237], with the carpal joint specifically showing much analogy to human knee OA [238, 239]. This would make the results of this study not only relevant for equine healthcare, but also for the potential development of novel human OA treatment options.

## 2. Materials and Methods



### 2.1 Materials.

PEG standards, polyvinyl alcohol (PVA 13-23) and sodium dodecyl sulphate (SDS) were purchased from Sigma Aldrich (Zwijndrecht, The Netherlands). Carboxymethyl cellulose (CMC) was purchased from Aqualon (Barendrecht, The Netherlands). Dichloromethane (DCM, p.a. stabilized with EtOH), sodium azide ($NaN_3$) and Tween-20 were purchased from Across (Geel, Belgium). Ultrapure water was purchased from B. Braun Medical B.V. (Oss, The Netherlands). Mannitol was purchased from Fagron (Barbsbütel, Germany). NIR780 was purchased from Li-Cor Inc (Nebraska, USA). Lumogen F Red 300 (Perylene red) was purchased from BASF (Ludwigshafen, Germany). Hexabrix 320®, a clinical iodine-based contrast agent, was obtained from Guerget, The Netherlands. All reagents were used as received.

### 2.2 Polymer synthesis

SynBiosys Pro [PDLLA-$PEG_{1000}$-PDLLA]-*b*-[PLLA] multi-block copolymers with various [PDLLA-$PEG_{1000}$-PDLLA] / [PLLA] block ratios were synthesized by InnoCore Pharmaceuticals (Groningen, The Netherlands) as described before [231, 240]. Typically, L-lactide and DL-Lactide were dried for 17 h at 50°C under vacuum. Poly(ethylene glycol) with a molecular weight of 1000 g/mol (PEG1000) was dried for 17 h at 90°C under vacuum. 1,4-Butanediol and 1.4 butanediisocyanate were distilled under

reduced pressure. The purity of distilled 1,4-butanediol and 1,4-butanediisocyanate was confirmed by $^{1}$H NMR ($CDCl_3$).

Low molecular weight poly(L-lactide) [PLLA] (Mw 4000 g/mol) and poly(DL-lactide)-polyethyleneglycol-poly(DL-lactide) [PDLLA-$PEG_{1000}$-PDLLA] (Mw 2000 g/mol) prepolymers were synthesized by standard stannous octoate catalysed ring-opening polymerization. Typically, to prepare PLLA with a target molecular weight of 4000 g/mol, 244.37 g (1.695 mol) of L-lactide was introduced into a three-necked bottle under nitrogen atmosphere and 5.63 g (62.47 mmol) of 1,4-butanediol was added to initiate ring-opening polymerization. Stannous octoate was added at a ratio of 11500 mol/mol monomer/catalyst. The mixture was magnetically stirred for 65 h at 140°C and subsequently cooled down to room temperature. PDLLA-$PEG_{1000}$-PDLLA prepolymer with a target molecular weight of 2000 g/mol, was synthesized in a similar way using 125 g (0.867mol) of DL-lactide, 125 g (0.125 mol) of $PEG_{1000}$ and stannous octoate at a ratio of 13500 mol/mol monomer/catalyst.

PLLA and PDLLA-$PEG_{1000}$-PDLLA prepolymers were subsequently chain-extended with 1,4-butanediisocyanate to yield [PDLLA-$PEG_{1000}$-PDLLA]-[PLLA] multiblock co-polymers with [PDLLA-$PEG_{1000}$-PDLLA] / [PLLA] block ratios of 10/90, 16/84, 20/80, 30/70 and 50/50 w/w. PLLA and PDLLA– $PEG_{1000}$-PDLLA pre-polymers were introduced into a three-necked bottle under nitrogen atmosphere. Then 65 ml of dry 1,4-dioxane (distilled over sodium wire) was added to obtain a 30 wt.% pre-polymer solution which was heated to 80°C to dissolve the prepolymers where after 4.23 g (30.18 mmol) of 1,4-butanediisocyanate was added. The reaction mixture was stirred mechanically for 20 h, cooled down to room temperature, where after it was transferred into a tray, frozen and vacuum-dried at 30 °C to remove 1,4-dioxane. The residual 1,4-dioxane content, as measured by GC headspace, was less than 200 ppm for all multi-block co-polymers. Residual contents of stannous ocoate as measured by inductively coupled plasma analysis was < 200 ppm for all multi-block co-polymers. Using $^{1}$H NMR analysis, only lactate/PEG ratios can be determined as it cannot be judged from the l actate signal in which block it resides. Hence the total LA/PEG mole/mole ratio equivalent for the block ratio is reported. In the table, it can be seen that the mole/mole ratios determined by NMR are close to the mole/mole ratios based on actual prepolymer in-weights, indicating that the actual block-copolymers have a block ratio very similar to their intended block ratio (table 1).

***Table 1.*** *Polymer block ratio, based on prepolymer in weight and determined by NMR.*

| Polymer type | PLLA (g) | PDLLA–$PEG_{1000}$-PDLLA (g) | Block ratio[a] (wt/wt ) | Lactate/PEG ratio (mole/mole) | |
|---|---|---|---|---|---|
| | | | | In weight[b] | 1H NMR[c] |
| 10[PDLLA-$PEG_{1000}$-PDLLA]-90[PLLA] | 119.93 | 12.83 | 9.7/90.3 | 270.4 | 258.8 |
| 16[PDLLA-$PEG_{1000}$-PDLLA]-84[PLLA] | 90.34 | 17.14 | 16.0/84.0 | 156.9 | 173.4 |
| 20[PDLLA-$PEG_{1000}$-PDLLA]-80[PLLA] | 88.05 | 21.84 | 19.9/80.1 | 124.7 | 126.9 |
| 30[PDLLA-$PEG_{1000}$-PDLLA]-70[PLLA] | 73.52 | 30.58 | 29.4/70.6 | 81.4 | 85.8 |
| 50[PDLLA-$PEG_{1000}$-PDLLA]-50[PLLA] | 48.37 | 46.91 | 49.2/50.8 | 42.9 | 46.1 |

[a] *[PDLLA-$PEG_{1000}$-PDLLA] / [PLLA] block ratio based on in weight of monomers and prepolymers.*
[b] *Molar Lactate/PEG ratio of the resulting multi-block copolymer as calculated based on in-weight of prepolymers*
[c] *Molar Lactate/PEG ratio of the resulting multi-block copolymer as determined from 1H NMR.*



## 2.2 Polymer characterization and in vitro polymer degradation

Thermal properties

Thermal properties of the synthesized polymers were measured by differential scanning calorimetry (DSC) using a Q1000 differential scanning calorimeter (TA instruments, Ghent Belgium) operated in the modulated mode (± 1.0 °C every 60 seconds) where the sample (5-10 mg) was heated from -85 to 180 °C at a rate of 5 °C/minute. During the measurement, the sample cell was purged with nitrogen. The reversed heat flow was used for determination of the glass transition temperature ($T_g$, midpoint), while the total heat flow was used for determination of the melting temperature (maximum of endothermic peak, $T_m$). The heat of fusion (ΔH (J/g)) was calculated from the surface area of the melting endotherm. Temperature and heat flow were calibrated using indium. Measurements were done in a single heating run by modulated DSC.

Chemical polymer composition evaluation

$^1$H NMR was used to determine the D,L-lactide/PEG (LA/PEG) monomer ratio of the multiblock copolymers after synthesis and during degradation. $^1$H NMR was performed on a VXR Unity Plus NMR spectrometer (Varian, California, USA) operating at 300 MHz. The d1 waiting time was set to 20 s, and the number of scans was 16–32. Spectra were recorded from 0 to 14 ppm. $^1$H NMR samples were prepared by dissolving 10 mg of polymer into 1 mL of deuterated chloroform ($CDCl_3$), and the spectrum was recorded from 0 to 8 ppm using $CHCl_3$ present as trace in $CDCl_3$ as reference. PDLLA/PEG

molar ratio was calculated from the -O-CH($CH_3$)C(O)- methine groups of PDLLA and D,L-lactide monomer at d 5.1–5.4 and d 5.0–5.1, respectively, and the -$CH_2CH_2$-O methine groups of PEG at d 3.6–3.7.

Molecular weight analysis

The number average molecular weight ($M_n$) and the weight average molecular weight ($M_w$) of synthesized polymers was determined using size exclusion chromatography (SEC-HPLC, Waters, Breeze, USA). Polymer samples (10 mg) were dissolved in DMF (1 mL) and PEG standards with molecular weights of 1-218 kg/mol were prepared likewise. Samples and PEG standards were injected (50 µL) onto the SEC column (Thermo Fischer, Column 1: Plgel 5 µm 500 Å, column 2: Plgel 5 µm 500 Å, column 3: Plgel 5 µm 104 Å, eluent: DMF with 0.1M LiBr, flow 1 mL/min). Polymers were detected by refractive index. The apparent molecular weights ($M_n$ and $M_w$) were then calculated with the aid of the PEG standards.

*In vitro* degradation

Polymer films with a thickness of 200-250 µm were prepared by dissolving 5 g of polymer in 45 g of DCM (10 wt.% polymer solution) and solvent casting of the solutions in Petri dishes and overnight incubation at RT to evaporate DCM followed by vacuum-drying at 50 °C for 5 days. Films were cut into 1x2 cm test samples with a weight of 50-150 mg and the obtained samples were then placed in test tubes containing 10-20 mL of 100 mM PBS (82 mM Na2HPO4, 18 mM $KH_2PO4$, 9 mM NaCl, and 0.2% $NaN_3$) pH 7.4 and incubated at 37 °C. At different time points test samples were collected, rinsed with demi-water over a 0.45 µm filter to remove buffer salts, blotted with tissue paper to remove excess of medium and weighed to determine their wet mass ($m_{wet,t}$) and swelling degree (SW). After vacuum-drying over silica gel, the weight of the sample was determined again ($m_{dry,t}$). The swelling degree and remaining mass were calculated as follows:

*(1)* $SW = (m_{wet,t} - m_{dry,t}) / m_{wet,t}$

*(2)* Remaining mass (%) = $100 \times m_{dry,t} / m_{dry,0}$

Where $m_{dry,o}$ and $m_{dry,t}$ are the masses of the dry sample at day 0 and dry sample at day t. GPC and $^1$H NMR measurements were performed in degraded samples as described above.

## 2.3 Preparation of monospheres

A membrane emulsification-based solvent extraction/evaporation process using microfabricated microsieve membranes with uniformly sized pores of 3.3 μm, 11 μm and 20 μm (Nanomi BV, The Netherlands) was used for the preparation of monospheres with target diameters of 5, 15 and 30 μm, respectively. To prepare the monospheres, approximately 0.5 g of 20[PDLLA-$PEG_{1000}$-PDLLA]-80[PLLA] was dissolved in 1.5 mL dichloromethane (DCM) to obtain a 20 % w/w solution which was subsequently filtered through a 0.2 mm PTFE filter. Using 35 mbar air-pressure, the filtered polymer solution (DP) was processed through the Microsieve membrane at an approximate rate of 0.12 mL/min into an aqueous solution containing 4 % w/v PVA (CP). The CP/DP volume ratio was around 35 v/v. The formed emulsion was stirred over a period of 3 hours at room temperature to extract and evaporate DCM. Hardened monospheres were collected by centrifugation at 2000 rpm for 3 min, washed twice with demiwater and twice with 0.05 % w/v aqueous Tween 20 solution and finally lyophilized. Tween 20 was used to facilitate the re-dispersion of the monospheres during re-constitution in the injection medium.

For the preparation of perylene red loaded monospheres, the dye was co-dissolved with 20[PDLLA-$PEG_{1000}$-PDLLA]-80[PLLA] (20 % w/w) in a 1:100 w/w ratio, where after the monospheres were prepared using the same membranes and procedures as described above. Similarly, monospheres containing 0.5 % w/w NIR-780F were prepared by co-dissolving the dye and 16[PDLLA-$PEG_{1000}$-PDLLA]-84[PLLA] (20% w/w ) in a 1:200 w/w ratio.

Prior to intra-articular injection in rats, monospheres were dispersed in freshly prepared sterile injection medium (0.4 wt.% CMC, 0.1 wt.% Tween 20 and 5.0 wt.% mannitol). For injection in mice and horses the monospheres were reconstituted in saline.

## 2.5 Monosphere characterization

Monospheres were visually examined by optical microscopy. Particle size was determined by dispersing 5-10 mg of monospheres in 50-100 mL of electrolyte solution (Beckman Coulter, Woerden, The Netherlands) and measuring the particle size distribution (PSD) with a Multisizer 3 Coulter Counter (Beckman Coulter, Woerden, The Netherlands) equipped with a 200 μm measuring cell. The volume average particle size (D50) and coefficient of variance (CV%) were determined from the PSD.

Surface morphology of the monopsheres was assessed by scanning electron microscopy (JCM-5000 Neoscope, Jeol, Germany). Freeze dried samples of monospheres were sputtered with a thin layer of gold using the JFC Neocoater (Jeol, Germany).

Residual dichloromethane content of lyophilized monopsheres was determined by GC-FID using a TraceGC gas chromatograph (Thermo Finnigan, Rodano, Milan, Italy) equipped with a CombiPal headspace module (CTC Analytics AG, Zwingen, Switzerland)

and an Agilent Column, DB-624/30 m/0.53mm and using dichloromethane standards in DMSO in the range of 0-2000 ppm.
Endotoxin evaluation was performed by Limulus amoebocyte lysate assay according to the chromogenic endpoint standard procedure, with a lower limit of detection of 0.05 EU/mL.

## 2.6 Intra-articular retention of injected monospheres

All experimental procedures were approved by the Subcommittee on Research Animal Care at Leiden University Medical Center. Male FVB mice (4–8 weeks of age, from the LUMC breeding facility) were used for both experiments. Initially, the capacity of the 20[PDLLA-$PEG_{1000}$-PDLLA]-80[PLLA] monospheres to remain intra-articular was tested. Two mice were injected intra-articularly with 10 µl of a NIR-780F suspension in saline (10 µg/ml) while 2 other mice received a 10 µl intra-articular injection of 1 % w/w NIR-780F loaded monospheres suspension in saline (1 mg /mL) using a 30 Gauge BD Micro-Fine syringe. In both groups the total amount of NIR-780F injected was of 0.10 µg. *In vivo* scans were made 24 hours post-injection to check intra-articular retention and biodistribution. For the second experiment, knee joints were injected bilaterally with monospheres of different sizes (5, 15 and 30 µm; n=3 knees/size), and the intra-articular presence of monospheres was determined by fluorescence imaging of the injected knees of the mice at t=0, t=1d, t=2d, t=6d, t=9d, t=39d and t=90d.
In the first experiment (free NIR-780F versus NIR-780F dye-loaded monospheres) fluorescence imaging of monospheres was performed with the Pearl Impulse (Li-cor, Lincoln, Nebraska USA). In the second experiment (differently sized monospheres) fluorescence imaging was performed with an IVIS Spectrum animal imaging system (Perkin Elmer/Caliper LifeSciences, Hopkinton, MA). For this second experiment, monospheres were loaded with perylene red. This dye was selected over NIR-780F because detectability was superior. Scans were made while the mice were anesthetized with 1.5% of Isoflurane balanced with oxygen. After the last scan (day 90), the mice were sacrificed, overlying skin was removed and *ex vivo* scans of the knees were made to check for remaining signal. For spectral unmixing, an image cube was collected on the IVIS Spectrum with 18 narrow band emission filters (20 nm bandwidth) that assist in significantly reducing autofluorescence by the spectral scanning of filters and the use of spectral unmixing algorithms. Fluorescence regions were identified and spectrally unmixed using Living Image 4.3.1 software. Because of the 3D character of the joints, a reliable quantification of the amount of signal over time could not be made. Therefore, we present results based on whether there was still any signal detectable or not.

## 2.7 Intra-articular biocompatibility in horses

All experimental procedures and protocols were approved by the Utrecht University Committee on the Care and Use of Experimental Animals in compliance with Dutch legislation on experimental animal use. Due to the limited number of horses available for experiments, we only tested the 30 μm monospheres. The horses used in this experiment had clinically normal middle carpal joints (radiographically confirmed). The left middle carpal joint was injected with 3 ml saline solution (control), while the right middle carpal joint was injected with 200 mg of 30 μm monospheres suspended in 3 ml saline.

### 2.7.1 Lameness

Lameness examinations were conducted at 0, 8, 24, 72 hours and 1, 2, 3, 4 weeks post injection, using a standardized scale of 0 to 5 [241]. Horses were monitored throughout the whole study for signs of discomfort.

### 2.7.2 Synovial fluid analysis

Synovial fluid was aspirated aseptically at the same time points the lameness examinations were conducted. A portion of the fluid was processed for white blood cell (WBC) count and total protein measurement. The remaining volume was centrifuged and analyzed for glycosaminoglycan (GAG) concentrations with a modified 1,9-dimethylmethylene blue dye-binding assay used previously in our laboratory [242]and collagen type 2 breakdown was measured by an antibody against a collagen type 2 epitope (C2C) as previously reported [242].

### 2.7.3 Synovial tissue analysis

To check the intra-articular retention of the monospheres in the equine joints, parts of the synovial tissue surrounding the third carpal bone were removed for histological analysis. After fixation in formalin, the synovial tissue was divided in two parts. The first part was used for light microscopic verification of the presence of monospheres within the synovial tissue 4 weeks after intra-articular injection. The second part was used for the same purpose using SEM.

## 2.8 Intra-articular biocompatibility in rats

The Animal Ethic committee of the Erasmus Medical Center, Rotterdam, The Netherlands, approved all conducted procedures. Twelve 16-week-old (400-450 g) male Wistar rats (Charles River Nederlands BV, Maastricht, The Netherlands) were housed in the animal facility of the Erasmus Medical Center, with a 12-h light-dark regimen, at 21°C. Animals were fed standard food pellets and water *ad libitum*. Experiments started after a 2 weeks acclimatization period. Since all monospheres of different sizes were retained in the knee joint (results of IVIS studies in mice), we choose to only test the

smallest and largest monospheres. The desired amounts of monopheres (5 μm: 2 mg/30 μl and 30 μm: 10 mg/50 μl) were re-suspended in injection medium and injected into the left knee of the rats (n=12) using a 27G syringe (Kendall, monoject). Contralateral knees were injected with the same volume of saline and served as controls. Scans of all knees were acquired at 3 different time points (t=0, t=6w and t=12w). Following the last scan, knees were harvested and EPIC μCT-scanning was performed [96].

2.8.1 μCT arthrography

Cartilage quality (sulphated glycosaminoglycan (sGAG) content) and quantity (thickness) was measured with *in vivo* μCT arthrography. Therefore, knees were injected with a radiographic contrast agent (Hexabrix (Hexabrix 320, Mallinckrodt, Hazelwood, MO, USA) mixed with 10 μg/ml Epinephrine) as described previously [96, 97]. Influx of Hexabrix into the cartilage correlates inversely with sGAG content [98, 99]; therefore, early changes in cartilage quality and quantity are measurable using *in vivo* μCT arthrography [96, 97]. After injecting Hexabrix, rats were placed in a custom-made scanner bed fixing the hind limb in extended position. Scans were made using an *in vivo* scanner (Skyscan model 1176, Skyscan, Kontich, Belgium) using the following scanner settings: isotropic voxelsize of 18 μm, 67 kV, 380 mA, 35 mm field of view, 1.0 mm Al filter, 0.5 rotation step over 198°, frame averaging of 2. Both knees were scanned at all 3 time points (t=0, 1 and 6 weeks). Due to incomplete Hexabrix influx in some knees, a total of 7 animals were available for longitudinal analysis.

2.8.2 EPIC μCT imaging

Equilibrium partitioning of a contrast agent using μCT (EPIC-μCT) shows a strong correlation with cartilage sulphated-glycosaminoglycan (sGAG) content [135]. Following the last *in vivo* μCT scan, rats were sacrificed and knees were dissected with removal of the surrounding soft tissue. The tibiae were incubated for 24 hr in a 40% Hexabrix solution at room temperature in order to achieve equilibrium between the contrast agent and the sGAG content of the cartilage [99]. After 24 hr, samples were scanned using the following settings: isotropic voxelsize of 18 μm, 60kV, 170 mA, 885 ms exposure time, 35 mm field of view, 0.5 mm Al filter, 0.8 rotation step over 198°, frame averaging of 3.

2.8.3 μCT data analysis

Obtained raw *in vivo* μCT images were converted into 3D reconstructions using the reconstruction software nRecon version 1.5 (SkyScan). With 3D Calc software segmentation into binary images [100] took place creating a mask overlaying bone and Hexabrix in the original gray value images (ImageJ; NIH, http://imagej.nih.gov/ij/index.html). Subsequently, regions of interest (ROIs) were drawn around the patellar cartilage (40 slices) for which attenuation and thickness were calculated. In the datasets

acquired with EPIC-μCT imaging ROIs were drawn directly around the Hexabrix saturated cartilage of both the medial and lateral tibial plateau of the 3D reconstructed images. Subsequently, global segmentation took place between the cartilage and the adjacent areas (subchondral bone and air) and attenuation and volume of the cartilage were measured.

2.8.4 Histological analysis

Directly following the EPIC scans, knee joints were fixed with formalin, decalcified and embedded in paraffin. Six μm sections were prepared sagitally at 300 μm intervals and stained with Safranin-O. At different time points, the infrapatellar folds containing the synovial membrane of the knees injected with 5 μm monospheres were removed and immunostained in order to check for the presence of macrophages due to the presence of particles < 10 μm. The tissue was embedded in paraffin and cut in 6 μm sections. These sections were dewaxed and pre-treated with heat mediated antigen retrieval (Dako S1699, Glostrup, Denmark) at 90°C for 20 minutes. Subsequently, sections were incubated with CD68 (1:100, Acris, Herford, Germany) for 60 minutes and visualized with AP link and label kit (Biogenex, Fremont, CA, USA), followed by a New Fuchsin substrate. Sections were dried overnight and mounted with Vectamount (Vectorlaboratories, Burlingame, CA, USA).



## 2.9 Statistical analysis

Differences in μCT-data and histological scoring between the microsphere-injected knees and the contralateral knees were all calculated using type-1, two-tailed, paired T-tests. The differences between monospheres-injected knees and the osteoarthritic control group was calculated using type-1, two-tailed unpaired T-tests. For the measurement in the horse SF samples, the control and monospheres-injected joints were compared using paired T-tests at all time-points. Additionally, the longitudinal data were analyzed using a lineair mixed model with post-hoc Bonferroni correction, CI 95%. All statistical tests were performed using SPSS-20. P-values<0.05 were considered statistically significant.

# 3. Results

## 3.1 Polymer synthesis and characterization

3.1.1 Polymer characterization

Block copolymers with different [PDLLA-$PEG_{1000}$-PDLLA] / [PLLA] ratios were synthesized and their characteristics are reported in table 2. This table shows that LA/PEG molar ratios of the xx[PDLLA-$PEG_{1000}$-PDLLA]-yy[PLLA] multi-block copolymers were between 46 and 285 mol/mol, close to the theoretical values (Table

2). GPC was performed relative to PEG standards and the apparent molecular weight values were obtained with values ranging from 33.6 to 49.6 kDa for $M_w$ and from 17.6 to 28.8 kD for $M_n$. Differential scanning calorimetry (DSC) thermograms showed a slight decrease of the melting temperature of the polymers (from 136ºC to 123ºC) upon increasing the block ratio of PDLA-$PEG_{1000}$ from 10/90 to 50/50. Whereas the $T_g$ decreased significantly from 53 °C to -5 °C. Swelling degrees (SW), as determined after 1 day of incubation, increased from 1.1 for 10[PDLLA-$PEG_{1000}$-PDLLA]-90[PLLA] to 1.5 for 50[PDLLA-$PEG_{1000}$-PDLLA]-50[PLLA].

*3.1.2 In vitro* polymer degradation

The degradation profile of films of the different polymers presented similar behavior. As shown in Figure 1-A, mass loss followed a two-phase behavior with an initial phase where fast degradation occurred and a second phase where the mass reduction rate was lower. The polymer with the highest PEG content (50[PDLLA-$PEG_{1000}$-PDLLA]-50[PLLA]) lost 46% of its weight after one week, whereas the polymer with the least PEG content (10[PDLLA-$PEG_{1000}$-PDLLA]-90[PLLA]) only lost 3% during the same period of time. The same behavior was observed for the PEG loss as a function of time (figure 1-B).

***Table 2**. Composition, PEG content, thermal properties and swelling degree of various xx[PDLLA-$PEG_{1000}$-PDLLA]-yy[PLLA] multi-block copolymers.*

| # | Polymer composition | PEG (wt%) | $M_w$ (Da) | $M_n$ (Da) | $T_g$ (°C) | $T_m$ (°C) | ΔHm J/g | Sw (-) |
|---|---|---|---|---|---|---|---|---|
| 1 | 10[PDLLA-$PEG_{1000}$-PDLLA]-90[PLLA] | 5 | 49600 | 28800 | 51 | 136 | 67.5 | 1.1 |
| 2 | 20[PDLLA-$PEG_{1000}$-PDLLA]-80[PLLA] | 10 | 33600 | 19200 | 39 | 130 | 43.9 | 1.1 |
| 3 | 30[PDLLA-$PEG_{1000}$-PDLLA]-70[PLLA] | 15 | 33800 | 17600 | 21 | 129 | 35.5 | 1.2 |
| 4 | 50[PDLLA-$PEG_{1000}$-PDLLA]-50[PLLA] | 25 | 46100 | 26700 | -5 | 122 | 17.5 | 1.5 |

*$M_w$: Weight average molecular weight; $M_n$: Number average molecular weight; $T_g$: glass transition temperature; $T_m$: melting temperature; ΔHm: melting enthalpy; $S_w$: swelling degree, as determined after 1 day of incubation.*

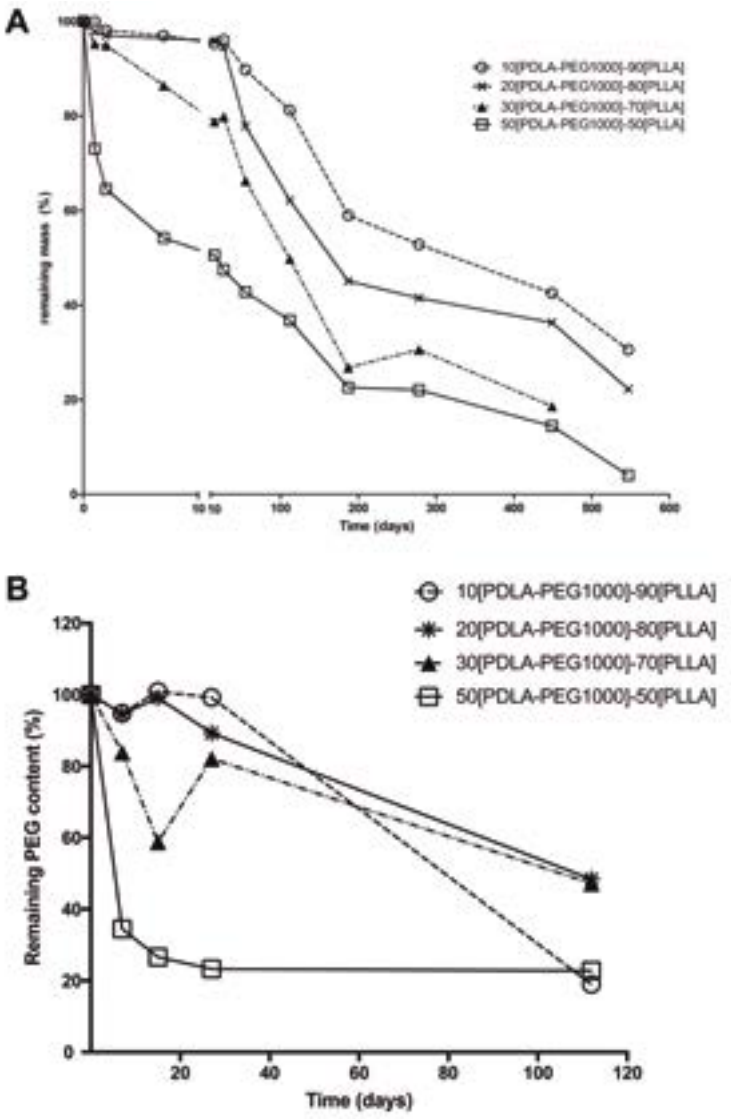


***Figure. 1**. **A**) In vitro degradation of xx[PDLLA-PEG1000-PDLLA]-yy[PLLA] multi-block copolymers expressed as remaining mass as a function of time [left] and PEG lost as a function of time [right] upon incubation in PBS, pH 7.4 and at 37 °C. **B**) The same degradation, expressed as PEG loss as a function of time.*

## 3.2 Monosphere characterization

Residual dichloromethane content of lyophilized monospheres was < 600 ppm and endotoxin levels were < 0.01 EU/mg, meeting the acceptance limits for parenteral injections [243]. Coulter Counter measurements indicated that the different

monospheres have a narrow particle size distribution (figure 2-A). The average diameter (and coefficient of variance (CV)) of the differently sized monospheres were respectively 4.7µm (CV 32.4%), 15.5 µm (CV 18.6%) and 34.4µm (CV 12.9%). Figure 2-B) shows a SEM picture of the three different monosphere sizes, clearly visualizing their size uniformity and their smooth and non-porous surface (non-spherical particles correspond to mannitol particles, which was used during washing and before freeze drying of the monospheres (see supplementary figure 1).

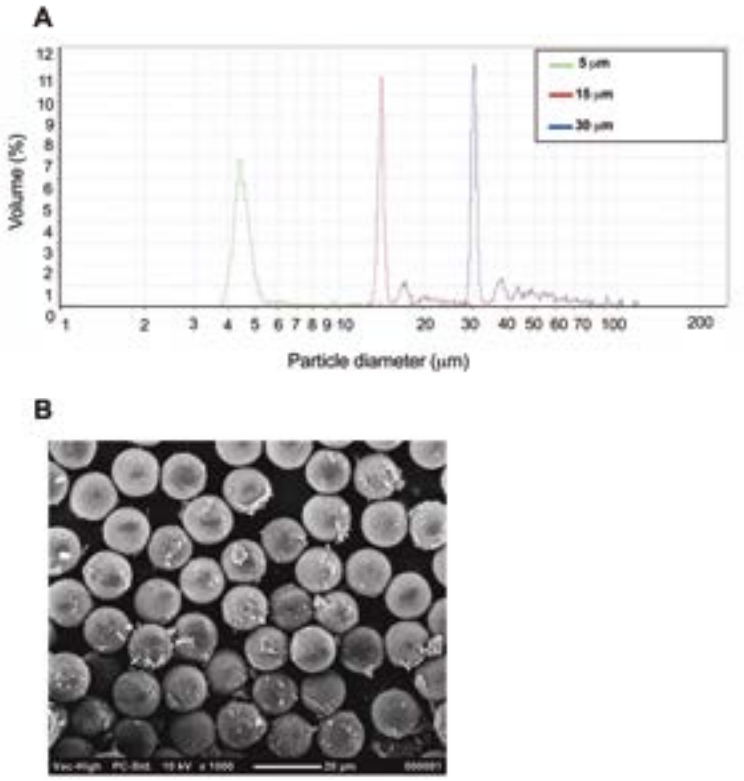


***Figure 2. A****) Particle size distribution of 20[PDLLA-PEG1000-PDLLA]-80[PLLA monospheres: 5, 15 and 30 µm.* ***B****) SEM picture of 15 µm 20[PDLA-PEG1000]-80[PLLA] monospheres. This picture shows the size uniformity of the batches. Mannitol was used during the washing and before freezing of the monospheres, explaining the irregularities seen in the picture. The surface of the monospheres appears smooth and without pores.*

## 3.3 Intra-articular retention and degradation kinetics

Equine intra-articular monosphere retention

*In vitro* evaluation of the perylene red loaded monospheres was performed to ensure that the dye was not released prematurely from the 20[PDLLA-$PEG_{1000}$-PDLLA]-80[PLLA]

monospheres. Therefore, the monospheres were incubated in release buffer (100 mM phosphate buffer, pH 7.4) at 55°C (to accelerate degradation) and the supernatant was inspected daily. The supernatant remained clear for up to 10 days, after which perylene red started to leak from the monospheres. To verify that the monospheres would retain enough perylene red during the course of the *in vivo* experiments, tissue surrounding the equine middle carpal joint was harvested 4 weeks after intra-articular injection with perylene red loaded monospheres. In all horses parts of the tissue were red (figure 3; left image) and upon microscopic evaluation this coloring was shown to indeed be due to the actual presence of perylene red loaded monospheres (figure 3; middle image).


***Figure 3.*** *Equine third carpal bone excised 4 weeks after intra articular injection of perylene red loaded monopsheres. In the surrounding tissue the red dye can be easily observed (left). Microscopic images of this tissue show that the red color is indeed due to the presence of monopsheres (middle). SEM pictures of these monospheres are shown on the right.*



IVIS scanning mice

IVIS analysis of intra-articularly injected NIR-780F encapsulated in monospheres showed a distinct signal only at the site of injection, contrary to the aqueous suspension of the free fluorescent dye which quickly redistributed from the knee throughout the whole body within the first 24 hours (figure 4). Up to 39 days, in all mice injected with perylene red-loaded monospheres, a clear signal was observed at the knee joint without re-distribution to other parts of the body. At 90 days post-injection, the signal was below detection limit in one animal only of the 5 µm monospheres group whereas in all other groups perylene fluorescence was still detected, demonstrating that at 90 days microspheres were still present. Subsequent *ex vivo* scans of the knee joints showed the presence of monospheres by remaining signal (figure 4) in all animals, irrespective of monosphere size.

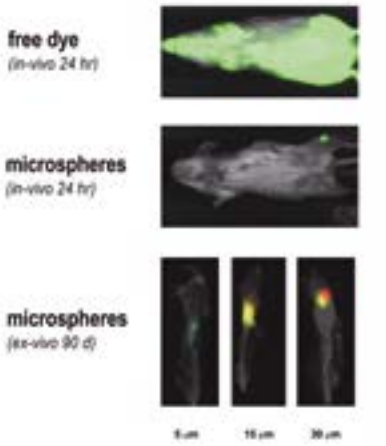


***Figure 4.*** *Fluorescent images of intra-articular retention of free dye and dye-loaded monopsheres in mice. Representative fluorescent images are shown for 24 h after intra- articular injection of free fluorescent dye, NIR-780F (upper picture) and monospheres (15 µm) containing the same dye (middle picture); the monospheres were able to retain the dye locally whereas the freely injected dye redistributed throughout the whole body quickly. The lower picture shows ex-vivo IVIS-scans of knees containing perylene red loaded 5 µm, 15 µm or 30 µm monospheres 90 days after injection. At this final time point, for all sizes there we still monospheres present within the knee joints.*

## 3.4 Intra-articular biocompatibility in horses

None of the horses showed any signs of discomfort following the intra-articular injection of 30 µm 20[PDLLA-$PEG_{1000}$-PDLLA]-80[PLLA] monospheres. Locomotion was not affected, as the lameness score for both monospheres and saline injected joints was 0 (maximum=5) for all horses throughout the whole study.

### 3.4.1 Synovial fluid analysis

Intra-articular injection of unloaded monospheres led to a significant increase of WBC in the synovial fluid 8 hrs after injection when compared to saline injected joints (figure 5-A). At t=24 and 72 hours post injection, elevated values were still found compared to the saline-injected joint, although no significance could be found in this small group. Compared to baseline values, both saline- and monospheres injected joints showed a trend of increased WBC in the SF for a period of 72 hours after the injection, which had returned to normal at one week after injection. Total protein content (figure 5-B) also increased from t= 8 hours until 1 week post injection due to the intra-articular injection of monospheres (significant differences at 8 hours, 24 hours and 1 week). At baseline (before injecting either saline of monospheres in the joints), a significant difference in GAG was found between the two groups. For all time points GAG release into the SF remained at or below baseline values. At some time points, significant differences were

seen when compared to the control joint (saline injected) but there was not a clear trend and the phenomenon seemed to appear quite randomly. Moreover, compared to values found in a previously conducted study, our values are in the range of what is normally found in healthy joints, and a tenfold lower than values found in inflamed joints [242] Also, Hyonate®, which is clinically accepted and used as an intra-articular intervention for OA, is proven to give rise of the GAG-content in synovial fluid of horses 1 day after injection [166]. No increase in C2C epitope content (collagen breakdown biomarker) was found at any time point (figure 5-D), indicating that no significant damage to the cartilage occurred due to the intra-articular injections. A significantly lower C2C content in the synovial fluid was detected at 8 hours after microsphere injection compared to the control joints. However, there is no clear explanation for this observation and this is therefore likely due to physiological fluctuation. Moreover, comparing our values to what was found in a previously conducted study, C2C epitope in the synovial fluid remained at base-line levels showing that the differences found are indeed a fluctuation of physiological levels and not considered to be clinically significant [166].

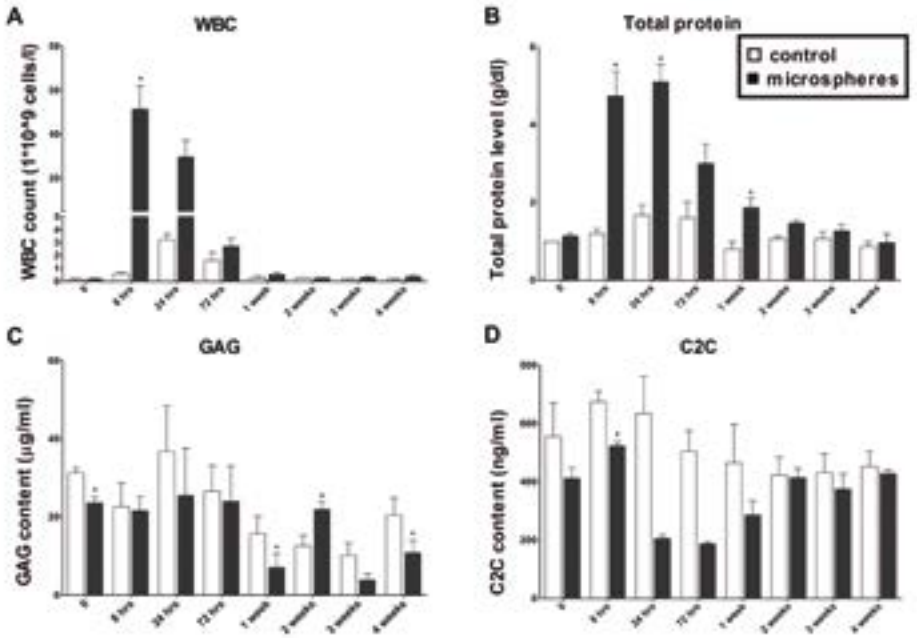


***Figure 5.*** *Synovial fluid analysis: White Blood Cell count (**A**), Total protein levels (**B**), GAG content (**C**) and C2C content (**D**). (n = 3, control: saline injected joints, monopsheres: monopsheres injected joints. Values are depicted as mean ± SD; *: $p < 0.05$ vs. control.*

## 3.5 Intra-articular biocompatibility in rats

3.5.1 *In vivo* μCT arthography scanning

Following the intra-articular injections, no toxic responses (e.g. changed locomotion, joint redness/swelling) occurred during the 12-weeks observation period. Arthographies at t=0 showed a small difference ($p<0.05$) in attenuation between microsphere- and saline injected knees (figure 6), however this difference is not clinically relevant since it is well within the range of what is normally found for healthy cartilage and much lower than diseased cartilage [136, 244]. Neither compared to baseline nor to the contralateral control knees (saline), changes in patellar cartilage quality or quantity occurred over the full course of the experiment (t=6 and 12 weeks).

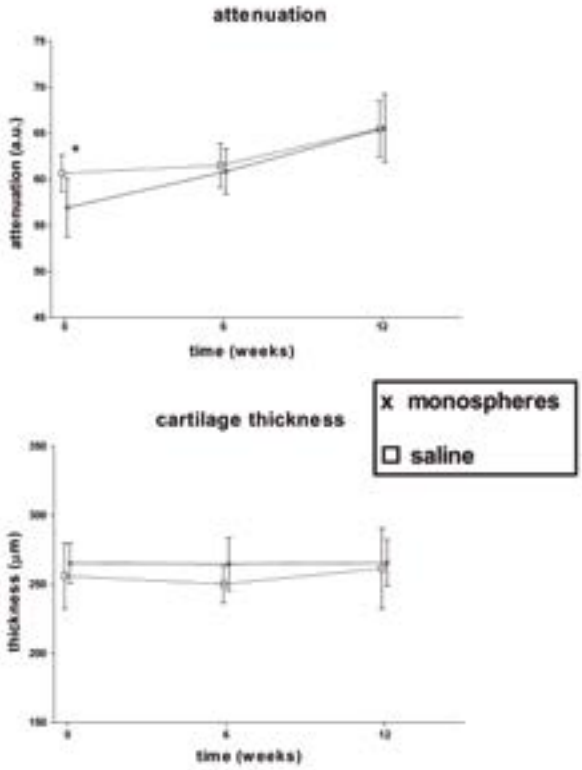


***Figure 6.*** *Attenuation (in arbitrary units) and cartilage thickness (in μm) of the patellar cartilage measured over time with the use of in vivo longitudinal μCT arthographies (5 μm and 30 groups combined; n = 7 in total). No significant changes occurred during the course of 12 weeks after intra-articular injection of unloaded monospheres when compared to both baseline measurement and control knees (saline injected).* $^{*}p < 0.05$.

3.5.2 EPIC scanning

Analysis of the rat tibial cartilage (figure 7-A with representative images shown in figure 7-B), both medial and lateral, showed that no differences were observed between the saline and monospheres injected knees with respect to either cartilage thickness or quality (sGAG content). Moreover, no surface irregularities due to possible indentation of the monospheres were seen in any of the samples. Data of EPIC scans made after unilateral osteoarthritis induction performed in a previous study by our group [136] are shown as well for comparison, showing changes in attenuation and cartilage thickness that are specifically found in rat knees affected by osteoarthritis.

3.5.3 Histology cartilage

Histology confirmed the findings of both the *in vivo* and EPIC scans. No differences in safranin O staining were found between monospheres injected rat knees (5 and 30 μm) and their controls. Also, morphologically the cartilage appeared healthy in all groups. In figure 7-C, representative histological images of saline and monospheres injected knees are shown, for comparison also a diseased knee (OA) is shown with clear signs of GAG leakage and loss of cartilage thickness.



3.5.4 Histology surrounding tissue

As stated earlier, 5 μm monospheres can be taken up by synovial macrophages while 30 μm monospheres would not be phagocytized [245, 246] and are therefore more likely to stay within the synovial fluid. This is indeed what was seen macroscopically after opening of injected knee joints; 5 μm monospheres were taken up already 24 hours after injection while 30 μm monospheres could still be identified in the synovial fluid 4 weeks post-injection. Based on these observations, we decided to more extensively investigate the macrophage infiltration of knees injected with 5 μm monospheres at several time points. The infrapatellar folds containing the synovial membrane were harvested at several time points. Immunohistochemistry on the excised tissues surrounding the knee joint indeed showed positive CD68 staining 24 hours and 4 days after intra-articular injection of the 5 μm monospheres, indicating macrophage infiltration (figure 7-D). More detailed analysis of the image with the highest amount of macrophages (day 4), showed that some macrophages had indeed phagocytosed monospheres. Two weeks after injection, macrophage infiltration had decreased significantly and 6 weeks after injection hardly any macrophages could be observed. At all time points after injection, some neutrophils were accumulated in the connective tissue, being most prevalent at t= day 4 and t= 2 weeks.

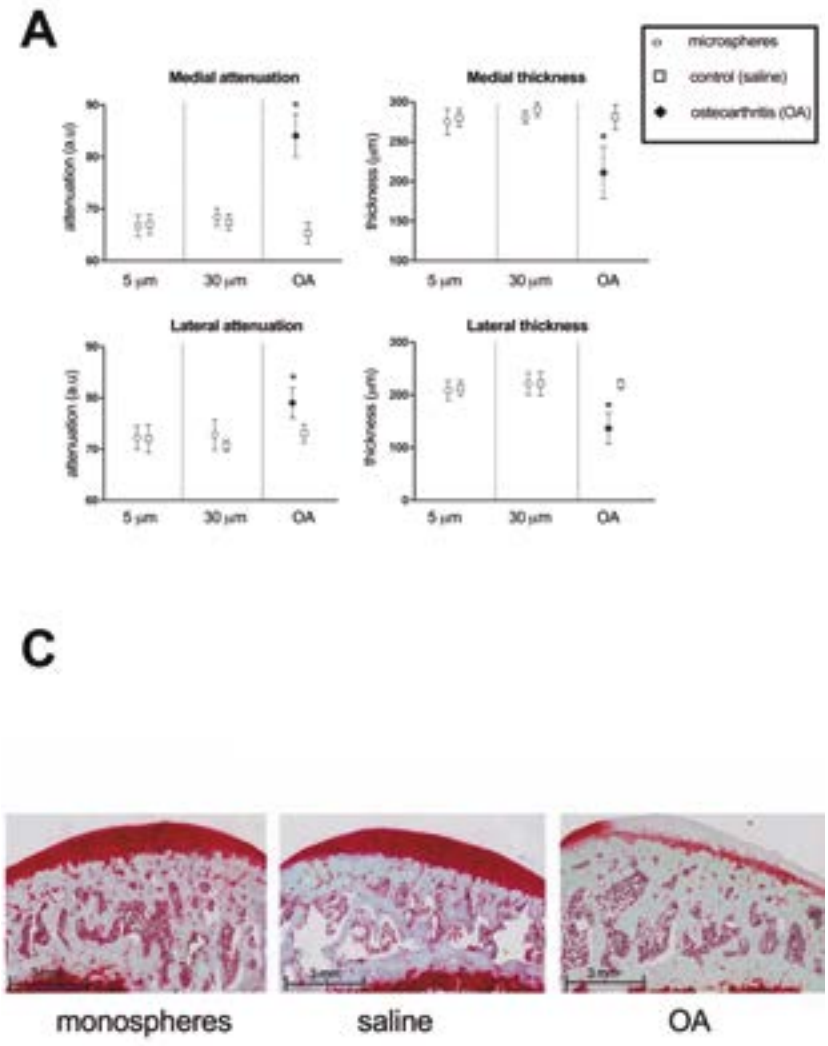


***Figure. 7. A****) Graphs representing cartilage quantity (thickness) and quality (attenuation) of monospheres injected knees vs. control knees (saline injected) measured with EPIC scanning. As a comparison, values of OA knees are also presented. No significant differences were found between monospheres- and saline injected knees.* $^{*}$*: All measurements of OA knees were significantly different from both saline- and monospheres injected knees.* ***B****) Representative EPIC images of the medial and lateral tibial plateau of monospheres (5 and 30 µm) and saline injected knees 12 weeks post-injection as well as a knee with induced OA. No changes in cartilage thickness and attenuation occurred (see color scheme) in monospheres injected knees* ***C****) representative histological images of knees injected with either monospheres or saline, stained with Saf-O (cartilage in red); on the right an OA specimen.* ***D****) Histology of macrophage-staining performed on synovial tissue retrieved at different time points related to intra-articular 5 µm mono-*

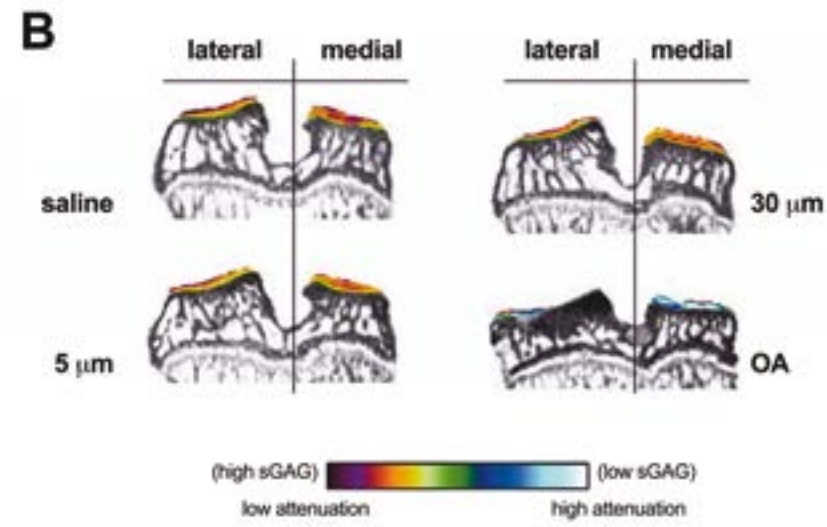


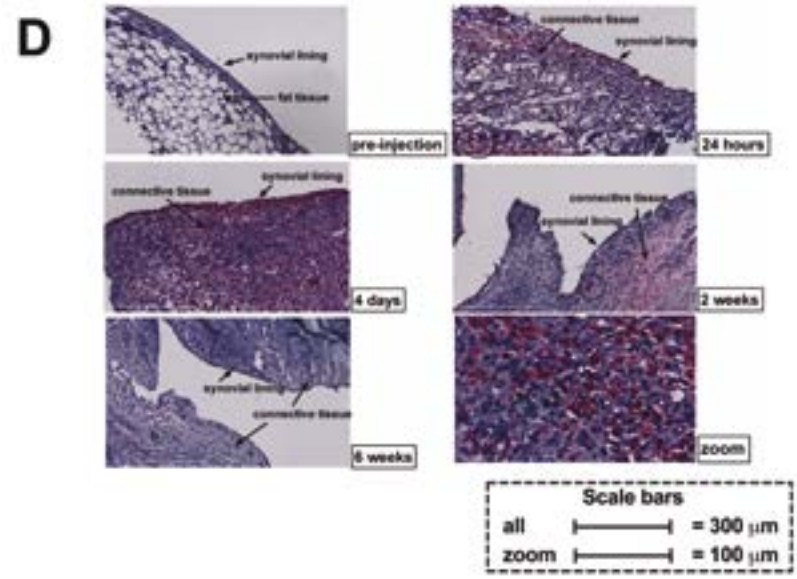


*spheres injection (before, after 24 h, 4 days, 2 weeks and 6 weeks). Macrophages are stained red. These images show that the presence of monospheres (which also seem to take up some of the staining) in the knee joint triggered an inflammatory macrophage reaction, which had returned to baseline at the 2 weeks time point. At all time points following the injection, neutrophils are present. Furthermore, these images show that some of the monospheres are taken up by the cells (likely macrophages) within the synovial tissue. This phenomenon did not occur yet at the 24 h time point, but was prevalent 4 days after injection (see 6x zoomed image).*

## 4. Discussion

The aim of this study was to investigate the suitability of different biodegradable multi-block copolymers for the development of injectable monospheres for local intra-articular drug delivery. First of all, we tested *in vitro* which copolymer would be most suitable for this application. Different xx[PDLLA-$PEG_{1000}$-PDLLA]-yy[PLLA] multi-block co-polymers of different composition were characterized on their composition, molecular weights and thermal properties (glass transition temperature and melting temperature/ enthalpy) as well as for their *in vitro* degradation characteristics. $^1$H NMR analysis confirmed that the LA/PEG molar ratios of the xx[PDLLA-$PEG_{1000}$-PDLLA]-yy[PLLA] multi-block copolymers were in line with their feed compositions. DSC confirmed the phase-separated nature of the xx[PDLLA-$PEG_{1000}$-PDLLA]-yy[PLLA] multiblock copolymers, showing a distinct glass transition temperature ($T_g$) for the PDLLA-$PEG_{1000}$-PDLLA based amorphous domains, along with a clear melting peak for the PLLA-based crystalline domains. These crystalline domains act as physical crosslinks and control the swelling of the amorphous PEG/PDLLA phase in the polymeric material under physiological conditions. The significant decrease in $T_g$ observed upon increasing the PDLLA-$PEG_{1000}$-PDLLA / PLLA block ratio from 10/90 to 50/50, is caused by PEG which acts as plasticizer and reduces the $T_g$ of the amorphous block due to the its complete miscibility with amorphous PDLLA [247, 248]. Although the changes in $T_m$ were not as noticeable as in the case of $T_g$, the decrease in the melting enthalpy ($\Delta$H) showed that the crystallinity of the multi-block copolymers decreased with increases of overall PEG-content in the polymer matrix ($\Delta$H decreased from 59.8 J/g for 5wt.% PEG-containing polymer to 16.1 J/g when 25wt.% PEG was present). Increasing the PEG content in the polymer composition also had an impact on the swelling of the matrix (table 2) due to the hydrophilic behavior of this polymer [249]. This could be relevant for future evaluation of drugs encapsulated within these matrices because the release of encapsulated compounds usually occurs via diffusion through the swollen polymer matrix. Furthermore, an accelerated mass loss during the initial phase of *in vitro* degradation was observed for the polymers with a higher content of the amorphous block, most probably caused by PEG loss. This is in line with our $^1$H NMR measurements and with other published studies on PEG-containing block co-polymers, where PEG preferentially leaves the material during early stages of degradation due to preferential cleavage of the ester bonds that connects PEG and the amorphous polyester block [58, 250-252]. Although a residual amount of tin octanoate was still present in the multiblock co-polymers, it was not expected to have a detrimental effect during in-vivo studies since it is below the maximum parenteral exposure stablished by the ICH guidelines (640µg/day) [253].

***Table 2**. Composition, PEG content, thermal properties and swelling degree of various xx[PDLLA-PEG$_{1000}$-PDLLA]-yy[PLLA] multi-block copolymers.*

| # | Polymer composition | PEG (wt%) | $M_w$ (Da) | $M_n$ (Da) | $T_g$ (°C) | $T_m$ (°C) | ΔHm J/g | Sw (-) |
|---|---|---|---|---|---|---|---|---|
| 1 | 10[PDLLA-PEG$_{1000}$-PDLLA]-90[PLLA] | 5 | 49600 | 28800 | 51 | 136 | 67.5 | 1.1 |
| 2 | 20[PDLLA-PEG$_{1000}$-PDLLA]-80[PLLA] | 10 | 33600 | 19200 | 39 | 130 | 43.9 | 1.1 |
| 3 | 30[PDLLA-PEG$_{1000}$-PDLLA]-70[PLLA] | 15 | 33800 | 17600 | 21 | 129 | 35.5 | 1.2 |
| 4 | 50[PDLLA-PEG$_{1000}$-PDLLA]-50[PLLA] | 25 | 46100 | 26700 | -5 | 122 | 17.5 | 1.5 |

*$M_w$: Weight average molecular weight; $M_n$: Number average molecular weight; $T_g$: glass transition temperature; $T_m$: melting temperature; ΔHm: melting enthalpy; $S_w$: swelling degree, as determined after 1 day of incubation.*



For *in vivo* evaluation of differently sized monospheres, the 20[PDLLA-PEG$_{1000}$-PDLLA]-80[PLLA] multi-block co-polymer was chosen because it presented little degradation during the first weeks, allowing release of potentially encapsulated drugs, and a second phase of accelerated degradation, which would facilitate the elimination of the monospheres from the treated joint. Besides, this polymer contains 10% PEG, making it soft enough for intra-articular use and a potential carrier for the sustained release of hydrophobic small drug molecules (MW 350 – 1000 g/mole) that are typically used for OA treatment such as steroid and non-steroid anti-inflammatory drugs [166, 213, 254]. We previously tested the mechanical compatibility of these monospheres with the cartilage. In short, the average Young's moduli of the materials in the swollen state are within the same range as the mechanical properties of healthy bovine cartilage and human osteoarthritic cartilage [228, 255]. This indicates that the presence of this type of monospheres within the joint would not be likely to cause cartilage damage due to surface indentation or grinding. Furthermore, the total water uptake and thus mechanical properties can be customized depending on the needs of any target tissue by simply changing the PEG content of the monospheres. The selected 20[PDLLA-PEG$_{1000}$-PDLLA]-80[PLLA] multi-block co-polymer was used to make microspheres of 3 different sizes with the use of the microsieve membrane emulsification process. Size uniformity was reached for all batches (target particle size of 5, 15 and 30 μm), as shown in figure 2-A and 2-B. These results confirm the suitability of this process to prepare monospheres with well-defined size and with a narrow particle size distribution. As stated before, narrow particle size distribution allows the use of smaller needles and consequently less painful injections. Indeed, monosphere suspensions were well

injectable through a 27G needle at concentrations up to 25% wt. (data not shown). Furthermore, the absence of very small microspheres could avoid particle-induced immunoactivation [217] and size uniformity allows more reproducible and predictable *in vivo* release kinetics [227, 228].

It is very important for a drug delivery system specifically designed for intra-articular use to be able to stay within the injected joint long enough to fully release the loaded drug locally, and in a timescale where it could potentially be effective for joint repair and/or pain relief. *In vitro* evaluation of the monospheres under the above described accelerated conditions retained the dye up to 10 days, which could be translated to approximately 80 days [256, 257] under physiological conditions. In short, an experiment was performed to determine whether the dye is retained in the monospheres during degradation.

Real time (37°C, pH7.4) degradation testing shows the presence of microspheres after 80 days. This was confirmed by the *in vivo* experiments on tissue surrounding the equine middle carpal joint. We also showed the potential of 5, 15 and 30 μm monospheres to remain intra-articular for at least 3 months, allowing the monospheres to act as a sustained local drug delivery system. After showing that the monospheres remained in the injected joints for a period long enough to release any encapsulated drug, we extensively tested the intra-articular biocompatibility of the monospheres. This is a very important part in the fabrication of any intra-articular drug delivery system, since the drug carrier intended to treat joint diseases like osteoarthritis should clearly not lead to negative effects in the joint upon intra-articular application. In horses, the intra-articular injection of unloaded monospheres gave rise to a mild transient inflammatory response, shown by a significant increase of WBC and total protein content in the synovial fluid (figure 5-A) of 72 hours and thereafter returned to baseline level quickly. A similar transient inflammatory reaction has been shown previously after intra-articular injection of hyaluronic acid (HA), a regulatory approved and widely used clinical treatment option in equine and human OA [258-260]. In fact, intra-articular injection of HA lead to an inflammatory response that is severe enough to cause transient lameness in horses, a reaction that is clinically known as a "flare" [261] a phenomenon that was clearly not present after injection of 30 μm [20PDLLA-$PEG_{1000}$-PDLLA]-80[PLLA] monospheres. This comparison therefore shows that the use of monospheres compares favorably with current clinical practice and can be considered safe for intra-articular use. It has been suggested that chronic inflammation plays an important role in the development of structural changes seen in osteoarthritis, since activated macrophages produce enzymes, growth factors and cytokines that will negatively affect joint structures like synovium, bone and cartilage [4]. Therefore, it was important to determine whether the inflammatory reaction followed by the intra-articular injection of monospheres had any deleterious effect on the joints. In order to do so, we first measured GAG content and C2C epitope (a neoepitope present on collagenase-cleavage fragments of type II collagen, hence a catabolic marker [262]) in the synovial fluid samples (figure 5-C).

An increase of these markers in the synovial fluid would indicate cartilage breakdown. The significant differences observed at baseline are most likely due to (small) differences in status of the joints due to the age and amount of exercise of the horses in the past, although the horses were all declared healthy based on X-ray before starting the experiments. GAG release into the SF remained at or below baseline values during the whole experiment, indicating that no loss of GAGs (an early sign of cartilage damage and OA) occurred due to the presence of intra-articular monospheres. Moreover, our values were approximately 10-fold lower compared to inflamed horse joints after LPS injection of around 300 μg/ml [242] all of our values remained in the range of values found for healthy joints. The C2C content has shown to be elevated in rheumatoid arthritis and OA when there is damage to the cartilage [263, 264], more specifically it indicates an inflammation-induced enhancement of collagen II cleavage [264]. In our study, this was clearly not the case, as there was no increase in C2C content at any time point (figure 5-D).

In theory, both 5 and 30 μm monospheres could have negative effects on cartilage, however via different mechanisms. Five μm monospheres can be taken up by synovial macrophages [68, 245, 246] which could potentially give rise to an inflammatory reaction, while 30 μm monospheres would not be phagocytized and therefore be more likely to stay within the synovial fluid, but with the potential risk of friction or indentation of the cartilage surface. Based on the equine SF analysis (section 3.2), we had strong indications to believe that the presence of monospheres within a joint does not harm the cartilage. To verify this assumption, 12 healthy rats were used to more accurately test the intra-articular biocompatibility of the unloaded 5 and 30μm 20[PDLLA-$PEG_{1000}$-PDLLA]-80[PLLA] monospheres compared to contra-lateral saline injections. Using *in vivo* μCT scanning (figure 6), followed by EPIC scans to even more accurately quantify cartilage thickness and quality (figure 7-A,B) and histology (figure 7-C), we indeed showed that no changes on cartilage thickness or cartilage quality (attenuation) occurred. The macrophage infiltration seen in the tissue surrounding the knees injected with monospheres (figure 7-D) correlates very well with the mild transient reaction in the first 2 weeks seen in the equine synovial fluid samples. The recruitment of macrophages and neutrophils following the intra-articular injection of a foreign material is considered physiological. Moreover, in the case of our monospheres it did not lead to any negative effects (as indicated by both μCT-scanning and histology of the injected joints). These findings show that monospheres composed of [PDLLA-$PEG_{1000}$-PDLLA]-[PLLA] multi-block copolymers are safe for intra-articular use. Recruitment of macrophages is one of the 5 phases of a foreign body response. These phases are: protein absorption, acute and chronic inflammation, foreign body giant cell formation and fibrosis [265]. The formation of fibrosis is an undesirable feature, since this would prevent drug release from the monospheres. More importantly, fibrosis within a joint lead to pain and loss of function. Joint capsules

consist of a dense fibrous connective tissue, lined with synovium, surrounding the joint. Therefore, it would be difficult to quantify fibrosis due to a foreign body reaction. The second phase of the foreign body reaction -acute inflammation- was seen in our horse study (significant increase of WBC and total protein count), as well as our rat study (presence of macrophages and neutrophils). Chronic inflammation was not the case for either of the animal models and the inflammatory response had returned to baseline 2 weeks post-injection. Additionally, no foreign body giant cell formation was observed at any time point. Therefore, the formation of a fibrous capsule is not very likely since this would follow chronic inflammation. Also, based on literature we know that adding PLLA to PEG largely reduced (90% reduction) capsule formation [266]. Another study, in which 5, 15 and 30 um monospheres were injected subcutaneously, no capsule formation was observed up until the end-point at 28 days post-injection [267].
Very interestingly, we see a portion of our monospheres being taken up by macrophages in the synovium (figure 7-D). In this current study, we only investigated the synovium of joint injected with 5 μm monospheres. From literature, we know that 5-10 μm is optimal for macrophage phagocytosis [254], because phagocytosis is ensured and therefore a prolonged retention in the joint is achieved. It has been suggested that phagocytosis ensures lower drug-exposure to the cartilage and hence less change of negative side-effect [25]; however, this assumption is not proven in this cited study nor has it, to our knowledge, been proven by other authors. It is also debatable, whether or not direct exposure of cartilage to a drug would necessarily have a negative outcome. Depending on the application and the type of drug encapsulated, one might opt for a different size of monospheres. For instance, when directly acting on inflammatory reactions, 5 μm monospheres might be preferable due to phagocytosis. It has been suggested that macrophages play an important role in the development of OA [268]. When macrophages become activated, they are able to produce a variety of enzymes [269], growth factors [270], and pro-inflammatory cytokines such as TNFα and interleukins [271, 272]. These, and other macrophage products play a major role in the OA development and may maintain the vicious circle by acting on the formation of synovial fibrosis and further induce the inflammatory state of the affected joint that leads to cartilage destruction [177, 269]. Injection of 5 μm monospheres containing an anti-inflammatory drug would therefore not only lead to a sustained local release of the drug, but might even lead to a more targeted effect on the local macrophages, thereby breaking the vicious circle of OA [67]. In contrast, when a drug that specifically acts on chondrocytes is injected, it would be reasonable to choose for larger monospheres (15 or 30 μm). From our current study, it can be concluded that the different sizes evaluated (5, 15, 30 μm) present equal levels of joint retention and biocompatibility. Therefore, the selection of the optimal size for intra-articular use should be based on the cells to be targeted.

## 5. Conclusion

Monospheres of different sizes (5, 15 and 30 μm) composed of biodegradable [PDLLA-$PEG_{1000}$-PDLLA]-*b*- [PLLA] multi-block copolymers were successfully obtained using a membrane emulsification process. Following intra-articular injection, both small (5 μm) and larger (30 μm) monospheres remained present in the joints of both small (mice and rats) and large animals (horses) for up to 3 months, which is likely long enough to release an incorporated drug. The monospheres elicited a mild transient inflammatory reaction similar to clinically used injectables, and did not harm the cartilage in any way in either of these animals. The excellent biocompatibility combined with the desirable intra-articular retention show that [PDLLA-$PEG_{1000}$-PDLLA]-*b*-[PLLA] monospheres have great potential as intra-articular drug delivery system for the treatment of arthritic diseases.

## Acknowledgment

This research forms part of the Project P2.02 OAcontrol of the research program of the BioMedical Materials institute, co-funded by the Dutch Ministry of Economic Affairs, Agriculture and Innovation.
This work was supported by the Dutch Arthritis Foundation (LLP-22)
Nanomi B.V. is acknowledged for providing the Microsieve Emulsification Technology

## Supplementary information

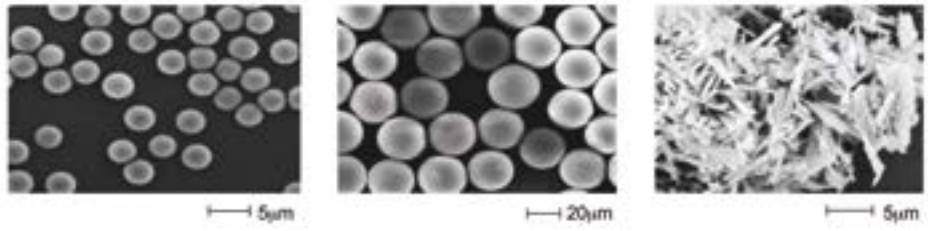


***Supplementary figure 1.*** *SEM images of 5μm- (left) and 30μm-sized (middle) monospheres prepared without washing with mannitol and mannitol-crystals (right) obtained after freeze-drying*

# Chapter 7

## Nanomechanical properties of multi-block copolymer microspheres for drug delivery applications

Moshtagh PR, Rauker J, Sandker MJ, Zuiddam MR, Dirne FW, Klijnstra E, Duque L, Steendam R, Weinans H, Zadpoor AA.

*J Mech Behav Biomed Mater. 2014 Jun; 34:313-9.*

## Abstract

Biodegradable polymeric microspheres are interesting drug delivery vehicles for site-specific sustained release of drugs used in treatment of osteoarthritis. We study the nano-mechanical properties of microspheres composed of hydrophilic multi-block copolymers, because the release profile of the microspheres may be dependent on the mechanical interactions between the host tissues and the microspheres that aim to incorporate between the cartilage surfaces. Three different sizes of monodisperse microspheres, namely 5, 15, and 30 μm, were tested in both dry and hydrated (swollen) states. Atomic force microscopy was used for measuring nanoindentation-based force-displacement curves that were later used for calculating the Young's moduli using the Hertz's contact theory. For every microsphere size and condition, the measurements were repeated 400-500 times at different surface locations and the histograms of the Young's modulus were plotted. The mean Young's modulus of 5, 15, and 30 μm microspheres were respectively 56.1 ± 71.1 (mean ± SD), 94.6 ± 103.4, and 57.6 ± 58.6 MPa under dry conditions and 226.4 ± 54.2, 334.5 ± 128.7, and 342.5 ± 136.8 kPa in the swollen state. The histograms were not represented well by the average Young's modulus and showed three distinct peaks in the dry state and one distinct peak in the swollen state. The peaks under dry conditions associated with the different parts of the co-polymeric material at the nano-scale. The measured mechanical properties of swollen microspheres are within the range of the nano-scale properties of cartilage, which could favor integration of the microspheres with the host tissue.

## 1. Introduction

Osteoarthritis is the most common joint disorder [273] and the most frequently reported cause of long-term disability [274]. Since disease-modifying drugs are not currently available for osteoarthritis, medicinal treatment often includes non-steroidal anti-inflammatory (NSAID) drugs [275] that are often used for pain management. The delivery of such drugs is a challenging task due to the chance of adverse reactions via conventional drug injections on the one hand [275, 276] and fast drug clearance that causes the drug concentration to rapidly drop below the therapeutically effective levels on the other hand [277]. Recently proposed approaches for the delivery of NSAID include the use of liposomes, nanoparticles, and microspheres for sustained and adjustable drug release [183, 278]. Among those, microspheres have the advantages of being easily adjustable in their release kinetic, allowing well-controlled sustained drug release varying from days to months [278].

It is known that the mechanical properties of the microspheres used for drug delivery applications influence their performance [279, 280]. The effects of mechanical properties are even more important for skeletal diseases where strong mechanical forces are transferred through the tissues and the microspheres interact with the surrounding tissues both chemically and mechanically. The release kinetics of the microspheres may change due to those mechanical interactions and the modulations that mechanics may have with diffusion kinetics and biodegradation behavior of the microspheres.

In this paper, we study the mechanical properties of monodisperse microspheres composed of hydrophilic phase-separated multi-block copolymers that are developed for delivery of drugs used in the management of osteoarthritis. We use atomic force microscopy (AFM) for nanoindentation tests and the Hertz's contact theory to calculate the nano-mechanical properties of the microspheres. The mechanical properties of microspheres with different sizes are measured both in the dry and swollen states. In the vast majority of the studies that report the mechanical properties of microspheres, a limited number of measurements are carried out and the obtained mechanical properties are averaged to calculate the mean values of the mechanical properties. In this study, we repeated the measurements several hundred times for every case to be able to measure the properties more accurately and to reveal nano-scale properties of the microspheres that cannot be identified using a few measurements.

## 2. Methods and materials

Monodisperse microspheres of different sizes, namely 5, 15 and 30 μm, were made of a biodegradable hydrophilic multi-block copolymer (SynBiosys®20LP10L20-LLA40, InnoCore Pharmaceuticals, Groningen, The Netherlands) using the Microsieve™ membrane emulsification equipment (Nanomi, Oldenzaal, The Netherlands) and were tested in both dry and swollen sates. The hydrophilic 20LP10L20-LLA40 multi-block copolymer is composed of hydrophilic poly (DL-Lactide)-PEG-poly (DL-Lactide) and hydrophobic poly (L-Lactide) segments that are randomly chain-extended with 1,4-butanediisocyanate. The poly (DL-Lactide)-PEG-poly (DL-Lactide) segments form amorphous domains, whereas the poly (L-Lactide) segments form crystalline domains, thereby forming a phase-separated multi-block copolymer in which the crystalline domains act as physical crosslinks (figure 1). Differently sized 20LP10L20-LLA40 microspheres were tested in both dry and swollen states to determine their mechanical properties. Before starting the test with AFM, the microspheres were attached to a firm substrate. A thin layer of a water-resistant epoxy-based glue (Bison, the Netherlands) was carefully applied to fix the microspheres on the microscope slide. For measurement under hydrated conditions, prior to testing, the microspheres were submerged in deionized water for three days to allow them reach their equilibrium swelling degree. The tests were carried out at room temperature.

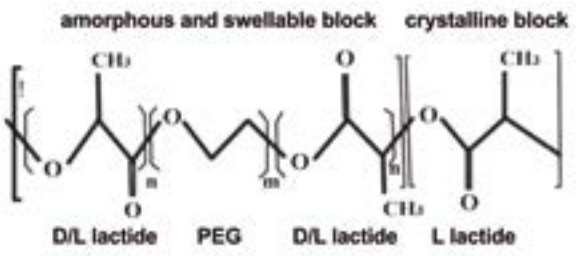


***Figure 1.*** *Molecular structure of SynBiosys 20LP10L20-LL40 multi-block copolymer.*

An AFM with a Nanoscope controller (Bruker, Dimension V, Japan) and a standard fluid cell (Bruker) was used for performing nanoindentation tests on the microspheres (figure 2). A symmetric triangular AFM probe (Bruker, Camarillo, USA) with a nominal diameter of 2 nm and a nominal cantilever spring constant of 0.35 N/m was used for the measurements to find the more symmetric characteristics of the microspheres [281]. The actual cantilever spring constant was determined using the thermal fluctuations technique [282]. The standard calibration process for finding the sensitivity factor for converting voltage to deflection was followed before the start of the measurements.

Using around 30 individual microspheres, 400-500 indentation curves were obtained at a frequency of 1 Hz and an indentation depth of around 500 nm. The Nanoscope analysis software (Bruker, version 1.4) was used for analyzing the obtained force-displacement curves and calculating the Young's modulus according to the Sneddon theory [281]. According to the Sneddon theory, force and displacement are related to each other through the following relationship:

$$F = \frac{\pi \tan\varphi}{2\gamma^2} \frac{E}{(1-\upsilon^2)} h^2 \qquad (1)$$

where $F$ is force, $h$ is displacement,  is the half angle of the cone, $\gamma=\pi/2$,  is the Poisson's ratio and $E$ is the Young's modulus of the microsphere [281, 283, 284]. A Poisson's ratio of 0.5 was assumed which is close to the value used in some other studies on cartilage nanomechanics [285, 286]. With such a value of the Poisson's ratio, the material behaves incompressibly.

The Young's moduli calculated for the swollen microspheres with different sizes were statistically assessed using the *one-way ANOVA* test followed by the Tukey-Kramer *post-hoc analysis*. Statistical significance threshold was set at $p< 0.05$. For the dry microspheres, the data was first rank-transformed using the non-parametric Kruskal-Wallis test. The post-hoc analysis could then be performed using the Tukey-Kramer test using the rank-transformed data.



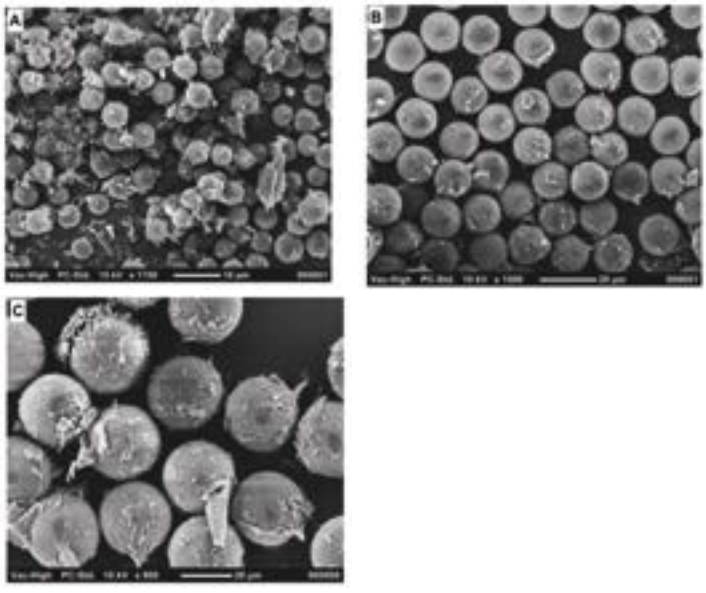


***Figure 2.*** *SEM pictures of 5 (a), 15 (b), and 30* ***μ****m (c) microspheres*

## 3. Results

In the dry state, the histogram of the Young's modulus shows several distinct peaks (figure 3). The peaks are more or less similar between the different microsphere sizes (table 1). The first and by far the largest peak is between 1 and 40 MPa for 5 μm microspheres, between 10 and 20 MPa for 15 μm microspheres and between 1 and 20 MPa for 30 μm microspheres (figure 3). A number of smaller peaks can be observed for all three microsphere sizes (Table 1), although the second and third peaks are more visible for 30 μm microspheres as compared to both other sizes. For 30 μm microspheres, the second peak occurs between 30 and 60 MPa while the third peak can be found around 120-130 MPa (figure 3c). Some less clear peaks can be observed for both other microsphere sizes around the same values of the Young's modulus (figure 3a-b). When averaged over all measurements, the Young's modulus of dry microspheres of 5, 15, and 30 μm were respectively 56.1± 71.1 (mean ± SD), 94.6 ± 103.4, and 57.6 ± 58.6 MPa. In dry state, the mean Young's moduli of the microspheres with different sizes were found to be significantly different (Table 1). Post-hoc analysis showed that the Young's modulus of 15 μm dry microspheres is significantly higher than those of both other sizes (also in dry state).

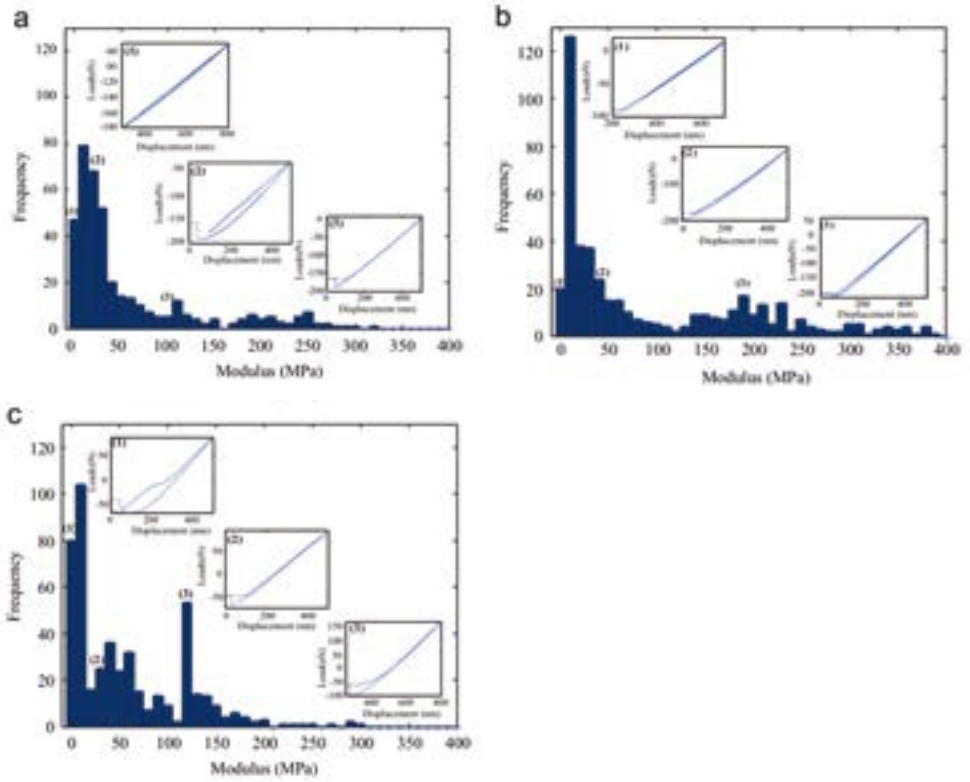


***Figure 3.*** *Histograms of the modulus of dry microspheres with typical force–displacement curve obtained from individual microspheres: (a) 5, (b) 15, and (c) 30 μm microspheres.*



The range of the Young's moduli measured by AFM of microspheres in the swollen state were several orders of magnitude lower than the Young's moduli of the microspheres measured in the dry state (figure 4). As opposed to the dry state where several peaks were observed in the histogram of the Young's modulus, there was only one clear peak in the histogram of the Young's modulus of the swollen microspheres (figure 4). This enabled us to fit a Gaussian distribution to the measured data points (figure 4a-c). When averaged over all measurements, the Young's moduli of swollen microspheres of 5, 15, and 30 μm were respectively 226.4 ± 54.2 (mean ± SD), 334.5 ± 128.7, and 342.5 ± 136.8 kPa. Statistical analysis of the Young's moduli of the swollen microspheres with different sizes showed that there is a significant difference between their Young's moduli (table 1). Post-hoc analysis showed that, in the swollen state, the Young's moduli of 15 and 30 μm microspheres are higher than those of the 5 μm microspheres. In the swollen state, there was no significant difference between the Young's moduli of 15 and 30 μm microspheres. Moreover, the Young's moduli of swollen microspheres generally tended to increase as the size of the microsphere increased.

***Table 1.*** *The main characteristics of the Young's modulus histograms found for microspheres with different sizes in dry and swollen states*

| Size (μm) | Young's modulus | | | | | | Primary and secondary peaks | |
|---|---|---|---|---|---|---|---|---|
| | Dry (MPa) | | | Swollen (kPa) | | | Dry (MPa) | Swollen (kPa) |
| | Mean | SD | Median | Mean | SD | Median | | |
| 5 | 56 | 71 | 25 | 226** | 54 | 216 | 1-40* | 197* |
| | | | | ($p$ =1.29×10$^{-68}$) | | | 40-50 | |
| | | | | | | | 120-130 | |
| 15 | 95** | 103 | 39 | 334 | 129 | 304 | 10-20* | 295* |
| | ($p$ =7.90×10$^{-8}$) | | | | | | 20-50 | 625 |
| | | | | | | | 190-200 | |
| 30 | 58 | 59 | 38 | 342 | 137 | 324 | 1-20* | 100 |
| | | | | | | | 30-60* | 315* |
| | | | | | | | 120-130* | |

** Peak with the highest frequency*
*** Microsphere size with significant difference in the Young's modulus from both other sizes*

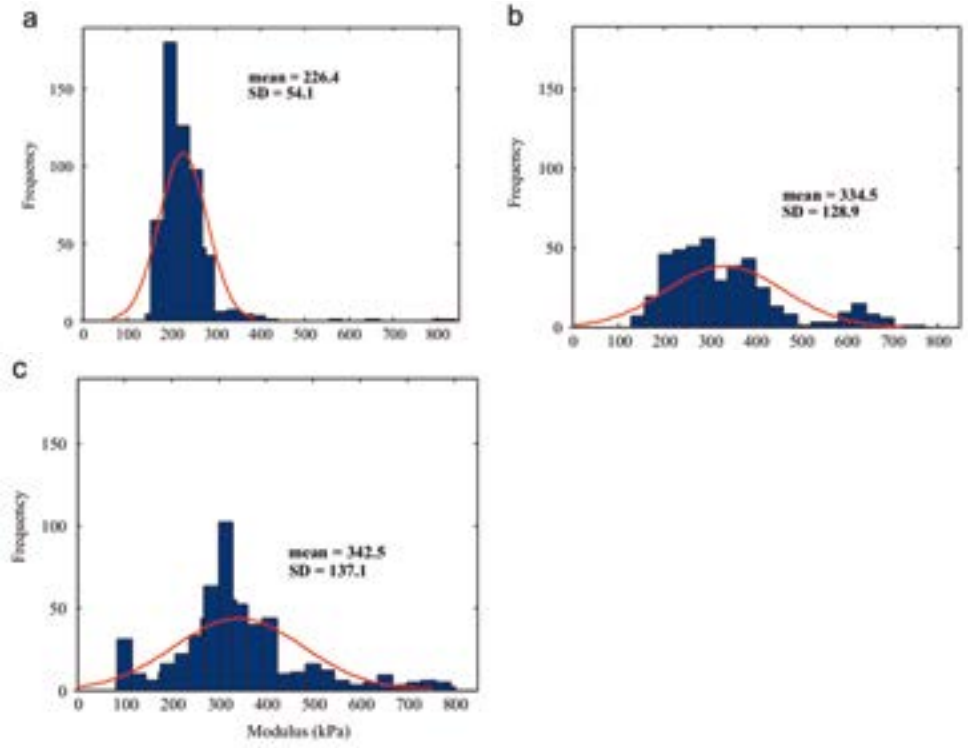


***Figure 4.*** *Histograms and corresponding normal distribution curves of swollen microspheres: (a) 5, (b) 15, and (c) 30* ***μ****m microspheres.*

## 4. Discussion

The hydrophilic 20LP10L20-LLA40 multi-block copolymer studied here contains two major components: an amorphous poly (DL-Lactide)-PEG-poly(DL-Lactide) (PDLA-PEG-PDLA) and a crystalline poly (L-Lactide) (PLLA) segment. The PDLLA-PEG-PDLLA part has water absorption functionality due to the presence of polyethylene glycol (PEG). PEG is known for its good biocompatibility and hydrophilicity [287-289], whereas PDLA is widely used in various sustained release drug delivery products due to its good biocompatibility and excellent biodegradability. The crystalline PLLA segments act as physical crosslinks and also give the microsphere appropriate stiffness that is needed for drug delivery applications in a cartilaginous environment. PLLA is widely used in biomedical implants especially where load-bearing properties are required. The specific molecular architecture and phase-separated morphology of the used multi-block copolymer gives the microspheres the desired hydrophilicity in combination with mechanical characteristics that are fairly similar to those of specially soft biological tissues such as cartilage, making it suitable for local delivery and controlled release applications [289-292].

### 4.1 Dry state

The first peak seen in the histogram of the Young's moduli of microspheres in the dry state can be attributed to the Young's modulus of PEG as the values are within the range of previously reported Young's moduli for PEG [293, 294]. As compared to crystalline PLLA, the PEG part is the softer part of the multi-block copolymer that constitutes the microspheres. The mean values of the second apparent peak in the histogram of the Young's modulus of 5, 15, and 30 μm microspheres are around 50 MPa. This second peak may be ascribed to the non-crystalline PDLA component of the PDLA-PEG-PDLA segment [289, 295]. It should be noted that the PDLA chains present in the PDLA-PEG-PDLA block studied here are relatively short. It is therefore not clear to what extent their properties are close to those of high molecular weight PDLA often studied elsewhere. The average values of the other recognizable peak, especially in 15 and 30 μm microspheres, exceed 100 MPa. This last peak might be indicative of the crystalline portion of the copolymer. It should be noted that the above-mentioned values of the Young's modulus and their relationship with the different parts of the copolymer are merely indicative. The actual values of the Young's modulus depend on many parameters including the molecular weight of the macromolecules, the length of the chains within polymeric network, the crosslinking density of the matrix, the ratio of the length of the PDLA portion to that of the PEG length in the PDLA-PEG-PDLA segment, and the optimized proportion between the PDLA-PEG-PDLA segment used for hydrophilicity and the PLLA block used for mechanical stiffness [287, 289-291].

## 4.2 Swollen state

The final functionality of the microsphere is in the swollen state, as they will be hydrated and perform their drug delivery role in the target cartilage tissue based on a combination of swelling, diffusivity [293, 296], and biodegradation. It is clear that there is a sharp decrease in the Young's modulus of the swollen microspheres as compared to the values found under dry conditions. The water molecules, with their polar groups, tend to interact with the hydrophilic domains of the multi-block copolymer and act as a plasticizer reducing the stiffness of the co-polymeric matrix [295]. The water uptake ratio can therefore be considered as a major factor for optimizing the mechanical properties of microspheres based on the principles of the swelling process. Moreover, the molecular weight of the crystalline PLLA segment have been narrowly tailored with respect to the molecular weight of the hydrophilic PDLA-PEG-PDLA segment [289, 291].
In the swollen state, the Young's moduli of 15 and 30 μm microspheres are significantly higher than those of 5 μm microspheres. This is due to the fact that the water adsorption ability of microspheres is size-dependent and is inversely related to the surface area, meaning that smaller microspheres show higher water adsorption tendency and lower stiffness values [297, 298].

## 4.3 The required number of measurements

This study is one of the rare studies in which more than a handful data points are used for characterizing the nano-mechanical properties of soft co-polymeric biomaterials particularly microspheres. In most other studies, the average of a few measurements is reported as the representative Young's modulus of the material at the nano-scale. The results of this study (figure 3-4) show that the mean of a few measurements may not necessarily be a good representative value. As for microspheres in the swollen state, the mean Young's modulus is a relatively good representative of the mechanical properties of the microspheres (figure 4) as most values seen in the histogram are distributed around the mean Young's modulus. In comparison, in the dry state, the mean Young's moduli of the microspheres vary between 55-95 MPa (figure 3). These mean values are several times larger than the first and by far the largest peak of the histograms of the young's modulus (figure 3a-c). Using the mean value of the Young's modulus as the representative Young's modulus of the microspheres will therefore grossly misrepresent the actual mechanical properties of microspheres at the nano-scale. Moreover, the histograms of the Young's modulus are very information-rich and could reveal additional information regarding the range and distribution of the mechanical properties of the microspheres at the nano-scale. This kind of information is totally lost when the average of a few data points are reported as the mechanical properties of the polymeric material.

## 4.4 Relevance for cartilage and drug delivery applications

Stolz *et al.* [299] measured the age-related dynamic elastic modulus of the human osteoarthritis articular cartilage tissue and fount it to be between 15.3 and 142 kPa. Han *et al.* [300] analyzed the modulus of the surface layer of the bovine articular tissue and found it to be between 120 and 200 kPa depending on the loading rate (0.1, 1, 10 μm/s). The Young's modulus of the microspheres in the swollen state under hydrated conditions are therefore well in the range of the mechanical properties of cartilage at the nano-scale, meaning that the microspheres should be able to well integrate within the host tissue and perform their functions.

The mechanical properties of drug delivery devices such as microspheres play important roles in regulating their controlled release performance. For example, it is known that mechanical interactions between the drug delivery devices and the surrounding tissues could influence the bio-degradation, surface area, and hydration and/or hydrolysis behavior of the involved biomaterials [301, 302]. Moreover, mechanical properties of drug delivery devices could be used as an indirect measure of their drug delivery performance. For example, it is known [303] that the degree of cross-linking in polyvinyl alcohol (PVA) hydrogels is intimately linked to both mechanical properties and drug delivery characteristics of the polymer [304]. One could therefore use mechanical properties of the polymer as an indirect measure of drug delivery characteristics. Probing the mechanical properties of the microsphere material is best done with AFM [305] and at the nano-scale, because accurate estimation of the mechanical properties using micro-scale indenters is extremely challenging particularly when micro-spheres are as small as 5 μm. That is partly because the surface of the micro-sphere cannot be considered to be flat anymore and the entire microsphere may start to deform considerably as a result of micro-scale indentations. These kinds of experiments are much more difficult to interpret and may necessitate the use of advanced computational techniques. Moreover, the mechanical properties at the micro-scale are related to the mechanical properties at the nano-scale and can theoretically be obtained from the nano-scale mechanical properties using homogenization techniques.



## 4.5 Limitations

This study has certain limitations that need to be considered when interpreting the presented data. First, the nano-indentation technique used for characterizing the mechanical properties of the microspheres is associated with certain complexities and sources of uncertainty. For example, the tip and cantilever geometry, the type of material from they are made, the depth and rate of indentation, adhesion forces, intermolecular forces, and electrostatic interactions could all play important roles in the accuracy of AFM measurements [306-310]. Second, the analytical solution used for interpretation of the force-displacement data has been derived based on specific assumptions that

are never perfectly satisfied in practice. Deviations from those conditions could cause inaccuracy in the measured mechanical properties. Finally, the mechanical properties of microspheres might be different *in vivo*, for example, due to the presence of different types of ions and enzymatic factors. Testing the microspheres in water is therefore only an approximation of the actual *in vivo* conditions.

## 5. Conclusions

In summary, the nano-mechanical properties of co-polymeric microspheres with different sizes were measured in both the dry and swollen states using atomic force microscopy. It was shown that the mechanical properties of the microspheres are in general much lower in the swollen state as compared to the dry state. In addition, the mechanical properties were found to be different for different microsphere sizes. In the swollen state, the Young's modulus tended to increase as the size of the microsphere increased. The mean Young's moduli of microspheres of 5, 15, and 30 μm were respectively 56.1 ± 71.1 (mean ± SD), 94.6 ± 103.4, and 57.6 ± 58.6 MPa in the dry state and 226.4 ± 54.2, 334.5 ± 128.7, and 342.5 ± 136.8 kPa in the swollen state. However, the mean values of the Young's modulus were not good representatives of the mechanical properties of the microspheres at the nano-scale, specifically in the dry state. A large number of measurements are therefore needed to establish the histogram of the Young's moduli in order to study the range and distribution of the Young's modulus of the microspheres at the nano-scale. Considering the range of cartilage tissue mechanical characteristics, the swollen microspheres demonstrate desired nano-scale elastic modulus data, due to which the microspheres are expected to exhibit the desired biocompatibility upon intra-articular administration besides well integration with their cartilaginous host tissue.

# Chapter 8

## Degradation, intra-articular biocompatibility, drug-release and bioactivity of tacrolimus-loaded poly(DL-lactide-PEG)-b-poly(L-lactide) multiblock copolymers based monospheres

Maria J Sandker, Luisa F Duque, Everaldo M Redout, Evelien C Klijnstra, Rob Steendam, Nicole Kops, Jan H Waarsing, Rene van Weeren, Wim E Hennink, Harrie Weinans.

*ACS Biomater. Sci. Eng., 2018 , 4 (7), pp 2390–2403*

## Abstract

The aim of this study was to develop a formulation with a sustained intra-articular release of the anti-inflammatory drug tacrolimus. Drug release kinetics from the prepared tacrolimus loaded monodisperse biodegradable microspheres based on poly(DL-lactide-PEG)-*b*-poly(L-lactide) multi-block copolymers were tunable by changing polymer composition, particularly hydrophobic-hydrophilic block ratio. The monospheres were 30 μm and released the drug, depending on the formulation, in 7 to >42 days. The formulation exhibiting sustained release for 1 month was selected for further *in vivo* evaluation. Rat knees were injected with three different doses of tacrolimus (10 wt.%) loaded monospheres (2.5, 5.0 and 10 mg), contralateral control knees with saline. Micro-CT and histology showed no negative changes on cartilage, indicating good biocompatibility. Minor osteophyte formation was seen in a dose dependent fashion, suggesting local drug release and therapeutic action thereof. To investigate *in vivo* drug release, tacrolimus monospheres were injected into horse joints, after which multiple blood and synovial fluid samples were taken. Sustained intra-articular release was seen during the entire 4-week follow-up, with negligible systemic drug concentrations (< 1 ng/mL), confirming the feasibility of local intra-articular drug delivery without provoking systemic effects. Intra-articular injection of unloaded monospheres led to a transient inflammatory reaction, measured by total synovial leucocyte count (72 hours). This reaction was significantly lower in joints injected with tacrolimus loaded monospheres, showing not only the successful local tacrolimus delivery, but also local anti-inflammatory action. This local anti-inflammatory potential without systemic side-effects can be beneficial in the treatment of inflammatory joint diseases, amongst which osteoarthritis.

## I. Introduction

Osteoarthritis is a common joint disease with a complex, multifactorial pathogenesis that causes pain and loss of joint function in patients. The disequilibrium between anabolic and catabolic activities leads to up-regulation of catabolic enzymes and pro-inflammatory cytokines, eventually resulting in cartilage breakdown and joint destruction [4, 5]. No disease modifying osteoarthritic drugs are yet available and the current standard of care consists largely of pain management using oral medication [21]. Consequently, there is a constant search for new treatment options. A potential drug for osteoarthritis is tacrolimus (FK506, Figure 1), a calcineurin inhibitor that has been used as an immunosuppressant in transplantation surgery to prevent graft rejection [44, 45]. Tacrolimus has also shown to be a treatment option for patients with active rheumatoid arthritis, a chronic systemic inflammatory disease leading to joint destruction [47]. In patients with rheumatoid arthritis synovial fluid concentrations of catabolic (inflammatory) cytokines such as TNF (tumor necrosis factor), IL-1b (interleukin 1) and IL-6 (interleukin 6) and several matrix metalloproteinases (MMPs) are elevated [48]. Although the pathogenesis of osteoarthritis has not been fully unraveled and the stimuli leading to the initial onset are different from rheumatoid arthritis, the process of cartilage degeneration involves the same loop of cytokines and MMPs as seen in rheumatoid arthritis and synovial inflammation is also common in osteoarthritis [50, 51, 311, 312]. The suppressive effect on catabolic cytokines of tacrolimus as well as of another (less potent) calcineurin inhibitor, such as e.g. cyclosporin-A, has been demonstrated both *in vitro* [46, 52] and *in vivo* [53, 56, 313]. It has also been shown that calcineurin inhibition leads to less cartilage destruction in rheumatoid arthritis of *in-vivo* animal models [52, 54, 314]. It is likely that this encouraging effect is (partially) achieved through the suppression of the catabolic cytokines and that a similar positive effect can be accomplished in osteoarthritis. Furthermore, calcineurin inhibition induced chondrogenic differentiation of clonal mouse embryonic carcinoma cells [55] and improved regeneration of cartilage defects, which is likely related to its stimulation of endogenous TGFb [56]. These features potentially pose great opportunities for cartilage regeneration and the treatment of osteoarthritis. However, oral administration of tacrolimus in doses high enough to reach therapeutic levels in the knee joint is problematic due to the presence of severe toxic side-effects, especially renal toxicity, which makes monitoring of the concentration of tacrolimus in blood important [315]. Further, the mean oral bioavailability is ~25%, and also is highly variable (5–93%) [316] which is a serious drawback for the clinical application of this drug. Tacrolimus is hence a very attractive drug for local intra-articular sustained delivery, as it is a potent immunosuppressor with low aqueous solubility and poor and strongly variable oral bioavailability [317-319]. To circumvent the problems encountered with oral administration, the best option would be to administer tacrolimus directly to the joint via intra-articular injections. This route of

drug administration has, however, major disadvantages since the intra-articular drug turnover is rapid [62, 66, 320], necessitating repeated intra-articular injections which carry the risk of cartilage damage and/or infections and are not patient friendly [60, 63, 66, 320]. The osteoarthritis community is therefore urgently seeking for appropriate drug delivery systems (DDSs) for local, controlled intra-articular delivery of therapeutic drugs with sustained drug retention times [28, 67, 68, 213, 321]. We previously showed the suitability and potential capacity of monospheres (microspheres with a narrow particle size distribution) based on poly(DL-lactide-PEG)-*b*-poly(L-lactide) multi-block copolymers due to their excellent intra-articular biocompatibility and their retention in the knee joint for several weeks [322]. These polymers are composed of a semi-crystalline (poly(L-lactide)) and an amorphous (poly(DL-lactide-PEG)) block, allowing a more controlled polymer swelling and sustained drug release kinetics than the commonly used PLGA, where dugs are released in a bi- or three-phasic manner due to its degradation properties [323, 324].

In this study, we investigated the potential of poly(DL-lactide-PEG)-*b*-poly(L-lactide) based monospheres for intra-articular drug delivery of tacrolimus as potential formulation for clinical treatment of osteoarthritis. We therefore developed and characterized a suitable tacrolimus-loaded monosphere formulation and investigated its intra-articular biocompatibility and bioactivity and *in vivo* release kinetics in both rats and horses.

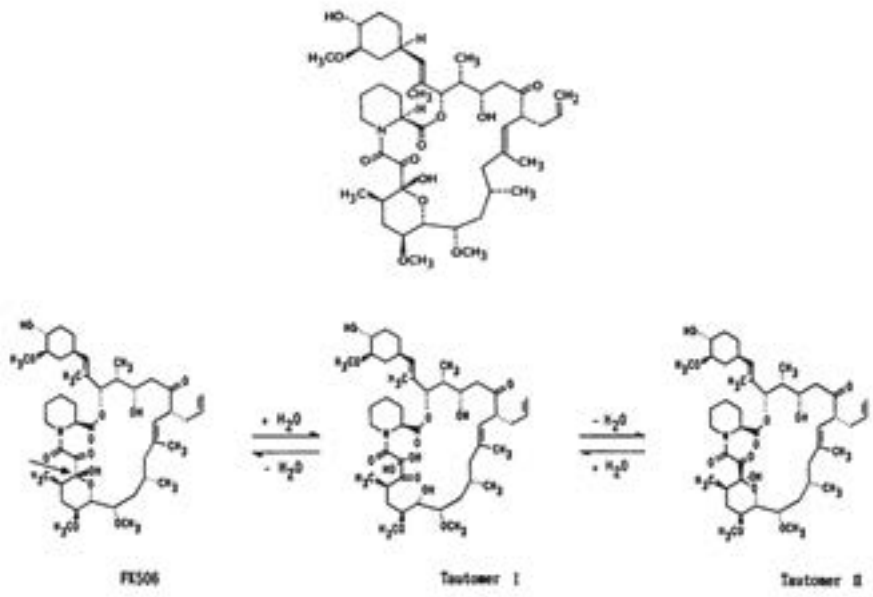


***Figure 1**. Chemical structure of tacrolimus[325] and its tautomers as reported by Akashi et al.[326]. Reproduced with permission from ref[326]. Copyright Elsevier.*

## Materials and Methods

**Materials**. Tacrolimus (FK506) was purchased from LC laboratories. [PDLA-$PEG_{1000}$]-*b*-[PLLA] multiblock co-polymers were synthesized by InnoCore Pharmaceuticals as described previously [322]. In short, low molecular weight poly(L-lactide) [PLLA] (Mw 4000 g/mol) and poly(DL-lactide)-polyethyleneglycol$_{1000}$-poly(DL-lactide) [PDLA-$PEG_{1000}$] (Mw 2000 g/mol) prepolymers were synthesized by standard stannous octoate catalyzed ring-opening polymerization. PLLA and PDLA-$PEG_{1000}$ prepolymers were then chain-extended in dioxane using1,4-butanediisocyanate to yield xx[PDLA-$PEG_{1000}$]-yy[PLLA] multiblock co-polymers with [PDLA-$PEG_{1000}$] / [PLLA] block ratios (xx/yy) of 10/90, 16/84 and 20/80(%w/w). The characteristics of the polymers used in this study are shown in table 1. The number average molecular weight (Mn) and the weight average molecular weight (Mw) of synthesized polymers were determined as described previously [322].

**Table 1.** *Properties of xx[PDLA-$PEG_{1000}$]-yy[PLLA] multiblock co-polymers used in the present study*

| # | Polymer composition | PEG content (wt%) | $M_w$ (Da) | $M_n$ (Da) | $T_g$ (°C) | $T_m$ (°C) | ΔHm (J/g) |
|---|---|---|---|---|---|---|---|
| 1 | 10[PDLA-$PEG_{1000}$]-90[PLLA] | 5 | 49600 | 28800 | 55 | 136 | 67.5 |
| 2 | 16[PDLA-$PEG_{1000}$]-84[PLLA] | 8 | 36100 | 17700 | 42 | 130 | 41.9 |
| 3 | 20[PDLA-$PEG_{1000}$]-80[PLLA] | 10 | 33600 | 19200 | 39 | 130 | 43.9 |

Polyvinyl alcohol (PVA, molecular weight 13-23 kDa), sodium dodecyl sulphate (SDS), acetone, sodium chloride (NaCl) and phosphoric acid were purchased from Sigma Aldrich (Zwijndrecht, The Netherlands). Carboxymethyl cellulose (CMC, type 7HF-PH) was purchased from Aqualon (Barendrecht, The Netherlands).
Dichloromethane (DCM, p.a. stabilized with EtOH), dimethyl sulfoxide (DMSO), sodium azide ($NaN_3$), Brij-35, and Tween-20 were purchased from Across (Geel, Belgium). Ultrapure water was purchased from B. Braun Medical B.V. (Oss, the Netherlands). Mannitol was purchased from Fagron (Barbsbütel, Germany). Hyaluronidase and ascomycin were both purchased from Sigma-Aldrich (Zwijndrecht, The Netherlands). Hexabrix 320®, a clinical iodine-based contrast agent, was obtained from Guerget, The Netherlands. All reagents were used as received. Saline was purchased from Gibco (Bleiswijk, the Netherlands).

## Preparation of tacrolimus loaded microspheres

Microspheres with a target diameter of 30 μm and with a narrow size distribution (referred to as 'monospheres') were prepared under best clean conditions by a membrane emulsification-based solvent extraction/evaporation process using microfabricated microsieve membranes with uniformly sized pores of 20 μm (Iris-20) (Nanomi BV, The Netherlands) as described in detail elsewhere [322]. Selection was based on findings of our previous study [322] in which this size showed to be most suitable for intra-articular delivery due to its retention for several weeks and only limited phagocytosis. In short, 50 mg of tacrolimus and 450 mg of the respective polymer were co-dissolved in 1.5 mL dichloromethane (DCM) to obtain a 20% w/w polymer solution followed by filtration through a 0.2 μm PTFE filter. Using 35 mbar air pressure, the filtered polymer solution was processed through the microsieve membrane into a sterile aqueous solution containing 4 % w/v PVA and 5% NaCl. The formed emulsion was stirred for 3 hours at room temperature to extract and evaporate DCM. Hardened monospheres were collected by centrifugation, washed twice with demiwater and twice with 0.05 % w/v aqueous Tween 20 solution and finally lyophilized. Prior to intra-articular injection in rats, monospheres were reconstituted in injection medium (0.4 wt.% CMC, 0.1wt% Tween 20 and 5.0wt.% mannitol sterile solution). For injection in horses the microspheres were reconstituted in saline.

## Microsphere characterization

Monospheres were visually examined by optical microscopy. Particle size was determined by dispersing 5-10 mg of monospheres in 50-100 mL of electrolyte composition solution (Beckman Coulter, Woerden, The Netherlands) and measuring the particle size distribution (PSD) with a Multisizer 3 Coulter Counter (Beckman Coulter, Woerden, The Netherlands) equipped with a 200 μm measuring cell. The volume average particle size (D50) and coefficient of variance (CV%) were determined from the PSD. Surface morphology of the monospheres was assessed by scanning electron microscopy (JCM-5000 Neoscope, Jeol, Germany). Samples were sputtered with a thin layer of gold using the JFC Neocoater (Jeol, Germany).

To determine the drug content of the obtained microspheres, 10 mg monospheres was incubated in 1.0 mL of an acetone–ethanol mixture (2:1) for 1 hour at room temperature to extract Tacrolimus. Previously conducted experiments in our lab confirmed that 1 hour was sufficient to fully extract the loaded drug (Extraction and HPLC method for tacrolimus quantification after extraction are shown in supporting information). 0.9 mL aliquot was withdrawn and replaced by 0.9 mL of a 5 w/v% Brij-35 aqueous solution to preserve the stability of the dissolved drug and avoid its

tautomerization. The 0.9 ml withdrawn samples showed no recovered drug. Avoiding tautomerization [326] was important to avoid peak shifting and erroneous integration during analysis. The tautomers have a different retention time and less stability, which could lead to less recovery of the drug. These samples containing Brij solution were then centrifuged at 15.000 rpm for 5 minutes, and the tacrolimus containing-supernatant was subsequently filtrated through a 0.2 μm filter to prevent blocking of the column. The drug concentration was determined by HPLC are described below.

The drug loading and encapsulation efficiency (EE) were calculated as follows:
(1) Drug loading (%) = (drug mass in the monospheres / mass of monospheres) x 100%
(2) Encapsulation efficiency (EE) (%) = (Drug loading $_{\text{Experimental}}$ / Drug loading $_{\text{Theoretical}}$) x 100%

The concentration of tacrolimus in the different samples was determined by RP-HPLC using an Alliance 2695 HPLC system (Waters Chromatography BV, The Netherlands) equipped with a UV/VIS detector PDA 2998 (Waters Chromatography BV, The Netherlands). A C18 Waters Xterra LC/MS reversed phase column (3.5μm 150x4.6mm column) at a temperature of 50 °C was used in isocratic mode using 70/29/1 v/v/v acetonitrile/water/phosphoric acid using a flow rate of 1.7 mL/min. Detection of tacrolimus was done spectrophotometrically at a wavelength of 210 nm. A calibration curve of tacrolimus in the range of 0.1 μg/ml to 120 μg/ml was prepared using the acetone/ethanol (2:1) mixture system as described before. The calibration standards and samples were stabilized in a 5 w/v% Brij-35 solution to avoid tacrolimus tautomerization prior analysis [326].

Tacrolimus monospheres (5 – 10 mg) were suspended in 2 mL of 100 mM PBS +0.1wt/v % SDS (added to allow re-suspension of monospheres, to avoid caking and to solubilize the released drug, pH 7.4, in glass tubes that were placed in a shaking water bath thermostated at 37 °C were drawn and replaced by 1.8 ml of fresh buffer. The concentration of tacrolimus in the different samples was determined by HPLC as described before. Sink conditions were maintained by refreshing 90% of the release buffer after each sampling point.

Residual DCM content of lyophilized microspheres was determined by GC-FID using a TraceGC gas chromatograph (Thermo Finnigan, Rodano, Milan, Italy) equipped with a CombiPal headspace module (CTC Analytics AG, Zwingen, Switzerland) and an Agilent Column, DB-624/30 m/0.53mm and using dichloromethane standards in dimethylsulfoxide in the range of 0-2000 ppm. Endotoxin concentrations in the different microsphere batches was performed by Limulus amoebocyte lysate assay according to

the chromogenic endpoint standard procedure, with a lower limit of detection of 0.05 EU/mL [234].

## *In vivo* biocompatibility study in rats

The Animal Ethic committee of the Erasmus Medical Center, Rotterdam, the Netherlands, approved all procedures (agreement number EMC2255(116-11-02). A total of twenty 16-week-old (400-450 g) male Wistar rats (Charles River Nederland BV, Maastricht, the Netherlands) were housed in the animal facility of the Erasmus Medical Center, with a 12-h light-dark regimen, at 21 °C. Animals were fed standard food pellets and water *ad libitum*. Experiments started after an acclimatization period of 2 weeks. For the first experiment, in which we assessed *in vivo* biocompatibility of tacrolimus loaded monospheres, all rats received an IA injection of 50 µl tacrolimus microsphere dispersion in saline (n=5 low dose, n=5 medium dose, n=5 high dose) in the left knee; contralateral 50 µl of saline was injected and served as a control. The different groups represent the following injected dosages. Low dose: 2.5 mg monospheres (8.8% loading) containing a total of 220 µg tacrolimus; medium dose: 5 mg monospheres (8.8% loading) containing a total of 440 µg tacrolimus; and high dose: 10 mg monospheres (8.8% loading) containing a total of 880 µg tacrolimus. Micro-CT scans of all knees were acquired at 3 different time points (t=0, t=6w and t=12w) as specified below. Following the last scan, knees were harvested and EPIC µCT-scanning was performed at 18 microns resolution as a quantitative measure of sulphated glycosaminoglycan content in the cartilage [96, 97, 135, 327] followed by histology. The tissue surrounding the injected rat knees, including synovial tissue, was harvested after the last µCT scan and used to evaluate possible remains of monospheres and tacrolimus locally. For this, the samples were vacuum dried at 30 ºC overnight. Presence of monospheres was evaluated by scanning electron microscopy and remaining tacrolimus was extracted and detected through the use of HPLC as described in the supplementary files (Figure S.1 and S.2). At 0, 6 and 12 weeks, the weight of the rats was measured as a clinical outcome parameter for systemic toxicity of the drug. Only for the weight experiment, as a negative control, a group of n=10 rats (equal in strain, gender and age) was used. These rats were treated with a daily oral dosage of 3.2 mg tacrolimus/kg bodyweight (suspended in NaCl 0.9%/ethanol), a proven tolerated dose [314]. As a positive control for all experiments, a group from a previously conducted study, consisting of rats of the same strain, age and gender but with osteoarthritic knee joints [136] was used.

µCT scans of both knees from all groups were performed to measure bone changes at the three time points (t=0, 1 and 6 weeks). Scans were made using an *in vivo* scanner (Skyscan model 1176, Skyscan, Kontich, Belgium). Rats were placed in a custom-made

scanner bed under isoflurane anaesthesia, fixing the hind limb in extended position. Scanner settings were the following: isotropic voxel size of 18 μm, 67 kV, 380 mA, 35 mm field of view, 1.0 mm Al filter, 0.5 rotation step over 198°, frame averaging of 2.

Following the last *in vivo* μCT scan, EPIC-CT scanning (equilibrium partitioning of an ionic contrast agent) of the joints was performed [97, 135]. Rats were killed and the knee joints were dissected into femur, tibia and patella with removal of the surrounding soft tissue. These samples were incubated for 24 hr. in 40% Hexabrix solution (Hexabrix 320, Mallinckrodt, Hazelwood, MO, USA) at room temperature in order to achieve equilibrium between the contrast agent and the sGAG (sulphated glycosaminoglycans) content of the cartilage [99], which is a direct measurement for cartilage quality. The influx of Hexabrix into cartilage correlates well with the inverse of sGAG content; therefore, cartilage degeneration is measurable using μCT (expressed as attenuation) [135, 327]. Samples were scanned using the following settings: isotropic voxelsize of 18 μm, 60kV, 170 mA, 885 ms exposure time, 35 mm field of view, 0.5 mm Al filter, 0.8 rotation step over 198°, frame averaging of 3.

The obtained images were converted into 3D reconstructions using nRecon version 1.5 (Skyscan). All *in vivo* bone scan datasets were segmented with a local threshold algorithm, the tibial epiphysis was selected and cortical and trabecular bone were automatically separated after which the subchondral plate thickness of the medial and lateral compartment of the tibial plateau were measured as described previously [136]. In all EPIC-μCT datasets, X-ray attenuation (arbitrary gray values inversely related to sGAG content) and thickness (μm) were calculated separately for cartilage of the medial and lateral tibial plateau [136]. Using Skyscan analysis software (CT-An), all datasets were segmented using a fixed attenuation threshold between air (attenuation 30) and subchondral bone (attenuation 120). In the segmented μCT datasets, regions of interest (150 slices) were drawn around the cartilage of the medial and lateral plateau of the tibia separately and for these regions, cartilage attenuation and thickness (μm) were calculated. As stated before, osteoarthritic knee joints of rats of the same strain, age and gender from a previous study were used in which cartilage damage was generated using a strenuous running protocol combined with 3 unilateral i.a. papain injections as a positive control [136].

Following EPIC scans, the knee parts were fixed with formalin, decalcified and embedded in paraffin. Six μm sections for histology were cut sagitally at 300 μm intervals and stained with Safranin-O and Hematoxylin-Eosin (HE) to assess cartilage quality and synovium tissue.

**Equine *in vivo* study** The study design was approved by the Ethics Committee on the Care and Use of Experimental Animals of Utrecht University in compliance with Dutch legislation on animal experimentation. Three ml of saline was used to disperse 200 mg of unloaded monospheres and was administered into the right middle carpal joint of three healthy horses with normal carpal and talocrural joints, as determined by radiographic and clinical evaluation. Three ml saline (control) was injected into the contralateral middle carpal joint. Additionally, three ml of saline was used to disperse 200 mg tacrolimus (8.8% loading; 17.6 mg tacrolimus) loaded monospheres and was injected into the right talocrural joint. Three ml saline was injected into the left talocrural joint to serve as a control. Lameness examinations (scored on a standardized 0 to 5 scale [241]) were conducted at 0, 8, 24, 72 hours and 1, 2, 3, 4 weeks post injection. Horses were monitored throughout the study for signs of discomfort.

From the horses, synovial fluid samples as well as blood samples were taken at the same predetermined time points when the lameness examinations were performed (0, 8, 24, 72 hours and 1, 2, 3, 4 weeks post injection) and tacrolimus concentrations were measured in order to establish the local and systemic drug concentrations that were achieved. To determine the tacrolimus concentrations in whole blood samples, tacrolimus was extracted as described earlier. Synovial fluid samples were pretreated with hyaluronidase before performing tacrolimus extraction using the same method. In short, the precipitation reagent methanol/1.125 M $ZnSO_4$ in water (66/34, v/v) containing 20 ng/mL ascomycin as internal standard was prepared immediately before sample preparation. Blood samples (100 µL) were transferred into a 1.5 ml test tube and 200 µl precipitation reagent was added. Samples were subsequently vortexed for 30 sec and left 5 min at room temperature. After vortexing for an additional 5 seconds, the tubes were centrifuged for 10 min at 15,000 × g at 4 °C. The supernatant was transferred into an autosampler vial and a 5 µl sample was injected onto a HyPURITY® $C_{18}$ (50 × 2.1 mm, particle size of 3 µm) analytical column (Thermo Fisher Scientific, Utrecht, NL). Separation was performed at a flow rate of 500 µl/min, with a total run time of 3 min. The mobile phases consisted of 10 mM ammonium acetate pH 3.5 in water (A), and 10 mM ammonium acetate pH 3.5 in methanol (B). Samples were separated using the following gradient A/B vol/vol: 0–0.8 min, 65/35; 0.8–0.9 min, 21/79; 0.9–2.0 min, 21/79 to 13/87; 2.0–2.1 min, 13/87 to 0/100; 2.1–2.6 min, 0/100; 2.6–2.7 min, 0/100 to 65/35; 2.7–3.2 min, 65/35 at a column temperature of 40 °C. The first 0.8 min of the column effluent was discarded, to prevent non-volatile components to enter the ionisation interface, where after the effluent was introduced by an electospray ionization (EPI) interface (Sciex, Toronto, ON) into a 4000 Q TRAP mass spectrometer. For maximal sensitivity and for linearity of the response, the mass spectrometer was operated in multiple-reaction monitoring (MRM) mode at unit mass resolution. Peaks were identified by comparison of retention time and mass

spectra of standards. For each component one ion transition was monitored, ascomycin: 809.5→756.5 (collision energy: 21 V), and FK-506: 821.5→768.4 (collision energy: 26 V). The following MS parameters were used: curtain gas: 10 psi; ion spay voltage: 5500 V; source temperature: 360 °C; gas flow 1: 50 psi; gas flow 2: 40 psi; decluster potential: 80 V and entrance potential: 10 V. Data were analyzed with Analyst software version 1.6.2 (Applied Biosystems, Nieuwerkerk a/d IJssel, The Netherlands). FK-506 peak areas were corrected for the ascomycin recovery, and concentrations were calculated using a FK-506 reference line ranging from 0.5 ng to 1000 ng/ml which was linear in this range ($r$ = 0.9997).

A second portion of synovial fluid was processed for white blood cell (WBC) count and total protein measurement, which are known to be elevated during inflammatory responses [328]. The remaining volume was centrifuged, and the supernatant was stored at -80 ºC until further analysis. Analyses consisted of measuring the glycosaminoglycan (GAG) concentrations using a modified 1,9-dimethylmethylene blue dye-binding assay used previously in our laboratory [242] and of the C2C epitope concentration, which are markers for proteoglycan and collagen damage respectively [329]. All values were compared to saline injected joints as well as to the response after intra-articular injections of unloaded monospheres to check for possible anti-inflammatory action of the locally released tacrolimus.

## Statistical analysis

Differences in μCT-data between the tacrolimus loaded microsphere-injected knees and the contralateral knees were assessed using type-1, two-tailed, paired T-tests. For the measured weight-gain, differences between t=0 and 6 weeks were analyzed for each independent group using a paired T-test. For the difference in weight gain (6w-t0) between the different groups, a one-way ANOVA with a post-hoc Bonferroni correction was used. For all tests, p-values<0.05 were considered statistically significant. All data are presented as mean ± SD.



## Results and discussion

### Preparation and *in vitro* characterization of tacrolimus monospheres

The different tacrolimus loaded microsphere formulations were obtained in a high yield (>75%) with average particle size in a narrow range from 28 - 33 μm (see Table 2 and figure 2a) and smooth and non-porous surface (Figure 2b). An encapsulation efficacy of ≥70% tacrolimus was obtained for the different formulations prepared.

***Table 2.*** *Polymer composition and characteristics of tacrolimus-loaded monospheres, data acquired by Coulter Counter*

| Formulation # | Polymer ratio (%) | | PEG content (wt%) | Tacrolimus monospheres characteristics | | |
|---|---|---|---|---|---|---|
| | 20[PDLA-PEG$_{1000}$]-80[PLLA] | 10[PDLA-PEG$_{1000}$]-90[PLLA] | | Average particle size (μm) | Particle size CV (%) | Loading (EE %) |
| **F1** | 100 | 0 | 10 | 30.1 | 14.2 | 79.3 |
| **F2** | 80 (18) | 20 | 9 | 28.9 | 10.4 | 70.6 |
| **F3** | 70 (17) | 30 | 8.5 | 29.2 | 10.9 | 72.0 |
| **F4** | 60 (16) | 40 | 8 | 33.4 | 11.5 | 72.7 |
| **F5** | 50 (15) | 50 | 7.5 | 32.0 | 12.1 | 70.0 |
| **F6** | 0 | 100 | 5 | 33.2 | 16.4 | 80.1 |

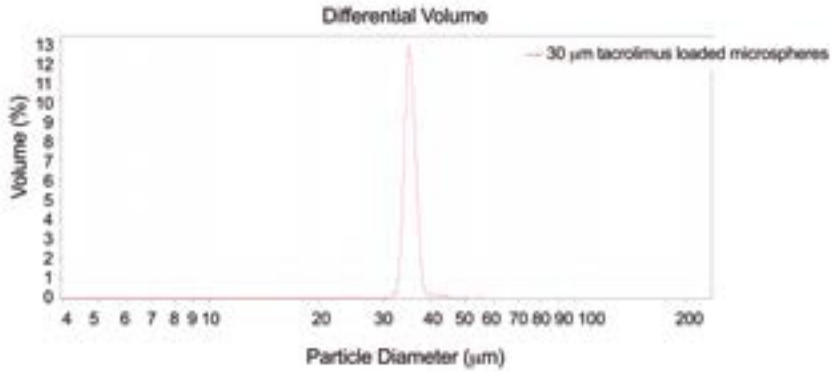


***Figure 2a****. Particle size distribution of tacrolimus loaded monospheres.*

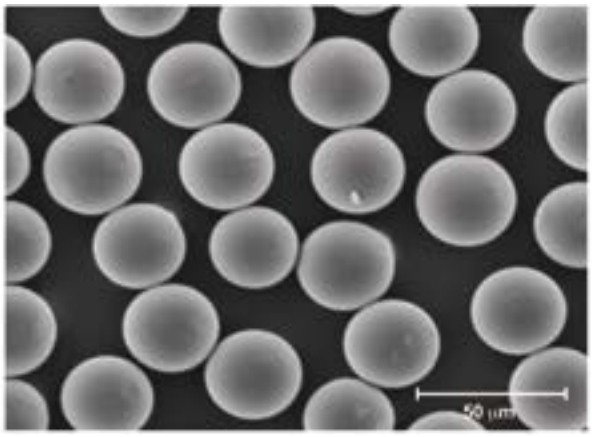


***Figure 2b****. SEM image of tacrolimus loaded monospheres.*

Analysis of the *in vitro* release of these different formulations showed that variations in polymer composition allowed tuning the release kinetics of tacrolimus over a period of 4-6 weeks (figure 3). Small variations in the content of the relatively hydrophilic amorphous block, (PDLA-$PEG_{1000}$) of the multiblock copolymer had an impact on the release kinetics of the tacrolimus loaded monospheres. Tacrolimus was released faster when there was an increase in this hydrophilic block most likely due to greater swelling of the matrix caused by an overall increase of PEG content within the polymer matrix, which facilitates diffusion of tacrolimus out of the polymer [322]. Tacrolimus is most probably released by a combination of diffusional and polymer degradation mechanisms as well as limited solubility of tacrolimus. Formulation F1 with 10 PEG % (see Table 2) showed a fast and complete release of tacrolimus within 7 days. In contrast, formulation F6 0/100 (having the lowest PEG content) was extremely stable and showed minor release (<2.0%) during 42 days. Interestingly, blends of 20[PDLA-$PEG_{1000}$]-80[PLLA] and 10[PDLA-$PEG_{1000}$]-90[PLLA] in different ratios (table 2) allowed to control the lag phase time and release rate as shown in figure 3. Monospheres based on the more hydrophilic 20[PDLA-$PEG_{1000}$]-80[PLLA] polymer with a higher PEG-content showed a faster release, probably because these particles swell more in buffer, facilitating the diffusion of tacrolimus to the release medium and the influx of water to the matrix that promotes its degradation and pore formation when PEG leaves the matrix [58, 255, 330]. Pore formation likely occurred in all formulations, however we do not have data about the pore size of the monospheres during drug release and cannot exclude the fact that the size of the pores and the rate of their formation would differ between formulations based on the polymer composition. Therefore, differences in tacrolimus release rate between formulations could also be influenced by pore formation.

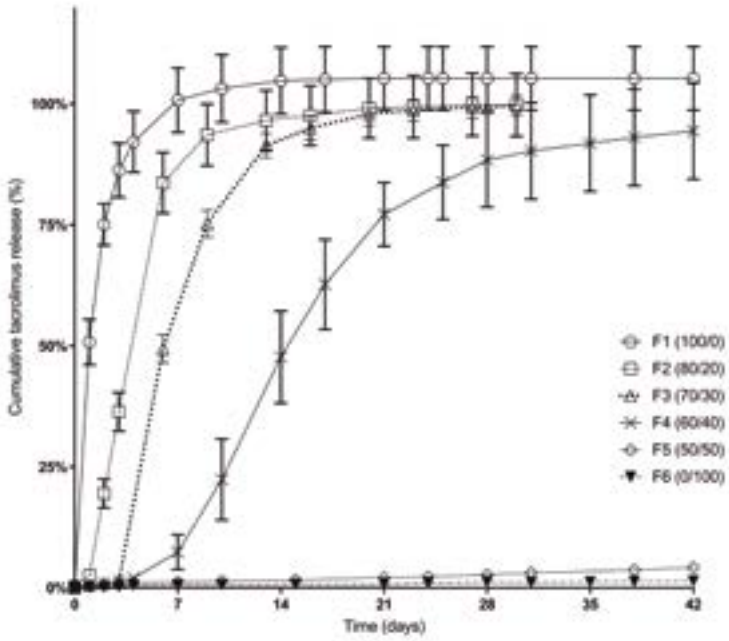


***Figure 3**. In vitro release of different tacrolimus loaded xx[PDLA-PEG$_{1000}$]-yy[PLLA] based monospheres (n=3 per time point). Composition of each monosphere formulation is shown in table 2.*

There is no literature about the *in vivo* use of tacrolimus for the treatment of osteoarthritis, therefore the most ideal release pattern is not known. Most articles focusing on the treatment of osteoarthritis via intra-articular drug delivery systems aim at a sustained release of several weeks [213], since shorter release periods would necessitate multiple injections which increases the risk of infection. Based on this information, formulation F4 showed the most suitable profile, because it presented a continuous *in vitro* release of tacrolimus for over 5 weeks, without showing a burst release. Formulations F1, F2 and F3 showed drug releases that were much faster than our aimed release period, with >75% being released within the first 10 days. Whereas formulations F5 and F6 were releasing the drug at a very slow rate, with only <5% of the drug being released after 42 days; this would lead to minimal local drug concentrations, which would very likely not be in the therapeutic range. Therefore, we choose to work with formulation F4 (blend of ratio of 60:40 of 20[PDLA-PEG$_{1000}$]-80[PLLA] over 10[PDLA-PEG$_{1000}$]-90[PLLA]). 60% of a polymer containing 20% [PDLA-PEG$_{1000}$] and 40% of a polymer containing 10% [PDLA-PEG$_{1000}$] will give 16% of this multi-block in the final blend. Hence, a polymer presenting this ratio (16[PDLA-PEG$_{1000}$]-84[PLLA]) was synthetized, and used to produce microspheres suitable for *in vivo* evaluation. The properties of this polymer are summarized in table 1. The decision to synthesize a new polymer instead of

using a blend of the two was made in order to facilitate easier manufacturing and up-scaling for clinical translation.

Three batches with the same composition were prepared under best clean conditions for *in vivo* evaluation. They had a residual dichloromethane content of < 600 ppm and very low endotoxins content < 0.01 EU/mg, complying with the acceptance limits for parenteral administration [243]. Monospheres with smooth and non-porous surfaces as observed by SEM (figure 4), and with an average diameter between 31.8 and 33.8µm (CV 13 -21%) were obtained. The size uniformity and absence of very small and very big microspheres represent additional advantages because possible particle-induced immunoactivation is avoided [39, 221, 228]. Moreover, more reproducible and predictable *in vivo* pharmacokinetics are obtained [227, 228], and injection is less painful due thanks to the possibility to use smaller needles. The drug encapsulation efficiency was >85% and the release kinetics was comparable to the release kinetics observed for monospheres of the 60:40 blend of 20[PDLA-$PEG_{1000}$]-80[PLLA] and 10[PDLA-$PEG_{1000}$]-90[PLLA] (figure 5), showing a lag phase of one week followed by a sustained release for over a period of 5 weeks. This lag phase could have an impact on the efficacy of tacrolimus in the joint. Nonetheless, it is known that differences between *in vitro* and *in vivo* release kinetics exist for polymer-based formulations due to the *in vivo* environment [155]. As a consequence of the presence of enzymes as well as cellular responses in the tissues, changes of polymer degradation and overall drug release (e.g. absence of lag phase) could be expected [221, 331]. We recently showed in an article regarding PCLA-PEG-PCLA, that after *in vivo* injection the polymer molecular weight decreased and composition determined by 1H NMR significantly changed over time during *in vivo* degradation. This indicates chain scission at the PEG-PCLA bonds and dissolution of the PEG rich chains, due to enzymatic degradation [122]. Because of expected differences between *in vitro* and *in vivo* release, an *in vivo* evaluation is required to assess the efficacy of the sustained release formulation. Consequently, further evaluation in two animal models was undertaken to evaluate the *in vivo* performance of the developed monospheres.



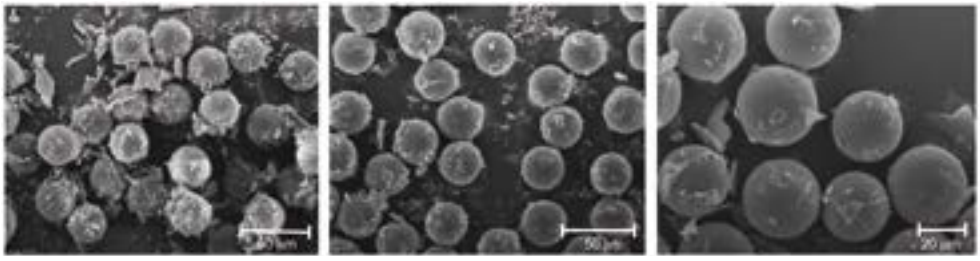

***Figure 4.*** *SEM picture of 30 µm 16[PDLA-$PEG_{1000}$]-84[PLLA] monospheres. This picture shows the size uniformity of the batches. Mannitol was used during the washing and before freezing of the monospheres, explaining the irregularities seen in the picture. The surface of the monospheres appears smooth and without pores.*

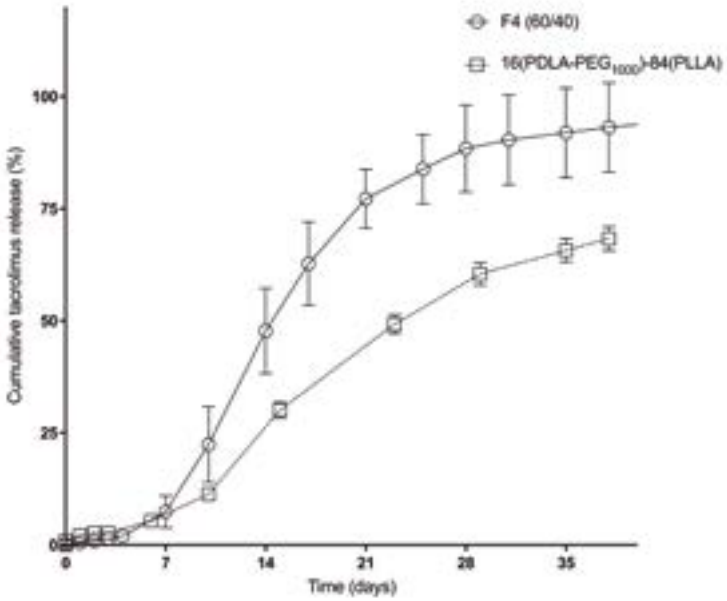


***Figure 5**. In vitro release (IVR) kinetics of 7.4-7.9 wt.% tacrolimus loaded monopsheres composed of 16[PDLA-PEG$_{1000}$]-84[PLLA] used for in vivo studies and the 60:40 20[PDLA-PEG$_{1000}$]-80[PLLA]: 10[PDLA-PEG$_{1000}$]-90[PLLA].*

***In vivo* tolerance study in rats** Neither local toxic responses (e.g. changed locomotion, joint redness/swelling) nor systemic effects occurred during the 12-week observation period after intra-articular injection.

Oral treatment with tacrolimus (figure 6: oral tacrolimus (OA)) led to a stagnation of growth (non-significant difference between weight at $t_0$ and after 6 weeks), whereas the intra-articular administration of tacrolimus loaded monospheres (figure 6: i.a. μspheres) did not hamper growth of the animals, indicating the absence of systemic toxic effects when administering the drug locally. A non-significant (only significant for highest loading) difference between growth of both OA induced groups (control (OA) and oral tacrolimus (OA)) versus the healthy animals injected with intra-articular tacrolimus-loaded monospheres was seen as well, which is likely due to the retarded growth of animals suffering from pain caused by OA.

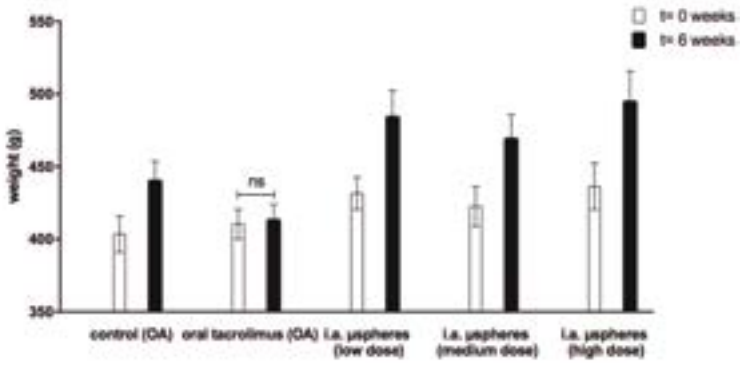


***Figure 6.*** *Weight gain of rats injected with intra-articular monospheres containing a low/medium or high dose of tacrolimus. As a control, untreated rats with induced OA and animals treated with daily oral tacrolimus administration (also induced OA) are shown. As can be seen, the oral treatment with tacrolimus led to a stagnation of growth (non-significant difference between weight at $t_0$ and after 6 weeks), whereas the intra-articular administration of tacrolimus loaded monospheres (by which in comparison to the oral administration much higher intra-articular concentrations could be achieved) did not hamper growth of the animals.*

Based on several studies in which oral bioavailability of tacrolimus was measured in rats [332-334] the oral dosage of 3.2 mg/kg/day would lead to a maximal systemic plasma concentration of 50 ng/ml, which in a steady state situation could maximally lead to 50 ng/ml intra-articularly. Those studies all showed that after oral administration, the plasma peak concentration occurs within the first 2 hours after administration, followed by a quick decrease to below detection level (thus < 0.3-1.0 ng/ml) within the first 24 hours. The total tacrolimus loads of the intra-articularly administered microspheres were respectively 220 µg (low), 440 µg (medium) and 880 µg (high). These loadings should, after local release, likely lead to very high intra-articular concentrations compared to what would be feasible with oral administration, with no systemic side effects (as shown in this study). However, as sequential synovial fluid sampling is impossible in rats without greatly influencing the pharmacokinetics of the drug delivery system, we were not able to generate data regarding this topic. Therefore, we did these measurements in horses, as described in section 3.5.

**Intra-articular retention of monospheres and tacrolimus in rats** In a previous study it has been shown that unloaded monospheres retain within the knee joint for at least 3 months [322]. Here, we examined the period that drug loaded monospheres retained in the joint and whether sustained intra-articular presence of the drug could be demonstrated. In samples of the surrounding tissue including the synovium harvested at the 12-week end-point, SEM imaging revealed the presence of monospheres (see figure 7a). Also, tacrolimus could be detected in four out of six samples by UV-HPLC as showed by the overlapping chromatogram (figure 7b). The sustained release of at

least 12 weeks is longer than what would be expected from the *in vitro* release data (figure 5). However, it is a well-known phenomenon for polymer-based sustained release formulations that *in vivo* and *in vitro* releases may differ significantly due to differences in the environmental conditions [155]. Anyhow, a longer release is a favorable feature for a local drug delivery system. The inability to detect tacrolimus in two of the six samples (1 low dosage, 1 medium dosage) may be due to either full release or harvesting an insufficient amount of tissue or tissue from a wrong area, since only a part of the tissue surrounding the joint was used for this analysis.

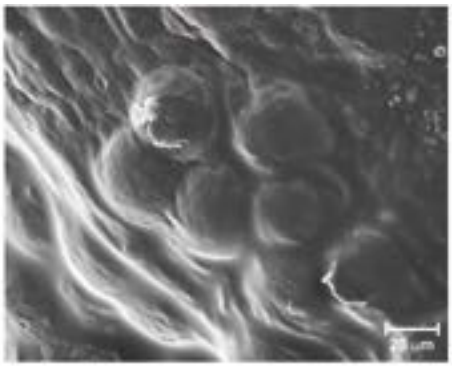

***Figure 7a.*** *SEM image of tissue surrounding the knee joint of a rat injected with tacrolimus loaded monospheres, 12 weeks after injection. Monospheres are still present in the joint, and are partly taken up by the surrounding tissue.*

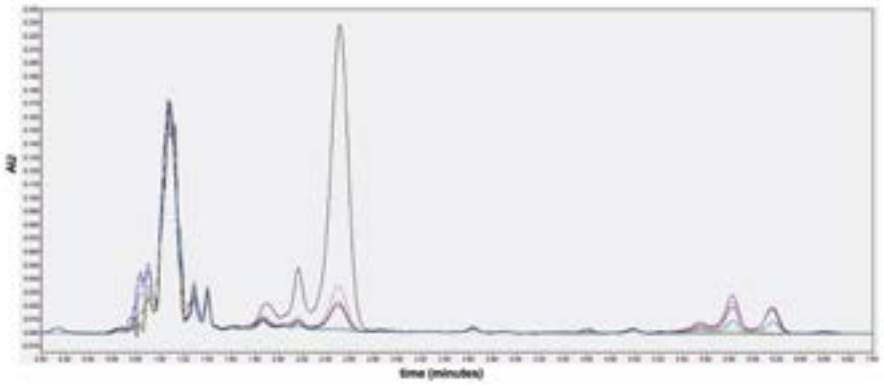


***Figure 7b.*** *Overlap chromatograms of tacrolimus in retrieved tissue 12 weeks post-injection. The black line (highest curve) represents a sample of pure FK-506, all other lines are samples derived from the FK506 injected rat joints. Four out of the six harvested knees showed presence of tacrolimus, in the joints of two rats (green and blue line) no tacrolimus was detected.*

## Intra-articular biocompatibility in rats

**Subchondral plate thickness** When longitudinally comparing healthy control knees (saline injected) to tacrolimus loaded monospheres injected knees, normal gain in subchondral plate thickness of both the lateral and medial compartment was seen for all groups, which is related to normal growth of the rat (figure 8). In contrast, we also correlated them to values found for osteoarthritic knee joints of rats (of the same strain, sex and age) from a previous study [136]. In these rats, the subchondral bone plate thickness of the medial tibia compartment in OA knees was slightly reduced after six and twelve weeks of follow up, while for the lateral compartment the thickness clearly increased over time compared to healthy control knees (saline injected).

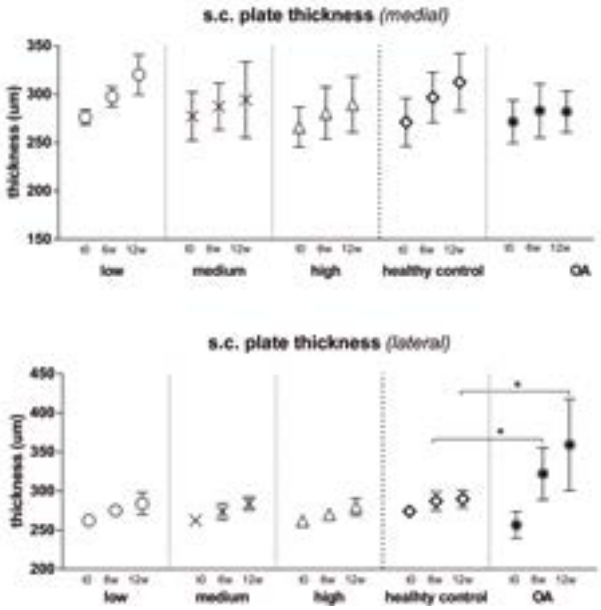


***Figure 8.*** *Subchondral plate thickness of knee joints injected with saline (healthy control), low/medium or high dose of tacrolimus loaded monospheres. Longitudinal in vivo scanning was performed at $t_0$ (before injection), 6 weeks and 12 weeks after injection. As a reference, values of OA knees are also shown. Generalized estimating equations were used to calculate differences between groups and over time, data is shown as mean ± SD, $p<0.05$ (*) is considered significant.*

Osteophytes are bony changes associated with osteoarthritis [335, 336], and therefore μCT scans were also inspected for these entities. A dose-dependent effect was seen, with no osteophyte formation for the lowest dose of tacrolimus loaded monospheres and some osteophyte formation in all knees injected with the highest dosage (figure

10, see μCT in high dose row). All osteophytes were very small and not visible during histological evaluation of the joints.

## Correlation of clinical outcome with bone changes

While there was no significant difference between healthy (saline injected) and tacrolimus loaded microspheres injected knees, there seemed to be a dose-dependent trend towards less increase of subchondral plate thickness for the tacrolimus loaded microsphere injected knees. This is in agreement with an earlier study in which we found that orally administered tacrolimus, in an OA model, led to a reduction of sclerotic bone formation, e.g. less thickening of the subchondral plate, when compared to untreated OA controls [337]. Tacrolimus is known to act directly on osteoclast and osteoblast activity, which can lead to bone changes. Indeed, tacrolimus was shown to be able to induce loss of bone density through anti-anabolic effects on osteoblastic cells [338] as well as by inhibiting osteoblast differentiation [339]. In contrast, there are studies suggesting the opposite, where tacrolimus treatment increased bone formation in patients with rheumatoid arthritis [340]. Further investigation of this topic is needed to clarify the direct actions of tacrolimus on bone, but with the doses used in our current study these actions are not relevant and were of no concern.
The formation of osteophytes is definitely not a desired effect and suggests that the medium and higher dosages of tacrolimus are probably not the best to be used in the treatment of osteoarthritis. It does, however, in combination with the fact that the osteophyte formation happened in a dose-dependent fashion, show that the monospheres are indeed a good drug delivery system and that the intra-articular administration led to local dosages (high enough to facilitate an effect) with low systemic concentrations.

Using EPIC-μCT (figure 9), we evaluated cartilage proteoglycan content and its quality. Knee joints injected with a low, medium or high dose of tacrolimus loaded monospheres showed no differences with respect to either attenuation (cartilage quality) nor thickness (cartilage quantity) when compared to the contralateral control knee. All values were within the range of what was found for healthy cartilage in a previous study using the same technique [136]. When comparing our results to the knees in which osteoarthritis was induced in this same previously conducted study [136], we see that significantly ($p<0.01$) worse attenuation and cartilage thickness were found.

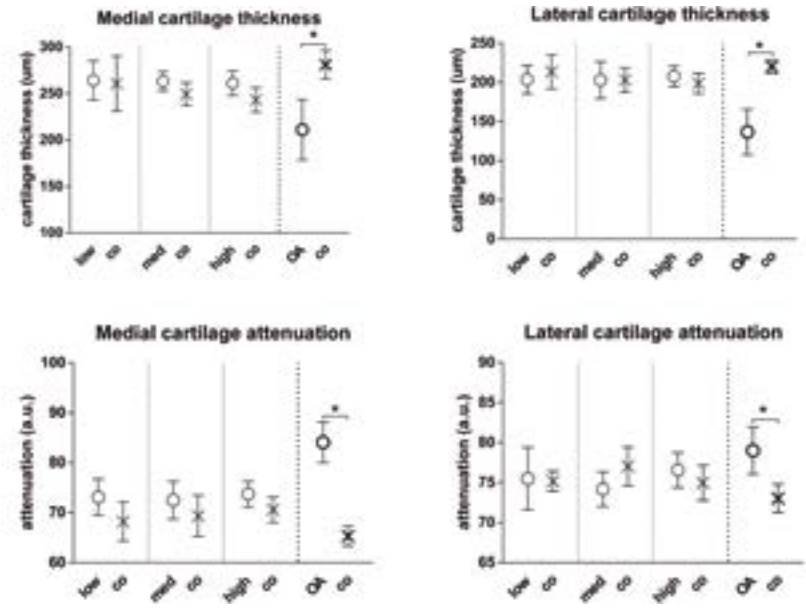


***Figure 9.*** *EPIC-μCT scanning to determine cartilage thickness (μm) and attenuation (arbitrary units) of knee joints injected with a low, medium or high dose of tacrolimus loaded monospheres, 12 weeks after injection vs. contralateral control knees (co). As a reference also values of OA knees are shown. Data is shown as mean ± SD, p<0.05 is considered significant. *: significant differences were found for all measurements of the OA knees when compared to the contralateral control knees and when compared to all doses of tacrolimus loaded monospheres.*

The histological images correlated nicely to the EPIC-μCT images (see figure 10, row 1 and 2). No differences in Saf-O staining were found between tacrolimus loaded monospheres injected knees (low, medium and high dosage) and controls. Morphologically, the cartilage appeared healthy in all groups. These results, together with the earlier shown harmlessness of the intra-articular injection of unloaded monospheres [322], pave the way to the possible exploration of the effectiveness of the intra-articular delivery of tacrolimus loaded monospheres for the treatment of osteoarthritis. However, the *caveat* with respect to osteophyte formation (see earlier) suggests the use of even lower dosages of tacrolimus in future experiments.

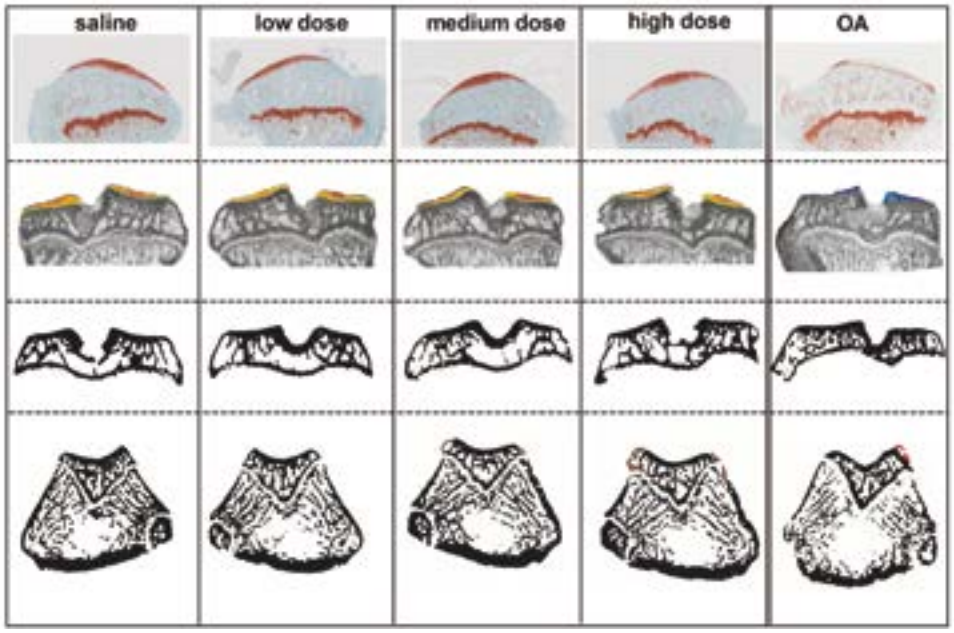


***Figure 10.*** *Histology and CT-images of saline injected knees, compared with low, medium and high doses of intra-articular injected tacrolimus loaded microspheres. Histologically and based on EPIC scanning, no differences are seen in cartilage thickness and quality. Also for subchondral bone thickness, no differences are seen between saline injected or tacrolimus microsphere injected knees. On the right, as a comparison images of an osteoarthritic joint are shown. Both cartilage quality and quantity are affected. Also, a difference (be it subtle) can be seen in terms of subchondral bone thickness of the lateral compartment. The lowest row of this figure shows the osteophyte formation, which is highlighted in red. No osteophyte formation is seen for the knees injected with saline and the low dose, whereas small osteophytes can be seen for the medium and high dose of tacrolimus microspheres and the osteoarthritic knee.*

***In vivo*** **tolerance in horses** There were no signs of lameness in either the saline injected or the tacrolimus loaded monospheres injected joints at any of the time points, indicating that the presence of these monospheres did not have any negative clinical effect on locomotion. *In vivo* tolerance in horses can hence be classified as excellent.

***In vivo*** **tacrolimus release kinetics** From the local synovial fluid and systemic plasma analyses in the three horse we demonstrate that tacrolimus was indeed being released after the tacrolimus loaded monospheres were injected intra-articularly (figure 11). Horse 2 was probably not injected properly into the joint since tacrolimus was not detected from 167 hours post-injection on. In the other two horses, a sustained local release (in the synovial fluid) was seen during the entire follow-up period of 4 weeks (672 hours). The three horses showed measurable systemic concentrations for the first 24 hours post-injection, that were substantially lower compared to the intra-articular concentrations at those time-points, indicating that most of the tacrolimus

was released locally. From 72 hours after injection until the end of the experiment, systemic concentrations were below detection limits (<1.5 ng/ml). Clinically, this was indirectly confirmed by the absence of any systemic side-effect. *In vivo*, we did not observe the lag phase which was observed during the in *vitro* release (figure 5). As stated before, differences between *in vitro* and *in vivo* release kinetics are a well-known phenomenon. Contributing environmental factors are for instance the different composition of synovial fluid compared to PBS which could influence drug solubility, the presence of proteins/enzymes that may change polymer degradation properties and volume available to dissolve tacrolimus (sink conditions) [155, 331]. To minimize the effect of tacrolimus solubility on the release kinetics, *in vitro* release experiments were performed under sink conditions. *In vivo* however, solubility might play a role in drug release due to the limited fluid volume and less predictable replenishment conditions (synovial fluid turn-over). Synovial fluid turn-over for healthy joints takes around 1 hour [341]. There is no literature yet about the solubility of tacrolimus in synovial fluid. Clearance of other substances from the synovial fluid have been tested, and vary from 2 hours for proteins to 5 hours for NSAIDS [213]. Based on this, we hypothesize that synovial fluid turn-over would not be a key factor in the *in vitro*/*in vivo* differences in release pattern, since clearance of intra-articular drugs appears to happen in a matter of hours, whereas our *in vitro* conditions were refreshed no more than once every 24 hours. Restricted amount of synovial fluid within the joint however (~50µL for rat knees, 2-5 mL for talocrural horse joints), could have a significant influence on drug solubility. Although the effects of synovial fluid volume and turn-over are intertwined, and rapid turn-over could diminish the effect of restricted volume, the amount of synovial fluid could have played an important role in the differences between *in vitro* and *in vivo* tacrolimus release.

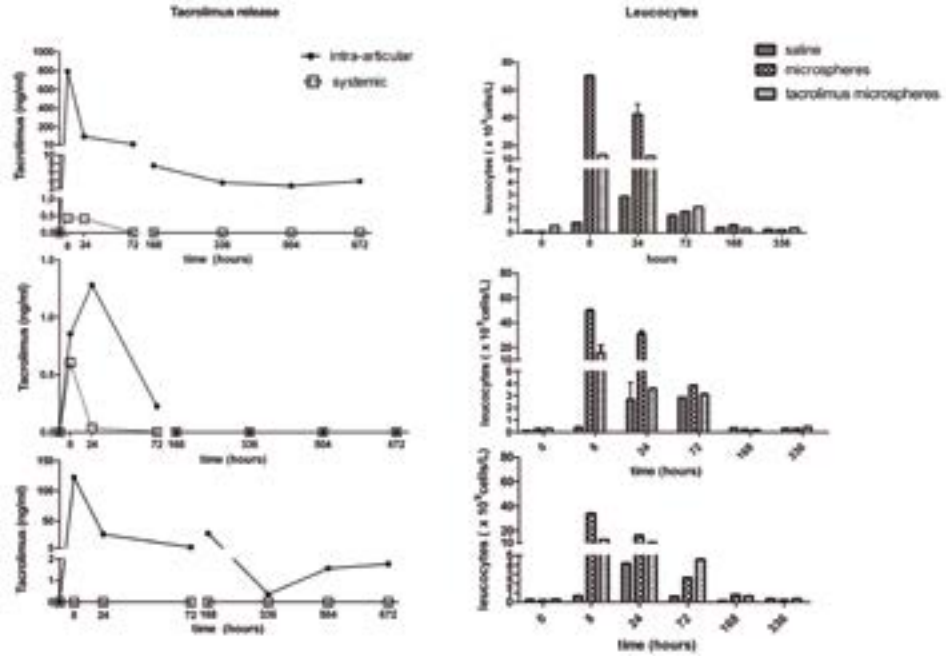


***Figure 11.*** *Tacrolimus concentrations in synovial fluid (intra-articular) and plasma (systemic) after intra-articular administration of tacrolimus loaded monospheres over time per individual horse (left). Right: for the same horse the amount of intra-articular leucocytes, a measure of inflammatory reaction, for joints injected with saline (negative control), unloaded monospheres (positive control) and tacrolimus loaded monospheres.*

***In vivo*** **bioactivity of released tacrolimus** After injection of the unloaded monospheres in the horse joints, a transient inflammatory reaction occurred (increased WBC and total protein in the synovial fluid), which lasted for 72 hours, as reported in our previous study [342]. This transient inflammatory reaction was also observed after the intra-articular injection of the same amount of tacrolimus loaded monospheres when compared to joints injected with saline alone. Macrophages within the synovial lining are activated by the presence of particles as well as by the (minimal) trauma of injecting the joint. These macrophages, whose primary role is to maintain the joint's homeostasis, attract inflammatory cells (amongst which WBC) [343]. A short period of leukocytosis (elevated leucocytes) is part of a healthy immune response. However, a chronic inflammatory state, would eventually lead to a disruption of the joint's homeostasis and might cause cartilage and bone damage, leading to osteoarthritis [344].
In a previous study, leucocyte count in synovial fluid of horses was measured after injection of different actives including Hyanote [166]. Injection of Hyonate led to increased leucocyte counts (>10^10/L) at 8 and 24 hours post-injection, and return to normal at 72 hours post injection. Since Hyonate is clinically approved for intra-

articular use in both humans and horses, we can conclude that mild inflammatory reaction seen in our current study is not a harmful one. Moreover, the inflammatory reactions of all joints injected with tacrolimus loaded monospheres were much less than for the joints injected with unloaded monospheres, indicating that the induced transient inflammatory reaction was less prominent (the same trend was seen for total protein count, see supplementary data figure S.3). At t=8 hours, for all horses the leucocyte count of the tacrolimus loaded microspheres injected joints was less than 50% of the leucocyte count for joints injected with unloaded microspheres. This reflects intra-articular release and a local anti-inflammatory action of tacrolimus [325]. In all horses, tacrolimus release lasted for at least the entire duration of the transient inflammatory reaction (72 hr.) and shows the potential of this medication to act on intra-articular inflammation, a hallmark of many joint diseases. The prolonged release as seen in 2 of the 3 horses shows the potential of the platform-active combination to influence any long-term inflammatory status of a joint, as for instance seen in OA.

**Intra-articular biocompatibility in horses** Chronic joint inflammation seems to play a major role in the structural changes of synovium, bone and cartilage seen in osteoarthritis, mainly through enzymes, growth factors and cytokines produced by activated macrophages [345, 346]. It is therefore important to determine whether the mild transient inflammatory reaction in the first 2 weeks caused by the injected monospheres had any negative effect on the joints. Recently, we have shown that the administration of unloaded microspheres in the horse joint did not have negative effects on the cartilage [342]. The intra-articular doses of tacrolimus would also not be likely to have a negative effect on the cartilage, since it was shown previously in our lab that tacrolimus, with doses up to 1000 ng/ml, did not affect cell proliferation and viability *in vitro* in human articular chondrocytes [56]. Moreover, a dose of 500 ng/ml was tested more extensively and showed to have anti-catabolic and even anabolic effects on chondrocytes.

Additionally, we analyzed GAG release and collagenase-cleavage fragments of type II collagen (C2C assay) in the synovial fluid samples of the horses, which can be considered indicative for cartilage breakdown. Neither of these two markers was elevated and the GAG marker showed even a trend towards less GAG release in the tacrolimus-treated joints compared to the unloaded microsphere treated joints (see supplementary data figure S.3). This correlates well with the positive effect of the tacrolimus loaded monospheres on the inflammatory reaction post injection and it could be hypothesized that the decrease of GAG release might be linked to this phenomenon.

It can be concluded that no negative changes in the cartilage occurred due to the injection of tacrolimus loaded monospheres, which is in line with the biocompatibility results in the rats.

## Conclusions

Poly(DL-lactide-PEG)-*b*-poly(L-lactide) multi-block copolymers provide a suitable platform for the development of injectable tacrolimus-loaded monospheres for intra-articular controlled drug delivery in the treatment of joint diseases, such as osteoarthritis. Tacrolimus-loaded monospheres were shown to be safe for intra-articular use while being retained in the synovial fluid and synovial lining of the rat knee and in the equine carpal joint for at least 4 weeks. Most importantly, local sustained drug release was achieved by the monospheres, since the drug was measurable in high concentrations in the joint without measurable systemic concentrations or toxic side effects. Effects of local tacrolimus delivery on peri-articular bony osteophytes were seen in a dose-dependent manner, indicating that indeed local release can be tuned and thereby achieving the desired local concentrations of an incorporated drug based on the therapeutic window and specific needs in different diseases. The locally released tacrolimus partially counteracted intra-articular inflammation, an action that is potentially beneficial in the treatment of arthritides. Not only have we shown tacrolimus to be a very interesting drug for further investigation in the field of osteoarthritis, but we also have shown monospheres to be excellent drug carriers for intra-articular delivery of potentially interesting drugs in general.

## Acknowledgements

This research was supported by the Dutch Arthritis Foundation (LLP-22) as well as BioMedical Materials institute (co-funded by the Dutch Ministry of Economic Affairs, Agriculture and Innovation (Project P2.02 OAcontrol).
Nanomi B.V. is acknowledged for providing the Microsieve Emulsification Technology.

## Supporting information

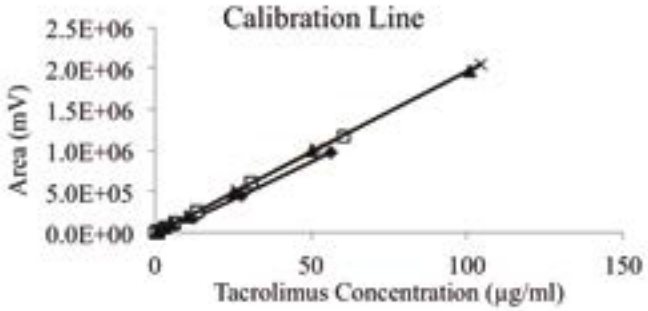


***Figure S.1*** *Extraction and HPLC method for tacrolimus quantification after extraction. Quantification and drug extraction method were developed based on literature. HPLC method showed high linearity and reproducibility between 0 – 100 µg/mL of Tacrolimus.*

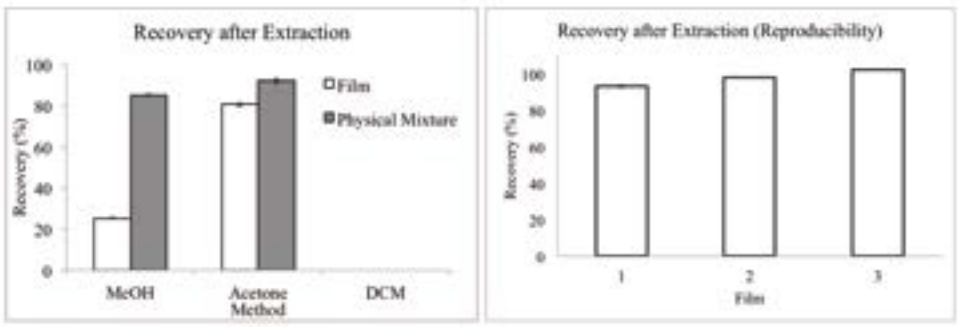


***Figure S.2*** *Three different organic solvents (methanol, acetone and dichloromethane) were tested for their suitability for extraction of tacrolimus from the polymer matrix. Physical blends and films of xx[PDLA-PEG$_{1000}$]-yy[PLLA] multiblock co-polymers and tacrolimus (1wt. %) were prepared in triplicate for the extraction tests. Acetone was finally selected because it showed the higher recovery and good reproducibility among the samples evaluated.*

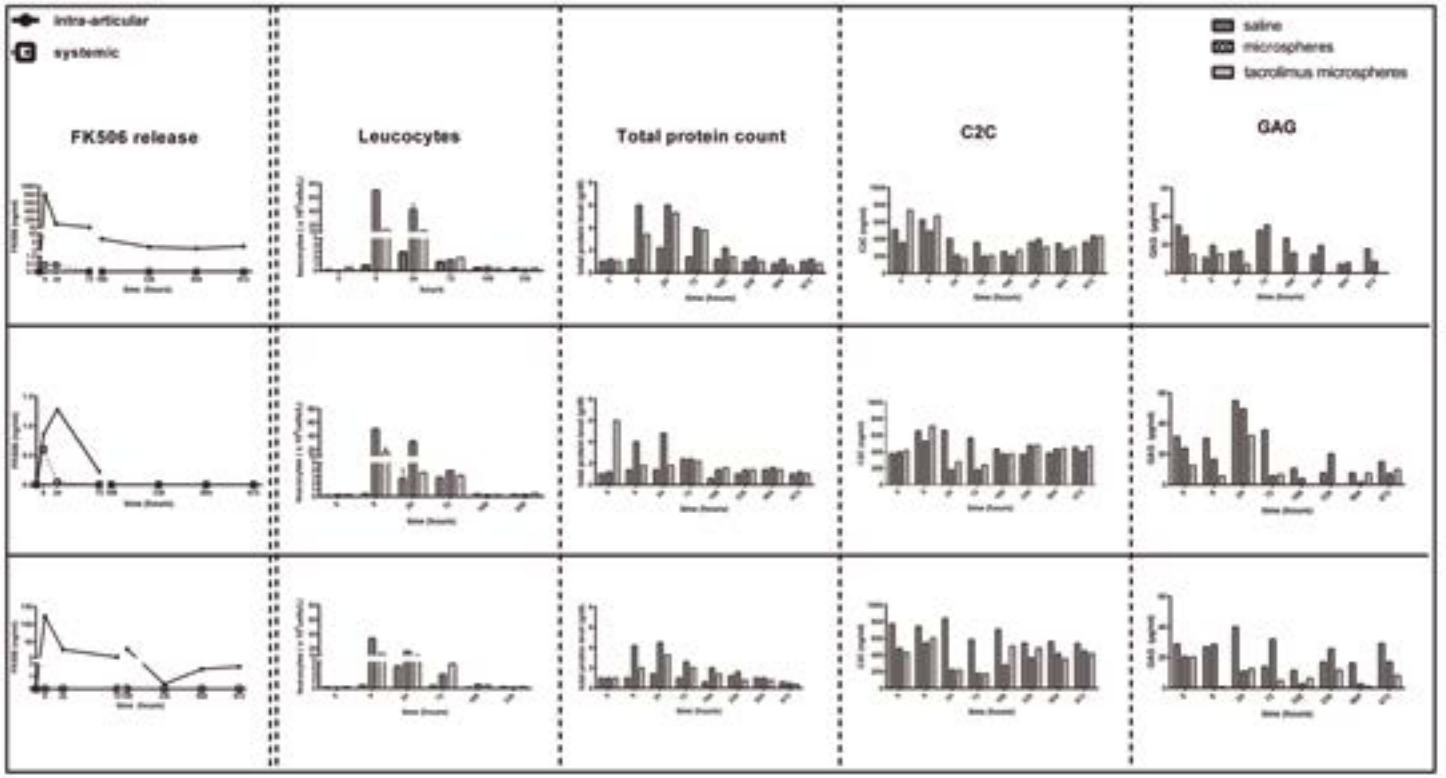


***Figure S.3*** *Tacrolimus concentrations in synovial fluid (intra-articular) and plasma (systemic) after intra-articular administration of tacrolimus loaded monospheres over time per individual horse (left). Right: for the same horse the amount of intra-articular leucocytes and total protein, measures of inflammatory reaction, for joints injected with saline (negative control), unloaded monospheres (positive control) and tacrolimus loaded monospheres. Also C2C and GAG content of the synovial fluid (indicative for cartilage breakdown) are shown. Neither of these two markers where elevated, indicating that neither the inflammation, nor the injection of FK-506 loaded monospheres led to cartilage breakdown during the study period.*


9

# Chapter 9

## General discussion and future perspectives

The aim of the research presented in this thesis was to develop new drug delivery systems for intra-articular use that release drugs aiming for the treatment of osteoarthritis. We focused on two different drug delivery systems, celecoxib loaded thermo-reversible hydrogels based on PCLA-PEG-PCLA and FK506 (tacrolimus) loaded poly(DL-lactide-PEG)-b-poly(L-lactide) multiblock copolymers based monospheres.
The results presented in this thesis demonstrate that substantial steps toward a potential treatment have definitely been made. We have successfully developed two drug delivery systems that have been shown to:

- Provoke no negative effects on the local injection site (the joint) nor provoke any negative systemic effects
- Remain at the site of injection and degrade over a period of several weeks
- Provide a prolonged local release of the loaded drug during this degradation period without leading to measurable systemic concentrations
- Specifically for the hydrogel system, the gel properties can be tailored to the aimed drug release profile, leading to customizable drug delivery systems that can be applied in a disease-specific of even patient-specific setting.

Requirements for biomaterials used in Orthopaedics are described in AAOS Comprehensive Orthopedic review. They state that " Biomaterials used in Orthopaedics must be biocompatible with the anatomic sites and tissues in which they are used, with the ability to function *in vivo* without electing detrimental local or systemic responses; must be resistant to corrosion and degradation (this is of course not applicable to biodegradable materials) and able to withstand their *in vivo* environment; and must have adequate mechanical and wear properties for the applications and settings in which they are to be used" [347]. Based on the work presented in this thesis, we feel confident to say that both developed drug delivery systems meet these requirements.

## Biocompatibility

Biocompatibility is one of the most important properties when designing a drug delivery system (DDS). Historically, biocompatibility is defined as "*the ability to perform with an appropriate host response in a specific application*" [348].
Upon mechanical loading, microspheres could potentially have a negative effect on tissues such as cartilage due to friction/shearing or indenting based on the materials hardness compared to that of the cartilage. Therefore, mechanical testing of our monospheres was conducted, as described in **Chapter 7**. Here we showed that the monospheres in their swollen state exhibit similar material stiffness (as reflected by the Young's modulus) compared to human cartilage. Therefore, the monospheres are very unlikely to cause cartilage damage by indentation which would be more likely when the hardness of the

microspheres would have exceeded that of cartilage. Shearing in a joint is naturally minimized by the presence of synovial fluid.
Indeed, after extensive *in vivo* testing, both of our DDSs were proven to be biocompatible when injected in both rat- and horse joints, since no adverse effects of the hydrogel or microspheres were seen on the location of injection (the joint) and also no adverse systemic effects were observed (**Chapter 2** and **Chapter 6**). We can conclude that the requirements of biocompatibility as decribed by Willams *et al.* are met.

## Translation to clinical application in human

To conclude, based on promising results in the animal experiments, that the DDSs studied in this thesis would be safe for human clinical use is a bit impetuous. Animal testing offers great benefits compared to human trials, for instance the results are quite consistent due to the homogeneity of a group of animals of the same sex, age and strain. Particularly interesting for orthopedic research, rat knees are anatomically almost identical to human knees [349]. Albeit all benefits of animal testing, results acquired in animals cannot be directly translated one-to-one to the clinical situation without any concerns regarding safety and effectivity.
Several reviews described that a therapeutic effect in an animal model does not always translate to efficacy in the human setting [350-352], although no orthopedic studies were analyzed in these studies. Hackam *et al.*[352] suggested different reasons contributing to this difference; for one, the presence of methodological bias in animal studies, such as not reporting an effect size and no blinding. For our studies however, power analyses have been performed prior to setting up our experiments. Also, overestimating the efficacy due to the lack of blinding is very unlikely for our experiments, since we used quantitative measurements like EPIC-CT scanning instead of histology, where the latter is subject to the interpretation of the examiner. A second potential reason for poor translation from animal to human, according to Hackem *et al.*, is the fact that animal models may not adequately represent human pathophysiology. Although, as stated before, the rat knee is anatomically close to identical to the human knee (with some small differences, such as ossicles within the menisci of rats [353]), this is a very valid argument. Items to consider when comparing results drawn from intra-articular experiments in rat knees to the human situation are for instance temperature, pH, the presence or absence of different cytokines and proteins as well as mechanical loading. When comparing rats to humans on these items, we can exclude the first two as contributors to possible differences in outcome, since they are the same in both species. Temperature of healthy rat knee joints is estimated between 30-35° [354], for human knee joints, resting temperature is 30-34° [355]. The pH of both healthy human and rat knee joints is 7.4 [356, 357]. Although degradation of poly(glycolic acid) based and poly(lactid acid)based biomaterials is mainly driven by hydrolysis [358], its degradation can be also affected by enzymes [359]

as we also showed in **Chapter 2** for the PCLA-PEG-PCLA hydrogel. So, while synovial fluids of rat and human are similar for both temperature and pH, the palette of proteins and enzymes present in a joint are numerous and might differ between the two species, leading to differences in degradation rate and profile. Also, upregulation of cytokines and chemokines is seen in diseases like rheumatoid arthritis and osteoarthritis [360], potentially leading to a faster degradation of an injected biomaterial in different stages of disease.

Joint loading obviously is different between rats and human, since rats are quadruped while human are biped. Also, rats weight about 300 to 500 grams while humans would usually be between 100-200 times this weight. This difference in mechanical loading on the injected biomaterials can affect their integrity and possibly the rate of degradation and release of loaded drugs. Both PLLA and PLGA are shown to degrade faster upon dynamic mechanical stress [361].

Therefore, although this was not examined, differences in effect of compressive forces on the intra-articular monospheres between rats and human can certainly not be ruled out. It must be stated that, through *in vivo* CT-visualization of intra-articular injected iodine-bound hydrogels (**Chapter 2**), we were able to conclude that the injected material mainly resides in the suprapatellar pouch and not between the articulating surfaces, thereby being less susceptible to mechanical loading. This would further minimize potential differences in degradation of the injected biomaterials and subsequently their drug release profiles. However, mechanical joint loading leads to enhanced flow of the intra-articular fluid in and out of the biomaterial, possibly enhancing diffusion of small molecules and degradation of the material itself [362]. It would be very interesting for future experiments concerning our hydrogels and monospheres to incorporate the effects of stress and mechanical loading on the degradation of the polymers and the drug release profiles. This could for instance be done by using the stress-modified Arrhenius equation [363]. Using this equation, the bond-rupture events in a polymer can be calculated based on the applied stress on the polymer.

Because of these foreseen differences between the results in the experimental animal setting and the human clinical setting, our recommendation would be to extensively test materials on items such as degradation kinetics and drug release profiles in human joints (for instance in patients awaiting total knee replacement). This in order to enable improvement of the biomaterials characteristics to match the requirements specifically for the human situation, before making the step to human efficacy studies.

## Hydrogels or monospheres?

In this thesis, two different drug delivery systems were extensively evaluated. There is quite some literature available on the intra-articular use of microspheres, while up to now, the use of injectable polymeric hydrogels for intra-articular use has been very

limited. The limited studies dealing with hydrogels for use in OA joints are however positive. It was e.g. shown that these gels are able to minimize the burst release seen with other drug delivery systems [26]. Based on our results presented in this thesis, we cannot easily point out one of the two as superior to the other, since they both show a good biocompatibility, are retained within the injected joints for several weeks and able to provide a sustained local drug release without provoking local or systemic side-effects. Also, the abovementioned advantage of hydrogels over microspheres in terms of lower burst release is not valid for our two systems, since our monospheres did not exhibit a burst release. There are however some pros and cons to both materials when comparing them. First of all, an advantage of the hydrogels is that the drug release period more or less equals the degradation rate of the polymer **(Chapter 2 and 3)**. For the monospheres however, *in vitro* drug release takes around 35 days **(Chapter 8)**, while full polymer degradation can take up to 550 days depending on the polymer composition **(Chapter 6)**. This leads to a long period that the empty drug delivery system is still present within the joint without actually being functional. Also, it should be stated that we did not test biocompatibility of the injected monospheres for the full course of degradation (an *in vivo* experiment of over 1 year would not be feasible) and we therefore cannot make any statements about the long-term biocompatibility. It has been shown in an animal experiment in which biodegradable poly(methylidene malonate) microspheres were injected into rat brains, that the material initially only evoked a mild inflammatory response, but upon visible degradation (after about 6 months) toxic effects on the surrounding tissue was elicited [364]. The authors speculate that the reason for this reaction to the degradation of the material is a direct effect of the acidic degradation products of the microspheres. Of course, we used a different material and cannot conclude that the same observations are valid on the long term after injection of our monospheres, but it is a pivotal step to research this fully before moving on to any type of clinical trial. An important difference between the abovementioned poly(methylidene malonate) and our hydrogel system is that due to the character of the PCLA-PEG-PCLA hydrogel, degradation products will leave the material in an easy and sustained manner, rather than having a bulk release at the end of the degradation period. This would lead to a less acidic environment and less potential tissue damage. Furthermore, brain tissue might be far more sensitive to environmental changes compared to cartilage or synovium. A major selling point of the hydrogels described in this thesis, is the fact that their *in vivo* release kinetics can be simply changed by altering the composition of the celecoxib/hydrogel formulation (see **Chapter 4**). This can lead to a drug delivery system that can be tailored specifically for a disease or even to meet the individual needs of single patients. For the monospheres, we did not execute such an *in vivo* experiment, but we did show that the degradation of the monopsheres can be altered by changing the [PDLA-PEG1000] / [PLLA] block ratios (**Chapter 8**). In addition to this, Innocore has shown for monospheres with a slightly different composition, namely

poly (E-caprolactone-PEG)-b-poly(E-caprolatone), by changing the PEG content of the polymer, the *in vivo* release kinetics could be predictably influenced [330]. By analogy, it is therefore likely that the *in vivo* release kinetics can also be influenced by choosing different block ratios for the monospheres used in this thesis.

In **Chapter 5**, the efficacy of celecoxib loaded PCLA-PEG-PCLA hydrogels was evaluated in a rat OA model. Unfortunately, no differences in either cartilage quality or quantity were found between treated and untreated animals. However, also no adverse effects were observed and the higher M2 macrophage activation following intra-articular administration of celecoxib loaded hydrogels is promising, since this could lead to less pain and less cartilage damage (although we were not able to measure this in the current OA model). Data regarding the efficacy of FK506 loaded monospheres in the same animal model also showed no differences between treated and untreated animals on cartilage quality or quantity (unpublished data, article in progress). Ten Broek *et al.* investigated the efficacy of tacrolimus in two different rat OA models, the MIA model (mono-iodoacetate) and the meniscal tear model [365]. Both systemic and intra-articular administration of tacrolimus lead to no significant differences compared to saline-treated knees in the MIA model, although a slight negative trend of intra-articular tacrolimus on cartilage histological score (5±0 versus 2.7±1.5 for saline injected knees) is described by the authors. In the meniscal tear model no significant effect on the histological scoring of the cartilage were found for intra-articular administered tacrolimus compared to significant positive effects of systemically administered tacrolimus (0.5±0.15 versus 1.83±0.31 in saline injected knees) in the same model. These results underline that it is very important to keep in mind that differences in efficacy between different studies can be (partly) due to the choice of OA model. Also, the results underline the need of a good intra-articular drug delivery system for tacrolimus, since the molecule is too toxic for systemic administration but apparently direct intra-articular injection of tacrolimus leads to some negative effects which might be attributed to high peak concentrations, whereas the use of a biomaterial would lead to sustained low concentrations, thereby minimizing the possibility of negative effects on cartilage. The fact that we found no positive effects of the released drug might also have to do with the achieved local concentrations, which might not have been within the therapeutic range. Although no effects on cartilage were observed, an unexpected effect was seen with the development of large osteophytes and even heterotopic ossifications in the surrounding soft tissue. This did not happen after injection of the same amount of FK506 loaded monospheres in healthy rat knees although some minor, dose dependent, osteophyte formation was seen after the injection of FK506 monospheres in **Chapter 8**. We also did not observe osteophyte formation after the treatment with celecoxib loaded hydrogels in the same OA animal model. It is therefore clear that the combination of this specific animal model with intra-articularly administered FK506 loaded monospheres provoked a reaction that led to osteophyte formation. Bone formation due to the administration of FK506

seems somewhat counterintuitive, since most studies where FK506 is administered to rats show loss of bone mass [366, 367]. However, osteophytes arise from periosteal and synovial cells, and although the mechanism behind the formation is not fully understood, the role of mechanical stress and chronic inflammation are thought to be a very important [201]. Activated macrophages producing TGF-ß, which induces BMP production; a trigger for osteophyte formation [11]. Loading was the same for all rats, so this was not the underlying cause of the osteophyte formation in only the group receiving intra-articular tacrolimus loaded monospheres. While effects of tacrolimus are known to be (partly) RANK/RANKL driven [368], inhibition of RANKL was shown to not have any effect on osteophyte formation [369], underlining the idea that the found osteophyte formation is not due to a direct effect of tarcrolimus on bone.
Apart from osteophytes, we also observed the formation of heterotopic ossifications.

Heterotopic ossifications are calcium deposition, usually in the form of bone in soft or hard tissue, these can occur in the case of genetic mutations, trauma or disease [370]. The induction of OA through injection of papain combined with the running model could be considered a trauma, although no heterotopic bone formation was observed in other cases with this combination. It was recently described however, in a rat model in which mesenchymal stem cells seeded on scaffolds were implanted ectopically, that the formation of ectopic bone was suppressed by T-cell and B-cell mediated immune response. This response could however effectively be abolished by the daily administration of 1 mg/kg FK506 intra-muscularly. In the rats treated with FK506, the formation of ectopic bone was profound [371]. This phenomenon could also have been the case in our study, where a trauma was inflicted by the induction of OA and the following immunosuppression lead to the formation of heterotopic ossifications.
The formation of osteophytes and heterotopic ossifications seems more likely to be a side-effect of the specific combination of OA induction, monospheres and FK506 and not to be linked to the use of monospheres only. Therefore, this difference between our celecoxib loaded hydrogels and FK506 loaded monospheres cannot be pinned down to a difference between monospheres and hydrogels, and we cannot conclude that one of the two is superior to the other based on these results. The pronounced effect on bone formation found in our study is however a very interesting finding and should be further investigated since it might be of interest for the treatment of for instance critical bone defects.

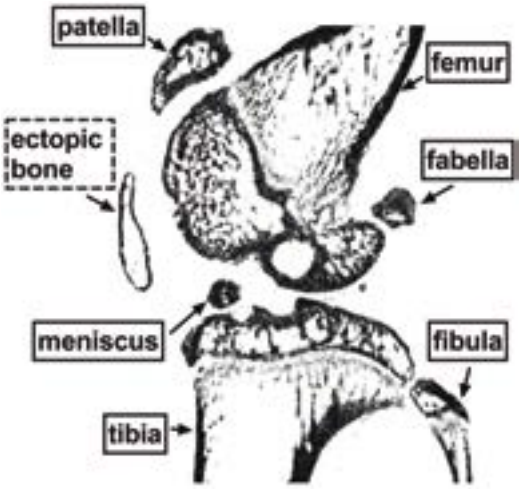


***Figure 1**. CT-image of ectopic bone formation in an FK506 treated rat OA knee (t= 12 weeks)*

The fate of intra-articular injected microspheres depends on their size. Particles <10 μm (optimally between 1 and 4 μm) are being phagocytosed by the macrophages residing in the synovium, whereas larger particles are not phagocytosed but instead sequester into subsynovial plaques [68]. Choosing different particle sizes for specifically targeting different cell types could be an interesting approach when searching for an optimal disease modifying drug, especially since the pathophysiology of OA has not been clarified yet and several authors propose macrophages to be very important players in the disease onset and progression [12, 193, 268, 344, 372]. Targeting the macrophages is especially interesting when anti-inflammatory drugs, such as NSAIDs are loaded in a drug delivery system, in order to directly reduce the inflammation and ideally break the vicious cycle of inflammation and cartilage degradation as seen in OA [185]. Choosing the site of operation with choosing the size of the particles is an advantage of micro/monospheres over hydrogel-based systems. There are some interesting developments in the field of drug delivery systems to even more precisely target specific tissues of interest. An example is the work of Bajpayee *et al.*, who published an article on a positively charged glycoprotein (avidin), as a nanocarrier for the targeted release of dexamethasone inside rabbit cartilage in an OA model [373]. Since cartilage matrix is negatively charged, electrostatic interactions led to a higher uptake of the drug into the tissue due to the positive charge. Full thickness penetration of the cartilage by avidin was shown by immunostaining. Another very interesting study involved near infrared fluorophore loaded immunoliposomes, of which the surface was functionalized with a collagen 2-antibody. After intra-venous injection, these liposomes selectively bind to damaged cartilage, thereby making it possible to visualize very early stages of osteoarthritis [374]. When these liposomes would be loaded with a drug instead of the near infrared label, very specific targeting of damaged cartilage could be achieved

potentially. Another interesting approach was done by Butoescu ea in 2009 [375]. In this paper, they present biodegradable PLGA-based microparticles for intra-articular administration of dexamethasone. What makes these particles interesting, is that they were also loaded with superparamagnetic iron oxide nanoparticles and that the retention of these particles within the joint could potentially be extended with the use of an external magnetic field. However, although the group did study *in vivo* release after intra-articular injection of these magnetic particles, they did not actually test the effect of the presence of a magnet on the intra-articular retention time. However, no follow-up study has been presented so far, and the reasons of not following up on this promising delivery system are not known. Although clinical application of magnetically responsive particles could be challenging, it is interesting to have a drug delivery system that could be externally influenced, since in theory an external magnet cannot only be used to keep the particles in place, but makes it also possible to remove them from the injected joint to the periphery in case of adverse effects, and even allows triggering drug release with an external magnet when desired.

## Which drug should be released?

In this thesis, we have focused on two different drugs for the delivery in the knee joint, with the aim of curing OA. However, although both the hydrogels and monospheres proved to be excellent local slow drug release systems, real efficacy of the released drugs on cartilage level was not shown (**Chapter 5** for celecoxib, FK506 data unpublished). The rationale behind the selection of these two drugs is discussed extensively in the introduction **(Chapter 1)** of this thesis. NSAIDS have a long history of intra-articular use, but until now no convincing data on the OA disease modifying properties have been shown in either a suitable animal model or a clinical trial, and even results on long-term pain relief are conflicting [23].

In this thesis, we were also not able to show an efficacy of locally release celecoxib in the treatment of OA **(Chapter 5)**, although higher M2 macrophage activation was found following intra-articular release of celecoxib from hydrogels potentially leading to less pain and cartilage damage when using a more severe OA model. FK506 showed promising *in vitro* results on chondrocytes [46, 56, 376]. Also, our group previously showed a positive effect of the oral administration in rats, which developed less pronounced OA when compared to a saline treated control group [337]. However, the difference between this previous study and the data discussed in this thesis might very well be linked to the timing of the experiments. In the study of Siebelt *et al.*, treatment began simultaneously with the induction of OA, while in our current study we choose to first induce osteoarthritis and start the treatment a couple of days later. This is a difference between a prophylactic treatment and treating early onset OA, the latter being

far more representative for the clinical setting since patients only present themselves after they experience clinical symptoms. Unfortunately however, the intra-articular treatment with FK506 did not result in slowing down the progression of OA compared to the saline treated animals. Again, this might also have been the case in our previous study had we not started treating before the first signs of OA appeared. Differences in results due to different experiment set ups rather than real treatment differences make animal studies difficult to compare and thus to extract overall conclusions from these varying experimental setups is rather complicated and ambiguous. Our general suggestion would therefore be to regulate animal studies like they do clinical studies, and to reach a consensus on the use of one or a few well-described animal models for the generation of reliable and comparable data.

Like stated before, although both of our released drugs were not able to halt the progression of OA, both drug delivery systems were able to deliver the drug in a sustained manner without local adverse effects and without systemic side-effect. The lack of therapeutic effects of the drugs could mean several things. For one, the local drug concentrations that are achieved by the sustained release from the DDSs might not have been in the therapeutic range. Since we did not observe toxic side effects of the formulations, it is recommended to carry out a dose-escalating study. Also, it cannot be ignored that efficacy of the released drugs is tested in an induced OA model in rats, rather than in the actual human situation in which we know the disease to have multiple phenotypes. Not seeing an effect might have to do with the choice of the model and/or the differences between rat and human, as stated before. Lastly, it is possible that both drugs indeed do not show any therapeutics effect in slowing down the progression of OA. It is therefore pivotal to look for new drug candidates to incorporate in these systems for local sustained release to facilitate chondropositive effects and treat OA. A number of different drugs are being tested *in vivo* in animal models and some even progressed to human clinical trials. There are some drugs that have gained interesting results. One of those drugs is verapamil, a suppressor of Wnt/β-catenin signaling in human OA chondrocytes which is able to inhibit OA progression in an OA rat model upon intra-articular injection [377]. These promising results have not been followed up yet by a clinical trial. Another active, sprifermin has gained some attention. Sprifermin, a recombinant human fibroblast growth factor 18, showed promising results in animals testing and a human trial followed [378]. In this trial, the drug was injected intra-articularly in OA knees 3 times over a course of 3 weeks while a control group was injected with saline and MRIs of the knees were conducted at baseline and at 12 months follow up. For the sprifermin group, significantly less severe degeneration of the patellofemoral joint cartilage was observed compared to the control group. Incorporating this drug in a DDS for local sustained release, and thereby lowering the number of injections would be extremely interesting. Another very interesting development in osteoarthritis research is the discovery of senescent cells and its relationship with OA. Cellular senescence is a cell-

cycle arrest, in which cells cease to proliferate [379] and protects against cancer [380]. Recently, it has been suggested by different groups that senescence is linked to OA [381, 382]. Xu *et al.* were the first to show a causal link between senescence and OA, since they observed the development of OA through histology and radiographs 3 months after transplanting senescent cells into knee joints of mice (histology score = 16.8±3.1) [383], while transplanting non-senescent cells showed only minor changes (histology score = 5.7±3.3). Senescent cells secrete different pro-inflammatory cytokines, amongst which IL-6, and Xu *et al.* indeed found a 20-fold increase of IL-6 secretion when comparing non-senescent cells to senescent cells. They postulate that the cells might contribute to the development and progression of OA via the induction of inflammation. One treatment option would therefore be the administration of anti-inflammatory drugs, like for instance celecoxib, one of the drugs used in this thesis. The lack of effectivity could be a dosage problem, and further research is needed to establish whether this is indeed the case. More novel are drugs specifically targeting senescent cells; these are so-called senolytic drugs [384, 385]. Navitoclax, one of these senolytic drugs, indeed showed, amongst other health span extending effects, that age-related GAG-loss from intervertebral discs was diminished after 10-12 weeks of treatment with a weekly oral dosage of the drug [384]. Since GAG-loss is also a key factor in the progression of OA, this drug is very interesting for the treatment of OA. Because the drug has to be administered weekly, there is a great potential for the use of a drug delivery system to achieve a sustained local drug concentration.

The most promising small molecule reported in the recent literature seems to be kartogenin. In 2012, 22.000 molecules were screened and kartogenin, a transcription factor CBFβ, was found to be able to induce chondrogenisis [386]. The authors describe not only a chondroprotective effect, but even cartilage matrix regeneration in a mouse collagenase OA model as well as a surgery-induced OA mouse model. It is however indicated by another group, that kartogenin at unwanted sites can induce overgrowth of normal tissues [387], demonstrating the need for a local release from a drug delivery system. In 2017, Hu *et al.* fabricated polyethylene glycol modified polyamidoamine nanoparticles loaded with kartogenin [388]. *In vitro*, the released kartogenin was able to upregulate chondrogenic markers, and the *in vivo* intra-articular retention time of the particles was >21 days. Efficacy of kartogenin loaded drug delivery systems has not been tested *in vivo* yet, but the abovementioned results are very encouraging.

Although all studies mentioned above showed promising results, it is important to acknowledge the fact that many drugs have shown chondroprotective effects based on *in vitro* experiments only, but the use of the same drugs in an *in vivo* environment fails to show significant effects [389]. It is difficult to determine the cause of this discrepancy, because the *in vivo* situation is far more complicated and unpredictable compared to standardized *in vitro* experiments using cell cultures. However, it might be a problem of

too low drug concentrations or too rapid clearance of the drug from the synovial fluid, both problems that can be solved by the administration of a DDS governing a sustained local drug release with tunable drug release kinetics.

## Current clinical developments

Up to now, when leaving hyonate (hyaluronic acid) out of the comparison, there is only one clinically available drug delivery system for intra-articular use in human. This is Lipotalon®, a liposomal corticosteroid formulation that is only available in Germany [390]. As stated in the Introduction of this thesis, liposomes have a few disadvantages compared to polymeric drug delivery systems. They are proven to be less stable, have a limited ability to be loaded with lipophilic drugs and also their resistance to mechanical loading is a problem mainly for their use in orthopedics [391]. Also, liposomes offer limited control over the release kinetic.

Very recently, a randomized, double blinded, placebo controlled multicenter study was published in which an intra-articular microsphere formulation, marketed under the name Zilretta (Flexion Therapeutics, USA), was used in a clinical setting [392]. In this study, 484 patients were treated with an intra-articular injection of either saline (n=162), 40 mg of freely injected triamcinolone acetonide (TA) (n=161), or triamcinolone acitonide (32 mg) loaded PLGA microspheres (n=161) with a size range of 20-100 μm. In an earlier conducted clinical study by this group, they found that after injecting around the same dose of TA encapsulated in microspheres rather than injected freely led to 11 times lower peak plasma concentrations, and intraarticular TA was measurable in the microspheres group for >12 weeks [393]. TA loaded microspheres offered around 50% improvement in average daily pain (ADP) intensity at t=12 weeks compared to saline, whereas ADP did not differ between free TA and TA loaded microspheres. Adverse events were mild and spread evenly throughout all treatment groups. However, on two patient outcome measurements based on questionnaires (KOOS-QOL and WOMAC A, B and C), significant differences were found in favor of the TA microspheres compared to the free drug at all time points (4, 8 and 12 weeks post injection). No serious adverse events linked to the injected study agents were reported, but 18.6%, 12.3%, and 9.9% for respectively TA microspheres, saline and TA, reported mild side-effects which was mainly arthralgia at day 3 post-injection, not related to a flare. The found differences are small, and the dosages of the free TA (40 mg) and TA released from the microspheres (32 mg) is not the same thus results are difficult to compare. However, this is the first ever trial with an intra-articular drug delivery system conducted in humans, and the fact that this step has now been made shows that there is a bright future for the whole research field focusing on intra-articular drug delivery systems. The two DDSs described

in this thesis show very promising results, and further research has to be carried out to fully explore their therapeutic potential for the treatment of osteoarthritis.


10

# Chapter 10

## Summary

Osteoarthritis (OA) is a common joint disease, patients afflicted by the disease suffer from pain and loss of function. The numbers of OA patients is expected to rise over the coming years, partly due to the increasing life expectancy as well as an increase in obesity amongst the general population [2]. Treatment options for OA are unfortunately limited, and are at present essentially based on treating the symptoms until the moment of joint replacement has become inevitable. The cornerstone of symptomatic OA treatment is pain management through the use of pain killers [21]. Oral administration of these painkillers can however result in serious side-effects [21, 22], while direct intra-articular injection of free drugs will lead to rapid drug clearance from the joint leading to a very short-lived effect [320]. Further, direct injections can be painful for patients. A way to circumvent the problem of rapid drug clearance from the joint and to avoid frequent administrations is the use of injectable drug delivery systems that release the therapeutic agent for a prolonged time [28, 68, 72, 183] [26]. For this thesis, two different drug delivery systems were studied for intra-articular use: monospheres and thermoreversible hydrogels.

In **Chapter 2** we studied the *in vitro* and *in vivo* properties of an acetyl-capped PCLA-PEG-PCLA based hydrogel. We showed good intra-articular biocompatibility of the gels, since no changes in cartilage quality or quantity was observed after intra-articular administration. In order to investigate *in vivo* gel degradation, a blend of polymers either capped with acetyl, or with 2-(2',3',5',-triiodobenzoyl, TIB) moieties was injected in rats, both subcutaneously and intra-articularly. TIB can be visualized using μCT, enabling longitudinal quantification of the degradation of the gel. With this method, we found that after subcutaneous injection, the gel degraded over a period of ~12 weeks. In contrast, after intra-articular injection, the gel was not detectable four weeks post-injection. The accelerated degradation after injection in the joints when compared to subcutaneous injection is likely caused by a combination of the following factors: dispersion of the gel in the synovial fluid, rapid synovial fluid turn-over, mechanical stress due to weight bearing and a higher surface/volume ratio.
After obtaining promising results for intra-articular use of the hydrogels based on acetyl-capped PCLA-PEG-PCLA polymers, we loaded it with celecoxib, a non-steroid anti-inflammatory drug, to be released from this gel. The celecoxib loaded hydrogel was tested both *in vitro* and *in vivo* and the results are presented in **Chapter 3**. In this chapter, both drug release kinetics and biocompatibility were investigated. The *in vitro* celecoxib release was governed by polymer dissolution and lasted for 90 days with a lag phase of ~10days. *In vivo* release occurred without a lag phase and an initial release of ~ 30% of the loaded drug during the first 3 days post-injection was followed by a sustained release of 4-8 weeks. The difference between *in vitro* and *in vivo* release is most likely due to enhanced solubility of celecoxib in biological fluids, turnover of synovial fluid and gel degradation by macrophages. Similar to the unloaded hydrogel tested in

**Chapter 2**, excellent intra-articular biocompatibility was shown in rats for the celecoxib loaded hydrogel through μCT scanning as well as histology.
After proving that the celecoxib-loaded PCLA-PEG-PCLA based hydrogels are safe for *in vivo* injection, and that these systems show sustained release of the loaded drug for several weeks, we were interested in obtaining more insight into the pharmacokinetics of these celecoxib PCLA-PEG-PCLA formulations as well as in the relation between the hydrogel composition and the pharmacokinetic. In **Chapter 4** we report on the release kinetics of 5 different celecoxib loaded gels which differed in terms of end-capping, injected volume, drug loading and polymer concentration, after subcutaneous injection. The *in vivo* celecoxib release period could be prolonged by increasing the injected volume from 100 to 500 μL, changing the end-capping from acetyl to propyl and also by increasing the celecoxib loading from 10 to 50 mg/mL. Not only the total release period, but also the serum concentrations of celecoxib per time point could be influenced by changing the specifications of the formulations. The fact that we are able to change the release period and kinetics by simply adjusting the gel adds great potential to this drug delivery system, since the drug release can be altered to meet disease or even patient specific needs.
**Chapter 5** describes the therapeutic efficacy of the celecoxib-loaded PCLA-PEG-PCLA gel in an OA rat model. Although we were not able to show a chondroprotective effect of celecoxib (either freely injected or released from a drug delivery system), celecoxib loaded gels proved to be superior to injection of free celecoxib on cartilage thinning. Increased macrophage activation was observed in knees injected with a celecoxib loaded hydrogel, based on current literature, most likely of the anti-inflammatory subtype. Clinically, the rats receiving the celecoxib loaded gels did not show any signs of inflammation or pain. The lack of efficacy on pain relief or chondroprotection might be due to the choice of a very mild OA model. In the future, we would like to repeat the experiment in a more severe OA model, combined with higher doses of celecoxib.
In **Chapter 6**, we developed and investigated monospheres composed of biodegradable poly(DL-lactide)-PEG-poly(DL-lactide)-b-poly(L-lactide) multiblock copolymers. Upon intra-articular injection in rat and horse knees, the unloaded monospheres were retained in the injected joints for up to 3 months and elicited a mild inflammatory response, but no negative effects on cartilage were observed.
In **Chapter 7**, the nano-mechanical properties of the monospheres are described and we found that the mechanical properties of swollen monospheres (their state in biological fluids) are within the range of the nano-scale properties of cartilage, making indentation or grinding damage of the monospheres to the cartilage less likely, which is indeed in line with the findings of **Chapter 6**.
In **Chapter 8** these same monospheres were loaded with tacrolimus (FK506). Tacrolimus is a calcineurin inhibitor that has been used as an immunosuppressant in transplantation surgery to prevent graft rejection [44, 45]. Upon injection of the tacrolimus loaded

monospheres in horse joints, sustained local drug release within the joint was obtained during the entire 4-week follow-up, with no measurable systemic concentrations. The inflammatory response seen after injection of unloaded monospheres was significantly lower in the tacrolimus loaded monospheres group, indicating a local anti-inflammatory action of the released drug.

In conclusion, two drug delivery systems were developed and both showed excellent biocompatibility for intra-articular use with favorable *in vivo* release kinetics. Anti-inflammatory actions were observed for the tacrolimus loaded monospheres, and the celecoxib loaded hydrogels proved to be superior to intra-articular injection of free celecoxib. However, we did not find actual therapeutic activity with either of the drug delivery systems in a pre-clinical OA model. Although both drug delivery systems show great potential for intra-articular use, further research is therefore needed. Firstly, since we found no negative effects of the released drugs from the injected formulations, but also no therapeutic effect, a dose-finding study is advised. If indeed the selected drugs show no disease modifying potential in OA, the selection of alternative drugs to be released from these systems should be carried out.

# Chapter II

## Appendices

*Nederlandse samenvatting*
*References*
*PhD portfolio*
*List of publications*
*Dankwoord*
*About the author*

# Nederlandse samenvatting

Arthrose is een veelvoorkomende gewrichtsaandoening, patiënten die lijden aan deze ziekte hebben vaak last van pijn en een functiebeperking van het aangedane gewricht. Het aantal patiënten dat lijdt aan arthrose zal naar verwachting de komende jaren stijgen, deels door de steeds verder stijgende levensverwachting, maar ook door een toename van obesitas onder de algemene populatie [2]. De behandelmogelijkheden zijn helaas beperkt, en op dit moment vooral gebaseerd op symptoombestrijding, tot het moment bereikt wordt waarop een chirurgische gewrichtsvervanging in de vorm van een prothese onvermijdelijk is geworden.
De belangrijkste pijler in de symptomatische behandeling van arthrose is pijnbestrijding met behulp van pijnstillers [21]. Orale toediening van deze pijnstillers kan echter lijden tot ernstige bijwerkingen [21, 22], terwijl het direct intra-articulair injecteren van deze medicijnen leidt tot een snelle klaring van het medicijn uit het gewricht (door de hoge turnover van synoviaal vloeistof), waardoor er maar een zeer beperkt effect verwacht kan worden [320]. Herhaaldelijk injecteren is echter geen optie, gezien de verhoogde risico's op infectie. Daarnaast is het aanprikken van het gewricht niet prettig voor de patiënt, wat nog een reden is om de prikfrequentie naar een minimum te reduceren. Een manier om deze problemen te omzeilen, is via het gebruik van injecteerbare drug delivery systems (DDSs) welke na het injecteren in een gewricht zorgen voor een langdurige lokale afgifte van het gewenste medicijn [26, 28, 68, 72, 183]. Voor dit proefschrift hebben we 2 verschillende DDSs voor intra-articulair gebruik onderzocht: monospheres en thermoreversibele hydrogels.

In **Hoofdstuk 2** beschrijven we de *in vitro* en *in vivo* eigenschappen van op acetyl-capped PCLA-PEG-PCLA polymeren gebaseerde hydrogels. We laten hier zien dat deze gels een goede intra-articulaire biocompatibiliteit hebben, aangezien de intra-articulaire toediening van deze gels op termijn niet leidde tot veranderingen in kraakbeen kwaliteit en/of kwantiteit. Om de *in vivo* degradatiesnelheid van de gel te kunnen onderzoeken, werd een mengsel van polymeren, met als endcap acetyl of 2-(2',3',5',-triiodobenzoyl; TIB), zowel subcutaan als intra-articulair geïnjecteerd in ratten. TIB is radio-opaak en kan daardoor afgebeeld worden met het gebruik van µCT, wat longitudinale kwantificatie van de geldegradatie mogelijk maakt. De gel bleek na subcutane injectie over een periode van ~12 weken af te breken. Na intra-articulaire injectie daarentegen, was de gel na 4 weken niet meer detecteerbaar. Deze versnelde degradatie na intra-articulaire

injectie in vergelijking met de subcutane situatie wordt waarschijnlijk veroorzaakt door een combinatie van de volgende factoren: dispersie van de gel in de synoviale vloeistof, snelle synoviale turnover, mechanische stress op de gel tijdens gewrichtsbelasting en een grotere oppervlakte/volume ratio.
Na deze veelbelovend resultaten ten aanzien van het intra-articulaire gebruik van op acetyl-capped PCLA-PEG-PCLA polymeren gebaseerde hydrogels, hebben we deze gels geladen met celecoxib, een bekende NSAID (non-steroid anti-inflammatory drug). Deze celecoxib geladen hydrogel werd vervolgens weer zowel *in vitro* als *in vivo* getest. In **Hoofdstuk 3** beschrijven we de afgifte kinetiek van celecoxib alsook de biocompatibiliteit van deze geladen gel. De *in vitro* celecoxib afgifte werd geleid door de ontbinding van de polymeren en duurde in totaal 90 dagen, met een "lag phase" van ~10 dagen. *In vivo* vond de afgifte plaats zonder "lag phase" en vond er een afgifte van ~ 30% van de geladen celecoxib plaats tijdens de eerste 3 dagen. Hierna volgde een continu gereguleerde afgifte voor 4-8 weken. Het verschil tussen de *in vitro* en *in vivo* afgifte wordt waarschijnlijk veroorzaakt door de verhoogde oplosbaarheid van celecoxib in biologische vloeistoffen, de turnover van de synoviale vloeistof en de degradatie van gel door macrofagen. Met μCT en histologie werd, net als de ongeladen gel die beschreven werd in **Hoofdstuk 2**, een goede intra-articulaire biocompatibiliteit van de celecoxib geladen gels aangetoond.
Na het aantonen dat de celecoxib geladen hydrogels veilig zijn voor *in vivo* gebruik en dat ze leiden tot een continu gereguleerde medicijn afgifte over een periode van enkele weken, waren we geïnteresseerd in het verkrijgen van meer inzicht in de farmacokinetiek van deze celecoxib geladen gels en tevens in de relatie tussen de hydrogel compositie en deze farmacokinetiek. In **Hoofdstuk 4** rapporteren we de afgifte kinetiek van 5 verschillende subcutaan geïnjecteerde celecoxib geladen gels. Deze gels verschilden van elkaar op het gebied van 'end-capping', geïnjecteerde volume, celecoxib loading en polymeer concentratie. De *in vivo* celecoxib afgifte periode kon worden verlengd door het geïnjecteerde volume van 100 naar 500 μL te verhogen, de end-capping van acetyl naar propyl te veranderen en ook door de celecoxib lading te verhogen van 10 naar 50 mg/mL. Niet alleen de totale periode van afgifte, maar ook de celecoxib-serum concentraties per tijdspunt kon worden beïnvloed door het veranderen van de gel specificaties. Het feit dat we op een relatief simpele manier de periode van afgifte en kinetiek kunnen beïnvloeden door het aanpassen van de gel, voegt een grote waarde toe aan dit drug delivery systeem, omdat we op deze manier de afgifte van medicijnen kunnen aanpassen aan de verschillende behoeften per ziektebeeld of zelfs per individuele patiënt.
In **Hoofdstuk 5** beschrijven we de therapeutische effectiviteit van de celecoxib geladen gels in ratten, waarbij we arthrose geïnduceerd hebben. Hoewel er geen chondroprotectief effect gevonden werd voor celecoxib (zowel de suspensie als afgegeven vanuit de gel), bleek de toediening van de celecoxib in gelvorm te beschermen tegen het milde kraakbeenverlies dat we vaststelden na injectie van de celecoxib suspensie. De knieën geïnjecteerd met de celecoxib geladen gels lieten een verhoogde macrofaag activatie zien.

Deze macrofaag activatie was, gebaseerd op de huidige beschikbare literatuur, meest waarschijnlijk van het anti-inflammatoire subtype. Klinisch lieten de ratten die de celecoxib gel hadden ontvangen geen tekenen van inflammatie of pijn zien. De keuze voor een mild arthrose model heeft er mogelijk toe geleid dat we geen positieve effecten van de celecoxib geladen gels hebben kunnen aantonen op kraakbeenniveau of in de vorm van pijnverlichting. In de toekomst zouden we graag dit experiment herhalen in een ernstiger model, gecombineerd met hogere doses van het medicijn.

**Hoofdstuk 6** beschrijft de ontwikkeling en de *in vitro* en *in vivo* prestaties van monopsheres opgebouwd uit biodegradeerbare poly(DL-lactide)-PEG-poly(DL-lactide)-b-poly(L-lactide) multiblock copolymeren. Na intra-articulaire injectie bleven deze monospheres detecteerbaar in het gewricht voor een periode van 3 maanden. Dit leidde tot een milde inflammatoire reactie, maar er werden geen negatieve effecten op kraakbeen niveau gedetecteerd.

In **Hoofdstuk 7** beschrijven we de nano-mechanische kenmerken van de monospheres. Hier tonen we aan dat de gezwollen monospheres (hun staat in biologische vloeistoffen) mechanische eigenschappen hebben die in dezelfde range liggen als kraakbeen. De kans op schade aan het kraakbeen door indentatie wordt hierdoor minder waarschijnlijk, wat inderdaad in lijn is met de bevindingen van **Hoofdstuk 6**.

In **Hoofdstuk 8** hebben we dezelfde monospheres geladen met tacrolimus (FK506). Tacrolimus is een calcineurine inhibitor en wordt gebruikt als immunosuppressief medicijn om afstoting van transplantatie-organen tegen te gaan [44, 45]. In een paardenmodel toonden we aan dat injectie van de tacrolimus-geladen monospheres leidde tot een gereguleerde lokale afgifte van het medicijn in het gewricht voor de volledige follow-up van vier weken, terwijl deze afgifte niet leidde tot meetbare systemische concentraties. De inflammatoire reactie die gezien werd na het injecteren van de ongeladen monospheres werd significant verlaagd door de lokale afgifte van tacrolimus, wat een lokale anti-inflammatoire werking van het afgegeven medicijn laat zien.

Concluderend hebben we twee drug delivery systemen ontwikkeld welke beide over een excellente intra-articulaire biocompatibiliteit beschikken en tevens een zeer gunstige *in vivo* afgiftepatroon vertonen. De tacrolimus geladen monospheres lieten een anti-inflammatoire werking zien, en de celecoxib geladen hydrogels bleken superieur ten opzichte van intra-articulaire injectie met een celecoxib suspensie. Hoewel beide systemen beschikken over goede potentie voor intra-articulair gebruik, is verder onderzoek geïndiceerd. Aangezien we geen negatieve effecten van de medicijn-geladen systemen hebben aangetoond, maar ook geen therapeutisch effect op de progressie van arthrose, is het uitvoeren van een zogeheten “dose-finding” studie aangewezen. Als wordt aangetoond dat celecoxib en tacrolimus beide geen ziektemodificerende werking blijken te hebben, zal er een selectie van alternatieve middelen om deze DDS mee te laden, moeten plaatsvinden.

# References

[1] RIVM, https://www.volksgezondheidenzorg.info/onderwerp/artrose. 2015).
[2] Y. Zhang, J.M. Jordan, Epidemiology of osteoarthritis, Clin Geriatr Med 26(3) (2010) 355-69.
[3] F.C. Breedveld, Osteoarthritis--the impact of a serious disease, Rheumatology (Oxford) 43 Suppl 1 (2004) i4-8.
[4] J.P. Pelletier, J. Martel-Pelletier, S.B. Abramson, Osteoarthritis, an inflammatory disease: potential implication for the selection of new therapeutic targets, Arthritis Rheum 44(6) (2001) 1237-47.
[5] M.B. Goldring, F. Berenbaum, The regulation of chondrocyte function by proinflammatory mediators: prostaglandins and nitric oxide, Clin Orthop Relat Res (427 Suppl) (2004) S37-46.
[6] H. Muir, The chondrocyte, architect of cartilage. Biomechanics, structure, function and molecular biology of cartilage matrix macromolecules, Bioessays 17(12) (1995) 1039-48.
[7] F. Kubaski, H. Osago, R.W. Mason, S. Yamaguchi, H. Kobayashi, M. Tsuchiya, T. Orii, S. Tomatsu, Glycosaminoglycans detection methods: Applications of mass spectrometry, Mol Genet Metab 120(1-2) (2017) 67-77.
[8] S. Castaneda, J.A. Roman-Blas, R. Largo, G. Herrero-Beaumont, Subchondral bone as a key target for osteoarthritis treatment, Biochem Pharmacol 83(3) (2012) 315-23.
[9] M.B. Goldring, S.R. Goldring, Articular cartilage and subchondral bone in the pathogenesis of osteoarthritis, Ann N Y Acad Sci 1192 (2010) 230-7.
[10] P.M. van der Kraan, W.B. van den Berg, Osteophytes: relevance and biology, Osteoarthritis Cartilage 15(3) (2007) 237-44.
[11] P.L. van Lent, A.B. Blom, P. van der Kraan, A.E. Holthuysen, E. Vitters, N. van Rooijen, R.L. Smeets, K.C. Nabbe, W.B. van den Berg, Crucial role of synovial lining macrophages in the promotion of transforming growth factor beta-mediated osteophyte formation, Arthritis Rheum 50(1) (2004) 103-11.
[12] H.M. de Visser, S.C. Mastbergen, A.E. Kozijn, K. Coeleveld, B. Pouran, M.H. van Rijen, F. Lafeber, H. Weinans, Metabolic dysregulation accelerates injury-induced joint degeneration, driven by local inflammation; an in vivo rat study, J Orthop Res 36(3) (2018) 881-890.

[13] A. Lahm, M. Uhl, M. Edlich, C. Erggelet, J. Haberstroh, P.C. Kreuz, An experimental canine model for subchondral lesions of the knee joint, Knee 12(1) (2005) 51-5.
[14] M. Mahjoub, F. Berenbaum, X. Houard, Why subchondral bone in osteoarthritis? The importance of the cartilage bone interface in osteoarthritis, Osteoporos Int 23 Suppl 8 (2012) S841-6.
[15] D.L. Goldenberg, M.S. Egan, A.S. Cohen, Inflammatory synovitis in degenerative joint disease, J Rheumatol 9(2) (1982) 204-9.
[16] A.D. Pearle, C.R. Scanzello, S. George, L.A. Mandl, E.F. DiCarlo, M. Peterson, T.P. Sculco, M.K. Crow, Elevated high-sensitivity C-reactive protein levels are associated with local inflammatory findings in patients with osteoarthritis, Osteoarthritis Cartilage 15(5) (2007) 516-23.
[17] G.A. Homandberg, F. Hui, Association of proteoglycan degradation with catabolic cytokine and stromelysin release from cartilage cultured with fibronectin fragments, Arch Biochem Biophys 334(2) (1996) 325-31.
[18] G.A. Homandberg, R. Meyers, J.M. Williams, Intraarticular injection of fibronectin fragments causes severe depletion of cartilage proteoglycans in vivo, J Rheumatol 20(8) (1993) 1378-82.
[19] C.R. Scanzello, S.R. Goldring, The role of synovitis in osteoarthritis pathogenesis, Bone 51(2) (2012) 249-57.
[20] G. Peat, E. Thomas, R. Duncan, L. Wood, E. Hay, P. Croft, Clinical classification criteria for knee osteoarthritis: performance in the general population and primary care, Ann Rheum Dis 65(10) (2006) 1363-7.
[21] T.E. McAlindon, R.R. Bannuru, M.C. Sullivan, N.K. Arden, F. Berenbaum, S.M. Bierma-Zeinstra, G.A. Hawker, Y. Henrotin, D.J. Hunter, H. Kawaguchi, K. Kwoh, S. Lohmander, F. Rannou, E.M. Roos, M. Underwood, OARSI guidelines for the non-surgical management of knee osteoarthritis, Osteoarthritis Cartilage 22(3) (2014) 363-88.
[22] S. Harirforoosh, W. Asghar, F. Jamali, Adverse effects of nonsteroidal antiinflammatory drugs: an update of gastrointestinal, cardiovascular and renal complications, J Pharm Pharm Sci 16(5) (2013) 821-47.
[23] N. Bellamy, J. Campbell, V. Robinson, T. Gee, R. Bourne, G. Wells, Intraarticular corticosteroid for treatment of osteoarthritis of the knee, Cochrane Db Syst Rev (2) (2005).
[24] C.H. Evans, V.B. Kraus, L.A. Setton, Progress in intra-articular therapy, Nat Rev Rheumatol 10(1) (2014) 11-22.
[25] J.H. Ratcliffe, I.M. Hunneyball, C.G. Wilson, A. Smith, S.S. Davis, Albumin microspheres for intra-articular drug delivery: investigation of their retention in normal and arthritic knee joints of rabbits, J Pharm Pharmacol 39(4) (1987) 290-5.

[26] M. Janssen, G. Mihov, T.J. Welting, J. Thies, P.J. Emans, Drugs and Polymers for Delivery Systems in OA Joints: Clinical Needs and Opportunities Polymers 6(3) (2014) 799-819.
[27] T.M. Allen, P.R. Cullis, Liposomal drug delivery systems: from concept to clinical applications, Adv Drug Deliv Rev 65(1) (2013) 36-48.
[28] C. Larsen, J. Ostergaard, S.W. Larsen, H. Jensen, S. Jacobsen, C. Lindegaard, P.H. Andersen, Intra-articular depot formulation principles: role in the management of postoperative pain and arthritic disorders, J Pharm Sci 97(11) (2008) 4622-54.
[29] S.A. Johnstone, D. Masin, L. Mayer, M.B. Bally, Surface-associated serum proteins inhibit the uptake of phosphatidylserine and poly(ethylene glycol) liposomes by mouse macrophages, Biochim Biophys Acta 1513(1) (2001) 25-37.
[30] J. Dong, D. Jiang, Z. Wang, G. Wu, L. Miao, L. Huang, Intra-articular delivery of liposomal celecoxib-hyaluronate combination for the treatment of osteoarthritis in rabbit model, Int J Pharm 441(1-2) (2013) 285-90.
[31] I. Elron-Gross, Y. Glucksam, I.E. Biton, R. Margalit, A novel Diclofenac-carrier for local treatment of osteoarthritis applying live-animal MRI, J Control Release 135(1) (2009) 65-70.
[32] Y. Barenholz, Doxil(R)--the first FDA-approved nano-drug: lessons learned, J Control Release 160(2) (2012) 117-34.
[33] T.E. Kavanaugh, T.A. Werfel, H. Cho, K.A. Hasty, C.L. Duvall, Particle-based technologies for osteoarthritis detection and therapy, Drug Deliv Transl Res 6(2) (2016) 132-47.
[34] A. Spitz, J.M. Young, L. Larsen, C. Mattia-Goldberg, J. Donnelly, K. Chwalisz, Efficacy and safety of leuprolide acetate 6-month depot for suppression of testosterone in patients with prostate cancer, Prostate Cancer Prostatic Dis 15(1) (2012) 93-9.
[35] J. Kopecek, Hydrogel biomaterials: a smart future?, Biomaterials 28(34) (2007) 5185-92.
[36] S.R. Van Tomme, G. Storm, W.E. Hennink, In situ gelling hydrogels for pharmaceutical and biomedical applications, Int J Pharm 355(1-2) (2008) 1-18.
[37] T. Vermonden, R. Censi, W.E. Hennink, Hydrogels for protein delivery, Chem Rev 112(5) (2012) 2853-88.
[38] L. Yu, J. Ding, Injectable hydrogels as unique biomedical materials, Chem Soc Rev 37(8) (2008) 1473-81.
[39] V.T. Tran, J.P. Benoit, M.C. Venier-Julienne, Why and how to prepare biodegradable, monodispersed, polymeric microparticles in the field of pharmacy?, Int J Pharm 407(1-2) (2011) 1-11.
[40] T. Saxne, D. Heinegard, F.A. Wollheim, Therapeutic effects on cartilage metabolism in arthritis as measured by release of proteoglycan structures into the synovial fluid, Ann Rheum Dis 45(6) (1986) 491-7.

[41] M.C. Zweers, T.N. de Boer, J. van Roon, J.W. Bijlsma, F.P. Lafeber, S.C. Mastbergen, Celecoxib: considerations regarding its potential disease-modifying properties in osteoarthritis, Arthritis Res Ther 13(5) (2011) 239.
[42] M. Janssen, U.T. Timur, N. Woike, T.J. Welting, G. Draaisma, M. Gijbels, L.W. van Rhijn, G. Mihov, J. Thies, P.J. Emans, Celecoxib-loaded PEA microspheres as an auto regulatory drug-delivery system after intra-articular injection, J Control Release 244(Pt A) (2016) 30-40.
[43] T. Kino, H. Hatanaka, S. Miyata, N. Inamura, M. Nishiyama, T. Yajima, T. Goto, M. Okuhara, M. Kohsaka, H. Aoki, et al., FK-506, a novel immunosuppressant isolated from a Streptomyces. II. Immunosuppressive effect of FK-506 in vitro, J Antibiot (Tokyo) 40(9) (1987) 1256-65.
[44] M.A. Hooks, Tacrolimus, a new immunosuppressant--a review of the literature, Ann Pharmacother 28(4) (1994) 501-11.
[45] P.A. Kelly, G.J. Burckart, R. Venkataramanan, Tacrolimus: a new immunosuppressive agent, Am J Health Syst Pharm 52(14) (1995) 1521-35.
[46] S. Sakuma, Y. Kato, F. Nishigaki, T. Sasakawa, K. Magari, S. Miyata, Y. Ohkubo, T. Goto, FK506 potently inhibits T cell activation induced TNF-alpha and IL-1beta production in vitro by human peripheral blood mononuclear cells, Br J Pharmacol 130(7) (2000) 1655-63.
[47] Y.H. Lee, J.H. Woo, S.J. Choi, J.D. Ji, S.C. Bae, G.G. Song, Tacrolimus for the treatment of active rheumatoid arthritis: a systematic review and meta-analysis of randomized controlled trials, Scand J Rheumatol 39(4) (2010) 271-8.
[48] M.A. van Leeuwen, J. Westra, P.C. Limburg, P.L. van Riel, M.H. van Rijswijk, Interleukin-6 in relation to other proinflammatory cytokines, chemotactic activity and neutrophil activation in rheumatoid synovial fluid, Ann Rheum Dis 54(1) (1995) 33-8.
[49] J.M. Dayer, D. Burger, Interleukin-1, tumor necrosis factor and their specific inhibitors, Eur Cytokine Netw 5(6) (1994) 563-71.
[50] J. Martel-Pelletier, N. Alaaeddine, J.P. Pelletier, Cytokines and their role in the pathophysiology of osteoarthritis, Front Biosci 4 (1999) D694-703.
[51] J. Sellam, F. Berenbaum, The role of synovitis in pathophysiology and clinical symptoms of osteoarthritis, Nat Rev Rheumatol 6(11) (2010) 625-35.
[52] S.A. Yoo, B.H. Park, H.J. Yoon, J.Y. Lee, J.H. Song, H.A. Kim, C.S. Cho, W.U. Kim, Calcineurin modulates the catabolic and anabolic activity of chondrocytes and participates in the progression of experimental osteoarthritis, Arthritis Rheum 56(7) (2007) 2299-311.
[53] J.W. Fuseler, M. Hearth-Holmes, M.B. Grisham, D. Kang, F.S. Laroux, R.E. Wolf, FK506 attenuates developing and established joint inflammation and suppresses interleukin 6 and nitric oxide expression in bacterial cell wall induced polyarthritis, J Rheumatol 27(1) (2000) 190-9.

[54] T. Sasakawa, Y. Sasakawa, Y. Ohkubo, S. Mutoh, FK506 ameliorates spontaneous locomotor activity in collagen-induced arthritis: implication of distinct effect from suppression of inflammation, Int Immunopharmacol 5(3) (2005) 503-10.
[55] F. Nishigaki, S. Sakuma, T. Ogawa, S. Miyata, T. Ohkubo, T. Goto, FK506 induces chondrogenic differentiation of clonal mouse embryonic carcinoma cells, ATDC5, Eur J Pharmacol 437(3) (2002) 123-8.
[56] A.E. van der Windt, H. Jahr, E. Farrell, J.A. Verhaar, H. Weinans, G.J. van Osch, Calcineurin inhibitors promote chondrogenic marker expression of dedifferentiated human adult chondrocytes via stimulation of endogenous TGFbeta1 production, Tissue Eng Part A 16(1) (2010) 1-10.
[57] G.J. van Osch, S.W. van der Veen, H.L. Verwoerd-Verhoef, In vitro redifferentiation of culture-expanded rabbit and human auricular chondrocytes for cartilage reconstruction, Plast Reconstr Surg 107(2) (2001) 433-40.
[58] A. Petit, B. Muller, R. Meijboom, P. Bruin, F. van de Manakker, M. Versluijs-Helder, L.G. de Leede, A. Doornbos, M. Landin, W.E. Hennink, T. Vermonden, Effect of polymer composition on rheological and degradation properties of temperature-responsive gelling systems composed of acyl-capped PCLA-PEG-PCLA, Biomacromolecules 14(9) (2013) 3172-82.
[59] E. Odding, H.A. Valkenburg, H.J. Stam, A. Hofman, Determinants of locomotor disability in people aged 55 years and over: the Rotterdam Study, Eur J Epidemiol 17(11) (2001) 1033-41.
[60] Recommendations for the medical management of osteoarthritis of the hip and knee: 2000 update. American College of Rheumatology Subcommittee on Osteoarthritis Guidelines, Arthritis Rheum 43(9) (2000) 1905-15.
[61] S.H. Roth, S. Anderson, The NSAID dilemma: managing osteoarthritis in high-risk patients, Phys Sportsmed 39(3) (2011) 62-74.
[62] C. Bahadir, B. Onal, V.Y. Dayan, N. Gurer, Comparison of therapeutic effects of sodium hyaluronate and corticosteroid injections on trapeziometacarpal joint osteoarthritis, Clin Rheumatol 28(5) (2009) 529-33.
[63] D.J. Hunter, In the clinic. Osteoarthritis, Ann Intern Med 147(3) (2007) ITC8-1-ITC8-16.
[64] X. Ayral, Injections in the treatment of osteoarthritis, Best Pract Res Clin Rheumatol 15(4) (2001) 609-26.
[65] N. Bellamy, J. Campbell, V. Robinson, T. Gee, R. Bourne, G. Wells, Intraarticular corticosteroid for treatment of osteoarthritis of the knee, Cochrane Database Syst Rev (2) (2006) CD005328.
[66] C.P. Charalambous, M. Tryfonidis, S. Sadiq, P. Hirst, A. Paul, Septic arthritis following intra-articular steroid injection of the knee--a survey of current practice regarding antiseptic technique used during intra-articular steroid injection of the knee, Clin Rheumatol 22(6) (2003) 386-90.

[67] N. Gerwin, C. Hops, A. Lucke, Intraarticular drug delivery in osteoarthritis, Adv Drug Deliv Rev 58(2) (2006) 226-42.
[68] S.H. Edwards, Intra-articular drug delivery: the challenge to extend drug residence time within the joint, Vet J 190(1) (2011) 15-21.
[69] M.C. Woodle, Surface-modified liposomes: assessment and characterization for increased stability and prolonged blood circulation, Chem Phys Lipids 64(1-3) (1993) 249-62.
[70] M.L. Immordino, P. Brusa, S. Arpicco, B. Stella, F. Dosio, L. Cattel, Preparation, characterization, cytotoxicity and pharmacokinetics of liposomes containing docetaxel, J Control Release 91(3) (2003) 417-29.
[71] H. Thakkar, R.K. Sharma, A.K. Mishra, K. Chuttani, R.S. Murthy, Celecoxib incorporated chitosan microspheres: in vitro and in vivo evaluation, J Drug Target 12(9-10) (2004) 549-57.
[72] Y. Shi, L.C. Li, Current advances in sustained-release systems for parenteral drug delivery, Expert Opin Drug Deliv 2(6) (2005) 1039-58.
[73] A. Sharma, U.S. Sharma, Liposomes in drug delivery: progress and limitations, Int J Pharm 154(2) (1997) 123-140.
[74] S.W. Larsen, A.B. Frost, J. Ostergaard, M.H. Thomsen, S. Jacobsen, C. Skonberg, S.H. Hansen, H.E. Jensen, C. Larsen, In vitro and in vivo characteristics of celecoxib in situ formed suspensions for intra-articular administration, J Pharm Sci 100(10) (2011) 4330-7.
[75] Z.P. Chen, W. Liu, D. Liu, Y.Y. Xiao, H.X. Chen, J. Chen, W. Li, H. Cai, W. Li, B.C. Cai, J. Pan, Development of brucine-loaded microsphere/thermally responsive hydrogel combination system for intra-articular administration, J Control Release 162(3) (2012) 628-35.
[76] B. Jeong, M.R. Kibbey, J.C. Birnbaum, Y.Y. Won, A. Gutowska, Thermogelling biodegradable polymers with hydrophilic backbones: PEG-g-PLGA, macromolecules 33 (2000) 8317-22.
[77] D.Y. Ko, U.P. Shinde, B. Yeon, B. Jeong, Recent progress of in situ formed gels for biomedical applications., Prog Polym Sci 38 (2013) 672-701.
[78] S. Jo, J. Kim, S.W. Kim, Reverse thermal gelation of aliphatically modified biodegradable triblock copolymers, Macromol Biosci 6(11) (2006) 923-8.
[79] L. Yu, G. Chang, H. Zhang, J. Ding, Temperature-induced spontaneous solegel transitions of poly(D, L-lactic acid-co-glycolic acid)-b-poly(ethylene glycol)-b- poly(D, L-lactic acid-co-glycolic acid) triblock copolymers and their end- capped derivatives in water. , J Polym Sci A Polym Chem 45 (2007) 1122-33.
[80] A. Petit, B. Muller, P. Bruin, R. Meyboom, M. Piest, L.M. Kroon-Batenburg, L.G. de Leede, W.E. Hennink, T. Vermonden, Modulating rheological and degradation properties of temperature-responsive gelling systems composed of blends of PCLA-

PEG-PCLA triblock copolymers and their fully hexanoyl-capped derivatives, Acta Biomater 8(12) (2012) 4260-7.
[81] N. Butoescu, C.A. Seemayer, G. Palmer, P.A. Guerne, C. Gabay, E. Doelker, O. Jordan, Magnetically retainable microparticles for drug delivery to the joint: efficacy studies in an antigen-induced arthritis model in mice, Arthritis Res Ther 11(3) (2009) R72.
[82] P.M. Mountziaris, D.C. Sing, A.G. Mikos, P.R. Kramer, Intra-articular microparticles for drug delivery to the TMJ, J Dent Res 89(10) (2010) 1039-44.
[83] E. Horisawa, K. Kubota, I. Tuboi, K. Sato, H. Yamamoto, H. Takeuchi, Y. Kawashima, Size-dependency of DL-lactide/glycolide copolymer particulates for intra-articular delivery system on phagocytosis in rat synovium, Pharm Res 19(2) (2002) 132-9.
[84] F. Mottu, D.A. Rufenacht, E. Doelker, Radiopaque polymeric materials for medical applications. Current aspects of biomaterial research, Invest Radiol 34(5) (1999) 323-35.
[85] C. Zaharia, T. Zecheru, M.F. Moreau, F. Pascaretti-Grizon, G. Mabilleau, B. Marculescu, R. Filmon, C. Cincu, G. Staikos, D. Chappard, Chemical structure of methylmethacrylate-2-[2',3',5'-triiodobenzoyl]oxoethyl methacrylate copolymer, radio-opacity, in vitro and in vivo biocompatibility, Acta Biomater 4(6) (2008) 1762-9.
[86] P.J. Emans, K. Saralidze, M.L. Knetsch, M.J. Gijbels, R. Kuijer, L.H. Koole, Development of new injectable bulking agents: biocompatibility of radiopaque polymeric microspheres studied in a mouse model, J Biomed Mater Res A 73(4) (2005) 430-6.
[87] M. Okamura, H. Uehara, T. Yamanobe, T. Komoto, S. Hosoi, T. Kumazaki, Synthesis and properties of radiopaque polymer hydrogels: polyion complexes of co-polymers of acrylamide derivatives having triiodophenyl and carboxyl groups and p-styrene sulfonate and polyallylamine, J Mol Struct 554(1) (2000) 35-45.
[88] L.L. Li, Name reactions: a collection of detailed reaction mechanisms, Mairdumont Gmbh & Co. Kg, new york, 2006.
[89] A. Benzina, M.A. Kruft, F.H. van der Veen, F.H. Bar, R. Blezer, T. Lindhout, L.H. Koole, A versatile three-iodine molecular building block leading to new radiopaque polymeric biomaterials, J Biomed Mater Res 32(3) (1996) 459-66.
[90] F. Mottu, D.A. Rufenacht, A. Laurent, E. Doelker, Iodine-containing cellulose mixed esters as radiopaque polymers for direct embolization of cerebral aneurysms and arteriovenous malformations, Biomaterials 23(1) (2002) 121-31.
[91] K. Saralidze, Y.B. Aldenhoff, M.L. Knetsch, L.H. Koole, Injectable polymeric microspheres with X-ray visibility. Preparation, properties, and potential utility as new traceable bulking agents, Biomacromolecules 4(3) (2003) 793-8.

[92] L. Yu, H. Zhang, J. Ding, A subtle end-group effect on macroscopic physical gelation of triblock copolymer aqueous solutions, Angew Chem Int Ed Engl 45(14) (2006) 2232-5.
[93] H. Abe, N. Takahashi, K.J. Kim, M. Mochizuki, Y. Doi, Effects of residual zinc compounds and chain-end structure on thermal degradation of poly(epsilon-caprolactone), Biomacromolecules 5(4) (2004) 1480-8.
[94] Y. Fan, H. Nishida, Y. Shirai, T. Endo, Thermal stability of poly (L-lactide); influence of end protection by acetyl group. , Polym Degrad Stab 84 (1) (2004) 143-9.
[95] I.C. Mcneill, H.A. Leiper, . Degradation studies of some polyesters and polycarbonates. 1. Polylactide e general features of the degradation under programmed heating conditions, Polymer Degradation and Stability 11(3) (1985) 267-285.
[96] M. Siebelt, J.H. Waarsing, N. Kops, T.M. Piscaer, J.A. Verhaar, E.H. Oei, H. Weinans, Quantifying osteoarthritic cartilage changes accurately using in vivo microCT arthrography in three etiologically distinct rat models, J Orthop Res 29(11) (2011) 1788-94.
[97] T.M. Piscaer, J.H. Waarsing, N. Kops, P. Pavljasevic, J.A. Verhaar, G.J. van Osch, H. Weinans, In vivo imaging of cartilage degeneration using microCT-arthrography, Osteoarthritis Cartilage 16(9) (2008) 1011-7.
[98] T.S. Silvast, J.S. Jurvelin, A.S. Aula, M.J. Lammi, J. Toyras, Contrast agent-enhanced computed tomography of articular cartilage: association with tissue composition and properties, Acta Radiol 50(1) (2009) 78-85.
[99] T.S. Silvast, J.S. Jurvelin, M.J. Lammi, J. Toyras, pQCT study on diffusion and equilibrium distribution of iodinated anionic contrast agent in human articular cartilage--associations to matrix composition and integrity, Osteoarthritis Cartilage 17(1) (2009) 26-32.
[100] J.H. Waarsing, J.S. Day, H. Weinans, An improved segmentation method for in vivo microCT imaging, J Bone Miner Res 19(10) (2004) 1640-50.
[101] H.J. Mankin, H. Dorfman, L. Lippiello, A. Zarins, Biochemical and metabolic abnormalities in articular cartilage from osteo-arthritic human hips. II. Correlation of morphology with biochemical and metabolic data, J Bone Joint Surg Am 53(3) (1971) 523-37.
[102] K.P. Pritzker, S. Gay, S.A. Jimenez, K. Ostergaard, J.P. Pelletier, P.A. Revell, D. Salter, W.B. van den Berg, Osteoarthritis cartilage histopathology: grading and staging, Osteoarthritis Cartilage 14(1) (2006) 13-29.
[103] S.R. Van Tomme, C.F. van Nostrum, M. Dijkstra, S.C. De Smedt, W.E. Hennink, Effect of particle size and charge on the network properties of microsphere-based hydrogels, Eur J Pharm Biopharm 70(2) (2008) 522-30.
[104] H. Seyednejad, D. Gawlitta, R.V. Kuiper, A. de Bruin, C.F. van Nostrum, T. Vermonden, W.J. Dhert, W.E. Hennink, In vivo biocompatibility and biodegradation

of 3D-printed porous scaffolds based on a hydroxyl-functionalized poly(epsilon-caprolactone), Biomaterials 33(17) (2012) 4309-18.
[105] J. Zeng, X. Chen, Q. Liang, X. Xu, X. Jing, Enzymatic degradation of poly(L-lactide) and poly(epsilon-caprolactone) electrospun fibers, Macromol Biosci 4(12) (2004) 1118-25.
[106] Z. Gan, D. Yu, Z. Zhong, Q. Liang, X. Jing, Enzymatic degradation of poly(e-caprolactone)/poly(DL-lactide) blends in phosphate buffer solution., polymer 40(10) (1999) 2859-62.
[107] S.J. Buwalda, P.J. Dijkstra, L. Calucci, C. Forte, J. Feijen, Influence of amide versus ester linkages on the properties of eight-armed PEG-PLA star block copolymer hydrogels, Biomacromolecules 11(1) (2010) 224-32.
[108] L. Yu, Z. Zhang, H. Zhang, J. Ding, Biodegradability and biocompatibility of thermoreversible hydrogels formed from mixing a sol and a precipitate of block copolymers in water, Biomacromolecules 11(8) (2010) 2169-78.
[109] A.D. Knight, J.R. Levick, The influence of blood pressure on trans-synovial flow in the rabbit, J Physiol 349 (1984) 27-42.
[110] Z. Zhang, J. Ni, L. Chen, L. Yu, J. Xu, J. Ding, Biodegradable and thermoreversible PCLA-PEG-PCLA hydrogel as a barrier for prevention of post-operative adhesion, Biomaterials 32(21) (2011) 4725-36.
[111] N.M. Davies, A.J. McLachlan, R.O. Day, K.M. Williams, Clinical pharmacokinetics and pharmacodynamics of celecoxib: a selective cyclo-oxygenase-2 inhibitor, Clin Pharmacokinet 38(3) (2000) 225-42.
[112] R. Tsutsumi, H. Ito, T. Hiramitsu, K. Nishitani, M. Akiyoshi, T. Kitaori, T. Yasuda, T. Nakamura, Celecoxib inhibits production of MMP and NO via down-regulation of NF-kappaB and JNK in a PGE2 independent manner in human articular chondrocytes, Rheumatol Int 28(8) (2008) 727-36.
[113] S.C. Mastbergen, J.W. Bijlsma, F.P. Lafeber, Selective COX-2 inhibition is favorable to human early and late-stage osteoarthritic cartilage: a human in vitro study, Osteoarthritis Cartilage 13(6) (2005) 519-26.
[114] S.K. Paulson, T.A. Kaprak, C.J. Gresk, D.M. Fast, M.T. Baratta, E.G. Burton, A.P. Breau, A. Karim, Plasma protein binding of celecoxib in mice, rat, rabbit, dog and human, Biopharm Drug Dispos 20(6) (1999) 293-9.
[115] L. Gong, C.F. Thorn, M.M. Bertagnolli, T. Grosser, R.B. Altman, T.E. Klein, Celecoxib pathways: pharmacokinetics and pharmacodynamics, Pharmacogenet Genomics 22(4) (2012) 310-8.
[116] A. Zvonar, J. Kristl, J. Kerc, P.A. Grabnar, High celecoxib-loaded nanoparticles prepared by a vibrating nozzle device, J Microencapsul 26(8) (2009) 748-59.
[117] P.A. McCarron, R.F. Donnelly, W. Marouf, Celecoxib-loaded poly(D,L-lactide-co-glycolide) nanoparticles prepared using a novel and controllable combination of

diffusion and emulsification steps as part of the salting-out procedure, J Microencapsul 23(5) (2006) 480-98.
[118] A.C. Amrite, S.P. Ayalasomayajula, N.P. Cheruvu, U.B. Kompella, Single periocular injection of celecoxib-PLGA microparticles inhibits diabetes-induced elevations in retinal PGE2, VEGF, and vascular leakage, Invest Ophthalmol Vis Sci 47(3) (2006) 1149-60.
[119] A. Bohr, J. Kristensen, E. Stride, M. Dyas, M. Edirisinghe, Preparation of microspheres containing low solubility drug compound by electrohydrodynamic spraying, Int J Pharm 412(1-2) (2011) 59-67.
[120] S.P. Ayalasomayajula, U.B. Kompella, Subconjunctivally administered celecoxib-PLGA microparticles sustain retinal drug levels and alleviate diabetes-induced oxidative stress in a rat model, Eur J Pharmacol 511(2-3) (2005) 191-8.
[121] M. Homar, N. Ubrich, F. El Ghazouani, J. Kristl, J. Kerc, P. Maincent, Influence of polymers on the bioavailability of microencapsulated celecoxib, J Microencapsul 24(7) (2007) 621-33.
[122] M.J. Sandker, A. Petit, E.M. Redout, M. Siebelt, B. Muller, P. Bruin, R. Meyboom, T. Vermonden, W.E. Hennink, H. Weinans, In situ forming acyl-capped PCLA-PEG-PCLA triblock copolymer based hydrogels, Biomaterials 34(32) (2013) 8002-11.
[123] G.M. Zentner, R. Rathi, C. Shih, J.C. McRea, M.H. Seo, H. Oh, B.G. Rhee, J. Mestecky, Z. Moldoveanu, M. Morgan, S. Weitman, Biodegradable block copolymers for delivery of proteins and water-insoluble drugs, J Control Release 72(1-3) (2001) 203-15.
[124] D.S. Lee, M.S. Shim, S.W. Kim, H. Lee, I. Park, T. Chang, Novel thermoreversible gelation of biodegradable PLGA-block-PEO-block-PLGA triblock copolymers in aqueous solution., macromol rapid commun 22(8) (2001) 587-92.
[125] G. Bonacucina, M. Cespi, G. Mencarelli, G. Giorgioni, G.F. Palmieri, Thermo-sensitive self-assembling block copolymers as drug delivery systems., polymers 3(2) (2011) 779-811.
[126] K.H. Bae, L. Wang, M. Kurisawa, Injectable biodegradable hydrogels: progress and challenges, J Mater Chem B 1(40) (2013) 5371-88.
[127] M. Qiao, D. Chen, X. Ma, Y. Liu, Injectable biodegradable temperature-responsive PLGA-PEG-PLGA copolymers: synthesis and effect of copolymer composition on the drug release from the copolymer-based hydrogels, Int J Pharm 294(1-2) (2005) 103-12.
[128] Y. Gao, F. Ren, B. Ding, N. Sun, X. Liu, X. Ding, S. Gao, A thermo-sensitive PLGA-PEG-PLGA hydrogel for sustained release of docetaxel, J Drug Target 19(7) (2011) 516-27.
[129] N.L. Elstad, K.D. Fowers, OncoGel (ReGel/paclitaxel)--clinical applications for a novel paclitaxel delivery system, Adv Drug Deliv Rev 61(10) (2009) 785-94.
[130] H. Bramfeldt, P. Sarazin, P. Vermette, Characterization, degradation, and mechanical strength of poly(D,L-lactide-co-epsilon-caprolactone)-poly(ethylene

glycol)-poly(D,L-lactide-co-epsilon-caprolactone), J Biomed Mater Res A 83(2) (2007) 503-11.
[131] A. Patist, S. Bhagwat, K. Penfield, P. Aikens, D. Shah, On the measurement of critical micelle concentrations of pure and technical-grade nonionic surfactants, J Surfactants Deterg 3(1) (2000) 53-8.
[132] S. Bozdag-Pehlivan, B. Subasi, I. Vural, N. Unlu, Y. Capan, Evaluation of drug-excipient interaction in the formulation of celecoxib tablets, Acta Pol Pharm 68(3) (2011) 423-33.
[133] H.G. Gika, A. Theodoridou, F. Michopoulos, G. Theodoridis, E. Diza, L. Settas, P. Nikolaidis, C. Smith, I.D. Wilson, Determination of two COX-2 inhibitors in serum and synovial fluid of patients with inflammatory arthritis by ultra performance liquid chromatography-inductively coupled plasma mass spectroscopy and quadrupole time-of-flight mass spectrometry, J Pharm Biomed Anal 49(3) (2009) 579-86.
[134] Y. Zhang, M. Huo, J. Zhou, S. Xie, PKSolver: An add-in program for pharmacokinetic and pharmacodynamic data analysis in Microsoft Excel, Comput Methods Programs Biomed 99(3) (2010) 306-14.
[135] A.W. Palmer, R.E. Guldberg, M.E. Levenston, Analysis of cartilage matrix fixed charge density and three-dimensional morphology via contrast-enhanced microcomputed tomography, Proc Natl Acad Sci U S A 103(51) (2006) 19255-60.
[136] M. Siebelt, H.C. Groen, S.J. Koelewijn, E. de Blois, M. Sandker, J.H. Waarsing, C. Muller, G.J. van Osch, M. de Jong, H. Weinans, Increased physical activity severely induces osteoarthritic changes in knee joints with papain induced sulfate-glycosaminoglycan depleted cartilage, Arthritis Res Ther 16(1) (2014) R32.
[137] H.A. Schneider, E.A. Di Marzio, The glass temperature of polymer blends: comparison of both the free volume and the entropy predictions with data. , polymer 33(16) (1992) 3453-61.
[138] E.A. Fouad, M. El-Badry, G.M. Mahrous, F.K. Alanazi, S.H. Neau, I.A. Alsarra, The use of spray-drying to enhance celecoxib solubility, Drug Dev Ind Pharm 37(12) (2011) 1463-72.
[139] G. Chawla, P. Gupta, R. Thilagavathi, A.K. Chakraborti, A.K. Bansal, Characterization of solid-state forms of celecoxib, Eur J Pharm Sci 20(3) (2003) 305-17.
[140] N. Seedher, S. Bhatia, Solubility enhancement of Cox-2 inhibitors using various solvent systems, AAPS PharmSciTech 4(3) (2003) E33.
[141] S.G. Vijaya Kumar, D.N. Mishra, Preparation, characterization and in vitro dissolution studies of solid dispersion of meloxicam with PEG 6000, Yakugaku Zasshi 126(8) (2006) 657-64.
[142] S. Biswal, J. Sahoo, P.N. Murthy, R.P. Giradkar, J.G. Avari, Enhancement of dissolution rate of gliclazide using solid dispersions with polyethylene glycol 6000, AAPS PharmSciTech 9(2) (2008) 563-70.

[143] C. Liu, C. Liu, K.G. Desai, Enhancement of dissolution rate of valdecoxib using solid dispersions with polyethylene glycol 4000, Drug Dev Ind Pharm 31(1) (2005) 1-10.
[144] T.G. fox, Influence of diluent and of copolymer composition on the glass temperature of a polymer system, The Bulletin of the American Physical Society 1 (1956) 123.
[145] P. Gupta, R. Thilagavathi, A.K. Chakraborti, A.K. Bansal, Role of molecular interaction in stability of celecoxib-PVP amorphous systems, Mol Pharm 2(5) (2005) 384-91.
[146] L. Yu, G.T. Chang, H. Zhang, J.D. Ding, Injectable block copolymer hydrogels for sustained release of a PEGylated drug, Int J Pharm 348(1-2) (2008) 95-106.
[147] W.S. Shim, J.H. Kim, K. Kim, Y.S. Kim, R.W. Park, I.S. Kim, I.C. Kwon, D.S. Lee, pH- and temperature-sensitive, injectable, biodegradable block copolymer hydrogels as carriers for paclitaxel, Int J Pharm 331(1) (2007) 11-8.
[148] A.J. de Graaf, S. Azevedo Prospero dos, II, E.H. Pieters, D.T. Rijkers, C.F. van Nostrum, T. Vermonden, R.J. Kok, W.E. Hennink, E. Mastrobattista, A micelle-shedding thermosensitive hydrogel as sustained release formulation, J Control Release 162(3) (2012) 582-90.
[149] W. Wang, L. Deng, S. Liu, X. Li, X. Zhao, R. Hu, J. Zhang, H. Han, A. Dong, Adjustable degradation and drug release of a thermosensitive hydrogel based on a pendant cyclic ether modified poly(epsilon-caprolactone) and poly(ethylene glycol)co-polymer, Acta Biomater 8(11) (2012) 3963-73.
[150] M. Qiao, D. Chen, T. Hao, X. Zhao, H. Hu, X. Ma, Effect of bee venom peptide-copolymer interactions on thermosensitive hydrogel delivery systems, Int J Pharm 345(1-2) (2007) 116-24.
[151] Y. Tang, J. Singh, Thermosensitive drug delivery system of salmon calcitonin: in vitro release, in vivo absorption, bioactivity and therapeutic efficacies, Pharm Res 27(2) (2010) 272-84.
[152] A. Dunne, T. O'Hara, J. Devane, Level A in vivo-in vitro correlation: nonlinear models and statistical methodology, J Pharm Sci 86(11) (1997) 1245-9.
[153] M.S. Guirguis, S. Sattari, F. Jamali, Pharmacokinetics of celecoxib in the presence and absence of interferon-induced acute inflammation in the rat: application of a novel HPLC assay, J Pharm Pharm Sci 4(1) (2001) 1-6.
[154] S.K. Paulson, M.B. Vaughn, S.M. Jessen, Y. Lawal, C.J. Gresk, B. Yan, T.J. Maziasz, C.S. Cook, A. Karim, Pharmacokinetics of celecoxib after oral administration in dogs and humans: effect of food and site of absorption, J Pharmacol Exp Ther 297(2) (2001) 638-45.
[155] M. Martinez, M. Rathbone, D. Burgess, M. Huynh, In vitro and in vivo considerations associated with parenteral sustained release products: a review based

upon information presented and points expressed at the 2007 Controlled Release Society Annual Meeting, J Control Release 129(2) (2008) 79-87.
[156] E. D'Aurizio, P. Sozio, L.S. Cerasa, M. Vacca, L. Brunetti, G. Orlando, A. Chiavaroli, R.J. Kok, W.E. Hennink, A. Di Stefano, Biodegradable microspheres loaded with an anti-Parkinson prodrug: an in vivo pharmacokinetic study, Mol Pharm 8(6) (2011) 2408-15.
[157] S.R. Smith, B.R. Deshpande, J.E. Collins, J.N. Katz, E. Losina, Comparative pain reduction of oral non-steroidal anti-inflammatory drugs and opioids for knee osteoarthritis: systematic analytic review, Osteoarthritis Cartilage 24(6) (2016) 962-72.
[158] J.N. Hoes, J.W. Jacobs, F. Buttgereit, J.W. Bijlsma, Current view of glucocorticoid co-therapy with DMARDs in rheumatoid arthritis, Nat Rev Rheumatol 6(12) (2010) 693-702.
[159] T. Thambi, Y. Li, D.S. Lee, Injectable hydrogels for sustained release of therapeutic agents, J Control Release 267 (2017) 57-66.
[160] A. Alexander, Ajazuddin, J. Khan, S. Saraf, S. Saraf, Poly(ethylene glycol)-poly(lactic-co-glycolic acid) based thermosensitive injectable hydrogels for biomedical applications, J Control Release 172(3) (2013) 715-29.
[161] K. Zhang, X. Tang, J. Zhang, W. Lu, X. Lin, Y. Zhang, B. Tian, H. Yang, H. He, PEG-PLGA copolymers: their structure and structure-influenced drug delivery applications, J Control Release 183 (2014) 77-86.
[162] B. Jeong, Y.H. Bae, D.S. Lee, S.W. Kim, Biodegradable block copolymers as injectable drug-delivery systems, Nature 388(6645) (1997) 860-2.
[163] B. Jeong, Y.H. Bae, S.W. Kim, Drug release from biodegradable injectable thermosensitive hydrogel of PEG-PLGA-PEG triblock copolymers, J Control Release 63(1-2) (2000) 155-63.
[164] S.S. Liow, A.A.X. Karim, J. Loh, Biodegradable thermogelling polymers for biomedical applications, MRS Bull 41(7) (2016) 557-566.
[165] A. Petit, M. Sandker, B. Muller, R. Meyboom, P. van Midwoud, P. Bruin, E.M. Redout, M. Versluijs-Helder, C.H. van der Lest, S.J. Buwalda, L.G. de Leede, T. Vermonden, R.J. Kok, H. Weinans, W.E. Hennink, Release behavior and intra-articular biocompatibility of celecoxib-loaded acetyl-capped PCLA-PEG-PCLA thermogels, Biomaterials 35(27) (2014) 7919-28.
[166] A. Petit, E.M. Redout, C.H. van de Lest, J.C. de Grauw, B. Muller, R. Meyboom, P. van Midwoud, T. Vermonden, W.E. Hennink, P. Rene van Weeren, Sustained intra-articular release of celecoxib from in situ forming gels made of acetyl-capped PCLA-PEG-PCLA triblock copolymers in horses, Biomaterials 53 (2015) 426-36.
[167] A.R. Tellegen, N. Willems, M. Beukers, G.C.M. Grinwis, S.G.M. Plomp, C. Bos, M. van Dijk, M. de Leeuw, L.B. Creemers, M.A. Tryfonidou, B.P. Meij, Intradiscal application of a PCLA-PEG-PCLA hydrogel loaded with celecoxib for the treatment of

back pain in canines: What's in it for humans?, J Tissue Eng Regen Med 12(3) (2018) 642-652.
[168] S.K. Paulson, J.Y. Zhang, A.P. Breau, J.D. Hribar, N.W. Liu, S.M. Jessen, Y.M. Lawal, J.N. Cogburn, C.J. Gresk, C.S. Markos, T.J. Maziasz, G.L. Schoenhard, E.G. Burton, Pharmacokinetics, tissue distribution, metabolism, and excretion of celecoxib in rats, Drug Metab Dispos 28(5) (2000) 514-21.
[169] D.N. McLennan, C.J. Porter, G.A. Edwards, M. Brumm, S.W. Martin, S.A. Charman, Pharmacokinetic model to describe the lymphatic absorption of r-metHu-leptin after subcutaneous injection to sheep, Pharm Res 20(8) (2003) 1156-62.
[170] Y. Zou, T.J. Bateman, C. Adreani, X. Shen, P.K. Cunningham, B. Wang, T. Trinh, A. Christine, X. Hong, C.N. Nunes, C.V. Johnson, A.S. Zhang, S.J. Staskiewicz, M. Braun, S. Kumar, V.B. Reddy, Lymphatic absorption, metabolism, and excretion of a therapeutic peptide in dogs and rats, Drug Metab Dispos 41(12) (2013) 2206-14.
[171] M.G. Sabbieti, A. Dubbini, F. Laus, E. Paggi, A. Marchegiani, M. Capitani, L. Marchetti, F. Dini, T. Vermonden, P. Di Martino, D. Agas, R. Censi, In vivo biocompatibility of p(HPMAm-lac)-PEG hydrogels hybridized with hyaluronan, J Tissue Eng Regen Med 11(11) (2017) 3056-3067.
[172] C.C. Lin, A.T. Metters, Hydrogels in controlled release formulations: network design and mathematical modeling, Adv Drug Deliv Rev 58(12-13) (2006) 1379-408.
[173] S.C. Sundararaj, M. Al-Sabbagh, C.L. Rabek, T.D. Dziubla, M.V. Thomas, D.A. Puleo, Comparison of sequential drug release in vitro and in vivo, J Biomed Mater Res B Appl Biomater 104(7) (2016) 1302-10.
[174] S. Wohl-Bruhn, M. Badar, A. Bertz, B. Tiersch, J. Koetz, H. Menzel, P.P. Mueller, H. Bunjes, Comparison of in vitro and in vivo protein release from hydrogel systems, J Control Release 162(1) (2012) 127-33.
[175] J.V. Andhariya, J. Shen, S. Choi, Y. Wang, Y. Zou, D.J. Burgess, Development of in vitro-in vivo correlation of parenteral naltrexone loaded polymeric microspheres, J Control Release 255 (2017) 27-35.
[176] V.R. Uppoor, Regulatory perspectives on in vitro (dissolution)/in vivo (bioavailability) correlations, J Control Release 72(1-3) (2001) 127-32.
[177] M.B. Goldring, S.R. Goldring, Osteoarthritis, J Cell Physiol 213(3) (2007) 626-34.
[178] W.L. Smith, D.L. DeWitt, R.M. Garavito, Cyclooxygenases: structural, cellular, and molecular biology, Annu Rev Biochem. 69 (2000) 145-182.
[179] S.C. Mastbergen, A.C. Marijnissen, M.E. Vianen, B. Zoer, P.M. van Roermund, J.W. Bijlsma, F.P. Lafeber, Inhibition of COX-2 by celecoxib in the canine groove model of osteoarthritis, Rheumatology (Oxford) 45(4) (2006) 405-13.
[180] D. Jiang, J. Zou, L. Huang, Q. Shi, X. Zhu, G. Wang, H. Yang, Efficacy of intra-articular injection of celecoxib in a rabbit model of osteoarthritis, Int J Mol Sci 11(10) (2010) 4106-13.

[181] P. Maudens, O. Jordan, E. Allemann, Recent advances in intra-articular drug delivery systems for osteoarthritis therapy, Drug Discov Today 23(10) (2018) 1761-1775.
[182] R.D. Signorell, P. Luciani, D. Brambilla, J.C. Leroux, Pharmacokinetics of lipid-drug conjugates loaded into liposomes, Eur J Pharm Biopharm 128 (2018) 188-199.
[183] N. Gerwin, C. Hops, A. Lucke, Intraarticular drug delivery in osteoarthritis, Adv Drug Deliver Rev 58(2) (2006) 226-242.
[184] P. Maudens, O. Jordan, E. Allemann, Recent advances in intra-articular drug delivery systems for osteoarthritis therapy, Drug Discov Today (2018).
[185] A.R. Tellegen, I. Rudnik-Jansen, B. Pouran, H.M. de Visser, H.H. Weinans, R.E. Thomas, M.J.L. Kik, G.C.M. Grinwis, J.C. Thies, N. Woike, G. Mihov, P.J. Emans, B.P. Meij, L.B. Creemers, M.A. Tryfonidou, Controlled release of celecoxib inhibits inflammation, bone cysts and osteophyte formation in a preclinical model of osteoarthritis, Drug Deliv 25(1) (2018) 1438-1447.
[186] R.A. Dionne, A.A. Khan, S.M. Gordon, Analgesia and COX-2 inhibition, Clin Exp Rheumatol 19(6 Suppl 25) (2001) S63-70.
[187] P.J. van Diest, No consent should be needed for using leftover body material for scientific purposes, 325 (2002) 648–51.
[188] S.E. Bove, S.L. Calcaterra, R.M. Brooker, C.M. Huber, R.E. Guzman, P.L. Juneau, D.J. Schrier, K.S. Kilgore, Weight bearing as a measure of disease progression and efficacy of anti-inflammatory compounds in a model of monosodium iodoacetate-induced osteoarthritis, Osteoarthritis Cartilage 11(11) (2003) 821-30.
[189] T.L. Mindt, C. Muller, F. Stuker, J.F. Salazar, A. Hohn, T. Mueggler, M. Rudin, R. Schibli, A “click chemistry” approach to the efficient synthesis of multiple imaging probes derived from a single precursor, Bioconjug Chem 20(10) (2009) 1940-9.
[190] T.M. Piscaer, C. Muller, T.L. Mindt, E. Lubberts, J.A. Verhaar, E.P. Krenning, R. Schibli, M. De Jong, H. Weinans, Imaging of activated macrophages in experimental osteoarthritis using folate-targeted animal single-photon-emission computed tomography/computed tomography, Arthritis Rheum 63(7) (2011) 1898-907.
[191] D. Clemett, K.L. Goa, Celecoxib: a review of its use in osteoarthritis, rheumatoid arthritis and acute pain, Drugs 59(4) (2000) 957-80.
[192] G.D. Searle, Celecoxib capsules prescribing information, http://pfizer.com/pfizer/download/uspi_celebrex.pdf.).
[193] M. Siebelt, N. Korthagen, W. Wei, H. Groen, Y. Bastiaansen-Jenniskens, C. Muller, J.H. Waarsing, M. de Jong, H. Weinans, Triamcinolone acetonide activates an anti-inflammatory and folate receptor-positive macrophage that prevents osteophytosis in vivo, Arthritis Res Ther 17 (2015) 352.
[194] X. Li, M. Ellman, P. Muddasani, J.H. Wang, G. Cs-Szabo, A.J. van Wijnen, H.J. Im, Prostaglandin E2 and its cognate EP receptors control human adult articular

cartilage homeostasis and are linked to the pathophysiology of osteoarthritis, Arthritis Rheum 60(2) (2009) 513-23.
[195] S.C. Mastbergen, A.C. Marijnissen, M.E. Vianen, P.M. van Roermund, J.W. Bijlsma, F.P. Lafeber, The canine 'groove' model of osteoarthritis is more than simply the expression of surgically applied damage, Osteoarthritis Cartilage 14(1) (2006) 39-46.
[196] D.M. Mosser, J.P. Edwards, Exploring the full spectrum of macrophage activation, Nat Rev Immunol 8(12) (2008) 958-69.
[197] G.B. Mackaness, Cellular resistance to infection, J Exp Med 116 (1962) 381-406.
[198] M. Stein, S. Keshav, N. Harris, S. Gordon, Interleukin 4 potently enhances murine macrophage mannose receptor activity: a marker of alternative immunologic macrophage activation, J Exp Med 176(1) (1992) 287-92.
[199] N.A. Jager, J. Westra, R. Golestani, G.M. van Dam, P.S. Low, R.A. Tio, R.H. Slart, H.H. Boersma, M. Bijl, C.J. Zeebregts, Folate receptor-beta imaging using 99mTc-folate to explore distribution of polarized macrophage populations in human atherosclerotic plaque, J Nucl Med 55(12) (2014) 1945-51.
[200] J. Ehrchen, L. Steinmuller, K. Barczyk, K. Tenbrock, W. Nacken, M. Eisenacher, U. Nordhues, C. Sorg, C. Sunderkotter, J. Roth, Glucocorticoids induce differentiation of a specifically activated, anti-inflammatory subtype of human monocytes, Blood 109(3) (2007) 1265-74.
[201] S.H. Wong, K.Y. Chiu, C.H. Yan, Review Article: Osteophytes, J Orthop Surg (Hong Kong) 24(3) (2016) 403-410.
[202] U.T. Timur, M.M.J. Caron, Y.M. Bastiaansen-Jenniskens, T.J.M. Welting, L.W. van Rhijn, G. van Osch, P.J. Emans, Celecoxib-mediated reduction of prostanoid release in Hoffa's fat pad from donors with cartilage pathology results in an attenuated inflammatory phenotype, Osteoarthritis Cartilage 26(5) (2018) 697-706.
[203] A. Ioan-Facsinay, M. Kloppenburg, An emerging player in knee osteoarthritis: the infrapatellar fat pad, Arthritis Res Ther 15(6) (2013) 225.
[204] L. Utomo, Y.M. Bastiaansen-Jenniskens, J.A. Verhaar, G.J. van Osch, Cartilage inflammation and degeneration is enhanced by pro-inflammatory (M1) macrophages in vitro, but not inhibited directly by anti-inflammatory (M2) macrophages, Osteoarthritis Cartilage 24(12) (2016) 2162-2170.
[205] F. Ren, M. Fan, J. Mei, Y. Wu, C. Liu, Q. Pu, Z. You, L. Liu, Interferon-gamma and celecoxib inhibit lung-tumor growth through modulating M2/M1 macrophage ratio in the tumor microenvironment, Drug Des Devel Ther 8 (2014) 1527-38.
[206] Y. Nakanishi, M. Nakatsuji, H. Seno, S. Ishizu, R. Akitake-Kawano, K. Kanda, T. Ueo, H. Komekado, M. Kawada, M. Minami, T. Chiba, COX-2 inhibition alters the phenotype of tumor-associated macrophages from M2 to M1 in ApcMin/+ mouse polyps, Carcinogenesis 32(9) (2011) 1333-9.
[207] T. Hayashi, K. Fujita, S. Nojima, Y. Hayashi, K. Nakano, Y. Ishizuya, C. Wang, Y. Yamamoto, T. Kinouchi, K. Matsuzaki, K. Jingushi, T. Kato, A. Kawashima, A.

Nagahara, T. Ujike, M. Uemura, M. Pena, J.B. Gordetsky, E. Morii, K. Tsujikawa, G.J. Netto, N. Nonomura, High-Fat Diet-Induced Inflammation Accelerates Prostate Cancer Growth via IL6 Signaling, Clin Cancer Res 24(17) (2018) 4309-4318.
[208] S. Gordon, A. Pluddemann, Tissue macrophages: heterogeneity and functions, BMC Biol 15(1) (2017) 53.
[209] Recommendations for the medical management of osteoarthritis of the hip and knee: 2000 update. American College of Rheumatology Subcommittee on Osteoarthritis Guidelines, Arthritis and Rheumatism 43(9) (2000) 1905-15.
[210] Z. Zhang, X. Bi, H. Li, G. Huang, Enhanced targeting efficiency of PLGA microspheres loaded with Lornoxicam for intra-articular administration, Drug Deliv 18(7) (2011) 536-44.
[211] R.O. Day, A.J. McLachlan, G.G. Graham, K.M. Williams, Pharmacokinetics of nonsteroidal anti-inflammatory drugs in synovial fluid, Clin Pharmacokinet 36(3) (1999) 191-210.
[212] W.J. Wallis, P.A. Simkin, Antirheumatic drug concentrations in human synovial fluid and synovial tissue. Observations on extravascular pharmacokinetics, Clin Pharmacokinet 8(6) (1983) 496-522.
[213] M.L. Kang, G.I. Im, Drug delivery systems for intra-articular treatment of osteoarthritis, Expert Opin Drug Deliv 11(2) (2014) 269-82.
[214] M. Fazil, A. Ali, S. Baboota, J.K. Sahni, J. Ali, Exploring drug delivery systems for treating osteoporosis, Expert Opin Drug Deliv 10(8) (2013) 1123-36.
[215] K. Fu, D.W. Pack, A.M. Klibanov, R. Langer, Visual evidence of acidic environment within degrading poly(lactic-co-glycolic acid) (PLGA) microspheres, Pharm Res 17(1) (2000) 100-6.
[216] A. Shenderova, T.G. Burke, S.P. Schwendeman, The acidic microclimate in poly(lactide-co-glycolide) microspheres stabilizes camptothecins, Pharm Res 16(2) (1999) 241-8.
[217] A. Giteau, M.C. Venier-Julienne, S. Marchal, J.L. Courthaudon, M. Sergent, C. Montero-Menei, J.M. Verdier, J.P. Benoit, Reversible protein precipitation to ensure stability during encapsulation within PLGA microspheres, Eur J Pharm Biopharm 70(1) (2008) 127-36.
[218] B.S. Zolnik, D.J. Burgess, Effect of acidic pH on PLGA microsphere degradation and release, J Control Release 122(3) (2007) 338-44.
[219] M.S. Shive, J.M. Anderson, Biodegradation and biocompatibility of PLA and PLGA microspheres, Adv Drug Deliv Rev 28(1) (1997) 5-24.
[220] S. Mao, C. Guo, Y. Shi, L.C. Li, Recent advances in polymeric microspheres for parenteral drug delivery--part 2, Expert Opin Drug Deliv 9(10) (2012) 1209-23.
[221] S. Mao, C. Guo, Y. Shi, L.C. Li, Recent advances in polymeric microspheres for parenteral drug delivery--part 1, Expert Opin Drug Deliv 9(9) (2012) 1161-76.

[222] Y.Y. Yang, H.H. Chia, T.S. Chung, Effect of preparation temperature on the characteristics and release profiles of PLGA microspheres containing protein fabricated by double-emulsion solvent extraction/evaporation method, J Control Release 69(1) (2000) 81-96.
[223] F. Ito, H. Fujimori, H. Honnami, H. Kawakami, K. Kanamura, K. Makino, Study of types and mixture ratio of organic solvent used to dissolve polymers for preparation of drug-containing PLGA microspheres, Eur. Polym. J 45(3) (2009) 658–667.
[224] T. Nakashima, M. Shimizu, M. Kukizaki, Particle control of emulsion by membrane emulsification and its applications, Adv Drug Deliv Rev 45(1) (2000) 47-56.
[225] T.S.M. Nakashima, M. Kukizaki, Membrane emulsification by microporous glass,, Key Eng. Mater. 61 (1991) 513-516.
[226] W. Rungseevijitprapa, R. Bodmeier, Injectability of biodegradable in situ forming microparticle systems (ISM), Eur J Pharm Sci 36(4-5) (2009) 524-31.
[227] J.C. De La Vega, P. Elischer, T. Schneider, U.O. Hafeli, Uniform polymer microspheres: monodispersity criteria, methods of formation and applications, Nanomedicine (Lond) 8(2) (2013) 265-85.
[228] J. Siepmann, N. Faisant, J. Akiki, J. Richard, J.P. Benoit, Effect of the size of biodegradable microparticles on drug release: experiment and theory, J Control Release 96(1) (2004) 123-34.
[229] F.Q. Wu, Y. Xia, G. Ma, Uniform-sized particles in biomedical field prepared by membrane emulsification technique, Chem. Eng. Sci 125 (2015) 85–97.
[230] F. Kazazi-Hyseni, M. Landin, A. Lathuile, G.J. Veldhuis, S. Rahimian, W.E. Hennink, R.J. Kok, C.F. van Nostrum, Computer modeling assisted design of monodisperse PLGA microspheres with controlled porosity affords zero order release of an encapsulated macromolecule for 3 months, Pharm Res 31(10) (2014) 2844-56.
[231] F. Ramazani, C. Hiemstra, R. Steendam, F. Kazazi-Hyseni, C.F. Van Nostrum, G. Storm, F. Kiessling, T. Lammers, W.E. Hennink, R.J. Kok, Sunitinib microspheres based on [PDLLA-PEG-PDLLA]-b-PLLA multi-block copolymers for ocular drug delivery, Eur J Pharm Biopharm 95(Pt B) (2015) 368-77.
[232] C.E. Hissink, patent P, , 2004.
[233] L. Li, S.P. Schwendeman, Mapping neutral microclimate pH in PLGA microspheres, J Control Release 101(1-3) (2005) 163-73.
[234] Y. Liu, S.P. Schwendeman, Mapping microclimate pH distribution inside protein-encapsulated PLGA microspheres using confocal laser scanning microscopy, Mol Pharm 9(5) (2012) 1342-50.
[235] J.P. Caron, R.L. Genovese, Chapter 85 - Principles and Practices of Joint Disease Treatment, in: M.W.D.S. Ross (Ed.), Diagnosis and Management of Lameness in the Horse, Elsevier, Philadelphia, 2003, pp. 746-764.
[236] J.P. Caron, R.L. Genovese, United States Department of Agriculture.
Lameness and laminitis in U.S. Horses. National Animal Health Monitoring

System. https://www.aphis.usda.gov/animal_health/nahms/equine/downloads/equine98/Equine98_dr_Lameness.pdf. 2000).
[237] G. Nilsson, Lameness and pathologic changes in the distal joints and the phalanges of the standardbred horse. A correlative study, Acta Vet Scand Suppl 44(0) (1973) 83-96.
[238] C.W. McIlwraith, D.D. Frisbie, C.E. Kawcak, The horse as a model of naturally occurring osteoarthritis, Bone Joint Res 1(11) (2012) 297-309.
[239] M.H. Gregory, N. Capito, K. Kuroki, A.M. Stoker, J.L. Cook, S.L. Sherman, A review of translational animal models for knee osteoarthritis, Arthritis 2012 (2012) 764621.
[240] M. Stankovic, H. de Waard, R. Steendam, C. Hiemstra, J. Zuidema, H.W. Frijlink, W.L. Hinrichs, Low temperature extruded implants based on novel hydrophilic multiblock copolymer for long-term protein delivery, Eur J Pharm Sci 49(4) (2013) 578-87.
[241] M.W. Ross, The lameness score: quantification of lameness severity, in: D. SJ (Ed.), Diagnosis and Management of Lameness in the Horse, W.B. Saunders, Philadelphia, 2003, pp. 66–67
.
[242] J.C. de Grauw, C.H. van de Lest, P.A. Brama, B.P. Rambags, P.R. van Weeren, In vivo effects of meloxicam on inflammatory mediators, MMP activity and cartilage biomarkers in equine joints with acute synovitis, Equine Vet J 41(7) (2009) 693-9.
[243] R. Kumar, M.J. Palmieri, Jr., Points to consider when establishing drug product specifications for parenteral microspheres, AAPS J 12(1) (2010) 27-32.
[244] M. Siebelt, H.C. Groen, S.J. Koelewijn, E. de Blois, M. Sandker, J.H. Waarsing, C. Müller, G.J. van Osch, M. de Jong, H. Weinans, Increased physical activity severely induces osteoarthritic changes in knee joints with papain induced sulphate-glycosaminoglycan depleted cartilage., Arthritis Res Ther 16(1) (2014) R32.
[245] R.L. Illgen, 2nd, T.M. Forsythe, J.W. Pike, M.P. Laurent, C.R. Blanchard, Highly crosslinked vs conventional polyethylene particles--an in vitro comparison of biologic activities, J Arthroplasty 23(5) (2008) 721-31.
[246] T.R. Green, J. Fisher, M. Stone, B.M. Wroblewski, E. Ingham, Polyethylene particles of a 'critical size' are necessary for the induction of cytokines by macrophages in vitro, Biomaterials 19(24) (1998) 2297-302.
[247] J.W. Lee, F. Hua, D.S. Lee, Thermoreversible gelation of biodegradable poly(epsilon-caprolactone) and poly(ethylene glycol) multiblock copolymers in aqueous solutions, J Control Release 73(2-3) (2001) 315-27.
[248] C.G. Mothe, A.D. Azevedo, W.S. Drumond, S.H. Wang, Thermal properties of amphiphilic biodegradable triblock copolymer of l, L-lactide and ethylene glycol, , J. Therm. Anal. Calorim 101(1) (2010) 229–233.

[249] J.E. Kim, S.R. Kim, S.H. Lee, C.H. Lee, D.D. Kim, The effect of pore formers on the controlled release of cefadroxil from a polyurethane matrix, Int J Pharm 201(1) (2000) 29-36.
[250] M.G. Carstens, C.F. van Nostrum, R. Verrijk, L.G. de Leede, D.J. Crommelin, W.E. Hennink, A mechanistic study on the chemical and enzymatic degradation of PEG-Oligo(epsilon-caprolactone) micelles, J Pharm Sci 97(1) (2008) 506-18.
[251] M.H. Huang, S. Li, D.W. Hutmacher, J.T. Schantz, C.A. Vacanti, C. Braud, M. Vert, Degradation and cell culture studies on block copolymers prepared by ring opening polymerization of epsilon-caprolactone in the presence of poly(ethylene glycol), J Biomed Mater Res A 69(3) (2004) 417-27.
[252] M.L. Zweers, G.H. Engbers, D.W. Grijpma, J. Feijen, In vitro degradation of nanoparticles prepared from polymers based on DL-lactide, glycolide and poly(ethylene oxide), J Control Release 100(3) (2004) 347-56.
[253] ICH guidelines. http://www.ich.org/fileadmin/Public_Web_Site/ICH_ Products/Guidelines/Quality/Q3D/Q3D_Step_4.pdf2014.).
[254] N. Butoescu, O. Jordan, E. Doelker, Intra-articular drug delivery systems for the treatment of rheumatic diseases: a review of the factors influencing their performance, Eur J Pharm Biopharm 73(2) (2009) 205-18.
[255] P.R. Moshtagh, J. Rauker, M.J. Sandker, M.R. Zuiddam, F.W. Dirne, E. Klijnstra, L. Duque, R. Steendam, H. Weinans, A.A. Zadpoor, Nanomechanical properties of multi-block copolymer microspheres for drug delivery applications, J Mech Behav Biomed Mater 34 (2014) 313-9.
[256] K. Makino, M. Arakawa, T. Kondo, Preparation and in vitro degradation properties of polylactide microcapsules, Chem Pharm Bull (Tokyo) 33(3) (1985) 1195-201.
[257] S.S. D'Souza, J.A. Faraj, P.P. DeLuca, A model-dependent approach to correlate accelerated with real-time release from biodegradable microspheres, AAPS PharmSciTech 6(4) (2005) E553-64.
[258] D.W. Jackson, T.M. Simon, Intra-articular distribution and residence time of Hylan A and B: a study in the goat knee, Osteoarthritis Cartilage 14(12) (2006) 1248-57.
[259] T. Adams, D. Band-Entrup, S. Kuhn, L. Legere, K. Mace, A. Paggi, M. Penney, Physical therapy management of knee osteoarthritis in the middle-aged athlete, Sports Med Arthrosc Rev 21(1) (2013) 2-10.
[260] A. Lussier, A.A. Cividino, C.A. McFarlane, W.P. Olszynski, W.J. Potashner, R. De Medicis, Viscosupplementation with hylan for the treatment of osteoarthritis: findings from clinical practice in Canada, J Rheumatol 23(9) (1996) 1579-85.
[261] L.A. Fortier, Systemic therapies for joint disease in horses, Vet Clin North Am Equine Pract 21(3) (2005) 547-57, v.

[262] T. Kojima, F. Mwale, T. Yasuda, C. Girard, A.R. Poole, S. Laverty, Early degradation of type IX and type II collagen with the onset of experimental inflammatory arthritis, Arthritis Rheum 44(1) (2001) 120-7.
[263] K.A. Elsaid, C.O. Chichester, Review: Collagen markers in early arthritic diseases, Clin Chim Acta 365(1-2) (2006) 68-77.
[264] A. Fraser, U. Fearon, R.C. Billinghurst, M. Ionescu, R. Reece, T. Barwick, P. Emery, A.R. Poole, D.J. Veale, Turnover of type II collagen and aggrecan in cartilage matrix at the onset of inflammatory arthritis in humans: relationship to mediators of systemic and local inflammation, Arthritis Rheum 48(11) (2003) 3085-95.
[265] R. Klopfleisch, Macrophage reaction against biomaterials in the mouse model - Phenotypes, functions and markers, Acta Biomater 43 (2016) 3-13.
[266] T. Ehashi, S. Kakinoki, T. Yamaoka, Water absorbing and quick degradable PLLA/PEG multiblock copolymers reduce the encapsulation and inflammatory cytokine production, J Artif Organs 17(4) (2014) 321-8.
[267] J. Zandstra, C. Hiemstra, A.H. Petersen, J. Zuidema, M.M. van Beuge, S. Rodriguez, A.A. Lathuile, G.J. Veldhuis, R. Steendam, R.A. Bank, E.R. Popa, Microsphere size influences the foreign body reaction, Eur Cell Mater 28 (2014) 335-47.
[268] J. Bondeson, A.B. Blom, S. Wainwright, C. Hughes, B. Caterson, W.B. van den Berg, The role of synovial macrophages and macrophage-produced mediators in driving inflammatory and destructive responses in osteoarthritis, Arthritis Rheum 62(3) (2010) 647-57.
[269] A.B. Blom, P.L. van Lent, S. Libregts, A.E. Holthuysen, P.M. van der Kraan, N. van Rooijen, W.B. van den Berg, Crucial role of macrophages in matrix metalloproteinase-mediated cartilage destruction during experimental osteoarthritis: involvement of matrix metalloproteinase 3, Arthritis Rheum 56(1) (2007) 147-57.
[270] E.N. Blaney Davidson, E.L. Vitters, F.M. Mooren, N. Oliver, W.B. Berg, P.M. van der Kraan, Connective tissue growth factor/CCN2 overexpression in mouse synovial lining results in transient fibrosis and cartilage damage, Arthritis Rheum 54(5) (2006) 1653-61.
[271] L.I. Sakkas, N.A. Johanson, C.R. Scanzello, C.D. Platsoucas, Interleukin-12 is expressed by infiltrating macrophages and synovial lining cells in rheumatoid arthritis and osteoarthritis, Cell Immunol 188(2) (1998) 105-10.
[272] M.K. Haynes, E.L. Hume, J.B. Smith, Phenotypic characterization of inflammatory cells from osteoarthritic synovium and synovial fluids, Clin Immunol 105(3) (2002) 315-25.
[273] N. Arden, M.C. Nevitt, Osteoarthritis: epidemiology, Best Pract Res Clin Rheumatol 20(1) (2006) 3-25.
[274] E. Badley, The effect of osteoarthritis on disability and health care use in Canada, The Journal of rheumatology. Supplement 43 (1995) 19-22.

[275] J. Lin, W. Zhang, A. Jones, M. Doherty, Efficacy of topical non-steroidal anti-inflammatory drugs in the treatment of osteoarthritis: meta-analysis of randomised controlled trials, BMJ 329(7461) (2004) 324-326.
[276] M. Mamdani, P.A. Rochon, D.N. Juurlink, A. Kopp, G.M. Anderson, G. Naglie, P.C. Austin, A. Laupacis, Observational study of upper gastrointestinal haemorrhage in elderly patients given selective cyclo-oxygenase-2 inhibitors or conventional non-steroidal anti-inflammatory drugs, BMJ 325(7365) (2002) 624-629.
[277] X. Ayral, Injections in the treatment of osteoarthritis, Best Practice & Research Clinical Rheumatology 15(4) (2001) 609-626.
[278] M.J. Sandker, A. Petit, E.M. Redout, M. Siebelt, B. Müller, P. Bruin, R. Meyboom, T. Vermonden, W.E. Hennink, H. Weinans, In situ forming acyl-capped PCLA–PEG–PCLA triblock copolymer based hydrogels, Biomaterials 34(32) (2013) 8002–8011.
[279] B. Chan, C. Li, K. Au-Yeung, K. Sze, A. Ngan, A microplate compression method for elastic modulus measurement of soft and viscoelastic collagen microspheres, Annals of Biomedical Engineering 36(7) (2008) 1254-1267.
[280] R. Mercadé-Prieto, Z. Zhang, Mechanical characterization of microspheres-capsules, cells and beads: a review, Journal of microencapsulation 29(3) (2012) 277-285.
[281] Y. Zhu, Z. Dong, U.C. Wejinya, S. Jin, K. Ye, Determination of mechanical properties of soft tissue scaffolds by atomic force microscopy nanoindentation, Journal of biomechanics 44(13) (2011) 2356-61.
[282] J. Notbohm, Poon, B., Ravichandran, G., Analysis of nanoindentation of soft materials with an atomic force microscope, Journal of Materials Research 27(01) (2011) 229-37.
[283] M.L. Oyen, R.F. Cook, A practical guide for analysis of nanoindentation data, Journal of the mechanical behavior of biomedical materials 2(4) (2009) 396-407.
[284] O. Franke, K. Durst, V. Maier, M. Goken, T. Birkholz, H. Schneider, F. Hennig, K. Gelse, Mechanical properties of hyaline and repair cartilage studied by nanoindentation, Acta biomaterialia 3(6) (2007) 873-81.
[285] M. Loparic, Wirz, D., Daniels, A. U., Raiteri, R., Vanlandingham, M. R., Guex, G., Martin, I., Aebi, U., Stolz, M., Micro- and nanomechanical analysis of articular cartilage by indentation-type atomic force microscopy: validation with a gel-microfiber composite, Biophysical journal 98(11) (2010) 2731-40.
[286] M. Stolz, Raiteri, R., Daniels, A. U., VanLandingham, M. R., Baschong, W., Aebi, U., Dynamic elastic modulus of porcine articular cartilage determined at two different levels of tissue organization by indentation-type atomic force microscopy, Biophysical journal 86(5) (2004) 3269-83.
[287] S.P. Zustiak, J.B. Leach, Hydrolytically degradable poly(ethylene glycol) hydrogel scaffolds with tunable degradation and mechanical properties, Biomacromolecules 11(5) (2010) 1348-57.

[288] C.B. Hutson, J.W. Nichol, H. Aubin, H. Bae, S. Yamanlar, S. Al-Haque, S.T. Koshy, A. Khademhosseini, Synthesis and characterization of tunable poly(ethylene glycol): gelatin methacrylate composite hydrogels, Tissue engineering. Part A 17(13-14) (2011) 1713-23.
[289] J.L. Ostroha, PEG-based degradable networks for drug delivery applications, Drexel 2006, p. 165.
[290] C.D. Brown, P.S. Stayton, A.S. Hoffman, Semi-interpenetrating network of poly(ethylene glycol) and poly(D, L-lactide) for the controlled delivery of protein drugs, Journal of Biomaterials Science, Polymer Edition 16(2) (2005) 189-201.
[291] D.K. Wang, S. Varanasi, D.J.T. Hill, F. Rasoul, A.L. Symons, A.K. Whittaker, The influence of composition on the physical properties of PLA-PEG-PLA-co-Boltorn based polyester hydrogels and their biological performance, Journal of Materials Chemistry 22(14) (2012) 6994.
[292] D. Garlotta, A Literature Review of Poly(Lactic Acid), Journal of polymers and the environment 9 (2001) 63-84.
[293] Z. Drira, V.K. Yadavalli, Nanomechanical measurements of polyethylene glycol hydrogels using atomic force microscopy, Journal of the mechanical behavior of biomedical materials 18 (2013) 20-8.
[294] S. Gäbler, Determination of the viscoelastic properties of hydrogels based on polyethylene glycol diacrylate (PEG-DA) and human articular cartilage, International Journal of Materials Engineering Innovation 1 (2009) 3-20.
[295] T. Yang, Mechanical and swelling properties of hydrogels, KTH 2012, p. 67.
[296] D.M. Ebenstein, L.A. Pruitt, Nanoindentation of soft hydrated materials for application to vascular tissues, Journal of biomedical materials research. Part A 69(2) (2004) 222-32.
[297] S.J. Eichhorn, W.W. Sampson, Relationships between specific surface area and pore size in electrospun polymer fibre networks, Journal of the Royal Society, Interface / the Royal Society 7(45) (2010) 641-9.
[298] K. Suttiponparnit, J. Jiang, M. Sahu, S. Suvachittanont, T. Charinpanitkul, P. Biswas, Role of surface area, primary particle size, and crystal phase on titanium dioxide nanoparticle dispersion properties, Nanoscale Research Letters (2010) 6-27.
[299] M. Stolz, R. Gottardi, R. Raiteri, S. Miot, I. Martin, R. Imer, U. Staufer, A. Raducanu, M. Duggelin, W. Baschong, A.U. Daniels, N.F. Friederich, A. Aszodi, U. Aebi, Early detection of aging cartilage and osteoarthritis in mice and patient samples using atomic force microscopy, Nature nanotechnology 4(3) (2009) 186-92.
[300] L. Han, E.H. Frank, J.J. Greene, H.Y. Lee, H.H. Hung, A.J. Grodzinsky, C. Ortiz, Time-dependent nanomechanics of cartilage, Biophysical journal 100(7) (2011) 1846-54.

[301] H. Kranz, N. Ubrich, P. Maincent, R. Bodmeier, Physicomechanical properties of biodegradable poly (D, L-lactide) and poly (D, L-lactide-co-glycolide) films in the dry and wet states, Journal of pharmaceutical sciences 89(12) (2000) 1558-1566.
[302] H.K. Makadia, S.J. Siegel, Poly lactic-co-glycolic acid (PLGA) as biodegradable controlled drug delivery carrier, Polymers 3(3) (2011) 1377-1397.
[303] I. Galeska, T.-K. Kim, S.D. Patil, U. Bhardwaj, D. Chatttopadhyay, F. Papadimitrakopoulos, D.J. Burgess, Controlled release of dexamethasone from PLGA microspheres embedded within polyacid-containing PVA hydrogels, The AAPS journal 7(1) (2005) E231-E240.
[304] C.M. Hassan, N.A. Peppas, Structure and applications of poly (vinyl alcohol) hydrogels produced by conventional crosslinking or by freezing/thawing methods, Biopolymers· PVA Hydrogels, Anionic Polymerisation Nanocomposites, Springer2000, pp. 37-65.
[305] J. Chen, Understanding the nanoindentation mechanisms of a microsphere for biomedical applications, Journal of Physics D: Applied Physics 46(49) (2013) 495303.
[306] E.M. Darling, Wilusz, R. E., Bolognesi, M. P., Zauscher, S., Guilak, F., Spatial mapping of the biomechanical properties of the pericellular matrix of articular cartilage measured in situ via atomic force microscopy, Biophysical journal 98(12) (2010) 2848-56.
[307] S. Thalhammer, Heckl, W. M., Zink, A., Nerlich, A. G., Atomic force microscopy for high resolution imaging of collagen fibrils—a new technique to investigate collagen structure in historic bone tissues, Journal of Archaeological Science 28(10) (2001) 1061-8.
[308] M. Salerno, Dante, S., Patra, N., Diaspro, A., AFM measurement of the stiffness of layers of agarose gel patterned with polylysine, Microscopy research and technique 73(10) (2010) 982-90.
[309] Y. Chen, B. Feng, Y. Zhu, J. Weng, J. Wang, X. Lu, Preparation and characterization of a novel porous titanium scaffold with 3D hierarchical porous structures, Journal of Materials Science: Materials in Medicine 22(4) (2011) 839-844.
[310] L. Calabri, Pugno, N., Menozzi, C., Valeri, S., AFM nanoindentation: tip shape and tip radius of curvature effect on the hardness measurement, J Phys-Condens Mat 20(47) (2008) 1-7.
[311] M.B. Goldring, M. Otero, Inflammation in osteoarthritis, Curr Opin Rheumatol 23(5) (2011) 471-8.
[312] E.B.P. Lopes, A. Filiberti, S.A. Husain, M.B. Humphrey, Immune Contributions to Osteoarthritis, Curr Osteoporos Rep 15(6) (2017) 593-600.
[313] A.E. van der Windt, E. Haak, N. Kops, J.A. Verhaar, H. Weinans, H. Jahr, Inhibiting calcineurin activity under physiologic tonicity elevates anabolic but suppresses catabolic chondrocyte markers, Arthritis Rheum 64(6) (2012) 1929-39.

[314] K. Magari, F. Nishigaki, T. Sasakawa, T. Ogawa, S. Miyata, Y. Ohkubo, S. Mutoh, T. Goto, Anti-arthritic properties of FK506 on collagen-induced arthritis in rats, Inflamm Res 52(12) (2003) 524-9.
[315] C.E. Staatz, S.E. Tett, Clinical pharmacokinetics and pharmacodynamics of tacrolimus in solid organ transplantation, Clin Pharmacokinet 43(10) (2004) 623-53.
[316] G.D. MacFarlane, L.M. Shaw, R. Venkataramanan, R. Mullins, D.G. Scheller, D.L. Ersfeld, Analysis of whole blood tacrolimus concentrations in liver transplant patients exhibiting impaired liver function, Ther Drug Monit 21(6) (1999) 585-92.
[317] B. Kaplan, K. Lown, R. Craig, M. Abecassis, D. Kaufman, J. Leventhal, F. Stuart, H.U. Meier-Kriesche, J. Fryer, Low bioavailability of cyclosporine microemulsion and tacrolimus in a small bowel transplant recipient: possible relationship to intestinal P-glycoprotein activity, Transplantation 67(2) (1999) 333-5.
[318] K. Yokogawa, M. Takahashi, I. Tamai, H. Konishi, M. Nomura, S. Moritani, K. Miyamoto, A. Tsuji, P-glycoprotein-dependent disposition kinetics of tacrolimus: studies in mdr1a knockout mice, Pharm Res 16(8) (1999) 1213-8.
[319] H. Saitoh, Y. Saikachi, M. Kobayashi, M. Yamaguchi, M. Oda, Y. Yuhki, K. Achiwa, K. Tadano, Y. Takahashi, B.J. Aungst, Limited interaction between tacrolimus and P-glycoprotein in the rat small intestine, Eur J Pharm Sci 28(1-2) (2006) 34-42.
[320] N. Bellamy, J. Campbell, V. Robinson, T. Gee, R. Bourne, G. Wells, Intraarticular corticosteroid for treatment of osteoarthritis of the knee, Cochrane Database Syst Rev (2) (2005) CD005328.
[321] A.G. Bajpayee, A.J. Grodzinsky, Cartilage-targeting drug delivery: can electrostatic interactions help?, Nat Rev Rheumatol 13(3) (2017) 183-193.
[322] M.J. Sandker, L.F. Duque, E.M. Redout, A. Chan, I. Que, C. Lowik, E.C. Klijnstra, N. Kops, R. Steendam, R. van Weeren, W.E. Hennink, H. Weinans, Degradation, intra-articular retention and biocompatibility of monospheres composed of [PDLLA-PEG-PDLLA]-b-PLLA multi-block copolymers, Acta Biomater 48 (2017) 401-414.
[323] C. Wischke, S.P. Schwendeman, Principles of encapsulating hydrophobic drugs in PLA/PLGA microparticles, Int J Pharm 364(2) (2008) 298-327.
[324] J. Siepmann, A. Streubel, N.A. Peppas, Understanding and predicting drug delivery from hydrophilic matrix tablets using the "sequential layer" model, Pharm Res 19(3) (2002) 306-14.
[325] T. Kino, H. Hatanaka, M. Hashimoto, M. Nishiyama, T. Goto, M. Okuhara, M. Kohsaka, H. Aoki, H. Imanaka, FK-506, a novel immunosuppressant isolated from a Streptomyces. I. Fermentation, isolation, and physico-chemical and biological characteristics, J Antibiot (Tokyo) 40(9) (1987) 1249-55.
[326] T. Akashi, T. Nefuji, M. Yoshida, J. Hosoda, Quantitative determination of tautomeric FK506 by reversed-phase liquid chromatography, J Pharm Biomed Anal 14(3) (1996) 339-46.

[327] J. van Tiel, M. Siebelt, M. Reijman, P.K. Bos, J.H. Waarsing, A.M. Zuurmond, K. Nasserinejad, G.J. van Osch, J.A. Verhaar, G.P. Krestin, H. Weinans, E.H. Oei, Quantitative in vivo CT arthrography of the human osteoarthritic knee to estimate cartilage sulphated glycosaminoglycan content: correlation with ex-vivo reference standards, Osteoarthritis Cartilage 24(6) (2016) 1012-20.
[328] A.L. Bertone, J.L. Palmer, J. Jones, Synovial fluid cytokines and eicosanoids as markers of joint disease in horses, Vet Surg 30(6) (2001) 528-38.
[329] J.C. de Grauw, C.H. van de Lest, P.R. van Weeren, Inflammatory mediators and cartilage biomarkers in synovial fluid after a single inflammatory insult: a longitudinal experimental study, Arthritis Res Ther 11(2) (2009) R35.
[330] M. Stankovic, J. Tomar, C. Hiemstra, R. Steendam, H.W. Frijlink, W.L. Hinrichs, Tailored protein release from biodegradable poly(epsilon-caprolactone-PEG)-b-poly(epsilon-caprolactone) multiblock-copolymer implants, Eur J Pharm Biopharm 87(2) (2014) 329-37.
[331] B.S. Zolnik, D.J. Burgess, Evaluation of in vivo-in vitro release of dexamethasone from PLGA microspheres, J Control Release 127(2) (2008) 137-45.
[332] M. von Suesskind-Schwendi, M. Gruber, D. Touraud, W. Kunz, C. Schmid, S.W. Hirt, K. Lehle, Pharmacokinetics of a self-microemulsifying drug delivery system of tacrolimus, Biomed Pharmacother 67(6) (2013) 469-473.
[333] T. Nassar, A. Rom, A. Nyska, S. Benita, Novel double coated nanocapsules for intestinal delivery and enhanced oral bioavailability of tacrolimus, a P-gp substrate drug, Journal of Controlled Release 133(1) (2009) 77-84.
[334] Y.J. Wang, J. Sun, T.H. Zhang, H.Z. Liu, F.C. He, Z.G. He, Enhanced oral bioavailability of tacrolimus in rats by self-microemulsifying drug delivery systems, Drug Dev Ind Pharm 37(10) (2011) 1225-1230.
[335] M.D. Grynpas, B. Alpert, I. Katz, I. Lieberman, K.P. Pritzker, Subchondral bone in osteoarthritis, Calcif Tissue Int 49(1) (1991) 20-6.
[336] A.J. Barr, T.M. Campbell, D. Hopkinson, S.R. Kingsbury, M.A. Bowes, P.G. Conaghan, A systematic review of the relationship between subchondral bone features, pain and structural pathology in peripheral joint osteoarthritis, Arthritis Res Ther 17 (2015) 228.
[337] M. Siebelt, A.E. van der Windt, H.C. Groen, M. Sandker, J.H. Waarsing, C. Muller, M. de Jong, H. Jahr, H. Weinans, FK506 protects against articular cartilage collagenous extra-cellular matrix degradation, Osteoarthritis Cartilage 22(4) (2014) 591-600.
[338] L.K. McCauley, T.J. Rosol, C.C. Capen, Effects of cyclosporin A on rat osteoblasts (ROS 17/2.8 cells) in vitro, Calcified tissue international 51(4) (1992) 291-7.
[339] L. Sun, H.C. Blair, Y. Peng, N. Zaidi, O.A. Adebanjo, X.B. Wu, X.Y. Wu, J. Iqbal, S. Epstein, E. Abe, B.S. Moonga, M. Zaidi, Calcineurin regulates bone formation by the osteoblast, Proc Natl Acad Sci U S A 102(47) (2005) 17130-5.

[340] K.Y. Kang, J.H. Ju, Y.W. Song, D.H. Yoo, H.Y. Kim, S.H. Park, Tacrolimus treatment increases bone formation in patients with rheumatoid arthritis, Rheumatol Int 33(8) (2013) 2159-63.
[341] M.B. Goldring, S.R. Goldring, Biology of the Normal Joint , in Kelley and Firestein's Textbook of Rheumatology 10 ed.2013.
[342] M.J. Sandker, L.F. Duque, E.M. Redout, A. Chan, I. Que, C.W. Lowik, E.C. Klijnstra, N. Kops, R. Steendam, R. van Weeren, W.E. Hennink, H. Weinans, Degradation, intra-articular retention and biocompatibility of monospheres composed of [PDLLA-PEG-PDLLA]-b-PLLA multi-block copolymers, Acta Biomater 48 (2017) 401-414.
[343] M. Kurowska-Stolarska, S. Alivernini, Synovial tissue macrophages: friend or foe?, RMD Open 3(2) (2017) e000527.
[344] X. Houard, M.B. Goldring, F. Berenbaum, Homeostatic mechanisms in articular cartilage and role of inflammation in osteoarthritis, Curr Rheumatol Rep 15(11) (2013) 375.
[345] J. Sellam, F. Berenbaum, The role of synovitis in pathophysiology and clinical symptoms of osteoarthritis, Nature Reviews Rheumatology 6(11) (2010) 625-35.
[346] J. Bondeson, S.D. Wainwright, S. Lauder, N. Amos, C.E. Hughes, The role of synovial macrophages and macrophage-produced cytokines in driving aggrecanases, matrix metalloproteinases, and other destructive and inflammatory responses in osteoarthritis, Arthritis Res Ther 8(6) (2006) R187.
[347] R. Ayers, K. Singh, Chapter 5; Biomaterials, in: M.I. Boyer (Ed.), AAOS Comprehensive Orthopaedic Review 22014.
[348] D.F. Williams, Definitions in biomaterials, Elsevier, Amsterdam, 1987.
[349] P.M. Treuting, S.M. Dintzis, K.S. Montine, Comparative Anatomy and Histology: A Mouse, Rat, and Human Atlas.
[350] P. Perel, I. Roberts, E. Sena, P. Wheble, C. Briscoe, P. Sandercock, M. Macleod, L.E. Mignini, P. Jayaram, K.S. Khan, Comparison of treatment effects between animal experiments and clinical trials: systematic review, BMJ 334(7586) (2007) 197.
[351] P. Pound, S. Ebrahim, P. Sandercock, M.B. Bracken, I. Roberts, G. Reviewing Animal Trials Systematically, Where is the evidence that animal research benefits humans?, BMJ 328(7438) (2004) 514-7.
[352] D.G. Hackam, D.A. Redelmeier, Translation of research evidence from animals to humans, JAMA 296(14) (2006) 1731-2.
[353] C. Hildebrand, G. Oqvist, L. Brax, F. Tuisku, Anatomy of the rat knee joint and fibre composition of a major articular nerve, Anat Rec 229(4) (1991) 545-55.
[354] S.C. Cheng, I.M. Jou, T.C. Chern, P.H. Wang, W.C. Chen, The effect of normal saline irrigation at different temperatures on the surface of articular cartilage: an experimental study in the rat, Arthroscopy 20(1) (2004) 55-61.

[355] C. Becher, J. Springer, S. Feil, G. Cerulli, H.H. Paessler, Intra-articular temperatures of the knee in sports - an in-vivo study of jogging and alpine skiing., BMC Musculoskelet Disord. 9(46) (2008).
[356] N.A. Cummings, G.L. Nordby, Measurement of synovial fluid pH in normal and arthritic knees, Arthritis Rheum 9(1) (1966) 47-56.
[357] S.E. Andersson, K. Lexmuller, A. Johansson, G.M. Ekstrom, Tissue and intracellular pH in normal periarticular soft tissue and during different phases of antigen induced arthritis in the rat, J Rheumatol 26(9) (1999) 2018-24.
[358] M. Vert, J. Mauduit, S. Li, Biodegradation of PLA/GA polymers: increasing complexity, Biomaterials 15(15) (1994) 1209-13.
[359] S.A. Ali, P.J. Doherty, D.F. Williams, Mechanisms of polymer degradation in implantable devices. 2. Poly(DL-lactic acid), J Biomed Mater Res 27(11) (1993) 1409-18.
[360] M.B. Goldring, K.B. Marcu, Cartilage homeostasis in health and rheumatic diseases, Arthritis Res Ther 11(3) (2009) 224.
[361] X. Li, C. Chu, P.K. Chu, Effects of external stress on biodegradable orthopedic materials: A review, Bioact Mater 1(1) (2016) 77-84.
[362] D.E. Thompson, C.M. Agrawal, K. Athanasiou, The effects of dynamic compressive loading on biodegradable implants of 50-50% polylactic Acid-polyglycolic Acid, Tissue Eng 2(1) (1996) 61-74.
[363] M.K. Beyer, H. Clausen-Schaumann, Mechanochemistry: the mechanical activation of covalent bonds, Chem Rev 105(8) (2005) 2921-48.
[364] E. Fournier, C. Passirani, N. Colin, S. Sagodira, P. Menei, J.P. Benoit, C.N. Montero-Menei, The brain tissue response to biodegradable poly(methylidene malonate 2.1.2)-based microspheres in the rat, Biomaterials 27(28) (2006) 4963-74.
[365] E.M. TenBroek, L. Yunker, M.F. Nies, A.M. Bendele, Randomized controlled studies on the efficacy of antiarthritic agents in inhibiting cartilage degeneration and pain associated with progression of osteoarthritis in the rat, Arthritis Res Ther 18 (2016) 24.
[366] J. Kanda, N. Izumo, M. Furukawa, T. Shimakura, N. Yamamoto, E.T. H, T. Asakura, H. Wakabayashi, Effects of the calcineurin inhibitors cyclosporine and tacrolimus on bone metabolism in rats, Biomed Res 39(3) (2018) 131-139.
[367] C.A. Kulak, V.Z. Borba, J. Kulak, Jr., M.R. Custodio, Osteoporosis after transplantation, Curr Osteoporos Rep 10(1) (2012) 48-55.
[368] R. Westenfeld, G. Schlieper, M. Woltje, A. Gawlik, V. Brandenburg, P. Rutkowski, J. Floege, W. Jahnen-Dechent, M. Ketteler, Impact of sirolimus, tacrolimus and mycophenolate mofetil on osteoclastogenesis--implications for post-transplantation bone disease, Nephrol Dial Transplant 26(12) (2011) 4115-23.
[369] G. Schett, M. Stolina, D. Dwyer, D. Zack, S. Uderhardt, G. Kronke, P. Kostenuik, U. Feige, Tumor necrosis factor alpha and RANKL blockade cannot halt bony spur

formation in experimental inflammatory arthritis, Arthritis Rheum 60(9) (2009) 2644-54.
[370] C.M. Giachelli, Ectopic calcification: gathering hard facts about soft tissue mineralization, Am J Pathol 154(3) (1999) 671-5.
[371] A. Chatterjea, V.L. LaPointe, J. Alblas, S. Chatterjea, C.A. van Blitterswijk, J. de Boer, Suppression of the immune system as a critical step for bone formation from allogeneic osteoprogenitors implanted in rats, J Cell Mol Med 18(1) (2014) 134-42.
[372] F. Berenbaum, Osteoarthritis as an inflammatory disease (osteoarthritis is not osteoarthrosis!), Osteoarthritis Cartilage 21(1) (2013) 16-21.
[373] A.G. Bajpayee, R.E. De la Vega, M. Scheu, N.H. Varady, I.A. Yannatos, L.A. Brown, Y. Krishnan, T.J. Fitzsimons, P. Bhattacharya, E.H. Frank, A.J. Grodzinsky, R.M. Porter, Sustained intra-cartilage delivery of low dose dexamethasone using a cationic carrier for treatment of post traumatic osteoarthritis, Eur Cell Mater 34 (2017) 341-364.
[374] H. Cho, J.M. Stuart, R. Magid, D.C. Danila, T. Hunsaker, E. Pinkhassik, K.A. Hasty, Theranostic immunoliposomes for osteoarthritis, Nanomedicine 10(3) (2014) 619-27.
[375] N. Butoescu, O. Jordan, P. Burdet, P. Stadelmann, A. Petri-Fink, H. Hofmann, E. Doelker, Dexamethasone-containing biodegradable superparamagnetic microparticles for intra-articular administration: physicochemical and magnetic properties, in vitro and in vivo drug release, Eur J Pharm Biopharm 72(3) (2009) 529-38.
[376] S.A. Yoo, B.H. Park, H.J. Yoon, J.Y. Lee, J.H. Song, H.A. Kim, C.S. Cho, W.U. Kim, Calcineurin modulates the catabolic and anabolic activity of chondrocytes and participates in the progression of experimental osteoarthritis, Arthritis and Rheumatism 56(7) (2007) 2299-311.
[377] A. Takamatsu, B. Ohkawara, M. Ito, A. Masuda, T. Sakai, N. Ishiguro, K. Ohno, Verapamil protects against cartilage degradation in osteoarthritis by inhibiting Wnt/beta-catenin signaling, PLoS One 9(3) (2014) e92699.
[378] F.W. Roemer, A. Aydemir, S. Lohmander, M.D. Crema, M.D. Marra, N. Muurahainen, D.T. Felson, F. Eckstein, A. Guermazi, Structural effects of sprifermin in knee osteoarthritis: a post-hoc analysis on cartilage and non-cartilaginous tissue alterations in a randomized controlled trial, BMC Musculoskelet Disord 17 (2016) 267.
[379] L. Hayflick, P.S. Moorhead, The serial cultivation of human diploid cell strains, Exp Cell Res 25 (1961) 585-621.
[380] M. Serrano, A.W. Lin, M.E. McCurrach, D. Beach, S.W. Lowe, Oncogenic ras provokes premature cell senescence associated with accumulation of p53 and p16INK4a, Cell 88(5) (1997) 593-602.
[381] R.F. Loeser, J.A. Collins, B.O. Diekman, Ageing and the pathogenesis of osteoarthritis, Nat Rev Rheumatol 12(7) (2016) 412-20.

[382] A. Mobasheri, C. Matta, R. Zakany, G. Musumeci, Chondrosenescence: definition, hallmarks and potential role in the pathogenesis of osteoarthritis, Maturitas 80(3) (2015) 237-44.
[383] M. Xu, E.W. Bradley, M.M. Weivoda, S.M. Hwang, T. Pirtskhalava, T. Decklever, G.L. Curran, M. Ogrodnik, D. Jurk, K.O. Johnson, V. Lowe, T. Tchkonia, J.J. Westendorf, J.L. Kirkland, Transplanted Senescent Cells Induce an Osteoarthritis-Like Condition in Mice, J Gerontol A Biol Sci Med Sci 72(6) (2017) 780-785.
[384] Y. Zhu, T. Tchkonia, T. Pirtskhalava, A.C. Gower, H. Ding, N. Giorgadze, A.K. Palmer, Y. Ikeno, G.B. Hubbard, M. Lenburg, S.P. O'Hara, N.F. LaRusso, J.D. Miller, C.M. Roos, G.C. Verzosa, N.K. LeBrasseur, J.D. Wren, J.N. Farr, S. Khosla, M.B. Stout, S.J. McGowan, H. Fuhrmann-Stroissnigg, A.U. Gurkar, J. Zhao, D. Colangelo, A. Dorronsoro, Y.Y. Ling, A.S. Barghouthy, D.C. Navarro, T. Sano, P.D. Robbins, L.J. Niedernhofer, J.L. Kirkland, The Achilles' heel of senescent cells: from transcriptome to senolytic drugs, Aging Cell 14(4) (2015) 644-58.
[385] Y. Zhu, T. Tchkonia, H. Fuhrmann-Stroissnigg, H.M. Dai, Y.Y. Ling, M.B. Stout, T. Pirtskhalava, N. Giorgadze, K.O. Johnson, C.B. Giles, J.D. Wren, L.J. Niedernhofer, P.D. Robbins, J.L. Kirkland, Identification of a novel senolytic agent, navitoclax, targeting the Bcl-2 family of anti-apoptotic factors, Aging Cell 15(3) (2016) 428-35.
[386] K. Johnson, S. Zhu, M.S. Tremblay, J.N. Payette, J. Wang, L.C. Bouchez, S. Meeusen, A. Althage, C.Y. Cho, X. Wu, P.G. Schultz, A stem cell-based approach to cartilage repair, Science 336(6082) (2012) 717-21.
[387] J. Zhang, J.H. Wang, Kartogenin induces cartilage-like tissue formation in tendon-bone junction, Bone Res 2 (2014).
[388] Q. Hu, B. Ding, X. Yan, L. Peng, J. Duan, S. Yang, L. Cheng, D. Chen, Polyethylene glycol modified PAMAM dendrimer delivery of kartogenin to induce chondrogenic differentiation of mesenchymal stem cells, Nanomedicine 13(7) (2017) 2189-2198.
[389] A.R. Barr, V.C. Duance, S.F. Wotton, A.E. Waterman, Influence of intra-articular sodium hyaluronate and polysulphated glycosaminoglycans on the biochemical composition of equine articular surface repair tissue, Equine Vet J 26(1) (1994) 40-2.
[390] M. Talke, W. Krempien, C. Bär, Wirksamkeit und Verträglichkeit von Dexamethasonpalmitat i.a.: Vergleich mit Dexamethason-Kristallsuspension im entzündlichen Schub, Aktuelle Rheumatologie 18(3) (1993) 104-111.
[391] M.V. chaubal, J. Kipp, B. Rabinow, Excipient selection and criteria for injectable dosage forms, in: A. Katdare, M.V. chaubal (Eds.), Excipient Development for Pharmaceutical, Biotechnology, and Drug Delivery Systems2006.
[392] P.G. Conaghan, D.J. Hunter, S.B. Cohen, V.B. Kraus, F. Berenbaum, J.R. Lieberman, D.G. Jones, A.I. Spitzer, D.S. Jevsevar, N.P. Katz, D.J. Burgess, J. Lufkin, J.R. Johnson, N. Bodick, F.X.P. Investigators, Effects of a Single Intra-Articular Injection of a Microsphere Formulation of Triamcinolone Acetonide on Knee Osteoarthritis Pain:

A Double-Blinded, Randomized, Placebo-Controlled, Multinational Study, J Bone Joint Surg Am 100(8) (2018) 666-677.
[393] V.B. Kraus, P.G. Conaghan, H.A. Aazami, P. Mehra, A.J. Kivitz, J. Lufkin, J. Hauben, J.R. Johnson, N. Bodick, Synovial and systemic pharmacokinetics (PK) of triamcinolone acetonide (TA) following intra-articular (IA) injection of an extended-release microsphere-based formulation (FX006) or standard crystalline suspension in patients with knee osteoarthritis (OA), Osteoarthritis Cartilage 26(1) (2018) 34-42.

# PhD portfolio

**Name PhD student:** Marjan (Maria Jannie) Sandker
**Erasmus MC Department:** Orthopaedics
**Promotor(s):** prof. H. Weinans, prof. W.E. Hennink

## PhD training

| | Year | Workload (ECTS) |
|---|---|---|
| **Courses** | | |
| Laboratory animals science course, artikel 9, Rotterdam | 2011 | **4** |
| Stralingshygiene 3B, Rotterdam | 2011 | **1** |
| AMIE (animal imaging workshop), Rotterdam | 2011 | **1.4** |
| Regenerative medicine module 1, Groningen | 2010 | **1.5** |
| **Seminars and workshops** | | |
| Molecular medicine day, Rotterdam | 2012 | **0.5** |
| Seminar Zuid-West Nederland overleg trauma (ZWOT), Rotterdam | 2014-2016 | **0.4** |
| **(Inter)national presentations** | | |
| Injectable gels for localized delivery of Celecoxib and Triamcinolone in the synovial cavity (oral presentation)<br>6th OAControl progress meeting, Utrecht, the Netherlands | 2012 | **1.0** |
| The Djoeni Project: development and assessment up to horse studies of controlled release products for Osteoarthritis (oral presentation)<br>BMM/ TeRM annual meeting, Ermelo, The Netherlands | 2012 | **1.0** |
| Intra-articular drug delivery through an *in situ* gelling system (poster presentation)<br>OARSI World Congress on Osteoarthritis, Philadelphia, USA | 2013 | **1.0** |
| The performance of gels and microspheres in a rat model (oral presentation)<br>BMM/ TeRM annual meeting, Ermelo, The Netherlands | 2013 | **1.0** |
| Intra-articular drug delivery, *biodegradable hydrogels* (oral presentation)<br>Opleidingsdag ROGO, Delft | 2016 | **0.5** |

| | | |
|---|---|---|
| Various presentations at research meetings at the department of Orthopaedics, Erasmus MC, Rotterdam | 2010-2013 | **4.0** |
| Science day, Department of Orthopaedics, Erasmus MC, Rotterdam (oral presentations) | 2012, 2014 | **1.0** |
| Conference attendences | | |
| NOV congres | 2015-2018 | **1.5** |
| Experimental Biology Meeting, Boston | 2013 | **0.5** |

## Teaching

| | **Year** | **Workload (ECTS)** |
|---|---|---|
| **Lecturing** | | |
| Biomedical research techniques, presentation on 'Computed Tomography' | 2013 | **1.0** |
| Lecturing 3rd year medical students attending the minor 'Orthopaedic Sports Traumatology' | 2012, 2013, 2016 | **3.0** |
| 'The knee' and 'spine' lectures for OR nurses in training, Fontys Hogeschool Eindhoven | 2018 | **2.0** |
| **Supervising practicals** | | |
| AMIE workshop, presentation and practical demonstration on 'Computed Tompography' | 2012 | **1.0** |
| AMIE workshop, presentation and practical demonstration on 'Computed Tompography' | 2013 | **1.0** |
| Supervising anatomy practicals ('snijzaal') and case presentations of medical students | 2016 | **2.0** |
| Supervision of medical students –writing of a systematic review | 2014, 2016 | **4.0** |
| Supervising bachelor thesis | | |
| Supervising BcS in scientific period | 2012 | **1.0** |

# List of publications

**Sandker MJ**, Petit A, Redout EM, Siebelt M, Müller B, Bruin P, Meyboom R, Vermonden T, Hennink WE, Weinans H. In situ forming acyl-capped PCLA-PEG-PCLA triblock copolymer based hydrogels. *Biomaterials. 2013 Oct;34(32):8002-11. doi: 10.1016/j.biomaterials.2013.07.046. Epub 2013 Jul 23.*

**Sandker M**, Petit A, Müller B, Meyboom R, van Midwoud P, Bruin P, Redout EM, Versluijs-Helder M, van der Lest CH, Buwalda SJ, de Leede LG, Vermonden T, Kok RJ, Weinans H, Hennink WE. Release behavior and intra-articular biocompatibility of celecoxib-loaded acetyl-capped PCLA-PEG-PCLA thermogels. *Biomaterials. 2014 Sep;35(27):7919-28. doi: 10.1016/j.biomaterials.2014.05.064. Epub 2014 Jun 19.*

**Maria J Sandker**, Paul M. van Midwoud, Wim E. Hennink, Leo G.J. de Leede, Alan Chan, Harrie Weinans. *In Vivo* Pharmacokinetics of Celecoxib Loaded Endcapped PCLA-PEG-PCLA Thermogels in Rats after Subcutaneous Administration. *Eur J Pharm Biopharm. 2018 Jul 31. pii: S0939-6411(18)30655-6. doi: 10.1016/j.ejpb.2018.07.026.*

**Maria J Sandker**, Paul van Midwoud, Stuart Koelewijn, Erik de Blois, Michiel Beekhuizen, Laura Creemers, Wim E. Hennink, Harrie Weinans. *In-vivo* efficacy of intra-articular injection of celecoxib-loaded thermoreversible hydrogels in a Rat Model of Osteoarthritis. *Submitted.*

**Sandker MJ**, Duque LF, Redout EM, Chan A, Que I, Löwik CWGM, Klijnstra EC, Kops N, Steendam R, van Weeren R, Hennink WE, Weinans H. Degradation, intra-articular retention and biocompatibility of monospheres composed of [PDLLA-PEG-PDLLA]-b-PLLA multi-block copolymers. *Acta Biomater. 2017 Jan 15;48:401-414. doi: 10.1016/j.actbio.2016.11.003. Epub 2016 Nov 2.*

Moshtagh PR, Rauker J, **Sandker MJ,** Zuiddam MR, Dirne FW, Klijnstra E, Duque L, Steendam R, Weinans H, Zadpoor AA. Nanomechanical properties of multi-block copolymer microspheres for drug delivery applications. *J Mech Behav Biomed Mater. 2014 Jun;34:313-9. doi: 10.1016/j.jmbbm.2014.03.002. Epub 2014 Mar 19.*

**Maria J Sandker**, Luisa F Duque, Everaldo M Redout, Evelien C Klijnstra, Rob Steendam, Nicole Kops, Jan H Waarsing, Rene van Weeren, Wim E Hennink, Harrie Weinans. Degradation, intra-articular biocompatibility, drug-release and bioactivity of tacrolimus-loaded poly(DL-lactide-PEG)-b-poly(L-lactide) multiblock copolymers based monospheres *ACS Biomater. Sci. Eng., 2018, 4* (7), pp 2390–2403 *DOI: 10.1021/acsbiomaterials.8b00116*

den Reijer PM, **Sandker M,** Snijders SV, Tavakol M, Hendrickx AP, van Wamel WJ. Combining in vitro protein detection and in vivo antibody detection identifies potential vaccine targets against Staphylococcus aureus during osteomyelitis. *Med Microbiol Immunol. 2017 Feb;206(1):11-22. doi: 10.1007/s00430-016-0476-8. Epub 2016 Sep 14.*

Siebelt M, van der Windt AE, Groen HC, **Sandker M,** Waarsing JH, Müller C, de Jong M, Jahr H, Weinans H. FK506 protects against articular cartilage collagenous extra-cellular matrix degradation. *Osteoarthritis Cartilage. 2014 Apr;22(4):591-600. doi: 10.1016/j.joca.2014.02.003. Epub 2014 Feb 19.*

Siebelt M, Groen HC, Koelewijn SJ, de Blois E, **Sandker M**, Waarsing JH, Müller C, van Osch GJ, de Jong M, Weinans H. Increased physical activity severely induces osteoarthritic changes in knee joints with papain induced sulfate-glycosaminoglycan depleted cartilage.
Arthritis Res Ther. 2014 Jan 29;16(1):R32. doi: 10.1186/ar4461.

van der Stok J, Wang H, Amin Yavari S, Siebelt M, **Sandker M**, Waarsing JH, Verhaar JA, Jahr H, Zadpoor AA, Leeuwenburgh SC, Weinans H. Enhanced bone regeneration of cortical segmental bone defects using porous titanium scaffolds incorporated with colloidal gelatin gels for time- and dose-controlled delivery of dual growth factors. *Tissue Eng Part A. 2013 Dec;19(23-24):2605-14. doi: 10.1089/ten.TEA.2013.0181. Epub 2013 Aug 17.*

Siebelt M, Jahr H, Groen HC, **Sandker M**, Waarsing JH, Kops N, Müller C, van Eden W, de Jong M, Weinans H. Hsp90 inhibition protects against biomechanically induced osteoarthritis in rats. *Arthritis Rheum. 2013 Aug;65(8):2102-12. doi: 10.1002/art.38000.*

Piscaer TM, **Sandker M**, van der Jagt OP, Verhaar JA, de Jong M, Weinans H.
Real-time assessment of bone metabolism in small animal models for osteoarthritis using multi pinhole-SPECT/CT. *Osteoarthritis Cartilage. 2013 Jun;21(6):882-8. doi: 10.1016/j.joca.2013.03.004. Epub 2013 Mar 14.*

# Dankwoord

Promoveren is als een lange reis, een waarvan je vooral terugblikkend pas ziet hoe bijzonder het eigenlijk was. Op het moment dat je "ja" zegt tegen het starten van een promotie heb je eigenlijk geen idee waar je aan begint, maar ik zou het zo weer doen! De ontwikkelingen die je als promovendus doormaakt, zowel op wetenschappelijk als persoonlijk vlak, zijn zeer waardevol. Zonder de hulp van anderen was het nooit gelukt, en ik zou via deze weg iedereen willen bedanken die mij hebben geholpen bij de totstandkoming van dit proefschrift.

Allereerst mijn promotor, professor Weinans, beste Harrie. Via professor Verhaar ben ik na mijn coschappen aan jou voorgesteld op het lab, omdat ik interesse had in het doen van onderzoek. Er was wel wat geld voor een onderzoekje van ongeveer een half jaar naar de loslating van prothesen. Het leek me erg leuk om dit te gaan doen, en alles was geregeld om hieraan te gaan starten. Op het laatste moment kreeg ik een telefoontje van jou, en ik was even bang dat het allemaal niet door zou gaan. Maar het was een compleet ander verhaal; er was een PhD-student gestopt met een project en je vroeg mij om in plaats van een onderzoekje van een half jaar een promotietraject te starten! Hierop heb ik direct volmondig 'ja' gezegd, en ik ben je nog steeds erg dankbaar voor de kans die je mij op deze manier gegeven hebt. Jouw enthousiasme werkt zeer aanstekelijk, en het was een van de vele redenen dat werken in het lab op de 16$^{e}$ verdieping zo prettig maakte. Na jouw vertrek naar Utrecht hebben we gelukkig altijd goed contact kunnen houden en heb je mij van een afstandje kunnen superviseren in het voltooien van dit boekje. Ik wil je hiervoor erg bedanken, zonder deze steun was het niet gelukt.

Professor Hennink, beste Wim. Pas later betrokken bij dit geheel, via Audrey Petit. De samenwerking met jou heb ik als bijzonder prettig ervaren. Altijd nauw betrokken en ongekend snel met reageren (zelfs in het weekend en tijdens vakanties). Jouw input heeft onze artikelen stuk voor stuk naar een hoger niveau kunnen tillen. Dit alles was van onschatbare waarde voor de totstandkoming van dit boekje en ik kan je niet genoeg bedanken dat je mijn copromotor wilde zijn.

Beste professor Verhaar, bedankt voor uw vertrouwen in mij. Vanuit mijn coschappen ben ik via U aangedragen bij professor Weinans, waarna ik mijn promotietraject heb kunnen starten. Hiervoor ben ik U bijzonder dankbaar. Vanaf de zijlijn bent U altijd

betrokken gebleven bij mijn promotie, en waar nodig kon ik altijd om advies vragen. Daarnaast heb ik in mijn eerste academische jaar van de opleiding tot Orthopedisch chirurg op uw afdeling mogen werken, waar ik ongelofelijk veel kennis heb mogen opdoen over ons prachtige vak. Ik zie ernaar uit om terug te keren en mijn opleiding in het Erasmus af te ronden.

Beste leescommissie, bedankt voor al jullie tijd en moeite.

Daarnaast wil ik graag de Universiteit van Utrecht bedanken voor de mogelijkheid om mijn promotie hier te laten plaatsvinden.

Mijn lieve paranifmen, Dineke en Jeanine. Wat bijzonder dat ik dit belangrijke moment in mijn leven mag delen met jullie, mijn twee zeer dierbare vriendinnen.
Dien, ik ken je inmiddels al weer meer dan 10 jaar. Bizar hoe de tijd vliegt. Wat hebben we veel mooie dingen mogen delen, van de uitjes met Euroturn tot samen naar festivals en zelfs een liftavontuur naar Hongarije die ik nooit zal vergeten. Wat ben ik blij om jou als vriendin te mogen hebben!
En Jeanine, Nientje. Jaren jonger dan ik, maar ik denk toch oud van ziel. Hoe wij vanaf het eerste moment dat we elkaar ontmoetten een connectie hebben gehad is ongelofelijk. Als ik jou zie is het van begin tot einde lachen geblazen, jouw positieve blik op het leven is iets om jaloers op te zijn. Er zijn te veel mooie momenten om op te noemen, eigenlijk is het altijd feest als jij in de buurt bent. Blijf altijd zoals je bent, dat is namelijk perfect!

Marianne. Helaas was je me net voor met jouw boekje, en dus ook jouw versie van het dankwoord, waardoor veel van mijn ideeën zijn al op papier gezet. Aan de andere kant valt er ook niet echt een andere versie van te schrijven. Vanaf het moment dat jij binnen kwam lopen op het lab voor je sollicitatiegesprek en ik je een kop koffie aanbood zijn we vriendinnen geweest en gelukkig gebleven. We hebben veel leuke dingen samen mee gemaakt, onder andere een tripje naar Berlijn en vorig jaar heb ik je bruiloft op Hvar mee mogen maken, wat onvergetelijk was. Op het maken van nog vele van zulke mooie herinneringen.

Johan, het was heel prettig om tegenover je te zitten in het lab en af en toe lekker samen te kunnen “zeuren” over van alles en nog wat. Je hebt een zwaar jaar achter de rug, maar nu is het tijd om weer naar de toekomst te kijken. Je bent een topper!!

Michiel, bedankt dat je mij wegwijs hebt gemaakt op het lab en in het bijzonder in het doen van dierexperimenteel onderzoek met behulp van onder andere CT en SPECT scannen. Je hebt me geleerd om dit alles zeer gestructureerd uit te voeren en te

documenteren, daarnaast heb je me veel geleerd over het wetenschappelijk juist opzetten van een studie en het analyseren hiervan.

Callie, my partner in crime. Thank you for all the awesome times we've had, in the lab but mostly outside. Our trips to Ireland and Ibiza are definitely ones to remember. I'm really glad you came to Holland from America and I got to become one of your friends!

Erwin, jouw expertise op het gebied van data-analyse en statistiek zijn voor onschatbare waarde voor de afdeling. Maar net zo belangrijk is jouw rust en jouw ongekende vriendelijkheid richting iedereen om je heen. Je bent werkelijk een voorbeeld.

Sandra, dagelijks een soepje met je halen was supergezellig. Je bent erg waardevol voor het lab.

Holger, jouw passie voor de wetenschap is ongeëvenaard en zeer aanstekelijk. Bedankt voor alle, soms onnavolgbare, input en daarnaast ook alle gezellige momenten.

Daarnaast wil ik alle andere mensen van de 16$^{e}$ verdieping in de toren bedanken, jullie hebben de 4 jaar die ik daar doorgebracht heb tot een onvergetelijke ervaring gemaakt met verschillende uitjes, de wekelijke "cake van de week" en natuurlijk alle koffie-momentjes; Rintje, Jasper, Mairead, Naimhe, Panithi, Wu, Maarten, Mieke, Nienke, Roberto, Nicole, Yvonne, Wendy, Lizette, Gerjo, Janneke.

Audrey, our collaboration was very fruitful from the beginning and your enthusiasm was very contagious. You taught me a lot about polymer chemistry and together we have achieved some awesome goals with 2 accepted papers in Biomaterials. I wish you all the best.

Paul, na mijn zeer positieve ervaringen met Audrey kwam jij als haar opvolger op het BMM-project vanuit Ingell. Het was erg prettig om met jou samen te werken, je bent op een rustige manier aanwezig, maar alles wat je aandraagt klopt als een bus. Nogmaals gefeliciteerd met de recente promotie en succes gewenst in de rest van je carrière.

Luisa; it took us some time to actually finish our joined articles, but once we did they were of an excellent level and I definitely thank you for all your hard work on the monosphere data. You are such a kind person and I wish you a great life and career in Berlin.

Verder wil ik alle mensen waarmee ik mee vanuit het BBM-OA-consortium innig mee samengewerkt heb op deze manier bedanken, in het bijzonder; Mike, Leo, Evelien, Everaldo, Renee, Ivo, Alan.

Collega's van het Maasstad Ziekenhuis, Erasmus MC en ETZ te Tilburg. Ik wil jullie erg bedanken voor de fantastische tijd die ik tot nu toe heb mogen hebben in de reis tot orthopedisch chirurg. Ik zou in het bijzonder mijn opleiders willen bedanken voor alle steun tijdens de soms lastige combinatie van een voltijd opleiding en het afronden van mijn promotietraject. Renee en Taco; bedankt!

Afleiding buiten het wetenschaps- en ziekenhuisleven is even belangrijk geweest voor het afronden van dit promotietraject. Milena, Roos, Yvonne, Astrid, Miljana, Thomas. Mijn vrienden uit Rotterdam die ik helaas wat minder zie door mijn verhuizing naar die andere stad (ik zal geen namen noemen). Uit het oog maar zeker niet uit het hart. Ik hoop dat we nog vele jaren van samen uit eten, feestjes en kletsen over het leven zullen meemaken.

Michelle, Diederick, Jeff, Stephanie, Mariska, Marcel, Coco, Chris, Shauna, Nathalie, Kevin, Max, Aranka en Ogy. Wat een bijeengeraapt zooitje, maar ik kan me geen betere groep voorstellen. Iedereen een andere achtergrond maar samen gekomen door onze gezamenlijke liefde voor muziek. Geen enkel moment is saai als ik samen ben met jullie. Ik hoop dat onze feestjes nog jaren door zullen gaan. TGL!

Pap en mam, ik zeg het niet vaak genoeg maar ik hou van jullie. Van kleins af aan hebben jullie me in alles gesteund en aangemoedigd om overal het beste van te maken. Zonder jullie had ik dit nooit kunnen bereiken. Bedankt voor jullie onvoorwaardelijke liefde en steun bij alles wat ik doe.

Gerwin, mijn lieve broer(tje). Wat was het leuk om samen met jou op te groeien in Valthermond. Ik kan me nagenoeg geen ruzies herinneren en we hebben altijd veel lol gehad samen. Vooral op latere leeftijd is onze band sterker geworden, het is erg gezellig om af en toe met jou een concert te pakken of samen een drankje te doen. Wat ben ik blij voor je dat je je plekje gevonden hebt in Nijmegen, en met Manon erbij is het helemaal compleet. Daarnaast ben je zelf dit jaar aan jouw promotietraject begonnen, wat je ongetwijfeld glansrijk zult afronden.

Sander, de mannelijke versie van mijzelf. Wat ben ik blij dat jij zo'n 3 jaar geleden in mijn leven bent gekomen. Beide niet per se op zoek naar een relatie, maar er dan achter komen dat samen zijn zo veel fijner is dan in je eentje. Ik ben je heel erg dankbaar voor jouw steun en ook geduld tijdens de laatste loodjes van dit boekje. Het was zwaar, maar zeker de moeite waard. Vanaf nu kan al mijn aandacht naar jou gaan in de spaarzame vrije uurtjes die we hebben, laten we gaan genieten! Ik hou van je.

# About the author

Marjan (Maria Jannie) Sandker werd geboren op 12 november 1985 te Valthermond. Zij ging naar het VWO aan de Regionale Scholengemeenschap (RSG) in Ter Apel, en behaalde in 2004 haar diploma. Datzelfde jaar startte ze met de opleiding Geneeskunde aan de Erasmus Universiteit in Rotterdam. Al op de middelbare school was er een bovengemiddelde interesse voor de Orthopedie, en tijdens de studie Geneeskunde groeide deze voorliefde voor het bewegingsapparaat. Daarop werd er voor zowel een keuze- en oudste coschap, als een wetenschappelijke stage op de afdeling Orthopedie gekozen. De studie Geneeskunde werd in 2010 succesvol afgerond. Er was tijdens de wetenschappelijke stage een interesse voor wetenschappelijk onderzoek aangewakkerd, en om de opleiding geneeskunde verdere verdieping te geven werd er gekozen voor een promotietraject. Deze werd direct aansluitend op het halen van het artsexamen gestart op het lab van de afdeling Orthopedie, onder begeleiding van prof. H. Weinans. In 2015 startte ze met haar vooropleiding Chirurgie in het Maasstad Ziekenhuis onder begeleiding van opleider dr. R. Klaassen, waar de eerste chirurgische vaardigheden werden ontwikkeld. In 2016 is ze begonnen met de opleiding tot orthopaedisch chirurg, welke ze in het Erasmus MC te Rotterdam (opleider Dr. P.K. Bos) en het ETZ te Tilburg (opleider dr. T. Gosens) zal afronden.